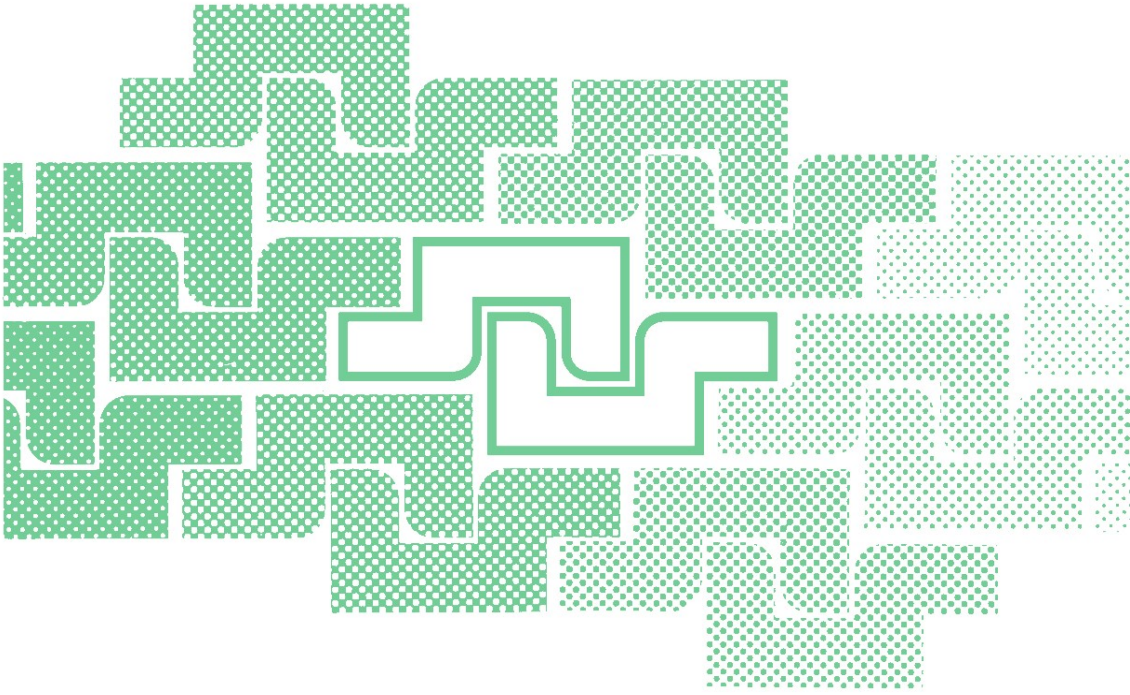

Regional Climate Variability and its Impacts in the Mediterranean Area

Edited by

A. Mellouki and
A.R. Ravishankara

NATO Science Series

IV. Earth and Environmental Sciences – Vol. 79

CD-ROM INCLUDED

REGIONAL CLIMATE VARIABILITY AND ITS IMPACTS IN THE MEDITERRANEAN AREA

NATO Science Series

A Series presenting the results of scientific meetings supported under the NATO Science Programme.

The Series is published by IOS Press, Amsterdam, and Springer (formerly Kluwer Academic Publishers) in conjunction with the NATO Public Diplomacy Division.

Sub-Series

I. Life and Behavioural Sciences	IOS Press
II. Mathematics, Physics and Chemistry	Springer (formerly Kluwer Academic Publishers)
III. Computer and Systems Science	IOS Press
IV. Earth and Environmental Sciences	Springer (formerly Kluwer Academic Publishers)

The NATO Science Series continues the series of books published formerly as the NATO ASI Series.

The NATO Science Programme offers support for collaboration in civil science between scientists of countries of the Euro-Atlantic Partnership Council. The types of scientific meeting generally supported are "Advanced Study Institutes" and "Advanced Research Workshops", and the NATO Science Series collects together the results of these meetings. The meetings are co-organized by scientists from NATO countries and scientists from NATO's Partner countries – countries of the CIS and Central and Eastern Europe.

Advanced Study Institutes are high-level tutorial courses offering in-depth study of latest advances in a field.
Advanced Research Workshops are expert meetings aimed at critical assessment of a field, and identification of directions for future action.

As a consequence of the restructuring of the NATO Science Programme in 1999, the NATO Science Series was re-organized to the Four Sub-series noted above. Please consult the following web sites for information on previous volumes published in the Series.

http://www.nato.int/science
http://www.springeronline.com
http://www.iospress.nl

Series IV: Earth and Environmental Sciences – Vol. 79

REGIONAL CLIMATE VARIABILITY AND ITS IMPACTS IN THE MEDITERRANEAN AREA

edited by

A. Mellouki

ICARE, CNRS,
Orléans, France

and

A.R. Ravishankara

NOAA, R/CSD,
Boulder, CO, U.S.A.

Published in cooperation with NATO Public Diplomacy Division

Proceedings of the NATO Advanced Research Workshop on
Regional Climate Variability and its Impacts
in the Mediterranean Area
Marrakech, Morocco
1 September 2006

A C.I.P. Catalogue record for this book is available from the Library of Congress.

ISBN 978-1-4020-6428-9 (PB)
ISBN 978-1-4020-6427-2 (HB)
ISBN 978-1-4020-6429-6 (e-book)

Published by Springer,
P.O. Box 17, 3300 AA Dordrecht, The Netherlands.

www.springer.com

Printed on acid-free paper

CONTENTS

CD-ROM with colour figures included.

PREFACE

A. Mellouki, A. R. Ravishankara, M. Kanakidou, K-H. Becker, L. Elmaimouni and A. Dakkina

Global change due to natural processes and anthropogenic activity as well as the natural variability of the climate system will impact all areas of the globe. However, the impact will not be uniform and different impacts of differing magnitude and nature will be felt in various regions of the globe. The Mediterranean region, like other regions of the world, will face some unique and different impacts of the climate change and variability on.

The uniqueness and difference in the Mediterranean are to be expected given some special dynamical, chemical, biological, and land characteristics of the region. Mediterranean is a landmass that surrounds a "sea," a body of saline water that does not exchange very rapidly with the rest of the oceans on Earth. It is apparent that the meteorology and chemistry in this region leads to two "distinct," but interlinked regions. In summer, two semi-permanent weather systems located at each end of the Mediterranean dominate the entire basin: at the west, the Azores anticyclone and at the east, a low pressure (monsoon) system, which extends from the middle-east to the whole of southwestern Asia. Between these two major weather systems the average air flow is diverted southward towards North Africa (close to the thermal equator in summer) via the Adriatic and Ionian seas and/or the Black sea, Agean Sea and the Levantine basin (*Millan M. et al., Photoxidant dynamics in the Mediterranean basin in summer: results from European research projects, JGR, 102, 8811-8823,1997; Barry R.G. and Chorley R.J., Atmosphere, Weather & Climate Methuen & Co Ltd, NewYork, ISBN 0-416-07142-2, 1987, pages 262-271*). Recirculation and regional patterns are more important in the west Mediterranean, basin that receives more precipitation with regard to the East basin that is drier and its seawater is more oligotrophic. The Mediterranean region has gradients in emissions of dust, hydrocarbons, and industrial pollutants (such as SO_2, NOx, and aerosols and their precursors). This is region that influenced by transport from such varied

landmasses as Europe, Africa, and Asia. The nature and intensities of the emissions from Europe are vastly different from those from Africa, which in itself is diverse given the change in terrain from vegetated regions of Central Africa to deserts of North Africa.

The Mediterranean region is often exposed to multiple stresses, such as a simultaneous water shortage and air pollution. This is a consequence of its unique location and emissions. One of the common stresses in North Africa is water shortage and distribution amongst the seasons. Air pollution can often add to the water stress. Air pollution occurs due to emissions in the region as well as from those transported from other areas and can occur when there is low water availability. Multiple stresses are likely to grow in the future when human induced stress is likely to increase due to the rapid industrialization of the region.

This NATO workshop was set up to discuss these issues in general, and the influence of chemical emissions and transformation in particular. This workshop was "special" because it involved a very large number of scientists (>75%) from the region, either from North Africa or the Mediterranean Europe. This participation greatly enabled infusion of key information about the region from the people who live in the region.

Many key issues, some of which are specific to this region, were identified after presentation and discussions for 3 days. These key findings are very briefly summarized here. Details of the finding and suggestions can be found in the articles in this volume.

Earth system science involves many highly diverse phenomena that are studies as processes in biology, ocean sciences, land surface changes, and atmosphere chemistry and dynamics. These phenomena are represented in models and are usually developed and sharpened by people involved in those disciplines. However, the superposition of these phenomena leads to additional requirements of connecting the processes across the regions, disciplines, and timescales. Often, the important issues involve phenomena occurring at the interface of these areas. Development of the necessary information and simultaneously

incorporating the differing areas are essential. Examples include atmospheric chemistry with biological processes and ocean chemistry with emissions and deposition. A strong sentiment was expressed by the participants for a larger emphasis on cross-discipline, interfacial, phenomena. Such a need is not unique to the Mediterranean region, but is essential for a clear understanding and predicting for this region.

Often, information on the details of an individual process is on a time and spatial scale that is very different from those with which it is coupled in the atmosphere. For example, the scale of the processes involved in the emissions of dust to the atmosphere are much shorter in time and smaller in space than the atmospheric transport and transformation of these particles. Therefore, including this information from in global climate and earth system models pose specific difficulties and challenges. Scaling up the information from the short time and space scale studies to global representation is essential and needs to be improved. Similarly, the time scales for some chemical processes can be very different than those for atmospheric processing. The range of such "scaling" of information, either as parameterizations or detailed process representation, is important in understanding various feedbacks in the climate system. As noted above, one of the specific processes of importance to the Mediterranean region is the incorporation of dust into the atmosphere.

The knowledge of the emissions into the atmosphere from various natural and human-induced sources is one of the largest uncertainties in climate studies as well as in the estimation of the impacts on regions and the globe. Inventories of the emissions are good for some sources (e.g., CO_2 from fossil fuel combustion) than for others (e.g., black carbon from biomass burning). The inventories have to include the amount, type, nature, the mix, and the temporal evolution of emissions. Such information is not currently available for most regions of the globe. This is particularly a problem for the Mediterranean region where the type, diversity, and nature of emissions are large and the time evolution of these emissions are different. Good emission inventories, in usable forms, from the Mediterranean region will be of great importance to not

only the global representation but also for assessing the contribution of the Mediterranean region and impacts on this region.

Deposition from the atmosphere appears to be a process that is not well understood, quantified, and represented in models. Currently, most depositions are presented in models as very simple parameterizations. Studies aimed at understanding the processes responsible for deposition are needed. When the understanding is sufficient, it will be a good idea to include deposition as a process, rather than a parameterization. An accurate representation of deposition will be essential for quantifying feedbacks, especially in such diverse areas as impact of land cover change and ocean uptake on atmospheric composition and its changes.

It was believed by the participants that the Mediterranean region is under-sampled, much more so than many parts of the globe. The lack observations in the Mediterranean region has led to inaccuracies in calculating emissions, atmospheric composition, and transport in and out of the region. Observations of processes that are unique to this region are needed. Further, it is clear that long-term monitoring of various atmospheric parameters and chemical composition is essential for understanding the contribution of this region to the globe and for assessing the impact of change on the unique Mediterranean region.

Even though there is a lack in observations from the Mediterranean region, compared to other parts of the world, in the current period, there are a relatively large number of historic and pre-existing observations available from this region. A thorough compilation, quality checking, and interpretation of these observations would be highly beneficial to not only the Mediterranean region but also for the global climate studies.

As noted earlier, the above are not all-inclusive, but represent a few of the key issues that were noted in the workshop. For full details, the reader is referred to other articles in this volume.

The workshop was held in Hotel Kenzi-Farah in Marrakech, Morocco, from 23rd to 26th November 2006.

ACKNOWLEDGEMENTS

The NATO Science Committee is very gratefully acknowledged for providing the main financial support for the workshop. Special thanks to the Moroccan Ministry of Environment for practical information as well as financial support. Additional financial support was received from CNRS-Orléans (France), University of Agadir (Morocco) and Eurochamp Project (EU) for which they are acknowledged.

The organising committee would like to thank V. Daële, J. Pagé, R. Herbin, A. Chehbouni and A. Melouki for their help.

Financial support of the workshop was by the following organizations:

- NATO Scientific and Environmental Affairs Division, Brussels
- Centre National de la Recherche Scientifique (CNRS)
- Institut de Combustion, Aérothermique, Réactivité et Environnement (ICARE)
- University of Agadir
- EUROCHAMP Project

LIST OF CONTRIBUTORS

Arsene Cecilia
Environmental Chemical Processes Laboratory
Department of Chemistry, University of Crete
P.O.Box 2208, Voutes, GR-71003 Heraklion, Greece
carsene@chemistry.uoc.gr

Azzi Abbès
Département de Génie-Maritime, Faculté de Génie-Mécanique
Université des Sciences et de la Technologie d'Oran (USTO)
BP. 1505 El-Mnaouar, 31000, Oran, Algeria
abbes.azzi@gmail.com

Balafrej Taha
Ministère de l'Aménagement du Territoire, de l'Eau et de l'Environnement
Point Focal de la CCNUCC
Agdal Rabat, Morocco
balafrej@minenv.gov.ma

Barnes Ian
Physikalische Chemie / Fachbereich C
Bergische Universitaet Wuppertal
Gauss Strasse 20, D-42097 Wuppertal, Germany
barnes@uni-wuppertal.de

Becker Karl H.
Institute of Physical Chemistry
Department of Chemistry, University Wuppertal
Gauss-Str. 20, D-42097 Wuppertal, Germany
khbecker@uni-wuppertal.de

Bergametti Gilles
Laboratoire Inter-Universitaire des Systèmes Atmosphériques (LISA)
Faculté des Sciences et Technologie
61 avenue du Général de Gaulle, F-94010 Créteil Cedex, France
bergametti@lisa,univ-paris12.fr

Bounoua Lahouari
Biospheric Sciences Branch, Code 614.4
NASA - Goddard Space Flight Center
Greenbelt MD 20771, USA
bounoua@ltpmail.gsfc.nasa.gov

Chehbouni Ahmed
Université Cadi Ayyad, Faculté des Sciences Semlalia
BP 2390, Marrakech, Morocco
chehbouni@ucam.ac.ma

Daële Véronique
CNRS, Laboratoire de Combustion et Systèmes Réactifs (LCSR)
1C, Avenue de la recherche scientifique
F-45071 Orléans cedex 02, France
daele@cnrs-orleans.fr

Dakkina Abdelali
Centre d'Information sur l'Energie Durable et l'Environnement (CIEDE)
Ministry of Environment
Rabat, Morocco
dakina2002@yahoo.fr

Elmaimouni Lahcen
Laboratoire de Chimie Physique, département de Chimie
FSA, Agadir, Morocco
lelmaimouni@yahoo.fr

George Christian
Laboratoire d'Application de la Chimie à l'Environnement (LACE)
Domaine Scientifique de la Doua, Batiment J. Raulin
43 Bd du 11 Novembre 1918, F-69622 Villeurbanne Cedex, France
Christian.George@univ-lyon1.fr

Hjorth Jens
Institute for Environment and Sustainability (IES)
The European Commission Joint Research Centre
TP 290, 21020 ISPRA (VA), Italy
jens.hjorth@jrc.it

Kanakidou Maria
Environmental Chemical Processes Laboratory
Department of Chemistry, University of Crete
P.O.Box 2208, Voutes, GR-71003 Heraklion, Greece
mariak@chemistry.uoc.gr

Karrouk Mohamed-Saïd
Université Hassan II Centre de Recherche de Climatologie (CEREC)
Laboratoire de Climatologie et de Télédétection (CLIMTEL)
BP 8220 Oasis, MA-20103 Casablanca, Morocco
Karrouk.MS@UnivH2M.Ac.Ma
KarroukSaid@Yahoo.Com

Kubilay Nilgün
Institute of Marine Sciences
Middle East Technical University
PO Box 28, Erdemli-Mersin, Turkey
kubilay@ims.metu.edu.t

Maione Michela
Universita' di Urbino Istituto di Scienze Chimiche
6, Piazza Rinascimento, 61029 Urbino, Italy
michela@uniurb.it
project.office@accent-network.org

Mallet Marc
Laboratoire d'Aérologie (LA), Observatoire Midi-Pyrenees
14 av Edouard Belin, F-31400 Toulouse, France
malm@aero.obs-mip.fr

Mellouki Wahid
CNRS, Laboratoire de Combustion et Systèmes Réactifs (LCSR)
1C, Avenue de la recherche scientifique
F-45071 Orléans cedex 02, France
mellouki@cnrs-orleans.fr
wmellouki@laposte.net

Mihalopoulos Nikos
Environmental Chemical Processes Laboratory
Department of Chemistry, University of Crete
P.O.Box 1470, Voutes, GR-71409 Heraklion, Greece
Mihalo@chemistry.uoc.gr

Millán Millán
Fundacion CEAM
Parque tecnologico c/4, Sector Oeste, Paterna
46980 Valencia, Spain
pilarz@ceam.es

Mohamed Mohamed A.
Atomic Energy Authority
National Centre for Nuclear Safety and Radiation Control (NCNSRC)
Material and Nuclear Fuel Cycle Dept.
3 Ahmed El-Zomer St. Nasr City, 11762, Cairo, Egypt, P.O.Box 7551
mageleel2000@yahoo.com

Mousa Ashraf
Crustal Movements Laboratory
National Research Institute of Astronomy and Geophysics
Elmarsad St., Helwan, Cairo, 11421, Egypt
ashrafkm@yahoo.com

Niedojadlo Anita
AGH University of Science and Technology
Faculty of Mining Surveying and Environmental Engineering
Department of Management and Protection of Environment
Al. Mickiewicza 30, C4, 30-059 Cracow, Poland
niedan@poczta.fm

Pilling Mike
School of Chemistry
University of Leeds
Leeds LS2 9JT, United Kingdom
M.J.Pilling@leeds.ac.uk

Prospero Joseph M.
RSMAS/MAC, University of Miami
4600 Rickenbacker Causeway
Miami, FL 33149, USA
jprospero@rsmas.miami.edu

Ravishankara A.R. (Ravi)
Chemical Sciences Division, Earth System Research Laboratory
NOAA, R/CSD 2
325 Broadway, Boulder CO 80305, USA
A.R.Ravishankara@noaa.gov

Saliba Najat A.
IBSAR - American University of Beirut
American University of Beirut
P.O.Box 11-0236 Riad El-Solh, Beirut 1107 2020, Lebanon
ns30@aub.edu.lb

Tanimoto Hiroshi
National Institute for Environmental Studies
Asian Environment Research Group Regional Atmospheric Modeling
Section & Center for Global Environment Research
16-2 Onogawa, Tsukuba, Ibaraki 305-8506, Japan
tanimoto@nies.go.jp

Wiesen Peter
Physikalische Chemie / Fachbereich C
Bergische Universitaet Wuppertal
Gauss Strasse 20, D-42097 Wuppertal, Germany
wiesen@uni-wuppertal.de

CLIMATE AND ITS VARIABILITY: GLOBAL AND REGIONAL PERSPECTIVE

LONG-RANGE TRANSPORT OF POLLUTANTS ABOVE THE EASTERN MEDITERRANEAN: IMPLICATIONS FOR AIR QUALITY AND REGIONAL CLIMATE

NIKOLAOS MIHALOPOULOS
University of Crete, Department of Chemistry, Voutes 71003, Heraklion, Greece, mihalo@chemistry.uoc.gr

Key Words: Transport parthways, Ozone, PM, aerosols, chemical composition, oxidation capacity, Eastern Mediterranean.

Abstract The present work provides an overview of the transport and transformation processes occurred above the Mediterranean with emphasis in the Eastern basin. It summarises the results from several campaigns performed since the last decade. The measurements gave evidence of a remarkably high level of air pollution from the surface to the top of the troposphere up to 15 km altitude. The strongest anthropogenic influence was observed in the lower 4 km by pollutants originating from both West- and East Europe transported by the northerly flow. The sources are industrial activity, traffic, forest fires, agricultural and domestic burning. Trajectory analysis and model results suggest also an important influence by Asian pollution plum near the tropopause from the east.

Near the surface the air pollution has several undesirable consequences. First, the European Union eight-hourly air quality standard for ozone is exceeded throughout the summer in the entire Mediterranean region. Second, the concentrations of aerosols are high as well, affecting human health. The aerosols furthermore influence the Mediterranean atmospheric energy budget by scattering and absorbing solar radiation. During summer, they reduce solar radiation absorption by the sea by about 10% and they alter the heating profile of the lower troposphere. As a consequence, evaporation and moisture transport, in particular to North Africa and the Middle East, are suppressed.

In the free troposphere, pollution is largely determined by intercontinental transport, whereas upper tropospheric pollution from Asia can reach the stratosphere. These “crossroads” carry large pollution loads over the Mediterranean, and the negative effects extend far beyond the region. International efforts are called for to reduce these atmospheric environmental stresses and to further investigate the links between Mediterranean and global climate change.

A. Mellouki and A.R. Ravishankara (eds.), Regional Climate Variability and its Impacts in the Mediterranean Area, 1–13.

1. Introduction

The Eastern Mediterranean is the cross road of air masses where emissions from pollution meet with natural ones. These emissions include trace gases like nitrogen oxides, carbon monoxide, volatile organic compounds, and particles. Pollution in the area results from industrial and traffic sources and domestic burning mainly from Europe, Balkans and the Black Sea. Forest fires and agricultural burning emissions are also affecting the area during the dry season. Natural emissions from the Sahara region, from the vegetation that surrounds the Mediterranean Sea and from the Mediterranean Sea itself also affect the area (Mihalopoulos et al., 1997; Lelieveld et al., 2002). Air masses transported from the Atlantic Ocean atmosphere but also from Asia (via the upper troposphere) can reach the area under favourable air flow conditions (Lelieveld et al., 2002; Kallos et al., 1998). South winds from Africa carry to the Eastern Mediterranean air masses with high loadings of Sahara dust and low levels of NO_x and O_3. This air flow is more frequently occurring during the transition periods in spring and fall.

Transport and transformation processes in the Eastern Mediterranean are the topic of intensive studies that aim to evaluate the intensity of these processes and their impact on regional air quality and visibility, climate and atmospheric composition change as well as on terrestrial and marine ecosystems.

2. Major Air Flow Patterns in the Eastern Mediterranean

During the MINOS campaign in July-August 2001, ground based, aircraft and remote sensing measurements gave evidence of a remarkably high level of air pollution from the surface to the top of the troposphere up to 15 km altitude and of the existence of 3 distinct atmospheric layers affected by different pollution sources (Figure 1).

The strongest anthropogenic influence was observed in the lower 4 km, originating from both West and East Europe transported by the northerly flow (Lelieveld et al., 2002). The sources are industrial activity, traffic, forest fires, agricultural and domestic burning (Gros et al., 2003). Biomass burning emissions in the area present large inter-annual variability, they maximized in 2000 when in July exceptionally intensive forest fires burnt a surface of more than 600 Km^2 that is about twice the annual mean burnt area over Greece the past 10 years (Latos et al., 2006). In addition to local fire events, biomass burning effluents from surrounding areas affect the area like those observed over the region north of the Black Sea during summer 2001 (Lelieveld et al., 2002).

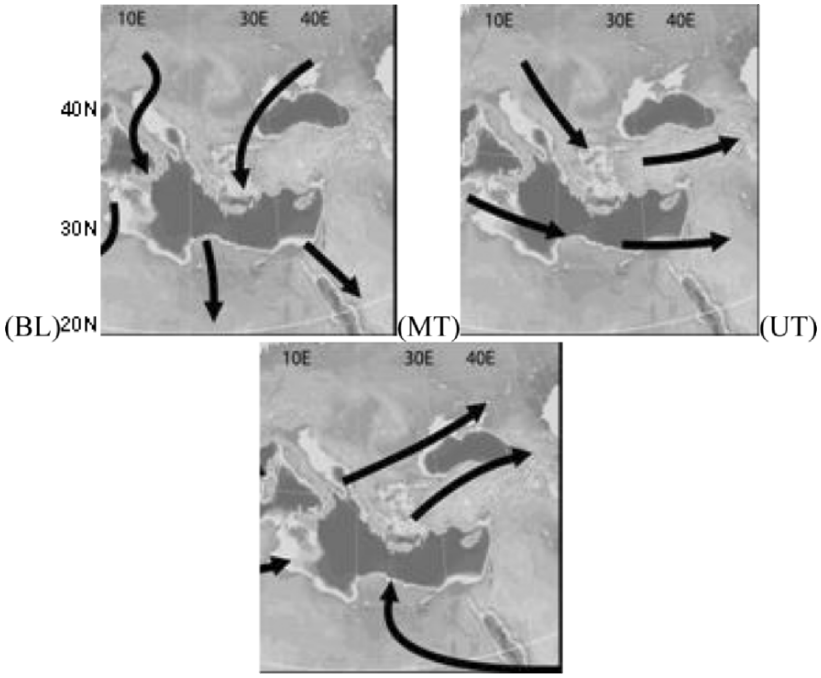

Figure 1. Major air mass flow pathways over the East Mediterranean during summer, in the boundary layer (BL), the middle troposphere (MT) and the upper troposphere (UT) – figure adopted from Lelieveld et al. (2002)

At higher altitudes, above 4 km, strong contributions from long-distance pollution transport from North America and Asia were detected during the MINOS campaign, for example, for carbon monoxide (CO) (Lawrence et al., 2002). It is quite remarkable that in summer 2001 about half of the mid-tropospheric CO over the Mediterranean originates from Asia and 25-30% from North America. These transports follow the prevailing westerly winds that are typical for the extra-tropics. Mid-troposphere is moreover substantially affected by ozone that is mixed down from the stratosphere (Roelofs et al., 2003). In addition, transport of anthropogenic O_3 and its precursor gases from the USA exerts a significant influence in the free troposphere.

In the upper troposphere, above 8 km altitude, another distinct layer was distinguished, especially over the eastern Mediterranean, associated with high levels of reactive species such as formaldehyde (Lelieveld et al., 2002). This was caused by anthropogenic emissions transported from South Asia, following convective lifting into the upper troposphere by thunderstorms in the Indian monsoon (Traub et al., 2003). Subsequently these air parcels followed the easterly tropical jet and turned north over the eastern Mediterranean in a large upper level anticyclone. The chemical "fingerprint" of biomass burning, in particular by biofuel use in India as also observed

during the Indian Ocean Experiment, was evident by measurements of enhanced levels of enhanced CH_3CN, CH_3Cl and C_2H_2 (Scheeren et al., 2003).

From the upper troposphere over the eastern Mediterranean these species can even penetrate the lowermost stratosphere. Thus especially the middle troposphere in summer is influenced by stratosphere-troposphere exchange, leading to a stratospheric contribution to column O_3 in the troposphere of nearly 30%. It appears that the Mediterranean region seems to be a preferred location for cross-tropopause exchanges, partly related to direct convective penetration of the lower stratosphere over southern Europe (Fischer et al., 2002; Galani et al., 2003).

3. Tropospheric Ozone and Aerosols Over the East Mediterranean

Experimental studies over the East Mediterranean (Zerefos et al., 2002; Kourtidis et al., 2002; Kouvarakis et al., 2002a) have demonstrated that the background conditions in O_3 are high over the area and that Finokalia sampling station on the island of Crete is a site representative of the area for such monitoring. A seven year time series (1997-2004) of surface ozone at Finokalia, Crete, identified transport from the European continent as the main mechanism that controls ozone levels in the Eastern Mediterranean, especially during summer when ozone presents a maximum (July) of 58 ± 10 ppbv (Gerasopoulos et al., 2005). Because the Mediterranean background O_3 levels are so high, it is difficult to control ozone in urban and industrial areas. Radon-222 has been proved a useful tool for the verification of the continental origin of ozone. The role of local photochemistry and pollution becomes important under western flow and stagnant wind conditions.

For the whole 7-year period, a profound ozone decreasing trend was also observed with a decline of 1.6 ± 0.2 ppbv y^{-1} (Figure 2). The sharp decline of ozone during the first 5 years (i.e. 3.4 ± 0.2 ppbv y^{-1} or 5.6% per year for 1998-2002) has been succeeded by an abrupt increase in 2003 (to the 1999 ozone levels), followed by a return to the "regular" ozone declining levels in 2004. Note that summer 2003 was a rather dry and warm summer over Europe with intensive photochemical activity. The rates of O_3 decline were higher for the spring and summer concentrations. In parallel with the ozone decline, a shift of the maximum ozone concentrations from summer to spring, attributed to a continuous decrease of the summer ozone concentrations, was also observed, with the year 2002 presenting a clear spring maximum. These changes in O_3 could be related (i) to the reduction of ozone precursors occurred both in western/central and eastern European countries, (ii) to the severe weather phenomena that influenced mainly central Europe in summer 2002 (rather wet and cold summer, incessant precipitation, devastating floods in Central and East Europe) and (iii) to the induced meteorological

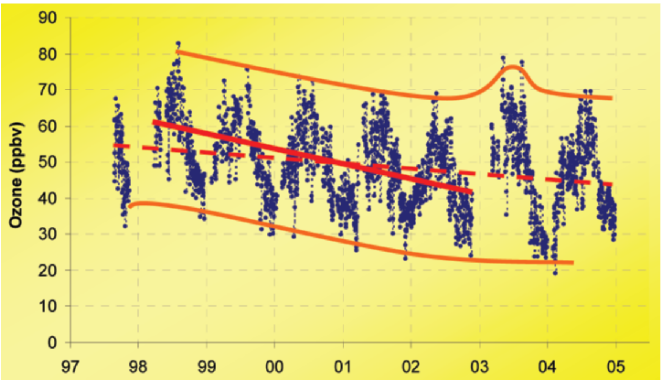

Figure 2. Observed surface O_3 levels from summer 1997 to 2004 at Finokalia monitoring station, Crete, Greece. Dashed red line indicates the trend for the whole period whereas the continuous red line indicates the 1998-2002 trend. Figure adopted from Gerasopoulos et al. (2005)

disturbance in 2002 that caused the prevalence of NW winds instead of the dominant NE flow (Gerasopoulos et al., 2005).

This dataset has been further analyzed in conjunction with simultaneously measured chemical and meteorological parameters (i) to investigate the factors that control the diurnal variability of ozone, and (ii) to evaluate the seasonally distributed ozone production/destruction rates in the area. The diurnal variability of ozone is small (~10%). The observed diurnal evolution of related chemical/physical parameters indicates that ozone morning built-up is driven by photochemistry while during summer the entrainment from the free troposphere is the dominant process in the afternoon. This was further supported by the observed similar behaviour of ozone maxima and Radon-222 minima. Ozone night time depletion has been mainly attributed to deposition and to a lesser extent to chemical reactions. On an annual basis the role of local photochemistry is found to be limited (–1 to 1.7 ppbv d^{-1}) contributing by less than 4% to the observed ozone levels. During summer the enhanced ozone destruction via deposition and chemistry are almost balanced by the chemical production and the entrainment of ozone rich air masses from the free troposphere that maximizes in summer (4-6% of the observed ozone levels). Chemical box model simulations also indicate low net chemical production in the area throughout the year that results from high chemical production and destruction terms. Especially during summer photochemical ozone depletion over the area is revealed both by model results and observations (0.5-1.0 ppbv d^{-1}) (Gerasopoulos et al., 2006a).

Observations over the East Mediterranean also show high concentrations of aerosols that can affect human health. The fine aerosol fraction (<1 μm) is mainly composed of sulfate (35-40%), organics (30-35%), ammonium

(10-15%) and black carbon (5-10%), mostly from fossil fuel and biomass combustion (Lelieveld et al., 2002; Bardouki et al., 2003).

High sulfate loadings in the area are mostly attributed to long range transport of pollution sources as also observed from space (SO_2 observations from space- Figure 3, see also in Eisinger and Burrows, 1998, Zerefos et al., 2000). Indeed, four-year aerosol observations performed by Amiridis et al. (2005) with a Raman lidar at Thessaloniki, Greece, in the framework of European Aerosol Research Lidar Network (EARLINET) indicate higher aerosol optical depth values and extinction to backscatter ratio mostly corresponding to air masses originating from the northeast Balkans and eastern Europe. Only about 20% of the non-sea-salt sulfate in the area is attribu ted to the oxidation of dimethylsulfide of marine origin (Kouvarakis and Mihalopoulos, 2002).

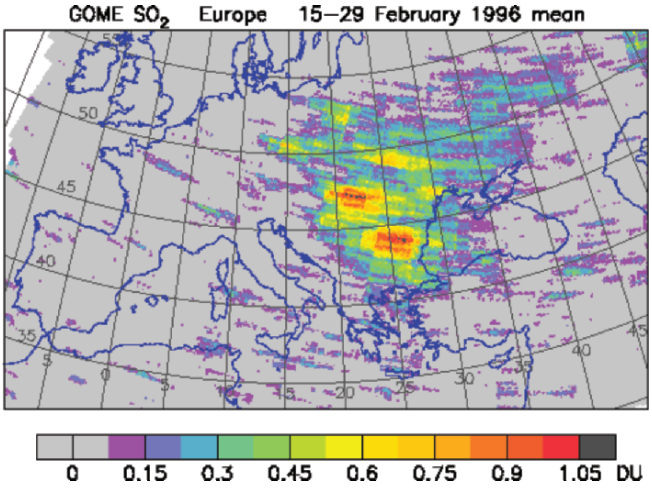

Figure 3. SO_2 column observations by GOME in 1996 (available at http://www.awi-potsdam.de/www-pot/atmo/gome/gome.html)

In addition to the particles of anthropogenic origin, significant amounts of naturally emitted airborn particles are present in the area. Large dust outbreaks from the Northern African continent are affecting the Mediterranean and to a lesser extend Central Europe (Figure 4). Dust reaches Europe either via vertically extended transport (VET) arriving over Crete simultaneously in the lower-free troposphere and inside the boundary layer, or via Free Troposphere Transport (FTT) arriving over Crete initially into the free troposphere with the heavier particles gradually being scavenged inside the boundary layer (Kalivitis et al., 2006). An analysis of southerly air masses arriving over Crete over a five year period (2000-2005), showed that both pathways present significant seasonal variations, but on an annual basis contribute almost equally to the dust transport in the area.

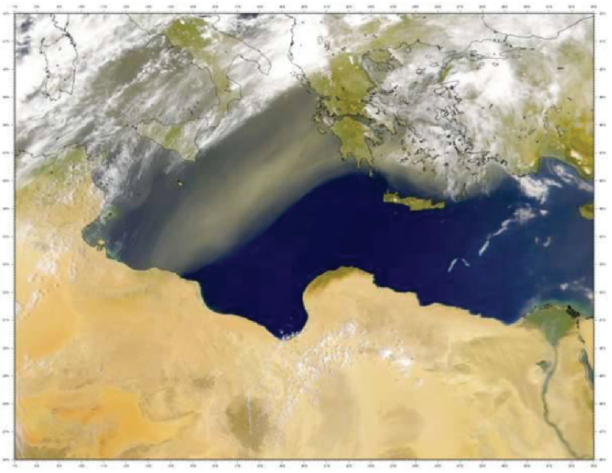

Figure 4. Observation of transport of dust over the east Mediterranean (SEAWIFS – Oct 2002)

Multiyear surface PM_{10} (airborn particles of diameter smaller than 10 um) measurements performed on Crete Island, Greece, have been analysed in conjunction with satellite (Total Ozone Mapping Spectrometer; TOMS) and ground-based remote sensing measurements (Aerosol Robotic Network; AERONET) (Kalivitis et al., 2006). They indicate that the majority of PM10 exceedences in the area seems to be related with mineral dust events that occur episodically over the Eastern Mediterranean. The EU limit of 50 μgm^{-3} is exceeded at Heraklion, one in 4 days, during winter and spring (50% due to transported dust) and half of the days during summer and fall (pollution). At Finokalia exceedences are observed in winter and spring during one in 5 days, 80-100% of which are associated with dust events. A significant covariance between PM_{10} and AOT was observed during VET indicating that aerosol optical thickness (AOT) levels from AERONET may be estimated by PM_{10} levels at the surface. During VET the Aerosol Index (AI) derived from TOMS (indicative of absorbing aerosol particles (airborne microscopic dust/smoke) was significantly correlated with surface PM_{10}, and in general AI was found to be adequate for the characterization of dust loadings over the Eastern Mediterranean on a climatological basis. The AI derived from TOMS was found to be adequate for the characterization of dust loading over the Eastern Mediterranean despite the fact that 20-30% of the dust related spikes in the PM_{10} time series that do not correspond to AI spikes. AI peaks are more frequent in spring indicating that the presence of dust can be detected to a certain extent by TOMS.

Simultaneous measurements of AOT at two distinct wavelengths, for instance 870 nm and 440 nm, can be used to distinguish the coarse (mainly

natural) form the fine (mainly anthropogenic) particles contribution. AOT in the near-infrared (870 nm), is more sensitive to coarse particles, and can be used to represent the seasonality of dust and sea-salt aerosols, while AOT in the near-ultraviolet (440 nm) shows the influence of anthropogenic sources. AOT at 870 nm maximizes primarily in spring and to a lesser extend in fall, whereas an extreme dust event has been observed on 27th of January 2005. AOT (at 440 nm) additionally exhibits a plateau in summer, probably related to the accumulation of fine anthropogenic particles due to the meteorological conditions. The difference in the covariance of the AOT at these two wavelengths attributed to either local or transported pollution, maximizes in summer Figure 5. These areas are confined to summer when pollution is shown to contribute significantly to the PM_{10} levels over the area (Gerasopoulos et al., 2006b). However, it remains an open question the involvement of volatile organic compounds in the formation of secondary organic particulate matter over the area.

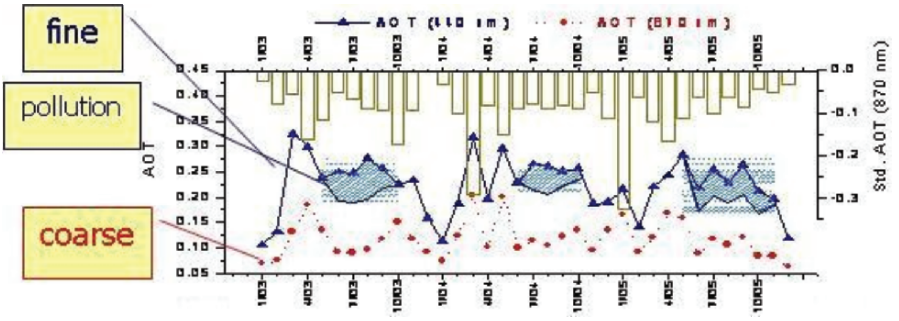

Figure 5. Monthly means of AOT at 440 and 870 nm over Crete during the period 2003-2005. Vertical bars are the standard deviation of the monthly means. The shaded areas indicate pollution aerosols (adopted from Kalivitis et al., 2006 where more explanations are provided)

4. Interactions Between Transported Pollution and Natural Emissions

A significant part of aerosols in the area is chemically formed in the atmosphere. In particular the Mediterranean atmosphere is a photochemical reactor with high levels of oxidants and particularly hydroxyl radicals that have been measured to reach mid-day maxima of approximately 2×10^7 molecules cm^{-3} (Berresheim et al., 2003). These oxidants initiate reactions that form acids including sulphuric and nitric acids. Hydroxyl radicals are efficient cleaning agents of the atmosphere and major removal pathway for persistent organics from the troposphere (Mandalakis et al., 2003; Mandalakis and Stephanou, 2002).

Nitrate radical (NO_3) measurements performed on the island of Crete for more than two years analysed together with ancillary measurements of chemical compounds and meteorological parameters show that night-time production of nitric acid (HNO_3) plus nitrate ions (NO_3^-), as initiated by NO_3 radicals, accounts for about 50-65% of the total production rate depending on season. The remainder is produced by the hydroxyl radical (OH) reaction with nitrogen dioxide during daytime. On a yearly mean basis, about 17% of the HNO_3 plus NO_3^- formation results from the reaction of NO_3 radicals with dimethylsulfide of marine origin (Figure 6). This shows important interactions between biogenic (volatile organics) and anthropogenic (nitrogen oxides and NO_3 radicals) compounds contributing to nutrient deposition to the sea (Vrekoussis et al., 2006, 2007).

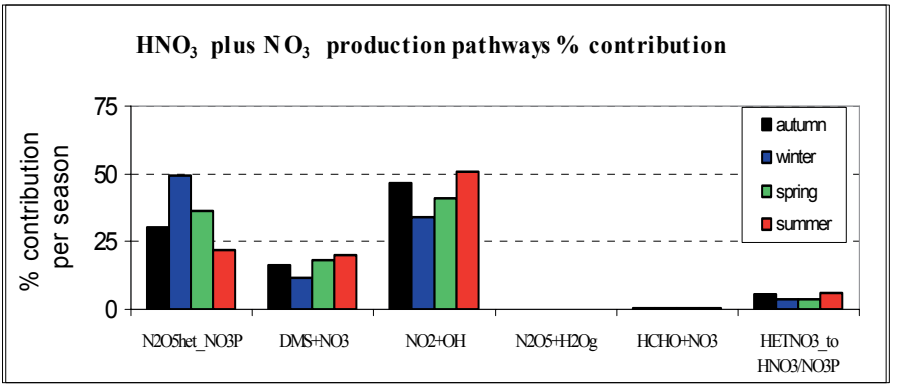

Figure 6. Percent contribution of the different pathways to the production of the sum of HNO_3 and NO_3^- (diel mean results). N2O5het_NO3p refers to the heterogeneous reaction of N_2O_5 on particles; HETNO3 refers to heterogeneous reactions of NO_3 on aerosols

5. Impacts

Near the surface the air pollution has several undesirable consequences. First, the European Union eight-hourly air quality standard for ozone (53 nmol/mol) is exceeded throughout the summer in the entire Mediterranean region. High ozone concentrations are harmful for human health and ecosystems, and they also cause agricultural crop loss.

The aerosols affect human health, visibility and furthermore influence the Mediterranean atmospheric energy budget by scattering and absorbing solar radiation (Figure 7). They reduce solar radiation absorption by the sea by about 10% and they alter the heating profile of the lower troposphere (Lelieveld et al., 2002; Markowicz et al., 2002; Vrekoussis et al., 2005). As a consequence, evaporation and moisture transport, in particular to North

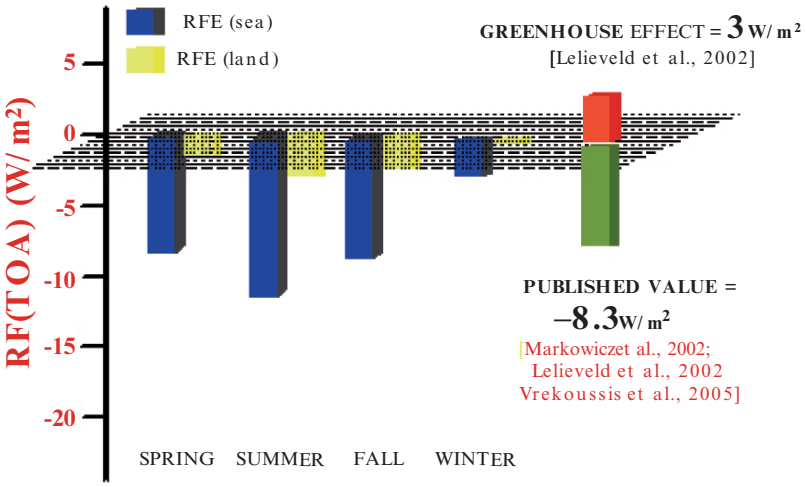

Figure 7. Radiative forcing at the Top Of the Atmosphere (RF(TOA)) induced by aerosols over sea (blue) and over land (yellow) during the 4 seasons as derived from aerosol observations and annual mean value (green) and comparison with the heating effect from the Greenhouse gases (red); figure adopted from Vrekoussis et al. (2005)

Africa and the Middle East, are suppressed. Furthermore, Rosenfeld (2000) studied satellite observations, indicating important perturbations of the cloud microstructure and convection by aerosols, probably decreasing precipitation.

The radiative forcing by aerosols (Figure 7) also influences the energy budget of the Mediterranean Sea, of which the consequences are yet poorly understood. Changing energy budget and anomalous winds are expected to influence the ocean circulation (Tragou and Lascaratos, 2003).

Therefore, aerosols may affect several components of the East Mediterranean atmosphere-ocean system including the regional water cycle. These effects by aerosols are substantial today, even though sulfate from Europe has actually decreased in the past two decades through the abatement of acidification.

Finally, during summer the persistent northerly winds carry large pollution loads from Europe that can deposit onto the Mediterranean Sea, for instance nitrate and phosphorus containing aerosols, which affect the water quality and could contribute to eutrophication (Kouvarakis et al., 2001).

6. Highlights–Conclusion Remarks

- Both observations and chemistry/transport models suggest that the troposphere of the Eastern Mediterranean is strongly polluted. Long range transport of European emissions is playing a key role in the built up of

oxidants and secondary aerosols that is also enhanced by the favourable weather conditions.

- Ozone and aerosol air quality limits are often exceeded over the entire Mediterranean in particular during summer. The contribution of natural emissions to these exceedences remains to be determined.
- Middle tropospheric CO can be strongly affected by Asian and N-American pollution under favorable air circulation patterns like those observed during summer 2001.
- Ozone increase is warming the atmosphere whereas aerosols cause strong surface radiative forcing and perturbation of the water cycle in the area.
- It remains an open question how is the climate changing due to the anthropogenic forcings to the East Mediterranean environment.

7. Acknowledgments

I wish like to thank Prof. Dr. J. Lelieveld as well as all the participants of the MINOS campaign for communicating their results, my co-workers Drs. H. Bardouki, G. Kouvarakis, E. Gerasopoulos, M. Vrekoussis, and Msc N. Kalivitis, S. Pilitsidis and P. Babasakalis for the excellent collaboration and Prof. Dr. Maria Kanakidou for helpful discussions.

8. References

Aleksandropoulou, V., and Lazaridis, M. (2004) Spatial Distribution of Gaseous And Particulate Matter Emissions in Greece*, Water, Air, and Soil Pollution*, Nov 02, 2004, **153**, 15-34, 10.1023/B:WATE.0000019923. 58620.58.

Amiridis, V., Balis, D. S., Kazadzis, S., Bais, A., Giannakaki, E., Papayannis, A., and Zerefos, C. (2005) Four-year aerosol observations with a Raman lidar at Thessaloniki, Greece, in the framework of European Aerosol Research Lidar Network (EARLINET), *J. Geophys. Res*., **110**, D21203, doi:10.1029/2005JD006190.

Balis, D., Papayannis, A., Galani, E., Marenco, F., Santacesaria, V., Hamonou, E., Chazette, P., Ziomas, I., and Zerefos, C. (2000) Tropospheric LIDAR aerosol measurements and sun photometric observations at Thessaloniki, Greece, *Atmos. Environment* **34**, 925-932.

Balis, D., Amiridis, V., Kazadzis, S., Papayannis, A., Tsaknakis, G., Tzortzakis, S., Kalivitis, N., Vrekoussis, M., Kanakidou, M., Mihalopoulos, N., Chourdakis, G., Pérez, C., Baldasano, J., and Drakakis, M. (2006) Optical characteristics of desert dust over the East Mediterranean during summer: a case study, *Annales Geophysicae*, **24**, 807-821.

Bardouki, H., Liakakou, H., Economou, C., Smolik, J., Zdimal, V., Eleftheriadis, K., Lazaridis, M., and Mihalopoulos, N., (2003) Chemical composition of size resolved atmospheric aerosols in the Eastern Mediterranean during summer and winter. *Atmospheric Environment* **37**, 195-208.

Berresheim, H., Plass-Dulmer, C., Elste, T., Mihalopoulos, N., and Rohrer, F. (2003) OH in the coastal boundary layer of Crete during MINOS: Measurements and relationship with ozone photolysis, *Atmos. Chem. Phys*., **3**, 639-649.

Eisinger M., and Burrows, J. P. (1998) *Tropospheric Sulfur Dioxide observed by the ERS-2 GOME Instrument*, Geophys. Res. Letters, **25** (22), 4177-4180.

Fischer, H., de Reus, M., Traub, M., Williams, J., Lelieveld, J., de Gouw, J., Warneke, C., Schlager, H., Minikin, A., Scheele, R., and Siegmund, P. (2002) Deep convective injection of boundary layer air into the lowermost stratosphere at midlatitudes, *Atmos. Chem. Phys*., **3**, 739-745.

Galani, E., Balis, D., Zanis, P., Zerefos, C., Papayannis, A., Wernli, H., and Gerasopoulos, E. (2003) Observations of stratosphere-to-troposphere transport events over the eastern Mediterranean using a ground-based lidar system, **108** (D12), 8527, doi:10.1029/ 2002JD002596.

Gerasopoulos, E., Kouvarakis, G., Vrekoussis, M., Kanakidou, M., and Mihalopoulos, N. (2005) Ozone variability in the marine boundary layer of the Eastern Mediterranean based on 7-year observations. J. Geophys. Res. **110**, doi:10.1029/2005JD005991.

Gerasopoulos, E., Kouvarakis, G., Vrekoussis, M., Donoussis, Ch., Mihalopoulos, N., and Kanakidou, M. (2006a) Photochemical ozone production in the Eastern Mediterranean, *Atmos. Environ*., **40**, 3057-3069.

Gerasopoulos, E., Kouvarakis, G., Babasakalis, P., Vrekoussis, M., Putaud, J.-P., and Mihalopoulos, N. (2006b) Origin and variability of particulate matter (PM10) mass concentrations over the Eastern Mediterranean, *Atmos. Environ*., **40**(25), 4679-4690.

Gros, V., Williams, J., van Aardenne, J.A., Salisbury, G., Hofmann, R., Lawrence, M., Von Kuhlmann, R., Lelieveld, J., Krol, M., Berresheim, H., Lobert J.M., and Atlas, E. (2003) Origin of anthropogenic hydrocarbons and halocarbons measured in the summertime European outflow (on Crete in 2001), *Atmos. Chem. Phys*., **3**, 1223–1235.

Holzinger, R., Klópfel, T., Salisbury, G., Williams, J., De Reus, M., Traub, M., Crutzen, P.J., and Lelieveld, J. (2003) Acetonitrile over the eastern Mediterranean and its use for assessing biomass burning contribution to the tropospheric burdens of CO, acetone, methanol and PAN, *Atmos. Chem. Phys*., **3**, 1589-1608.

Kalivitis, N., Gerasopoulos, E., Vrekoussis, M., Kouvarakis, G., Kubilay, N., Hatzianastassiou, N., Vardavas, I., and Mihalopoulos, N. (2006) Dust transport over the Eastern Mediterranean from TOMS, AERONET and surface measurements, *J. Geophys. Res*., in press.

Kallos, G., Kotroni, V., Lagouvardos, K., and Papadopoulos, A. (1998) On the long-range transport of air pollutants from Europe to Africa. *Geophys. Res. Lett*. **25**, 619-622.

Kourtidis, K., et al. (2002) Regional levels of ozone in the troposphere over eastern Mediterranean, *J. Geophys. Res*., **107**(D18), 8140, doi:10.1029/ 2000JD000140.

Kouvarakis, G., and Mihalopoulos, N. (2002) Seasonal variation of dimethylsulfide in the gas phase and of methanesulfonate and non-sea–salt sulfate in the aerosols phase in the Eastern Mediterranean atmosphere. *Atmos. Environ*. **36** (6), 929-938.

Kouvarakis, G., Tsigaridis, K., Kanakidou, M., Mihalopoulos, N. (2000*)* Temporal variations of surface regional background ozone over Crete Island in the southeast Mediterranean. *Journal of Geophysical Research* **105** (D4), 4399-4407.

Kouvarakis, G., Mihalopoulos, N., Tselepides, T., and Stavrakakis, S. (2001) On the importance of atmospheric nitrogen inputs on the productivity of Eastern Mediterranean, *Global Biogeochem*. Cycles, **15**, 805-818.

Kouvarakis, G., Vrekoussis, M., Mihalopoulos, N., Kourtidis, K., Rappenglueck, B., Gerasopoulos, E., and Zerefos, C. (2002) Spatial and temporal variability of tropospheric ozone (O3) in the boundary layer above the Aegean Sea (eastern Mediterranean), *J. Geophys. Res*., **107**, doi: 10.1029/2000JD000081.

Latos, M., Spyridaki, A., Flatoy, F., and Lazaridis, M. (2006) Contribution of forest fire emissions to atmospheric pollution in the eastern Mediterranean area, in the proceeding of the Environmental Conference Protection and Restoration of the Environment, Chania.

Lawrence, M. G., Rasch, P. J. et al. (2002) Global chemical weather forecasts for field campaign planning: predictions and observations of large-scale features during MINOS, CONTRACE, and INDOEX, *Atmos. Chem. Phys*., **3**, 267-289.

Lelieveld, J., Berresheim, H., et al. (2002) Global air pollution crossroads over the Mediterranean. *Science* **298**, 794-799.

Mandalakis, M., Berresheim, H., and Stephanou, E. G. (2003) Direct evidence for destruction of polychlorobiphenyls by OH radicals in the subtropical troposphere, *Environ. Sci. Technol*., **37**, 542–547.

Mandalakis, M., and Stephanou, E. G. (2002), Study of atmospheric PCB concentrations over the eastern Mediterranean Sea, *J. Geophys. Res*., **107**, doi:10.1029/2001JD001566.

Markowicz, K.M., Flatau, P.J., Ramana, M.V., Crutzen, P.J., and Ramanathan, V. (2002) Absorbing Mediterranean aerosols lead to a large reduction in the solar radiation at the surface*, Geophys. Res. Lett*., 29, doi:10.1029/2002GL015767.

Mihalopoulos, N., Stephanou, E., Kanakidou, M., Pilitsidis, S., and Bousquet, P. (1997) Troposheric aerosol ionic composition above the Eastern Mediterranean area. *Tellus* **49B**, 314–326.

Myriokefalitakis, S., Development of chemical code for the study of the global distribution of glyoxal and formaldehyde by using a 3-d global model, Master Thesis, Dept. of Chemistry, University of Crete, Dec. 2006.

Roelofs, G.-J., Scheeren, B., Heland, J., Ziereis, H., and Lelieveld, J. (2003) Distribution and origin of ozone in the eastern Mediterranean free troposphere during MINOS (August 2001), *Atmos. Chem. Phys. Discuss.*, **3**, 1247-1272.

Rosenfeld, D. (2000) Suppression of rain and snow by urban and industrial pollution, *Science*, **287**, 1793-1796.

Scheeren, H. A., Lelieveld, J., Roelofs, G.J., Williams, J. Fischer, H., de Reus, M., de Gouw, J. A., Warneke, C., Holzinger, R., Schlager, H., Klópfel, T., Bolder, M. van der Veen, C., and Lawrence, M. (2003) The impact of monsoon outflow from India and Southeast Asia in the upper troposphere over the eastern Mediterranean*, Atmos. Chem. Phys*., **3**, 1589-1608.

Tragou, E., and Lascaratos, A. (2003) Role of aerosols on the Mediterranean solar radiation, *J. Geophys. Res*., **108**, doi:10.1029/2001JC001258.

Traub, M., Fischer, H., de Reus, M., Kormann, R., Heland, J., Ziereis, H., Schlager, H., Holzinger, R. Williams, J. Warneke, C. de Gouw, J. and Lelieveld, J. (2003) Chemical characteristics assigned to trajectory clusters during the MINOS campaign, *Atmos. Chem. Phys*.,**3**, 459-468.

Vrekoussis, M., Liakakou, E., Kocak, M., Kubilay, N., Oikonomou, K., Sciare, J., Mihalopoulos, N. (2005) Seasonal variability of optical properties of aerosols in the Eastern Mediterranean. *Atmospheric Environment* **39**, 7083-7094.

Vrekoussis M., Liakakou, N., Mihalopoulos, M., Kanakidou, P.J., Ctutzen, J., Lelieveld (2006) Formation of HNO_3 and NO_3^- in the anthropogenically-influenced eastern Mediterranean marine boundary layer, *Geophys. Res. Letter*, **33**, L05811, doi:10.1029/ 2005GL025069.

Vrekoussis M., Mihalopoulos, N. Gerasopoulos, E. Kanakidou, M. Crutzen, P. J. and Lelieveld, J. (2007) Two-years of NO_3 radical observations in the boundary layer over the Eastern Mediterranean, *Atmos. Chem. Phys*., **7**, 315-327, www.atmos-chem-phys.net/ 7/315/2007/

Zerefos, C., Ganev, K., Kourtidis, K., Tzortziou, M., Vasaras, A., Syrakov, E. (2000) On the origin of SO_2 above northern Greece, *Geophys. Res. Lett*., **27**, 365-368.

Zerefos, C. S., et al. (2002) *Photochemical Activity and Solar Ultraviolet Radiation (PAUR)* Modulation Factors: An overview of the project, *J. Geophys. Res*., 107(DX), 10.1029/ 2000JD000134.

AFRICAN DUST: ITS LARGE-SCALE TRANSPORT OVER THE ATLANTIC OCEAN AND ITS IMPACT ON THE MEDITERRANEAN REGION

JOSEPH M. PROSPERO
University of Miami
Rosenstiel School of Marine and Atmospheric Science
Cooperative Institute for Marine and Atmospheric Studies
4600 Rickenbacker Causeway
Miami, FL 33149-1098
Tel: 305-421-4159
Fax: 305-421-4221
Email: jprospero@rsmas.miami.edu

Key Words: Atmospheric transport; atmospheric deposition; mineral dust; trace metals; chemical; transport models; trace elements; ocean fertilization; nitrogen species; aerosols; particulate matter;Mediterranean; North Atlantic Ocean.

Abstract Mineral dust is a major aerosol component over many regions of the world, especially arid areas. In satellite images dust is the most persistently visible aerosol component over the oceans. There is increased interest in dust because of its impact on climate and also because iron associated with dust is an essential micronutrient that can serve to enhance ocean primary productivity and, thus, impact the global carbon cycle. Africa is the world's largest dust source. Great quantities of African dust are transported over large areas of the North Atlantic and the Mediterranean. In this report I review recent research on African dust transport and discuss some of the possible impacts that dust might have. A major concern is the future trend in African dust transport under climate change conditions. It is very difficult to predict future trends because of our lack of understanding of the factors that affect the activity of dust sources. North Africa can serve as the ideal laboratory in which to study these important processes.

1. Introduction

Aerosols play an important role in climate. They can modify the Earth's radiative properties directly by scattering and absorbing radiation and indirectly

A. Mellouki and A.R. Ravishankara (eds.), Regional Climate Variability and its Impacts in the Mediterranean Area, 15–38.

by affecting the microphysical properties of clouds. Until recently research efforts have tended to focus on pollution aerosols such as sulfate particles. However, it is now recognized that mineral dust is an important aerosol component over large areas of the world. Indeed dust plumes are the most prominent, persistent, and widespread aerosol features visible in satellite images over the continents and the oceans. Dust also plays a role in ocean biogeochemistry. In many remote ocean regions, iron associated with dust particles is the only source of this element which is an important, and often limiting, micronutrient. Thus, to the extent that dust-Fe impacts on ocean primary productivity, dust could play a major role in the global carbon cycle (Jickells et al., 2005; Mahowald et al., 2005; Parekh et al., 2005) which, in turn, plays a role in climate. For this reason there is great interest in dust transport and its deposition to the oceans (Duce et al., 1991; Prospero, 1996).

Here I present an overview of the temporal and spatial distribution of dust over the global ocean. I place special emphasis on North African dust processes because this region is without a doubt the strongest source in the world. Great quantities of African dust are carried great distances because of the huge expanse of arid lands and because of the meteorological setting which acts as a uniquely-efficient mechanism for pumping dust into the large-scale wind systems. Winds routinely carry dust across the Atlantic to the Caribbean and to the southern and eastern United States. African dust is frequently carried across the Mediterranean to southern Europe, and into the Middle East. The deposition of this dust to the ocean and in particular to the Mediterranean can have a large impact on biogeochemical processes in these waters.

Our studies show large changes in dust concentration on daily, seasonal and interannual time scales. In some cases these changes can be linked to weather and climate variability. This variability demonstrates the extraordinary sensitivity of dust mobilization to changes in regional climate and also to human impacts. Of particular note is the great increase in dust transport out of North Africa in the past several decades because of the widespread and prolonged drought conditions. In my presentation I will identify some of the more critical processes that we must understand in order to improve our ability to model dust-weather-climate interactions.

2. Global Dust Transport and Dust Sources

There are many satellites that provide us with data on the distribution of aerosols over the ocean (Kaufman et al., 2002, 2005). An example is AVHRR

(Advanced Very High Resolution Radiometer) which measures the radiation backscattered to space by aerosols over the oceans; these data are converted to aerosol optical thickness (AOT) which is a measure of the column-integrated aerosol loading (Husar et al., 1997). Figure 1 shows the global average distribution of oceanic AOT in the four seasons. Clear temporal and spatial patterns are evident. First, the highest values of AOT (and, hence, the greatest column concentrations of aerosols) are found in regions close to the continents. This distribution affirms the fact that in most ocean regions the aerosol character is defined to a large extent by the transport of materials by winds from the continents. Second, there are large seasonal differences in aerosol concentrations - compare, for example, the December-January distributions with June-August in Figure 1. These differences are due to a variety of factors including the seasonal variability of source emissions and meteorology. Third, some continents emit more aerosols than others which suggests large differences in source and transport conditions.

A notable feature in the AVHRR product and other aerosol satellite products is the dominance of mineral dust. Mineral dust plumes are the most prominent aerosol feature in satellite images. Dust plumes yield the highest values of AOT over the largest ocean areas. Especially notable is that large plume of dust that extends over the tropical Atlantic from the coast of Africa to South America (in boreal winter) and to the Caribbean (in summer). The large region of high AOT over the Arabian Sea in summer is due to dust carried from Africa and the Middle East. During spring (Figure 1b) winds carry large quantities of dust out of Asia and over large areas of the North Pacific (Prospero et al., 1989) in some cases penetrating deep into North America (Husar et al., 2001; VanCuren, 2003).

Pollution aerosols are also prominent in satellite imagery - for example over the North Atlantic in summer due to transport from sources in North America and Europe and along the coast of Asia during most seasons. Also, plumes from biomass burning are visible - e.g., along the west coast of southern Africa during most seasons. But, in general, dust is the most prominent and persistent feature on a global scale.

Because aerosol transport varies so greatly from season-to-season we would expect that any impacts that aerosol transport might have on ocean processes should also show a large seasonal and spatial variability. Especially notable is the large seasonal migration of the African dust plume. The seasonal oscillation is consistent with the very large seasonal cycle of dust concentrations measured in South Florida, and Barbados, West Indies (Husar et al., 1997; Prospero, 1999; Prospero and Lamb, 2003). Indeed,

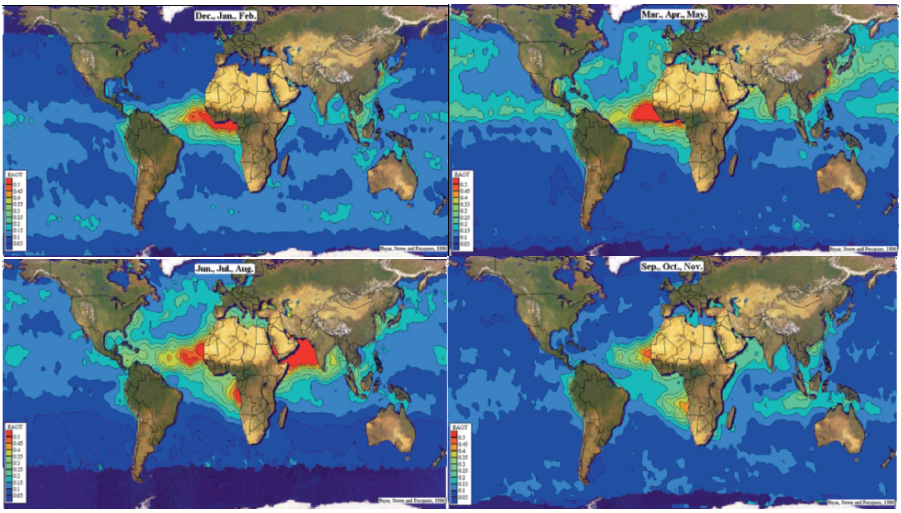

Figure 1. Aerosol distributions over the oceans derived from the National Oceanic and Atmospheric Administration (NOAA) advanced very high resolution radiometer (AVHRR) satellite (Husar et al., 1997). Distributions are shown in units of aerosol optical thickness (AOT) which is derived from measurements of visible-spectrum solar radiation reflected from aerosols back to space. Distributions are shown for each of the four seasons: top left, December-February; bottom left, March-May; top right, June-August; bottom right, September-November. Figure based on that in Husar et al., 1997

during the summer months African dust has been measured over the eastern United States as far north as the New England states (Perry et al., 1997; Kallos et al., 2006).

The TOMS (Total Ozone Mapping Spectrometer) provides information on the distribution of absorbing aerosols - predominantly mineral dust and smoke (Herman et al., 1997). The TOMS product is especially useful because (in contrast to AVHRR and many other satellites) TOMS can detect aerosols over land as well as over water surfaces. In many cases the distributions over land show a clearly defined geometry that can be matched to topographical features and geology. In Figure 2 (Prospero et al., 2002), TOMS absorbing aerosol data has been filtered to show the frequency of occurrence of intense dust events over the entire Earth. The dust sources in Figure 2 have several common characteristics: they are located in topographical lows or adjacent to highlands; they are located in arid regions; and they were flooded during the Pleistocene or Holocene (Prospero et al., 2002). Thus these

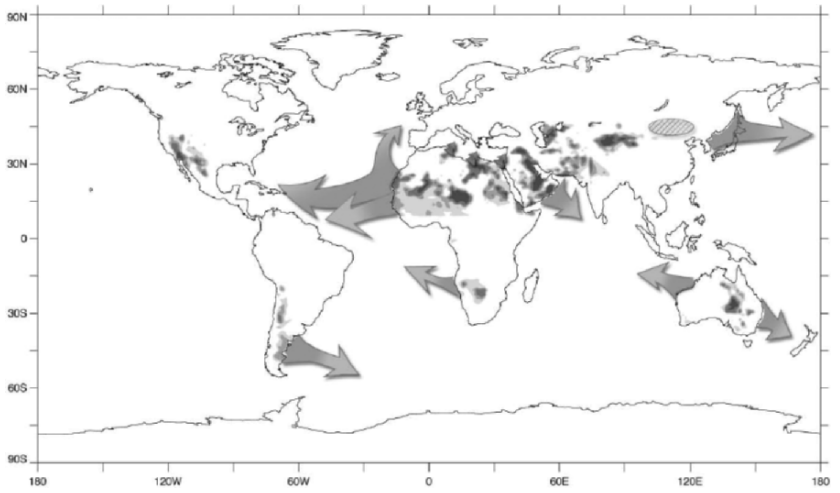

Figure 2. The global distribution of major dust sources and dust transport paths based on the Total Ozone Mapping Satellite (TOMS) aerosol product (Prospero et al., 2002). The darker gray tones show those regions were substantial concentrations of dust are lifted into the air more than 50% of the time during the dusty seasons of the year. The arrows show the main transport paths over the oceans. The arrow size is not indicative of the magnitude of the transport nor the distance that dust is carried. The hatched area in northeastern China identifies an intense dust source region that is not clearly identified in TOMS

terrains contain large deposits of fine-grained alluvial soils which can be readily mobilized by winds during arid phases (Engelstaedter et al., 2006).

It is clear, based on Figures 1 and 2, that the most active dust source regions lie in the Northern Hemisphere. Most notable is the broad band of active dust sources that extends from the west coast of North Africa, through the Middle East, and across Asia to the Pacific coast. Of these, North Africa is by far the most intense. In contrast there are only a few scattered sources in the southern hemisphere and these are rather weak producers of dust.

The emission of pollutants is also much greater in the Northern Hemisphere relative to the Southern. The combined effects of pollution and mineral dust has important implications both from the standpoint of climate issues and also the impact of aerosol transport on ocean biogeochemical processes.

3. The Annual Cycle of African Dust Transport Over the North Atlantic

Many dust studies have focused on the North Atlantic because of the heavy transport of African dust to the region. The University of Miami aerosol group has carried out extensive studies in the region with some measurements beginning in the mid-1960s. In the 1980s, an extensive aerosol network was established in the Atlantic (Figure 3).

The transport of dust across the region varies greatly on time scales ranging from days to decades. The short term variability is displayed in Figure 4 which shows daily dust concentrations measured at two sites during the summer of 1998: Izaña Observatory on Tenerife, Canary Islands; and at Barbados, West Indies. The sharp dust spikes are attributed to the passage of large dust outbreaks over the region. Dust outbreaks are associated with disturbances that cross the coast of Africa during the summer. The main transport occurs at higher altitudes in a layer (the Saharan air layer - SAL) that typically reaches to several kilometers and often to 5-6 km (Karyampudi et al., 1999). Concentrations aloft are usually several times greater than in the marine boundary layer (Reid et al., 2003). Because of the unusually

Figure 3. The University of Miami North Atlantic aerosol sampling network. African aerosol studies began on Barbados in 1965 and in Miami in 1974. The network expanded to other islands in the 1980s as a part of the Atmosphere-Ocean Chemistry Experiment (AEROCE)

high temperature and low relative humidity of the SAL, it can be identified in routine meteorological soundings as far west as the Caribbean (Reid et al., 2003) and over the Amazon basin in eastern Brazil (Swap et al., 1992).

It requires about 5-7 days for a dust outbreak to transit the Atlantic from the coast of Africa to the eastern Caribbean. The transit time can be computed from the data in Figure 4. A very large dust peak was observed at Izaña, Tenerife, on 22 June 1998, one of the largest measured during a 12 years of operations. The dust cloud reached Barbados on 28 June, 6 days later. Many coincident peaks are seen in Figure 4, but this is due to the fact that the transit time across the Atlantic is about the same as the time interval between dust outbreaks along the coast of Africa, typically about 5 days. Satellite imagery can also be used to track dust outbreaks across the Atlantic. Figure 5 shows a TOMS image obtained during the great dust storm in June 1998. The image on 23 June shows a plume of dust (coded in red, yellow, and green colors) extending across the central Atlantic to the Caribbean and

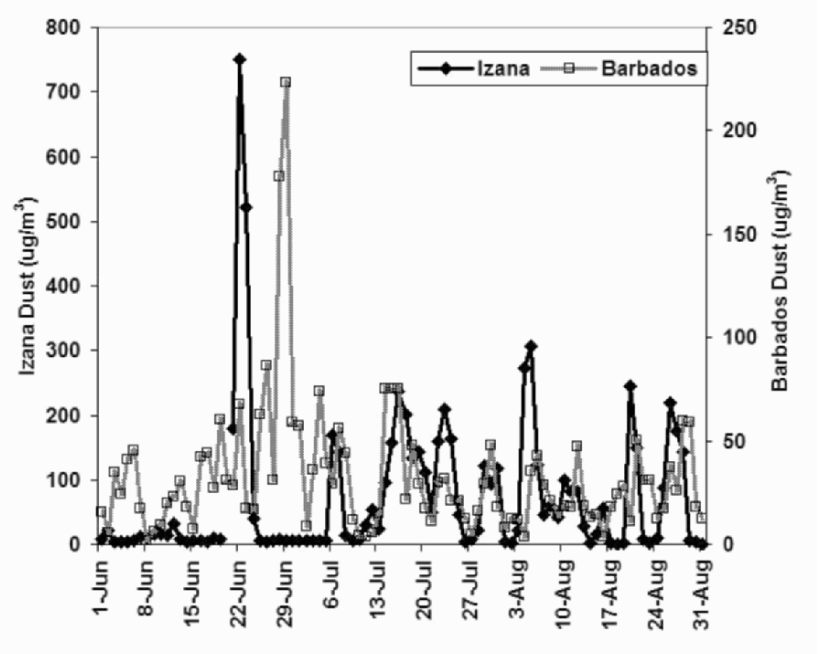

Figure 4. The transit of a dust outbreak across the tropical North Atlantic. The dust measurements carried out at Izaña Observatory, Tenerife, shows the beginning of a massive dust outbreak on 20 June 1998 and which reached a maximum on 22-23 June, yielding a dust concentration of 750 μg m^{-3}, one of the highest ever observed at this site. The dust cloud reached Barbados on 28 June (178 μg m^{-3}) and continued through 29-30 June (224 μg m^{-3}). The elapsed time to transit the tropical Atlantic, 5-6 days, is typical for such dust events

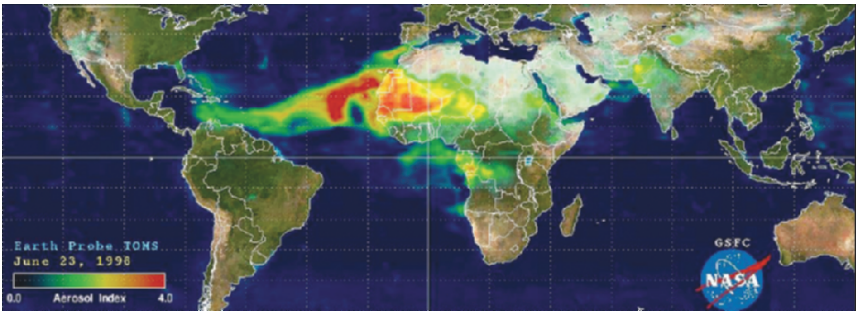

Figure 5. The great dust storm of June 1998 as recorded in the TOMS Absorbing aerosol product. The TOMS image on 23 June shows high concentrations of dust (red) extending to the central Atlantic which is attributed to the large dust outbreak associated with the peak at Izaña shown in Figure 4. (TOMS data obtained at http://jwocky.gsfc.nasa.gov/aerosols/aerosols.html)

over the Bahamas east of Florida. The region of heavy dust (shown in red) is attributed to the large dust outbreak that passed Tenerife on 22 June as seen in Figure 4. The TOMS image also shows continued and intense dust activity (in red coding) over West Africa.

The monthly mean dust concentrations measured in the North Atlantic network depicted in Figure 3 is shown in Figure 6. A number of features stand out. First of all, the highest dust concentrations are in the eastern tropical Atlantic (Sal Island and Izaña). The annual mean concentration at Sal Island (46 μg m^{-3}) is 60 times greater than that over the eastern North Atlantic as measured at Mace Head, Ireland. Second, there is a pronounced seasonal cycle in dust transport to the western Atlantic as seen in the seasonal distributions measured at Cayenne, Barbados, Miami, and Bermuda. This annual cycle matches that observed in AVHRR AOT, as shown in Figure 1. In late winter and in spring, African dust is carried to South America (Prospero et al., 1981) where African dust plays an important role in the nutrient balance in the soils of the Amazon Basin (Swap et al., 1992). Barbados experiences the longest annual cycle; substantial amounts of dust are present in most months of the year, with greatest concentrations in the summer and the least in winter (Prospero and Lamb, 2003). Miami (Prospero, 1999) and Bermuda (Arimoto et al., 2003; Savoie et al., 2002) are impacted by African dust every year in the summer. Indeed the entire central and eastern United States experiences African dust during the summer months, etc. (Perry et al., 1997).

The large scale synoptic character of African dust transport is clearly evident in Figure 7 which shows the monthly mean dust concentrations measured at Barbados, Miami, and Bermuda over the period 1989 to 1998.

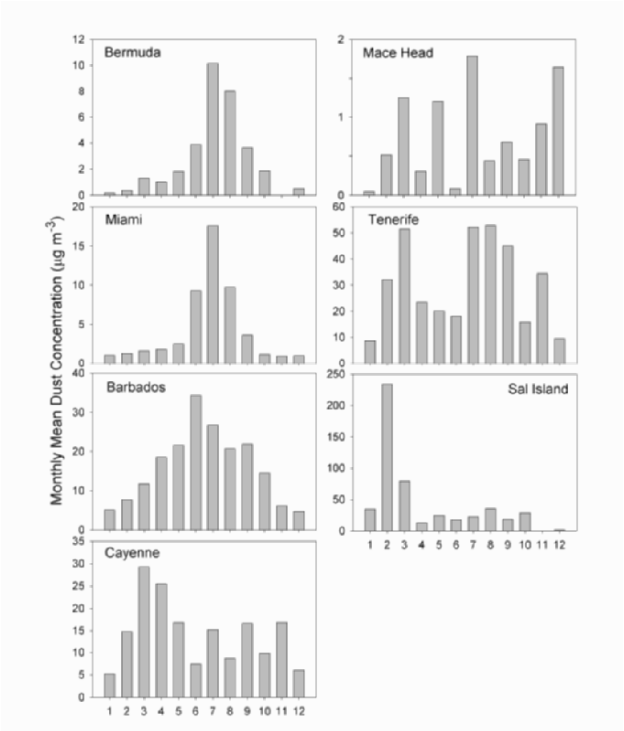

Figure 6. Monthly mean mineral dust concentrations measured at seven locations in the North Atlantic: Bermuda; Mace Head, Ireland; Miami, Florida; Izaña Observatory, Tenerife, Canary Islands; Barbados, West Indies; Sal Island, Cape Verde Islands; Cayenne, French Guiana. The figures are stacked according to latitude with the more northerly stations at the top; the stations in the eastern Atlantic are placed on the right and the western on the left. The ordinate is dust concentration: units, µg m^{-3}. Note the difference in the ordinate scales for each station. These data are based on daily measurements made over differing time periods; in all cases, at least one year of data are shown

At all sites, the maximum dust concentrations are observed in the summer months. The major differences among the sites are that dust concentrations are usually substantially greater at Barbados than those at Miami and Bermuda and the dust season is much longer. The effects of changes in transport meteorology are also evident in Figure 7. In some years, the relatively narrow dust peaks at Miami and Barbados are centered on the broad peak at Barbados (e.g., 1997) while in other years they are more asymmetrically located (e.g., 1998). These apparent differences are due more to changes in the timing and duration of the Barbados dust transport season than to changes in the higher latitudes where the dust peak is relatively stably

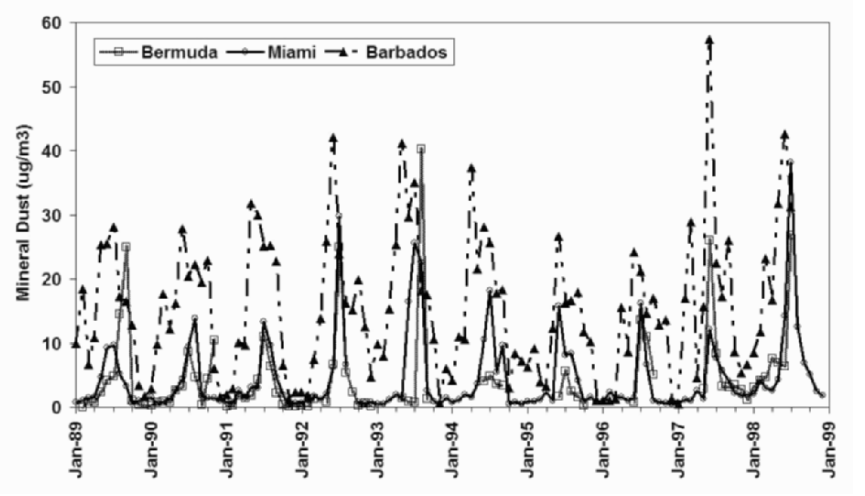

Figure 7. Large-scale temporal coherence of dust transport across the North Atlantic as reflected in the monthly mean mineral dust concentrations measured at Barbados, Miami, and Bermuda, 1989 to 1998

centered on June-July. Another major difference between these dust records is that at Barbados in some years there is a substantial transport of dust during the winter months while none is ever seen at the more northerly sites.

Over the eastern Atlantic, the synoptics of dust transport are more complicated. This is reflected in the distinct difference between the annual cycle at Sal Island compared to that at Izaña (Figure 6). This difference is linked to two factors: the meteorology of individual dust outbreaks (Karyampudi et al., 1999) and how it changes with season; the altitude of the sampling sites - Sal Island is located in the marine boundary layer and Izaña at an altitude of 2360 m which place it in the free troposphere at night. During the winter months along the coast of Africa dust transport takes place largely at lower altitudes. It is at this time of year that one sees dramatic satellite imagery of dust storms sweeping out of the coastal areas of Morocco and Mauritania and enveloping the Canary Islands and the Cape Verde Islands. Often the higher elevations on the islands can be clearly seen rising above the dense dust layer that obscures the lower elevations; also clear-air "wakes" can be seen downwind of the islands. In contrast during the summer months, as stated above, dust transport takes place in a very deep elevated layer, often extending to 5-6 km. Consequently at Sal Island the major dust peak occurs early in the year while in the summer months the major transport takes place above the island although there are very substantial concentrations during the summer as well, a fact not readily seen in Figure 6

because of the scale. On the other hand at Izaña the annual dust cycle is bimodal with a peak early in the year, reflecting the winter transport, and a peak during the summer season when dense dust hazes envelope the site and extend far above it.

4. Long-term Trends in African Dust Transport and the Link to Climate

Aerosol measurements began on Barbados in 1965 and continue to the present (Prospero and Lamb, 2003), making it the longest continuous aerosol data set available. The monthly mean dust concentrations for the period 1965 to 2004 are shown in Figure 8. The previously noted annual cycle stands out clearly across the entire record with summer maxima and winter minima. But there are large year-to-year changes. It is particularly notable that dust concentrations were much lower early in the record. They increased shar ply in the early 1970s and they have remained high, albeit with large fluctuations. Particularly large dust peaks are noted in some years. These appear to be linked to El Niño events as indicated by arrows in the figure (Prospero and Lamb, 2003). The major peaks generally appear to lag the onset of El Niño by one year.

The monthly mean minimum concentrations occur during the boreal winter months. It is notable that there has been a great change in winter dust concentrations over the record. In the early years, concentrations were vanishingly

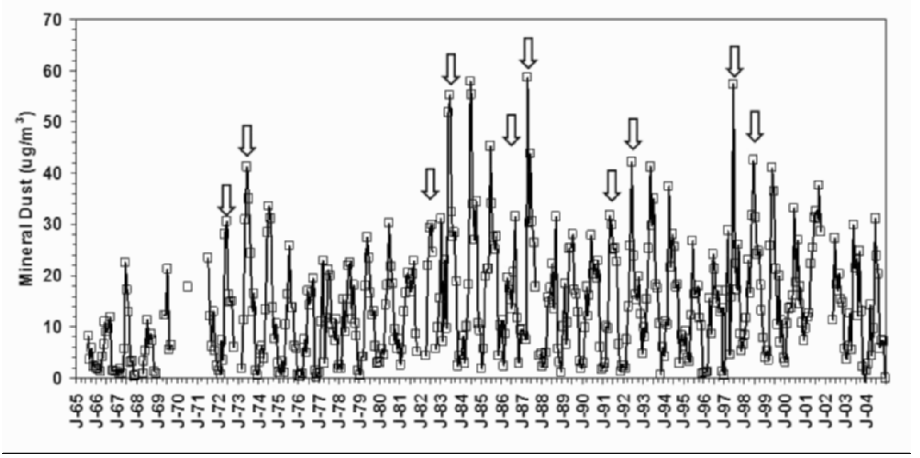

Figure 8. Barbados monthly mean mineral dust concentrations, 1965-2004. The abscissa scale marks January of each year. Arrows mark major El Niño events: 1972-73, 1982-83, 1986-87, 1991-92, 1997-98 [NOAA-CIRES Climate Diagnostics Center Multivariate ENSO Index web site: http://www.cdc.noaa.gov/~kew/MEI/mei.html]

small but beginning in the late 1970s winter concentrations increased markedly. Indeed, during the El Niño winter of 1983-1984 dust concentrations peaked at a higher value than those of the preceding summer! This had never before been seen in our studies and it has not occurred since.

Previous studies suggest that during an El Niño phase there is a decrease in rainfall in the Soudano-Sahel region of Africa, an area that is a major dust source as shown in Figure 2. Indeed, Prospero and Lamb (2003) show that dust concentrations in Barbados were highly correlated with rainfall deficits in this region (Figure 9) with a one year lag. The sharp increase in dust transport in the early 1970s is linked to the onset of prolonged drought in North Africa. The periods of intense transport (e.g., 1972-1973, 1983-1984, etc.) were associated with particularly severe drought phases.

The monthly mean minimum concentrations occur during the boreal winter months. It is notable that there has been a great change in winter dust concentrations over the record. In the early years, concentrations were vanishingly small but beginning in the late 1970s winter concentrations increased markedly. Indeed, during the El Niño winter of 1983-1984 dust concentrations peaked at a higher value than those of the preceding summer! This had never before been seen in our studies and it has not occurred since.

Winter dust activity over North African and its transport over the Atlantic are linked to the strength of the North Atlantic Oscillation - NAO (Figure 10, Ginoux et al., 2004). The NAO index (NAOI) is defined as the difference between the normalized sea-level atmospheric pressures at Lisbon, Portugal, and at Stykkisholmur, Iceland (Hurrell, 1995). Winters with high NAOI are characterized by a deepening of the Icelandic low and a stronger Azores anticyclone. This results in higher surface pressure, stronger winds, and drier conditions over Northern Africa. In contrast during low NAOI conditions, there is an increase of precipitation over the Mediterranean and North Africa. Figure 10 shows the year-to-year variability of the NAO winter index values (http://www.cgd.ucar.edu/~jhurrell/nao.html) and the GOCART model simulated concentrations at Barbados in winter (January–March) (Ginoux et al., 2001). In contrast, the NAOI does not seem to have any significant impact on summer dust transport intensity mainly because the summer pressure difference between Iceland and Portugal is much weaker along with the consequent meteorological effects. It is notable that the dust activity most highly correlated with the NAOI is that over the Bodele depression in Chad (Ginoux et al., 2004). The Bodele is without doubt the most active dust source on Earth (Prospero et al., 2002, Washington et al., 2006). The Bodele stands out in Figure 2 as the large dark spot in central North Africa.

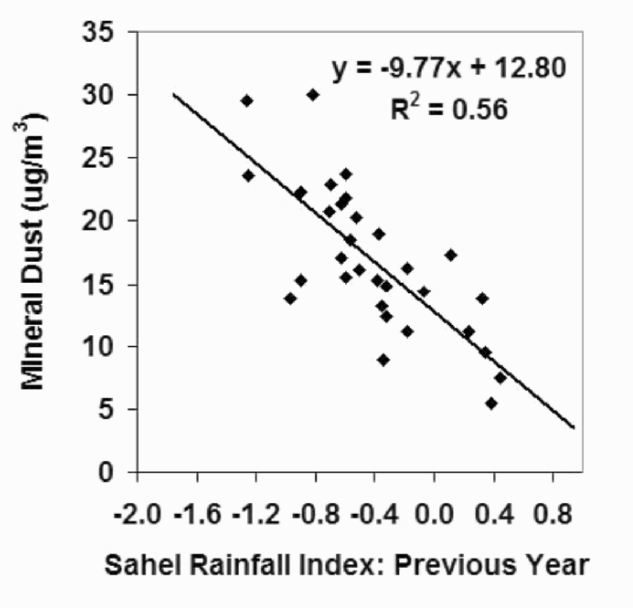

Figure 9. Barbados annual mean dust concentrations plotted against the prior-year Lamb Soudano-Sahel normalized rainfall index (in standard deviations from mean) over the period 1965-1998. The solid line shows the linear regression. For details see Prospero and Lamb, 2003

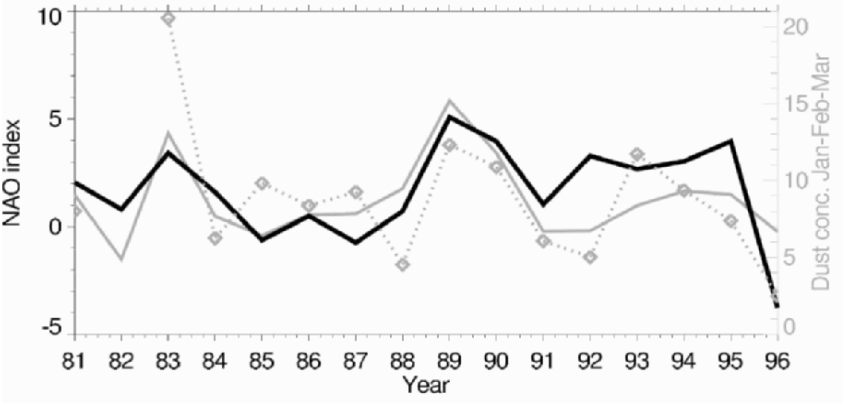

Figure 10. Comparison between NAO index (bold black line), the observed winter dust surface concentration at Barbados (diamonds and gray dashed line), from 1981 to 1996, and the GOCART model-derived dust concentrations (solid gray line) in units of μg m^3. (Ginoux et al., 2004)

In general, the year-to-year variability of dust concentrations in winter seems to be correlated with the NAO over much of the North Atlantic and the western part of North Africa. In a later section I show that the NAOI also seems to modulate dust activity over the Mediterranean.

5. Atmospheric Dust Transport and Deposition to the North Atlantic Ocean

One of the major motivations in studying dust transport phenomena is to estimate the impact of dust deposition on the biogeochemistry of the oceans and to assess the possible impact of climate change in coming decades. Given the dearth or total absence of dust measurements over many ocean regions, it is necessary to use atmospheric transport models to this end.

Over the past decade a major effort has focused on dust model development. In a recent comparison of chemical transport models (Textor et al., 2005), there were 13 models that included dust. There are many difficulties in developing such models. Dust generation is a highly nonlinear processes that depends on many factors, especially wind speed, soil moisture, soil composition, vegetation cover, topography, and the state of the soil surface (especially soil disturbances such as those resulting from grazing and agriculture). While experimental studies can characterize the effect of one or perhaps several of these factors in isolation, extrapolating to the larger world is very difficult. In general models have difficulties in reproducing the spatial and temporal pattern of dust emissions. Model development is severely limited by the general lack of information of soil and terrain properties, especially land use. The spatial quality of wind data sets is also highly variable. (Luo et al., 2003), for example, show that the use of two different meteorological data sets (NCEP/NCAR and NASA DAO) in their dust model resulted in very large differences in their global dust emission estimates; the differences between the models was greater than the differences within the models where they were attempting to assess the impact of variables such as land use.

Nonetheless models are capable of producing dust distributions that compare well with satellite products. Figure 11 is an example from one model which shows total column dust load for each of the four seasons (Cakmur et al., 2006). Note that the seasonal migration of the African dust plume compares well with that from AVHRR in Figure 1. In boreal spring (Figure 11b) there is, in effect, a global band of dust that extends over much of the mid- and low-latitude northern hemisphere. Although the model might exaggerate the magnitude of dust transport especially in the mid latitudes, it nonetheless is correct in showing that dust is carried great distances. For example, dust from Asia is believed to be a major component in the soil particles found in snow and ice cores from Greenland (Bory et al., 2003) and in some cases in

the Alps (Grousset et al., 2003). In contrast Figure 11 shows relatively little dust in the Southern Hemisphere.

A typical model estimate of dust deposition rates to the oceans is shown in Figure 12 (Jickells et al., 2005). In the tropical North Atlantic rates typically range between 2 to 10 g m^{-2} y^{-1}; over the Arabian Sea they are as high as 20 g m^{-2} y^{-1}. Over much of the North Pacific, rates are in the range 0.5 to 1 g m^{-2} y^{-1}, increasing to 1 to 2 g m^{-2} y^{-1} closer to the coast of Asia. Deposition to the Mediterranean Sea is also very high, comparable to that over the Tropical Atlantic; rates in the eastern region are higher (5-10 g m^{-2} y^{-1}) than in the western region (2-5 g m^{-2} y^{-1}). Dust deposition rates in Figure 12 tend to mirror the aerosol distributions shown in Figure 1 which, as previously stated, is largely linked to the presence of dust and, in some regions, smoke from biomass burning. High rates are also consistent with the model dust column concentrations shown in Figure 11.

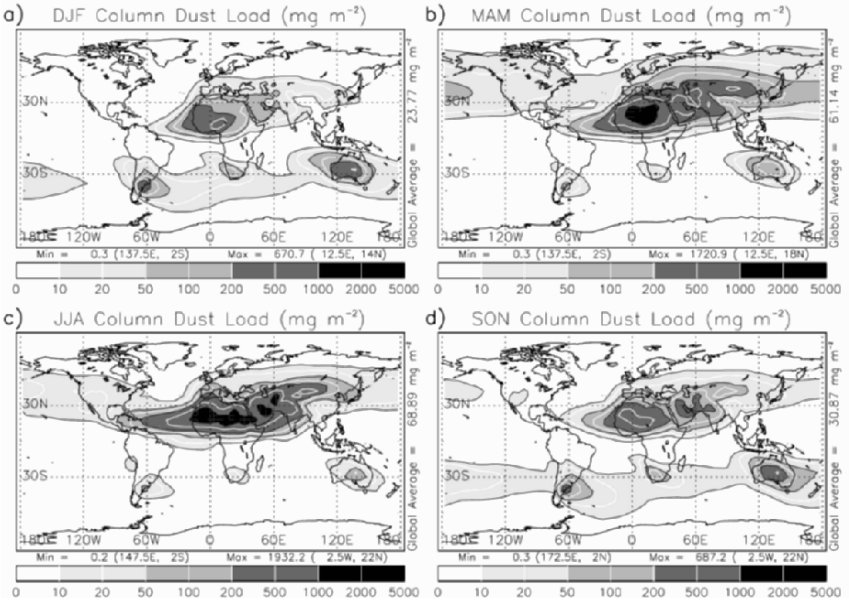

Figure 11. Seasonal global column dust load: units, mg m^{-2}: (a) DJF, (b) MAM, (c) JJA, and (d) SON. (Cakmur et al., 2006). Dust aerosol is calculated using the AGCM model of the NASA Goddard Institute for Space Studies

Table 1 shows estimates of deposition rates to the major ocean basins obtained from eight commonly-used models (Engelstaedter et al., 2006). There is considerable agreement for the North Atlantic because models are generally tuned to African sources. In contrast there is a substantial spread in the estimates for other regions especially the Indian Ocean and South

Pacific. Despite these differences, current models yield a reasonable, albeit broad, match with sediment trap measurements in the oceans (Mahowald et al., 2005).

Attempts have been made to estimate the quantities of dust mobilized through human activities. This is a difficult task. Estimates range from 0% to 50% (Mahowald et al., 2005). The wide range is a reflection of the uncertainties involved in these analyses and the dearth of data needed to better quantify anthropogenic contributions to dust mobilization.

The model studies summarized in Table 1 emphasize the point that North Africa is the World's most active dust source followed by the Middle East and Central Asia. In effect, these combine to form a global dust belt that dominates transport to the oceans. These sources account for the much greater deposition rates to the Northern Oceans compared with Southern Oceans. Nonetheless there are a few substantial and important dust sources in the Southern Hemisphere in Australia, southern Africa, and southern South America. There is evidence that many of these currently weak sources were much more active under previous climate regimes, e.g., the last glacial (Harrison et al., 2001).

TABLE 1. Estimates of mean annual dust deposition to the global ocean and to various ocean basins

	Annual Dust Deposition Rate (10^{12}g y^{1})*						
References#	NAO	SAO	NPO	SPO	NIO	SIO	GO
Duce et al. (1991)	220	24	480	39	100	44	910
Prospero (1996)	220	5	96	8	20	9	358
Ginoux et al. (2001)	184	20	92	28	154		478
Zender et al. (2003)	178	29	31	8	36	12	314
Luo et al. (2003)	230	30	35	20	113		428
Ginoux et al. (2004)	161	20	117	28	164	15	505
Tegen et al. (2005)	259	35	56	11	61		422
Kaufman et al. (2005)	140						

*Abbreviations: North Atlantic Ocean (NAO), South Atlantic Ocean (SAO), North Pacific Ocean (NPO), South Pacific Ocean (SPO), North Indian Ocean (NIO), South Indian Ocean (SIO), global oceans (GO)

#Adapted from Engelstaedter et al., 2006

6. Dust Transport to the Mediterranean Basin

Large quantities of aerosol are transported over the Mediterranean during much of the year. Aerosol concentrations, as measured by AVHRR (Figure 1), SeaWiFS (Antoine and Nobileau, 2006), and TOMS (Kubilay et al., 2005;

Kalivitis et al., 2007), are greatest in the spring and summer months but decrease in the fall. The high aerosol loadings are attributable to two fundamentally different components: pollution, largely derived from Europe, and dust carried from North Africa (Lelieveld et al., 2002). The major sources of Mediterranean dust (Figure 2) are located in Tunisia, Algeria, Mali, and Libya and, to a lesser extent, Egypt (Engelstaedter et al., 2006).

Engelstaedter et al. (2006) discuss the meteorology of Mediterranean dust outbreaks and the linkage to sources areas. Dust transport typically takes place in conjunction with strong low pressure systems that travel across North Africa and the Mediterranean. As the systems move rapidly to the east, typically 7°-8° per day, they generate strong surges of dust which are swept in a northerly direction across the Mediterranean and into Europe as far north as England and Scandinavia (Engelstaedter et al., 2006) and Iceland (Sodermann et al., 2006). In the later stages, the cyclones carry dust into the eastern Mediterranean and the Middle East (Barkan et al., 2005). Dust is carried over the Mediterranean at altitudes ranging from the surface (Kalivitis et al., 2007) to as high as 8 km (Alpert et al., 2004). High altitude transport is quite common as evidenced by the frequent presence of African dust in snows in the high Alps (Maggi et al., 2006; Sodermann et al., 2006).

While the northward flow on the eastern side of the cyclones carries dust to Europe, the southward flow behind the systems carries pollutants to North Africa. Thus every passage of a cyclone results in a massive exchange of aerosols across the region. This was noted in the context of the distribution AOT in AVHRR in Figure 1. In actual satellite images (e.g., MODIS, SeaWiFS), there is a distinct difference in the color of the aerosol plumes: the dust has a red-yellow coloration while the pollution is typically blue-gray. The mixing of European pollutants with suspended dust over the Mediterranean and North Africa has a number of implications including the role that they might play in changing cloud properties and, possibly, precipitation over the region (Levin et al., 1996; Rosenfeld et al., 2001).

Pollutant aerosols are carried deep into North Africa (Lelieveld et al., 2002) and over the tropical Atlantic to the Caribbean. On Barbados, European pollutants are measured along with African dust. Measurements of Pb isotopes in Barbados dust during the 1980s (Hamelin et al., 1989), when leaded gasoline was still in use, yielded a Pb isotopic signature that suggested a European origin. On Barbados about half of the nss-sulfate and nitrate are attributed to anthropogenic sources which are believed to be largely in Europe (Savoie et al., 2002). Nonetheless over the Mediterranean a large fraction of the column aerosol loading is clearly linked to dust transport (Figures 1 and 11). The periodic incursions of dust into Europe complicates the task of characterizing aerosols with regard to compliance with European air quality standards (Rodriguez et al., 2002, 2003).

The sporadic transport and deposition of African dust could play an important role in the chemistry of rainwater and in the biogeochemistry of Mediterranean waters (Guerzoni et al., 1999; Kubilay et al., 2000). Studies in the Laggo Maggiore watershed carried out since 1975 show increasing pH values in precipitation over the past 15-20 years. This trend is attributed in part to the increase in alkaline events attributed to Saharan dust (easily distinguished by the visible presence of red deposits). The deposition of African dust may explain why there are many low-alkalinity lakes in the Alps and the Pyrenees that did not become acidic in recent decades whereas lakes in areas which are rarely influenced by dust depositions (e.g., in Scandinavia) have acidified (Psenner, 1999). Similar effects are noted in high mountain lakes in Spain (Morales-Baquero et al., 2006).

Given the large quantities of dust transported over the Mediterranean, it is not surprising that substantial amounts are deposited to these waters (Guerzoni et al., 1999). As previously noted, the model-estimated deposition rates (Jickells et al., 2005) are quite high, 2 to 5 g m^{-2} y^{-1} over the western region and 5 to 10 g m^{-2} y^{-1} over the eastern region (see Figure 12). These estimates are comparable to actual measurements at island and coastal measurement sites around the basin (Guerzoni et al., 1999). In the western Mediterranean, the dissolution of Fe from African dust accounts for the relatively high concentration of Fe measured in surface waters and demonstrates the importance of dust as a source of Fe to this basin (Guieu et al., 2002). The dust-associated deposition of Fe and other dust-nutrients apparently has an impact on primary production. Herut et al. (2002) carried out a series of on-board microcosm experiments to track the response of Eastern Mediterranean surface seawaters to the addition of fresh Saharan dust. The dust triggered an increase in phytopigments and primary production. In addition to Fe, Saharan dust is a good source of P, also an important nutrient (Carbo et al., 2005; Ridame and Guieu, 2002) although the solubility of dust-P appears to be rather low.

There has been a trend of increasing dust transport to the Mediterranean similar to that noted in the transport across the Atlantic. Although there are no long-term aerosol measurements comparable to those on Barbados, there are various proxy measurements that provide evidence of trends. The concentration of African dust in snow and ice cores from the Alps shows an increased frequency of large dust events starting in the 1970s, the time period when transport to Barbados was observed (De Angelis and Gaudichet, 1991; Maggi et al., 2006). Similarly the increase in rainfall pH in northwest Italy since 1975 is attributed in part to an increase in African dust. (Rogora et al., 2004). The interannual trends of dust transport over the Mediterranean appear to be correlated with the NAO index, similar to what was found with

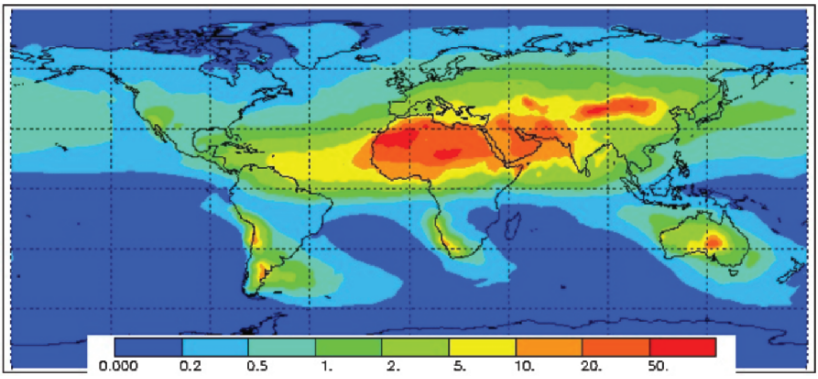

Figure 12. Dust deposition to the world oceans: units, g m^{-2} y^{-1}). Deposition values are a composite of three models: Ginoux et al., 2001; Mahowald and Luo, 2003; Tegen et al., 2004. Total atmospheric dust inputs to the oceans: 450 Tg y^{-1}. Percentage inputs to ocean basins based on this model are as follows: North Atlantic, 43%; South Atlantic, 4%; North Pacific, 15%; South Pacific, 6%; Indian, 25%; and Southern Ocean, 6%. (Jickells et al., 2005)

the winter dust transport to Barbados. This conclusion is based on satellite estimates of AOT (Meteosat and SeaWiFS) over the period 1984 to 2004 (Antoine and Nobileau, 2006).

7. Discussion and Conclusions

North Africa is clearly one of the most active dust sources on Earth. Over recent decades there appears to have been a substantial increase in the generation and transport of dust out of Africa. This change has been most thoroughly documented over the Atlantic by measurements which began in 1965. But there is considerable evidence that transport to the Mediterranean and to Europe has also increased over this period. This increase has a number of implications regarding climate and the biogeochemistry of Mediterranean waters. It also has implications for air quality and public health. A substantial fraction of African dust in the size range below 2.5 μm diameter (Prospero, 1999) and, consequently, these particles can readily penetrate the human respiratory system. Although there is little data to suggest that African dust is specifically a health hazard, it is generally acknowledged that the inhalation of aerosol particles of any type can be a threat to some degree. Thus, efforts are underway to better characterize the concentrations of respirable dust and their health effects.

A major issue not addressed here is the relative importance of "anthropogenic" dust, generally thought of as soil dust liberated through land-use impacts. It has been estimated that as much as 50% of the present-day

suspended dust mass is due to such impacts although other estimates are much smaller, approaching zero. But there is another source of "anthropogenic" dust - that is dust generated as a result of climate change brought on by the effects of green-house gases. As discussed herein, studies show that the increase in African dust since the late 1960s is linked to drought in North Africa. However recent studies suggest that the drought was to a considerable extent linked to climate change (Held et al., 2005). Thus, to the degree that this is true, the increased dust of recent decades can be considered to be "anthropogenic".

There have been a number of efforts to assess what impact global warming will have on dust emissions in the future (Harrison et al., 2001). This is a difficult task. There is much that we do not understand about dust source processes. Until we have a better understanding of the distribution and characteristics of global dust sources and how these sources respond to changes in weather and climate, we will not be able to satisfactorily assess the effects that climate change will have on future dust loads. Where is dust generated, under what conditions, in what quantities, and where is it transported? Africa, being such a rich source of dust, is an excellent laboratory for the study of such processes. African dust is both a challenge and an opportunity for researchers in this field.

8. References

Alpert, P., Kischa, P., Shivelman, A., Krichak, S. O., and Joseph, J. H., 2004, Vertical distribution of Saharan dust based on 2.5-year model predictions, *Atmos. Res.* **70:**109-130.

Antoine, D., and Nobileau, D., 2006, Recent increase of Saharan dust transport over the Mediterranean Sea, as revealed from ocean color satellite (SeaWiFS) observations, *J. Geophys. Res.* **111:**D12214, doi:10.1029/2005JD006795.

Arimoto, R., Duce, R. A., Ray, B. J., and Tomza, U., 2003, Dry deposition of trace elements to the western North Atlantic, *Global Biogeochem. Cycles* **17**(1)**:** 1010,doi:10.1029/ 2001GB001406.

Barkan, J., Alpert, P., Kutiel, H., and Kishcha, P., 2005, Synoptics of dust transportation days from Africa toward Italy and central Europe, *J. Geophys. Res.* **110:**D07208, doi:10.1029/2004JD005222

Bory, A. J.-M., Biscaye, P. E., and Grousset, F. E., 2003, Two distinct seasonal Asian source regions for mineral dust deposited in Greenland (NorthGRIP), *Geophys. Res. Lett.* **30**(4)**:**1167, doi:10.1029/ 2002GL016446.

Cakmur, R. V., Miller, R. L., Perlwitz, J., Geogdzhayev, I. V., Ginoux, P., Koch, D., Kohfeld, K. E., Tegen, I., and Zender, C. S., 2006, Constraining the magnitude of the global dust cycle by minimizing the difference between a model and observations, *J. Geophys. Res.* **111:**D06207, doi:10.1029/ 2005JD005791.

Carbo, P., Krom, M. D., Homoky, W. B., Benning, L. G., and Herut, B., 2005, Impact of atmospheric deposition on N and P geochemistry in the southeastern Levantine basin, *Deep Sea Res. II: Topical Studies in Oceanography* **52(**22-23)**:**3041-3053.

De Angelis, M. D., and Gaudichet, A., 1991, Saharan dust deposition over Mont Blanc (French Alps) during the last 30 years, *Tellus* **43B:**61-75.

Duce, R. A., Liss, P. S., Merrill, J. T., Atlas, E. L., Buat-Menard, P., Hicks, B. B., Miller, J. M., Prospero, J. M., Arimoto, R., Church, T. M., Ellis, E. W., Galloway, J. N., Hansen, L., Jickells, T. D., Knap, A. H., Reinhardt, K. H., Schneider, B., Soudine, A., Tokos, J. J., Tsunogai, S., Wollast, R., and Zhou, M., 1991, The atmospheric input of trace species to the world ocean, *Global Biogeochem. Cycles.* **5:**193-259.

Engelstaedter, S., Tegen, I., and Washington, R., 2006, North African dust emissions and transport, *Earth-Science Reviews* **79**(1-2)**:**73-100.

Ginoux, P., Chin, M., Tegen, I., Prospero, J. M., Holben, B., Dubovik, O., and Lin, S. J., Sources and distributions of dust aerosols simulated with the GOCART model, 2001, *J. Geophys. Res.*, **106**(D17)**:** 20255-20273.

Ginoux, P., Prospero, J. M., Torres, O., and Chin, M., 2004, Long-term simulation of dust distribution with the GOCART model: Correlation with the North Atlantic Oscillation, *Environ. Modelling Software* **19:**113-128.

Grousset, F. E., Ginoux, P., Bory, A., and Biscaye, P. E., 2003, Case study of a Chinese dust plume reaching the French Alps, *Geophys. Res. Lett.* **30**(6), 10.1029/2002GL016833.

Guieu, C., Bozec, Y., Blain, S., Ridame, C., Sarthou, G., and Leblond, N., 2002, Impact of high Saharan dust inputs on dissolved iron concentrations in the Mediterranean Sea, *Geophys. Res. Lett.*, **29**(19)**:**1911, doi:10.1029/2001GL014454.

Guerzoni, S., Chester, R., Dulac, F., Herut, B., Loye-Pilot, M.-D., Measures, C., Migon, C., Molinaroli, E., Moulin, C., Rossini, P., Saydam, C., Soudine, A., and Ziveri, P., 1999, The role of atmospheric deposition in the biogeochemistry of the Mediterranean Sea, *Prog. Oceanogr.* **44:**147-190.

Hamelin, B., Grousett, F. E., Biscaye, P. E., Zindler, A., and Prospero, J. M., 1989, Lead isotopes in trade wind aerosols at Barbados: The influence of European emissions, *J. Geophys. Res.*, **94:**16,243-16,250.

Harrison, S. P., Kohfeld, K. E., Roeland, C., and Claquin, T., 2001, The role of dust in climate today, at the last glacial maximum and in the future, *Earth-Science Reviews* **54:**43-80.

Held, I. M., Delworth, T. L., Lu, J., Findell, K. L., and Knutson T. R., 2005, Inaugural Article: Simulation of Sahel drought in the 20th and 21st centuries, *Proc. Natl. Acad. Sci. USA* **102:**17,891-17,896.

Herut, B., Zohary, T., Krom, M. D., Fauzi, R., Mantoura, C., Pitta, P., Psarra, S., Rassoulzadegan, F., Tanaka, T., and Thingstad, T. F., 2005, Response of East Mediterranean surface water to Saharan dust: On-board microcosm experiment and field observations, *Deep Sea Res. II: Topical Studies in Oceanography* **52(**22-23**)**:3024-3040, doi:10.1016/j.dsr2.2005.09.003.

Husar, R. B., Prospero, J. M., and Stowe, L. L., 1997, Characterization of tropospheric aerosols over the oceans with the NOAA advanced very high resolution radiometer optical thickness operational product. *J. Geophys. Res.* **102**(D14):16,889-16,909.

Husar, R. B., Tratt, D. M., Schichtel, B. A., Falke, S. R., Li, F., Jaffe, D., Gasso, S., Gill, T., Laulainen, N. S., Lu, F., Reheis, M. C., Chun, Y., Westphal, D., Holben, B. N., Gueymard, C., McKendry, I., Kuring, N., Feldman, G. C., McClain, C., Frouin, R. J., Merrill, J., DuBois, D., Vignola, F., Murayama, T., Nickovic, S., Wilson, W. E., Sassen, K., Sugimoto, N., and Malm, W. C., 2001, Asian dust events of April 1998, *J. Geophys. Res.-Atmos.* **106**(D16):**1**8,317-18,330.

Hurrell, J. W., 1995, Decadal trend in the North Atlantic Oscillation: Regional temperatures and precipitations, *Science* **269:**676-679.

Jickells, T., An, Z. A., Baker, A. R., Bergametti, G., Brooks, N., Boyd, P. W., Duce, R. A., Hunter, K. A., Junji, C., Kawahata, H., Kubilay, N., Andersen, K. K., laRoche, J., Liss, P. S., Mahowald, N., Prospero, J. M., Ridgwell, A. J., Tegen, I., and Torres, R., 2005, Global iron connections: Desert dust, ocean biogeochemistry and climate, *Science* **308:**67-71.

Kalivitis, N., Gerasopoulos, E., Vrekoussis, M., Kouvarakis, G., Kubilay, N., Hatzianastassiou, N., Vardavas, L., and Mihalopoulos, N., 2007, Dust transport over the eastern Mediterranean derived from Total Ozone Mapping Spectrometer, Aerosol Robotic Network, and surface measurements, *J. Geophys. Res.* **112:**D03202, doi:10.1029/2006JD007510.

Kallos, G., Papadopoulos, A., Katsafados, P., and Nickovic, S., 2006, Transatlantic Saharan dust transport: Model simulation and results, *J. Geophys. Res.* **111:**D09204, doi:10.1029/2005JD006207.

Karyampudi, M.V., Palm, S. P., Reagen, J. A., Fang, H., Grant, W. B., Hoff, R. M., Moulin, C., Pierce, H. F., Torres, O., Browell, E. V., and Melfi, S. H., 1999, Validation of the Saharan Dust Plume Conceptual Model Using Lidar, Meteosat, and ECMWF Data, *Bull. Am. Met. Soc.* **80**(6)**:**1045-1076.

Kaufman, Y. J., Tanre´, D., and Boucher, O., 2002, A satellite view of aerosols in the climate system, *Nature* **419:**215-223.

Kaufman, Y. J., Koren, I., Remer, L. A., Tanre´, D., Ginoux, P., and Fan, S., 2005, Dust transport and deposition observed from the Terra-Moderate Resolution Imaging Spectroradiometer (MODIS) spacecraft over the Atlantic Ocean, *J. Geophys. Res.* **110:**D10S12, doi:10.1029/2003JD004436.

Kubilay, N., Nickovic, S., Moulin, C., and Dulac, F., 2000, An illustration of the transport and deposition of mineral dust onto the eastern Mediterranean, *Atmos. Environ.* **34:**1293-1303.

Kubilay, N., Oguz, T., Koçak, M., and Torres, O., 2005, Ground-based assessment of Total Ozone Mapping Spectrometer (TOMS) data for dust transport over the northeastern Mediterranean, *Global Biogeochem. Cycles.* **19:**GB1022, doi:10.1029/2004GB002370.

Lelieveld, J., Berresheim, H., Borrmann, S., Crutzen, P. J., Dentener, F. J., Fischer, H., Feichter, J., Flatau, P. J., Heland, J., Holzinger, R., Korrmann, R., Lawrence, M. G., Levin, Z., Markowicz, K. M., Mihalopoulos, N., Minikin, A., Ramanathan, V., de Reus, M., Roelofs, G. J., Scheeren, H. A., Sciare, J., Schlager, H., Schultz, M., Siegmund, P., Steil, B., Stephanou, E. G., Stier, P., Traub, M., Warneke, C., Williams, J., and Ziereis, H., 2002, Global Air Pollution Crossroads over the Mediterranean, *Science* **298:**794-799.

Levin, Z., Ganor, E., and Gladstein, V., 1996, The effects of desert particles coated with sulfate on rain formation in the Eastern Mediterranean, *J. Appl. Meteor.* **35:**1511-1523.

Luo, C., Mahowald, N. M., and del Corral, J., 2003, Sensitivity study of meteorological parameters on mineral aerosol mobilization, transport, and distribution, *J. Geophys. Res.* **108**(D15)**:**4447, doi:10.1029/2003JD003483, 2003.

Mahowald, N. M., and Luo, C., 2003, A less dusty future?, *Geophys. Res. Lett.* **30**(17):**1**903, doi:10.1029/2003GL017880.

Mahowald, N. M., Baker, A. R., Bergametti, G., Brooks, N., Duce, R. A., Jickells, T. D., Kubilay, N., Prospero, J. M., and Tegen, I., 2005, Atmospheric global dust cycle and iron inputs to the ocean, *Global Biogeochem. Cycles* **19:**GB4025, doi:10.1029/2004GB002402.

Maggi, V., Villa, S., Finizio, A., Delmonte, B., Casati, P., and Marino, F., 2006, Variability of anthropogenic and natural compounds in high altitude – high accumulation Alpine Glaciers, *Hydrobiologia* **562:**43-56, doi:10.1007/s10750-005-1804-y.

Morales-Baquero, R., Pulido-Villena, E., and Reche, I., 2006, Atmospheric inputs of phosphorus and nitrogen to the southwest Mediterranean region: Biogeochemical responses of high mountain lakes, *Limnol. Oceanogr.* **51**(2)**:**2006, 830-837.

Parekh, P., Follows, M. J., and Boyle, E. A., 2005, Decoupling of iron and phosphate in the global ocean, *Global Biogeochem. Cycles* **19:**GB2020, doi:10.1029/2004GB002280.

Perry, K. D., Cahill, T. A., Eldred, R. A., Dutcher, D. D., and Gill, T. E., 1997, Long-range transport of North African dust to the eastern United States, *J. Geophys. Res.* **102**(D10)**:**11,225-11,238.

Prospero, J. M., 1996, The Atmospheric transport of particles to the Ocean, in: *Particle Flux in the Ocean*, SCOPE Report 57, V. Ittekkot, P. Schäfer, S. Honjo, and P. Depetris, eds., John Wiley and Sons, Chichester, pp. 19-52.

Prospero, J. M., 1999, Long-term measurements of the transport of African mineral dust to the Southeastern United States: Implications for regional air quality, *J. Geophys. Res.* **104:**D13, 15,917-15,927.

Prospero, J. M., and Lamb, P. J., 2003, African Droughts and Dust Transport to the Caribbean: Climate Change Implications, *Science* **302:**1024-1027.

Prospero, J. M., Glaccum, R. A., and Nees, R. T., 1981, Atmospheric transport of soil dust from Africa to South America, *Nature* **289:**570-572.

Prospero, J. M., Uematsu, M., and Savoie, D. L., 1989, Mineral aerosol transport to the Pacific Ocean, in: *Chemical Oceanography, Vol. 10*, J. P. Riley, ed., Academic Press, New York, pp. 187-218.

Prospero, J. M., Ginoux, O., Torres, O., Nicholson, S. E., and Gill, T. E., 2002, Environmental characterization of global sources of atmospheric soil dust identified with the NIMBUS 7 Total Ozone Mapping Spectrometer (TOMS) absorbing aerosol product, *Rev. Geophys.* **40**(1):1002, doi:10.1029/2000RG000095.

Psenner, R, 1999, Living in a Dusty World: Airborne Dust as a Key Factor for Alpine Lakes, *Water Air Soil Poll.* **112:**217-227, doi:10.1023/A:1005082832499,

Reid, J. S., Kinney, J. E., Westphal, D. L., Holben, B. N., Welton, E. J., Tsay, S.-C., Eleuterio, D. P., Campbell, J. R., Christopher, S. A., Colarco, P. R., Jonsson, H. H., Livingston, J. M., Maring, H. B., Meier, M. L., Pilewskie, P., Prospero, J. M., Reid, E. A., Remer, L. A., Russell, P. B., Savoie, D. L., Smirnov, A., and Tanré, D., 2003, Analysis of measurements of Saharan dust by airborne and ground-based remote sensing methods during the Puerto Rico Dust Experiment (PRIDE), *J. Geophys. Res.* **108**(D19)**:**8586, doi:10.1029/2002JD002493.

Ridame, C., and Guieu, C., 2002, Saharan input of phosphate to the oligotrophic water of the open western Mediterranean Sea, *Limnol. Oceanogr.* **47**(3)**:**856-869.

Rodríguez, S., Querol, X., Alastuey, A., and Plana, F., 2002, Sources and processes affecting levels and composition of atmospheric aerosol in the western Mediterranean, *J. Geophys. Res.* **107**(D24)**:**4777, doi:10.1029/2001JD001488.

Rodríguez, S., Querol, X., Alastuey, A., and Viana, M-M., 2003, Events Affecting Levels and Seasonal Evolution of Airborne Particulate Matter Concentrations in the Western Mediterranean, *Environ. Sci. Technol.* **37**(2)**:**216-222.

Rogora, M., Mosello, R., and Marchetton, A., 2004, Long-term trends in the chemistry of atmospheric deposition in Northwestern Italy: the role of increasing Saharan dust deposition, *Tellus B* **56:**5 426.

Rosenfeld, D., Rudich, Y., and Lahav, R. 2001, Desert dust suppressing precipitation, a possible desertification feedback loop, *Proceed. Nat. Acad. Sci.* **98**(11)**:**5975-5980.

Savoie, D. L., Arimoto, R., Keene, W. C., Prospero, J. M., Duce, R. A., and Galloway, J. N., 2002, Marine biogenic and anthropogenic contributions to non-sea-salt sulfate in the marine boundary layer over the North Atlantic Ocean, *J. Geophys. Res.* **107**(D18):4356, doi:10.1029/2001JD000970.

Sodermann, H., Palmer, A. S., Schwierz, C., Schwikowski, M., Wernli, H., 2006, The transport history of two Saharan dust events archived in an Alpine ice core, *Atmos. Chem. Phys.* **6:**667-688.

Swap, R. M., Garstang, M., Greco, S., Talbot, R., and Kallberg, P., 1992, Saharan dust in the Amazon basin, *Tellus B* **44:**133-149.

Tegen, I., Werner, M., Harrison, S. P.,and Kohfeld, K. E., 2004, Relative importance of climate and land use in determining present and future global soil dust emission, *Geophys. Res. Lett.* **31:**L05105.

Textor, C., Schulz, M., Kinne, S., Guibert, B. Y., Bauer, S. E., Berntsen, T., Berglen, T., Boucher, O., Chin, M., Dentener, F., Diehl, T., Easter, R., Feichter, H., Fillmore, D.,

Ghan, S., Ginoux, P., Gong, S. Grini, A., Hendricks, J., Horowitz, L., Huang, P., Isaksen, I., Iversen, T., Kirkevåg, A., Kloster, S., Koch, D., Kristjansson, E., Krol, M., Lauer, A., Lamarque, J. F., Liu, X., Montanaro, V., Myhre, G., Penner, J., Pitari, G., Reddy, S., Seland, Ø., Stier, P., Takemura, T., and Tie, X., 2005, Analysis and quantification of the diversities of aerosol life cycles within AeroCom, *Atmos. Chem. Phys. Discuss* **5:**8331-8420.

VanCuren, R. A., 2003, Asian aerosols in North America: Extracting the chemical composition and mass concentration of the Asian continental aerosol plume from long-term aerosol records in the western United States, *J. Geophys. Res.* **108**(D20)**:**4623, doi:10.1029/2003JD003459.

Washington, R., Todd, M. C., Engelstaedter, S., Mbainayel, S., and Mitchell, F., 2006, Dust and the low-level circulation over the Bodélé Depression, Chad: Observations from BoDEx 2005, *J. Geophys. Res.* **111:**D03201, doi:10.1029/2005JD006502.

Zender, C. S., Bian, H., and Newman, D., 2003, Mineral Dust Entrainment and Deposition (DEAD) model: Description and 1990s dust climatology, *J. Geophys. Res.* **108**(D14)**:**4416, doi:10.1029/2002JD002775.

RADIATIVE AND PHYSIOLOGICAL EFFECTS OF INCREASED CO_2: HOW DOES THIS INTERACTION AFFECT CLIMATE IN THE MEDITERRANEAN REGION?

LAHOUARI BOUNOUA
NASA Goddard Space Flight Center
Greenbelt MD 20071, USA

Key Words: Doubling CO_2; physiological and radiative interactions; Mediterranean region.

Abstract The radiative and physiological effects of doubled atmospheric carbon dioxide concentration (CO_2) on climate are described using climate simulations. When CO_2 was increased for vegetation only assuming no radiative effect, the response was a decrease in stomatal conductance followed by a temperature increase. This temperature increase was stronger when the vegetation physiological "down-regulation" was allowed in the model. The radiative forcing alone did not affect the global mean photosynthesis, however, some stimulation was observed in cold places. The interactions between the physiological and the radiative effects of doubled CO_2 are not linearly "additive" and when acting together they tend to reduce the warming in the Mediterranean region.

1. Background

Climate change and variability occur because of changes in natural forcing such as volcanic eruption, or anthropogenic forcing such as greenhouse gases and aerosols. Variations in atmospheric concentration of greenhouse gases and aerosols, solar radiation and land surface properties affect the climate system by altering its energy budget. It is widely expected that over next couple of centuries, the human forcing of climate will exceed the natural forcing.

Carbon dioxide (CO_2), a long lasting greenhouse gas exerts the largest radiative effect on the climate system of about 1.66 Wm^{-2} (IPCC 2007) and remains the most studied impact of human activity on climate change. The radiative effect of increased atmospheric CO_2 concentration has been extensively described (e.g., Henderson-Sellers et al., 1995, Sellers et al., 1996, Bounoua et al., 1999, and references therein). A recent assessment of the responses generated by several climate models to an increase in atmospheric CO_2 shows that, relative to a 1980-1999 baseline, the global average

A. Mellouki and A.R. Ravishankara (eds.), Regional Climate Variability and its Impacts in the Mediterranean Area, 39–50.

surface air temperature could increase from 1.8°C to 4.0°C by the end of the century-2090-2099 (IPCC 2007). For an equilibrium doubling of CO_2, which measures the amplitude of the model's climate response to a continuous 2 × CO_2 forcing, the report indicates a temperature increase between 2 and 4.5°C. It is recognized, however, that water vapor and clouds feedbacks represent the largest sources of uncertainties in these best estimates.

Feedbacks and internal interactions are often difficult to distinguish at smaller scales because at these scales the local variability is higher than the large scale forcing and therefore masks the signal. It is a fair assessment to state that according to current state of the art in climate modeling, a large part of the warming due to greenhouse gases will arise from internal feedback mechanisms rather than form direct effects, and that a substantial part of the uncertainty in the projected results is due to our limited knowledge of these internal interactions. In this presentation, we document some of the feedback mechanisms acting between carbon, water and energy cycles in several climate model simulations subjected to an instantaneous doubling of atmospheric CO_2 concentration with an emphasis on the interaction between the physiological and radiative effects.

CO_2 in the atmosphere affects the radiation by absorbing more in the longwave length creating thus a greenhouse effect. Vegetation takes up CO_2 from the atmosphere as a part of photosynthesis and at the same time diffuses water out to the atmosphere through transpiration. Plants control the leaf water-CO_2 exchange through adjustment of their stomates. Stomatal adjustment is a function of environmental and physiological conditions and is done in a manner that optimizes the amount of carbon assimilated for a given rate of transpiration (Cowan, 1977). Leaf-scale models of net photosynthetic assimilation and stomatal conductance have been formulated to describe these relations (Collatz et al., 1991; Collatz et al., 1992). The physiological responses to increased atmospheric CO_2 concentration that have potential consequences for climate result mainly from the dependence of photosynthesis and stomatal conductance on CO_2 partial pressure as shown by the theoretical models in Figure 1. Two types of photosynthetic physiologies are considered here, C3 and C4. The C3 type occurs in most woody plants and temperate herbaceous plants and the C4 type is dominant in tropical and subtropical herbaceous vegetation. These two types are distinguished by their different responses to temperature and CO_2 partial pressure (Figure 1A). Short-term exposure of C3 plants to a doubling of CO_2 concentration stimulates photosynthesis (Figs. 1A and B) and decreases the stomatal conductance (Figure 1C) from C (control ($1 \times CO_2$)) to P (physiological response to CO_2 doubling ($2 \times CO_2$)).

After a long-term exposure to increased CO_2 concentration, some plants have been observed to "down-regulate" their maximum photosynthesis capacity to maintain about the same rate of photosynthesis as if they were

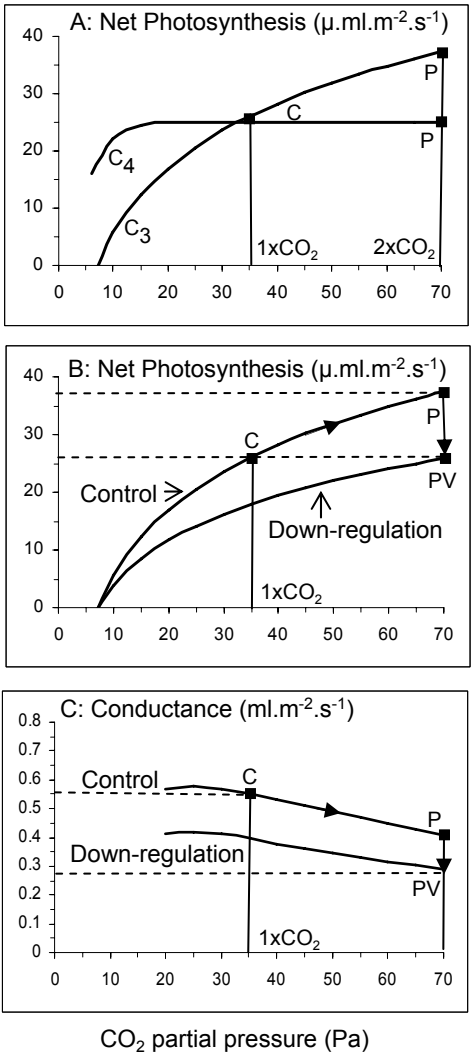

Figure 1. Leaf photosynthesis and conductance response to atmospheric CO_2 concentration (see text for details)

under normal ($1 \times CO_2$) conditions (Field et al., 1992; Tissue et al., 1993). The extent of this ''down regulation'' of physiological capacity depends on species, nutrient availability, and environmental stress (Field et al., 1991; Gunderson and Wullschleger, 1994). The theoretical model response of photosynthesis for the case of down regulation at ($2 \times CO_2$) is indicated by PV in (Figs. 1B,C.). These calculations, made at constant temperature, high shortwave radiation, and unstressed conditions, show that doubling CO_2 causes reductions in stomatal conductance of about 25% in the P-case, and 50% in the PV-case, which are within the range observed for trees and herbaceous species (Morison, 1987; Field et al., 1995). On the other hand, analyses of stomatal densities in fossilized or otherwise preserved leaf surfaces have shown that leaf stomatal conductance is negatively correlated with past changes in atmospheric CO_2 concentration (Woodward, 1987; Penuelas and Matamala, 1990; Beerling and Woodward, 1996). The line segments joining the P and PV points in (Figs. 1B and C) thus describe the likely range of leaf-scale physiological responses to doubling of atmospheric CO_2 concentration in the absence of other climate effects. Photosynthesis could increase significantly, with an associated small reduction in stomatal conductance (P-case), or it might remain more or less constant with a larger reduction in stomatal conductance and consequently transpiration (PV-case). The actual response probably lies between these two cases.

2. Model Experiments

The coupled land atmosphere ocean model used to carry out these simulations is extensively described in (Randal et al., 1996) and (Sellers et al., 1996a,b). The simulations are also described in (Sellers et al., 1996c) and (Bounoua et al., 1999). Basically, six 30-year simulations were run in which sea surface temperature and sea ice were allowed to evolve with atmospheric conditions (Figure 2). For all six experiments, global satellite data for 1987 were used to characterize land surface parameters at monthly intervals (Sellers et al., 1996c; Randall et al., 1996).

1) The first run is the control (C) simulation. The coupled model was integrated for 30 years using the current atmospheric CO_2 concentration for both radiative and physiological modules.
2) The second simulation, ''physiology-only'' (P) run consisted of operating the radiative transfers module under $1 \times CO_2$ whereas the CO_2 concentration in the physiological module was instantaneously doubled to 700 ppm, thus directly influencing the photosynthesis–conductance sub-model (Figs. 1A,C).
3) The third experiment (PV) simulated the case where the plant's physiological activity is "down regulated". The expected result is that, at $2 \times CO_2$,

the assimilation rates in this experiment should approach those of the C case (Figure 1B) and stomatal conductance to water vapor should be substantially reduced (Fig. 1C). This case suggests that vegetation may adapt to increased CO_2. The P and PV simulations show the sensitivity of climate to decreasing conductance in the absence of radiative forcing.

4) The fourth run, radiation-only (R), is an experiment in which only the atmospheric radiative module is affected by the 2 × CO_2 concentration, whereas the land surface vegetation module operates at 1 × CO_2. This experiment assesses the impact of physical climate change on the vegetation physiological activity.
5) The radiation and physiology (RP) run is a combination of the R and P experiments; both the radiation and the physiology modules operate under 2 × CO_2.
6) The sixth experiment (RPV) is identical to the fifth one (RP) except that vegetation is allowed to down-regulate its physiological activity.

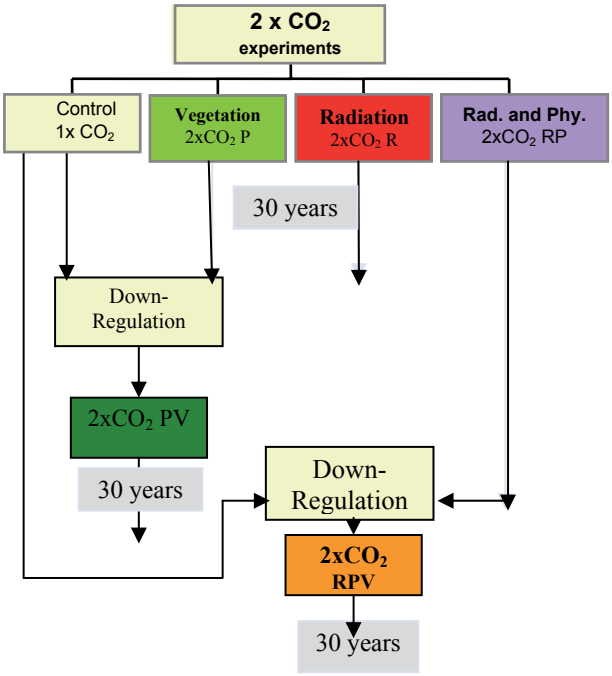

Figure 2. This Experimental design

3. Results and Discussion

The monthly mean surface air temperature response for selected experiments is shown in Figure 3. Responses of the PV, R, and RPV cases are displayed as differences from the control (C). In both the R and RPV simulations, the mean temperature response to the impulsively doubled CO_2

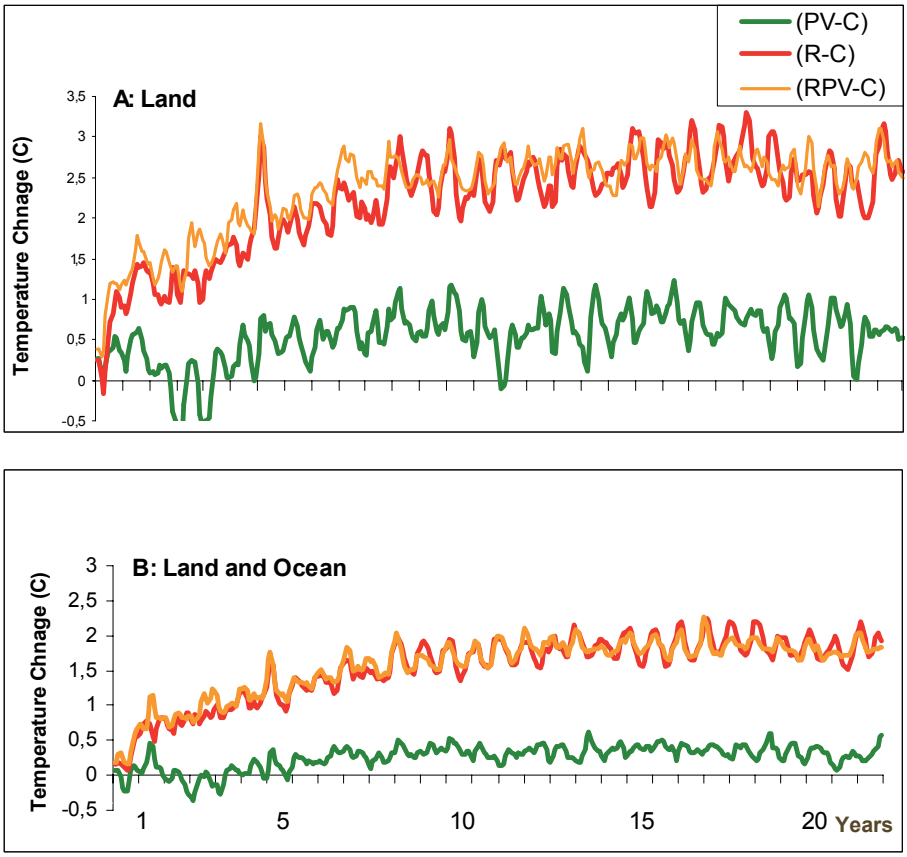

Figure 3. Three-month running mean surface temperature response for A) Land and B) Land and ocean

concentration was almost instantaneous. After about 20 years of integration, the surface temperature response has reach equilibrium. Over land masses, the temperature increase due to doubling CO_2 with down-regulation of the physiology (PV-C) resulted in a warming of about 0.5°C. It is worth noting that inter-annual variability in the simulated air temperature is large enough at times to obscure the physiological effects.

4. Global Response

The monthly mean response to increased CO_2 is illustrated for the month of July corresponding to the northern hemisphere growing season for most plants. Averaged over all land points, the doubling of CO_2 had a large stimulation of carbon assimilation for the P and RP-cases where plant physiology was subjected to a doubling of CO_2 without down-regulation.

Positive but smaller stimulation in photosynthesis occurred when plants' physiology was down-regulated (PV and RPV). The radiation only R-case resulted in a small inhibition of photosynthesis (Figure 4A). As expected, canopy conductance decreased in all experiments with the strongest reduction in down-regulated cases (Figure 4B). The reduction in conductance is mirrored in transpiration (Figure 4C), the largest component of evapotranspiration, which caused the temperature to increase (Figure 4d). Over land the temperature increased by 2.7°C. Globally (land and ocean), however, the temperature increased only 1.8°C. This is rather in the lower range of the increase of 2 to 4.5°C estimated by the IPCC models (IPCC 2007). In our simulations, the radiative forcing due to doubling CO_2 caused the transpiration to increase, but the physiological response more than compensated for this increase.

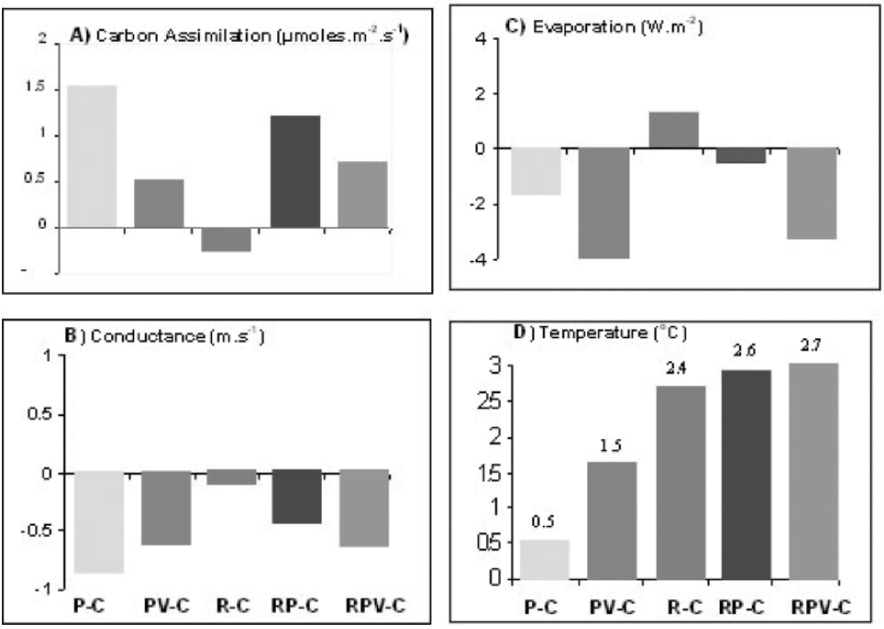

Figure 4. July mean difference for all vegetated land for A) Carbon assimilation, B) Stomatal conductance, C) Evaporation and D) Temperature

5. Regional Response

At regional scale the warming was more intense, especially in the southern shores of the Mediterranean basin where vegetation is rather sparse. There, the down-regulation of the physiology caused the annual mean temperature to increase by about 1 to 2°C along the Northern African coast. This is

likely related to the reduced vegetation cover over the region. In this case, most of the radiative energy absorbed by the surface is converted to sensible heating since the latent heat component is small or negligible (Figure 5a). The radiative forcing alone R-case resulted in an additional warming over the entire region (Figure 5b) and when the radiative and down-regulated physiology were combined, the warming was even stronger. The scaling down of the physiological activity, although small over the region, contributed to warming above and beyond the radiative forcing (Figure 5c).

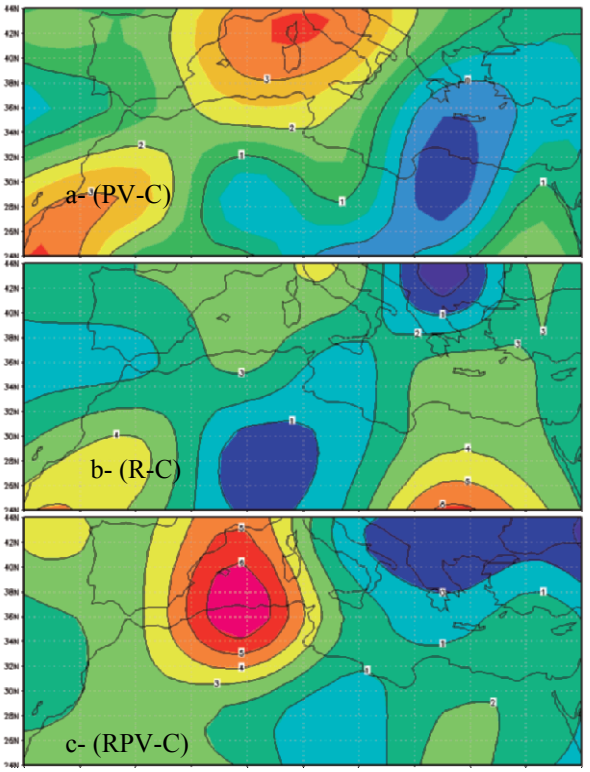

Figure 5. Annual mean surface temperature difference over the Mediterranean region for a) the down-regulated physiology, b) the radiative forcing alone and c) the radiative and down-regulated physiological forcing

Figure 6 shows the annual response of assimilation, temperature and precipitation over the Mediterranean region and the local semi-arid region of Marrakech (Morocco). At regional and local levels, the physiological response was as expected and similar to that observed globally. Even when down-regulation was imposed on vegetation, the canopy carbon assimilation increased. Interestingly, however the radiative forcing R-case which inhibited assimilation at global scale has stimulated it over the local region of

Marrakech. This is likely associated with increase in temperature over the cold Atlas Mountain which stimulates more growth during early fall and spring when vegetation is normally stressed by cold temperatures and assimilation is inhibited. The physiological response alone caused the temperature to increase by about 1°C over the Mediterranean region with negligible effect on precipitation. Precipitation increased in both PV and

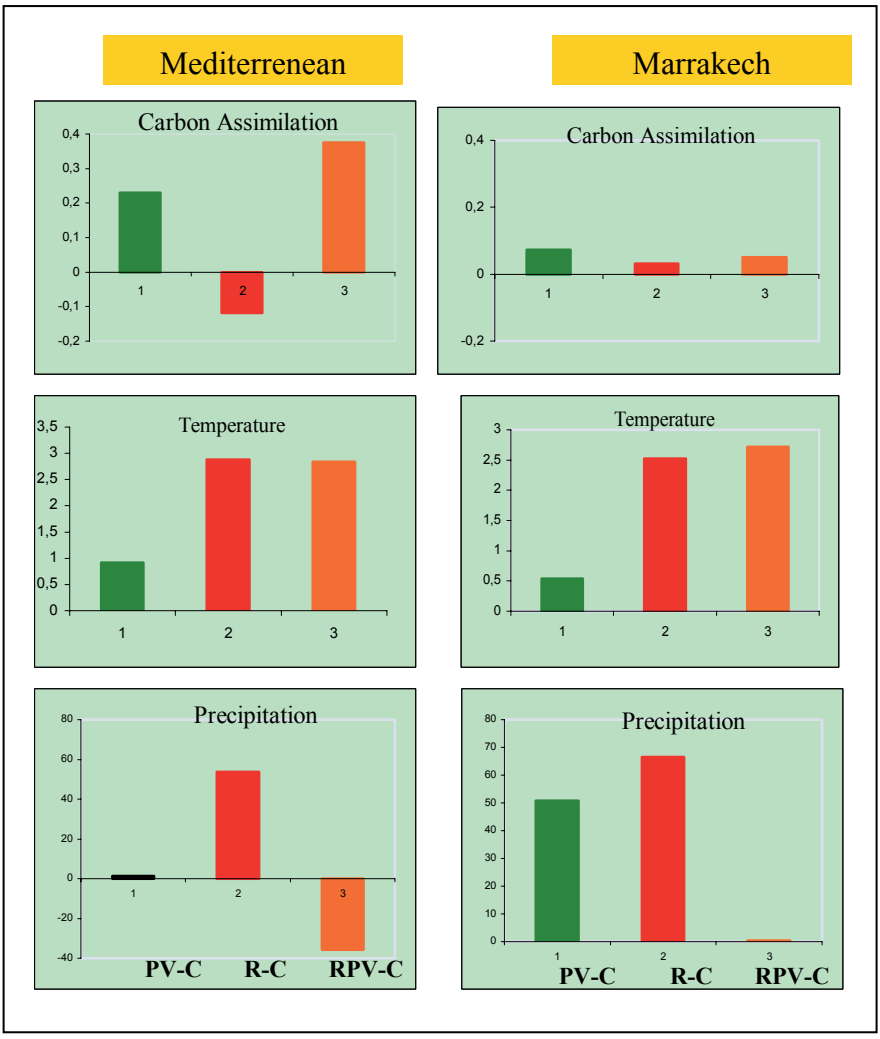

Figure 6. Annual mean difference of carbon assimilation [micro-moles-$m^{-2}.s^{-1}$] (top panel), surface temperature (Celsius) (middle panel) and precipitation (mm) (bottom panel) for the Mediterranean region (left panels) and the semi-arid region of Marrakech (right panels)

R-cases; however the RPV-case resulted in a reduced precipitation over the entire region. This result suggests that vegetation could play an important role in the climate of the region in case of doubling atmospheric CO_2 concentration. Over the semi-arid region of Marrakech the doubling of CO_2, even with down-regulation of the physiology, resulted in a sensible increase in precipitation of about 50 mm annually, but as the radiative and physiological forcings were combined the vegetation was forced to reduce its stomatal conductance to water vapor and lower its transpiration rate. Consequently, the gain in precipitation caused by the radiative forcing was almost offset by the down-regulation resulting in a small precipitation increase.

This nonlinearity in the response of the climate system to a combined radiative and physiological forcing can be evidenced by examining the variation in assimilation as a function of variation in temperature. Figure 7 illustrates these variations for the month of July and for all experiments. Results are shown for the Mediterranean and Marrakech regions as well as the global land area. The radiation (R) only case had no effect on the carbon assimilation when averaged over all land; however over the Mediterranean region, assimilation is inhibited. This suggests that around this region vegetation is sensitive to a temperature increase regardless of CO_2 concentration because in the R-case the vegetation operated under normal $1 \times CO_2$ conditions and therefore the simulated inhibition of assimilation is an indirect effect from the climate warming caused by radiative forcing. Over the semi-arid region if Marrakech, assimilation has slightly increased and this is believed to be related to the relief of low temperature stress during the cold months. If the radiative and physiological effects were linear, one would expect the added effects of R and PV-cases would be similar to those of RPV-case. Our results show that this is not the case. When these forcings are added separately the resulting effect is more warming. The dashed line

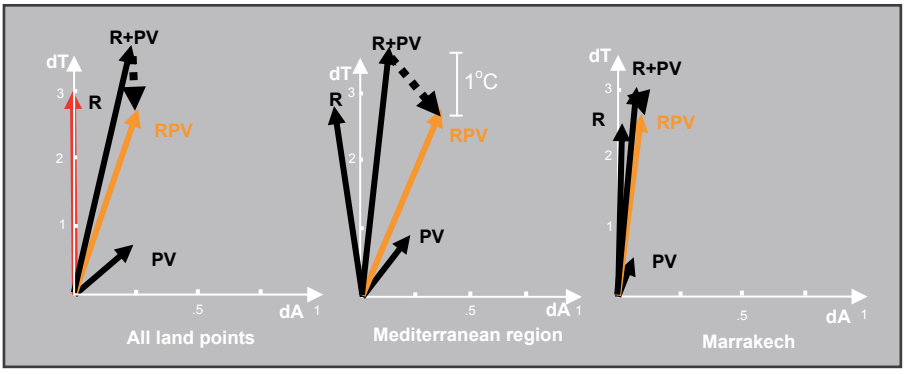

Figure 7. Nonlinearity in the interactions between radiative and physiological forcing in a $2 \times CO_2$ environment (see text for details)

joining vectors (R + PV) and RPV in Figure. 7 represent the feedback between vegetation physiology and the radiative forcing. This feedback results in increasing the carbon assimilation (dA) and reducing the temperature (dT). For the Mediterranean region this feedback accounted for a temperature reduction of about $1^{o}C$.

6. References

Beerling, D. J., and Woodward, F. I., 1996, Palaeo-ecophysiological perspectives on plant responses to global change, *Tree,* **11**: 20-23.

Bounoua, L., Collatz, G. J., Sellers, P. J., Randall, D. A., Dazlich, D. A., Los, S. O., Berry, J. A., Fung, I. C., Tucker, J., Field, C. B., and Jensen, T. G., 1999, Interactions between Vegetation and Climate: Radiative and Physiological Effects of Doubled Atmospheric CO_2, *J. Climate,* **12**: 309-324.

Collatz, G. J., Ball, J. T., Grivet, C., and Berry, J. A., 1991, Physiological and environmental regulation of stomatal conductance, photosynthesis and transpiration: A model that includes a laminar boundary layer, *Agric. For. Meteor.,* **54**: 107-36.

Collatz, G. J., Ribas-Carbo, M., and Berry, J. A., 1992, Coupled photosynthesis-stomatal onductance model for leaves of C4 plants, *Aust. J. Plant Physiol.,* **19**: 519-538.

Cowan, I. R., 1977, Stomatal behavior and environment, *Adv. Bot. Res.,* **4**: 117-228.

Field, C. B., 1991, Ecological scaling of carbon gain to stress and resource availability, In *Integrated Responses of Plants to Stress,* H. A. Mooney, W. E. Winner, and E. J. Pell, Eds., Academic Press, pp. 35-65.

Field, C. B., Chapin, F. S., Matson, P. A., and Mooney, H. A., 1992, Responses of terrestrial ecosystems to the changing atmosphere: A resource-based approach, *Annu. Rev. Ecol. Syst.,* **23**: 201-235.

Field, C. B., Jackson, R. B., and Mooney, H. A., 1995, Stomatal responses to increased O2: Implications from the plant to the global scale, *Plant, Cell Environ.,* **18**: 214-1225.

Gunderson, C. A., and Wullschleger, S. D., 1994, Photosynthetic acclimation in trees to rising atmospheric CO2: A broader perspective, *Photosyn. Res.,* **39**: 369-388.

Henderson-Sellers, A., McGuffie, K., and Gross, C., 1995, Sensitivity of global climate model simulations to increased stomatal resistance and CO2 increases, *J. Climate,* **8**: 1738-1756.

IPCC WG1 Fourth Assessment Report: Working Group I contribution to the Intergovernmental Panel on climate Change, fourth Assessment Report. Climate change 2007: The physical Science Basis.

Morison, J. I. L., 1987, Intercellular CO2 concentration and stomatal response to CO_2, In *Stomatal Function,* E. Zeiger, G. D. Farquhar, and I. R. Cowan, Eds., Stanford University Press, pp. 229-252.

Penuelas, J., and Matamala, R., 1990, Changes in nitrogen and sulfur leaf content, stomatal density and specific leaf area of 14 plant species during the last three centuries of carbon dioxide increase, *J. Exp. Botany,* **41**: 1119-1124.

Randall, D. A., and Co-authors, 1996, A revised land surface parameterization (SiB2) for GCMs. Part III: The greening of the Colorado State University General Circulation Model, *J. Climate,* **9**: 738-763.

Sellers, P. J., and Co-authors, 1996a, Comparison of radiative and physiological effects of doubled atmospheric CO_2 on climate, *Science,* **271**: 1402-1406.

Sellers, P. J., Randall, D. A., Collatz, G. J., Berry, J. A., Field, C. B., Dazlich, D. A., Zhang, C., and Bounoua, L., 1996b, A revised land surface parameterization (SiB2) for atmospheric GCMs. Part I: Model formulation, *J. Climate,* **9**: 676-705.

Sellers, D. A., Los, S. O., Tucker, C. J., Justice, C. O., Dazlich, D. A., Collatz, G. J., and Randall, D. A., 1996c, A revised land surface parameterization (SiB2) for atmospheric GCMs. Part II: The generation of global fields of terrestrial biophysical parameters from satellite data, *J. Climate,* **9**: 706-737.

Tissue, D. T., Thomas, R. B., and Strain, B. R., 1993, Long-term effects of elevated CO_2 and nutrients on photosynthesis and Rubisco in loblolly pine seedlings, *Plant, Cell Environ.,* **16**: 859-865.

Woodward, F. I., 1987, Stomatal numbers are sensitive to increases in CO_2 from pre-industrial levels, *Nature,* **327**: 617-618.

CLIMATE ALTERING TRACE GASES IN THE MEDITERRANEAN AREA: TRENDS AND SOURCE ALLOCATION

PAOLO BONASONI
ISAC-CNR, Bologna, Italy

RICCARDO SANTAGUIDA
Italian Air Force Meteorological Service, Sestola, Italy

UMBERTO GIOSTRA, MICHELA MAIONE*
University of Urbino, Italy

Key Words: Climate Altering Gases, Carbon dioxide, Halocarbons, Ozone, Continuous observations.

Abstract The site of Mt. Cimone, located to the south of the Alps and the Po Valley and to the north of the Mediterranean Sea, is considered to be representative of European background conditions. At the site a number of atmospheric studies are carried out in the frame of different International Research Projects. Among these, continuous observations of climate altering gases are carried out and are here reported.

1. Introduction

Mt. Cimone is the highest peak of northern Apennines (44°12'N, 10°42'E, 2165 m a.s.l.). Due to both its altitude (above the atmospheric boundary layer for most of the year) and geographical position to the south of the Alps and the Po Valley and to the north of the Mediterranean Sea, the site is considered to be representative of the European continental background conditions (Fischer et al., 2003; Bonasoni et al., 2000). It is characterized by a completely free horizon for 360°, with major towns and industrial areas situated in the lowlands, about 40 km away; Tyrrhenian and Adriatic Seas are respectively at about 45 and 130 km of distance.

As all high mountain areas, this is an ideal site where atmospheric background conditions and environmental change processes can be studied thanks to continuous monitoring activities that constitute also an important

* To whom correspondence should be addressed.

A. Mellouki and A.R. Ravishankara (eds.), Regional Climate Variability and its Impacts in the Mediterranean Area, 51–61.

aid to understand global change processes. Moreover, the inclusion of such activities in several International Research Projects allows to better understand atmospheric processes and assess emission patterns.

Measurements are carried out at the Observatory of the Italian Air Force Meteorological Service and at the "O. Vittori" Station of the Italian National Research Council, lodged in the buildings of the first one. This is a baseline site operating within the GAW (Global Atmosphere Watch) of the WMO (World Meteorological Organization) for the measurements of CO_2 and surface O_3. A detailed descriptions of the activities, of the instrumentation used, and indication of the research groups involved is available under http://www.isac.cnr.it/cimone/. In the following, an overview of research activities on climate altering trace gases is reported.

2. Climate Altering Trace Gases

2.1. CARBON DIOXIDE

Since 1979 CO_2 has been continuously monitored at the site by the Italian Air Force Meteorological Service, thus producing a record which is one of the longest available in Europe (Ciattaglia et al., 1987; Colombo et al., 2000; Santaguida et al., in press). The average amplitude for the diurnal cycle as a function of month for the period 1980-2006 is shown in Figure 1.

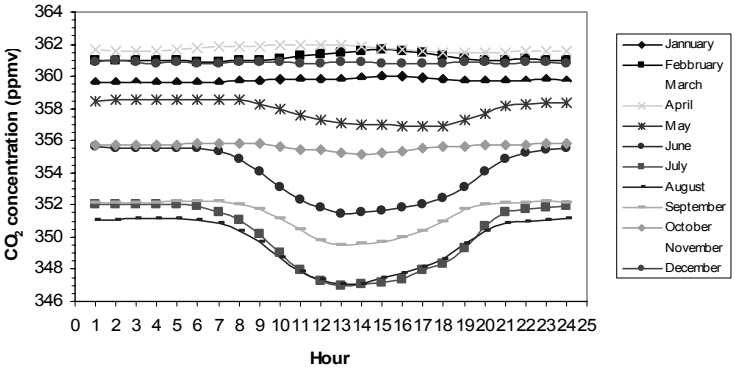

Figure 1. Average diurnal cycle for the period 1980-2006 at Mt. Cimone

A rather large amplitude can be observed at Mt. Cimone during summer months. This is due to air lifting from the surrounding valleys and reaching the top of the mountain during daytime hours. During the remaining months the site is usually above the planetary boundary layer and the amplitude of the diurnal cycle is very small. In order to select hourly means unaffected by local processes, a procedure based on Thoning et al. (1989) is routinely

used, which can be summarised as follows: Visual inspection of the raw data; hourly means with standard deviation greater than a cutoff value are discarded; hourly means with a difference with respect to the previous hour greater than a preset value are discarded; summer data between 9:00 AM and 9:00 PM are temporarily discarded; a cubic spline curve passing through the daily means is created; an iterative routine discards data too far from the resulting curve. The monthly means of the selected data are shown in Figure 2, meanwhile growth rates of the trends are shown in Figure 3. A positive peak is evident on June/July 1998 occurring with a lag of about 7/8 months after an intense El Nino event. In 2001/2003 another positive peak can be observed, not related to any El Nino event. It's also worth noting the minimum in the growth rate at Mt. Cimone on January 1992, seven months after the eruption of Mt. Pinatubo and the maximum in 1983, 7/8 months after another El Nino event.

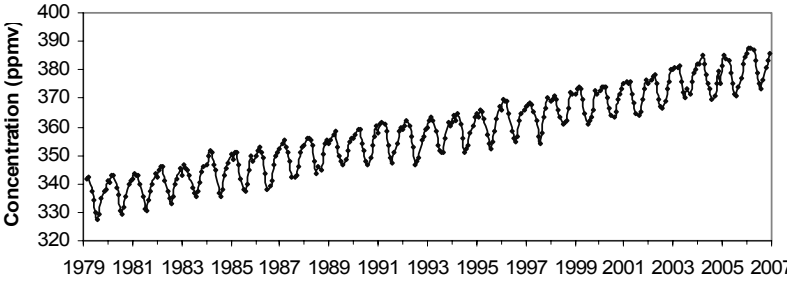

Figure 2. CO_2 monthly averages at Mt. Cimone 1979-2006

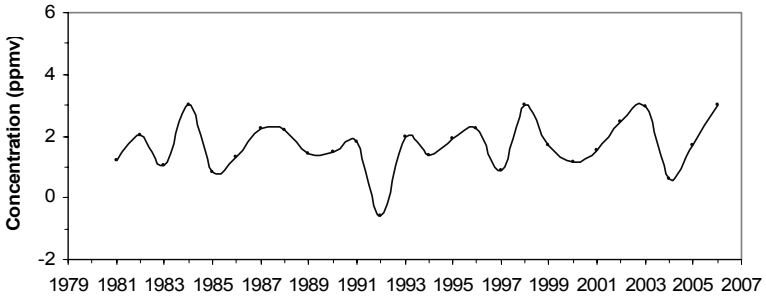

Figure 3. Annual growth rates of CO_2 mixing ratio 1980-2006

2.2. TROPOSPHERIC OZONE

Tropospheric ozone is ranked in the IPCC Third Assessment Report (IPCC-TAR) as the third climate forcing gas after carbon dioxide and methane. At Mt. Cimone, surface ozone is monitored since 1996 by a UV analyzer

(DASIBI 1108) with an accuracy and precision of ±2 ppbv. Over the period 1996-2004 (see Figure 4), the yearly mean value recorded has been of 54± 11 ppbv (one standard deviation) with a monthly behaviour exhibiting a seasonal cycle characterized by a minimum in winter, a principal maximum in summer (mean value: 63 ppbv) and a secondary one in spring (mean value: 59 ppbv). The spring ozone maximum is typical of the seasonal ozone cycles in the clean northern hemispheric atmosphere (Logan, 1985).

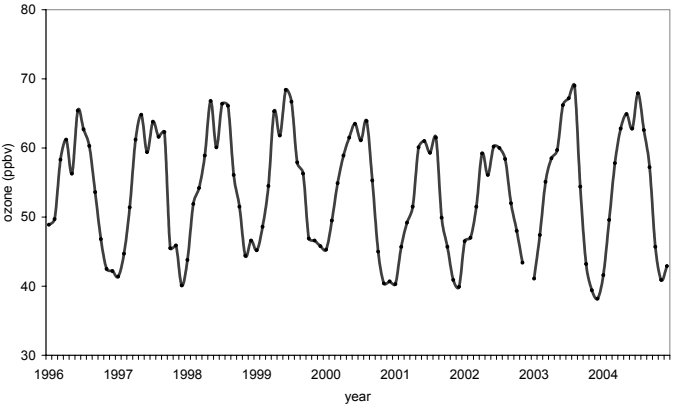

Figure 4. Monthly ozone variation at the Mt. Cimone

A contribution to high O_3 values in high mountain remote areas, can be provided by stratospheric intrusion events (Sthol et al., 2000) that may transport downwards O_3-rich air coming from the stratosphere or upper troposphere.

However, using three years of statistical back-trajectory analyses, high O_3 values have been typically related to air masses coming from the north Italy and central Europe areas (Bonasoni et al., 2000) especially during the warm season. In fact, persistent high pressure and temperature facilitate a strong increase in O_3 concentration in densely inhabited urban and industrialized areas, from where polluted air masses can reach the Apennine peak.

During summer 2003, when West and South Europe were affected by a heath wave, the fair weather conditions favoured the build-up of anthropogenic pollutants, giving rise to an increased O_3 production. At Mt. Cimone, extremely high O_3 concentrations were recorded in connection with air masses coming from continental Europe and the Po basin boundary layer (Cristofanelli et al., 2007), with O_3 concentration similar to those measured in the cities lying in the Po basin area. Such high O_3 levels were clearly related to the increased photochemical production which characterized the lower troposphere during the period. Therefore, the O_3 diurnal variation for polluted days was considerably higher than for unpolluted days, i.e., when

O_3 concentrations are representative of the free troposphere conditions, how shown in Figure 5, where daily O_3 variation for polluted and unpolluted periods are shown. The same figure also shows how the anomalous O_3 concentrations recorded in summer 2003 were considerably higher than those registered in the years before.

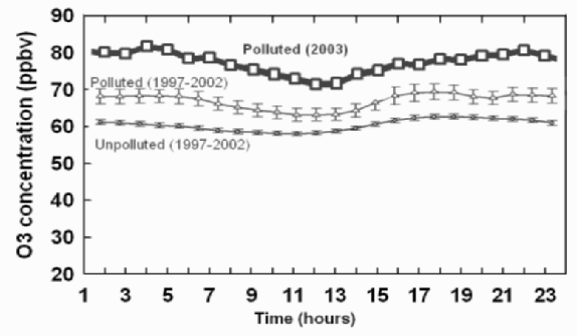

Figure 5. Mean daily O_3 variations at Mt. Cimone during the August heat wave (upper line) and for the 1997-2202 summer period (middle an lower lines, respectively) (Adapted from Cristofanelli et al., 2007)

On the contrary, when low O_3 values are recorded at Mt. Cimone, these are usually related to air masses flowing from low latitudes with a slight O_3 latitudinal gradient characterizing the data. Such variations have been related to Saharan dust transport episodes (Bonasoni et al., 2004). The presence of a desert area like the Sahara feeding Aeolian transport, determined by recurrent meteorological phenomena, facilitates the transport of particulate over the Mediterranean Sea and the Europe (Prodi and Fea, 1978). As a matter of fact, Mt. Cimone is particularly suitable to study these transport phenomena, being Apennines the first mountain chain met by Saharan air masses on their way to Europe. During several episodes of dust transports recorded at the Mt. Cimone station, an anti-correlation between high dust loadings and low ozone concentrations were found (Figure 6).

Previous studies (Schmitt et al., 1998; Zhang et al., 1994; Dentener et al., 1996; Martin et al., 2002; Bian and Zender, 2003) investigated possible mechanisms responsible for O_3 destruction and two possible results have been suggested: i) change of the photolysis rates in dust plumes and ii) heterogeneous destruction of ozone on mineral dust. The fact that the dust-loaden air masses already carried lower ozone concentrations before they received the dust injections is an unlikely scenario, since air masses arriving from the same North African source regions without strong dust loading had higher ozone concentrations than the dust-loaden ones.

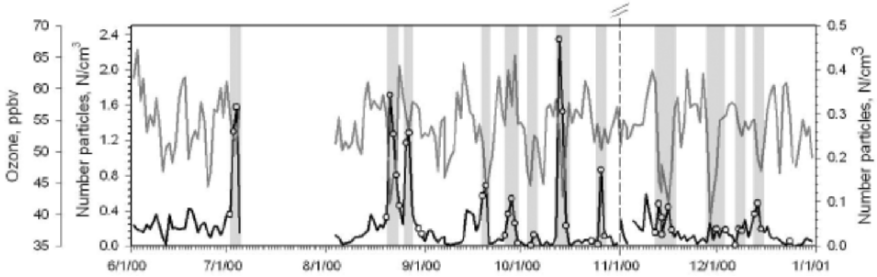

Figure 6. Daily coarse aerosol concentration (black line) and daily de-trended ozone (grey line) recorded at MTC during the period Jun–Dec 2000 (for coarse aerosol: Nov–Dec right scale). White circles represent days during which BTs originated from north Africa. Grey bars indicate the periods of the dust transport events. (Source, Bonasoni et al., 2004)

2.3. HALOCARBONS

Halocarbons contribute directly to surface climate change being powerful greenhouse gases able to absorb long-wave radiation re-emitted by the earth's surface in the 8-13 μm atmospheric window, a region of the spectrum where other greenhouse gases have only a small effect. Another way in which halocarbons containing chlorine and bromine affect climate is via ozone layer depletion which has an indirect effect on temperature. At Mt. Cimone 27 halocarbons are continuously monitored under the EU funded Project SOGE (System for Observations of Halogenated Greenhouse Gases in Europe) which consists of an integrated system based on a combination of in situ continuous observations, carried out at four European measuring stations, and models. Measurements are conducted at the four stations in a similar fashion (gas chromatography with mass spectrometric detection preceded by enrichment on specific adsorbent resins) (Maione et al., 2004; Reimann et al., 2004). Moreover, all the stations are linked internally and also to international measurement networks through the use of the same calibration scale. In Figure 7, time series (raw data) recorded at Mt. Cimone since 2002 are reported for four halocarbons, three of them being anthropogenic fluorinated hydrocarbons (HFCs) and one a methyl halide.

The three HFCs are used as refrigerant fluids, foam blowing agents and fire extinguisher in replacement for the ozone depleting gases. They were introduced into the market after 1990 but atmospheric measurements carried out so far suggest significant increases for their European emissions over

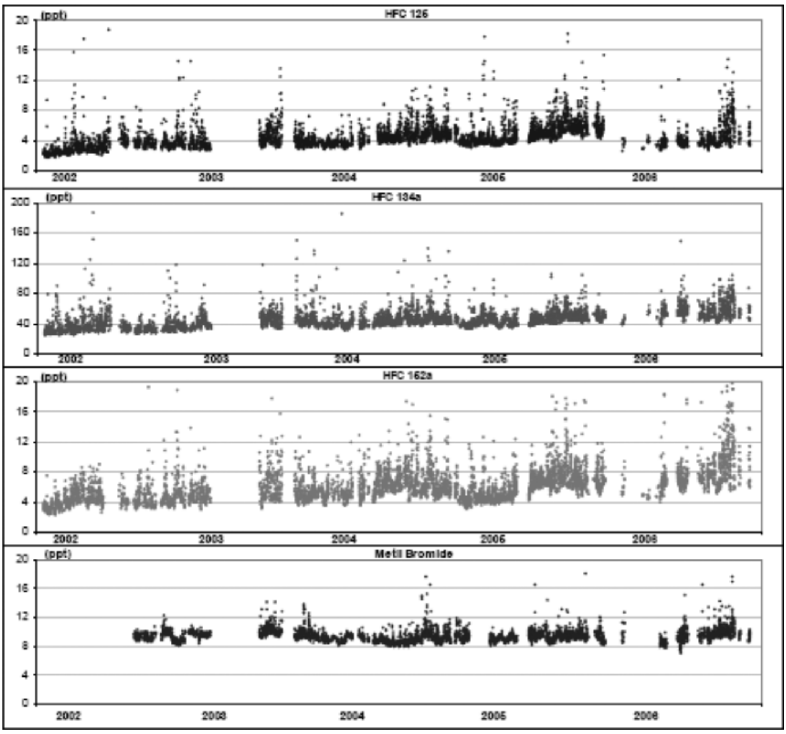

Figure 7. Time series (raw data) recorded at MTC during the period 2002-2005 for three anthropogenic fluorinated gases (HFC-125, 134a, 152a) and methyl bromide

the past decade (Greally et al., in press; O'Doherty et al., 2004; Reimann et al., 2004). Methyl bromide is the most abundant bromine-containing species in the troposphere. Unlike other halocarbons, biogenic emissions play an important role in determining its atmospheric burden. In the Mediterranean basin biogenic sources are essentially marine, meanwhile anthropogenic sources are entirely land based, including its use as fumigant and emissions from forest fires. Methyl bromide production and consumption are regulated under the Montreal Protocol which calls for its complete phase out since January 2005 in developed countries. Italy, however, asked and obtained large exemptions in critical use, i.e., cultivation of high value-added agricultural products. Smaller exemptions have been obtained by other European countries. Identification and quantification of natural sources with respect to anthropogenic ones is important because the calculated atmospheric budget of this compound is largely out of balance, with identified sinks outweighing identified sources.

In order to identify source regions of halocarbons, a combination of in situ measurements and back trajectory (BT) analysis is used: when air masses containing concentration peaks higher than background value reach the station, the BT approach allows to identify potential source regions.

Applying this method, HFCs potential source distributions confirm a high frequency of occurrence in the whole considered domain (Europe), with maxima values of frequency of occurrence mainly occurring in the Po Basin. On the contrary, methyl bromide potential sources show a more scattered spatial distribution with intense potential sources in the Mediterranean area.

However, all methods based on such approach assign a potential probability to each grid cell crossed by a marked back-trajectory along its way. Therefore, "ghost" potential sources can be generated in the lee of real source. Such an inconvenience can be overcome combining results from different stations. Such an approach has been shown in a recent study (Maione et al., submitted) where data from Mt. Cimone have been combined with those from the Alpine station of Jungfraujoch (Switzerland). In this case, the method has been applied to the anthropogenic HFCs, for which a very strong source region (i.e., Po basin) is located in between the two stations. In Figure 8, results referred to HFC-152a are shown. Maps *a* and *b* report potential source region as from concentration data collected at Mt. Cimone

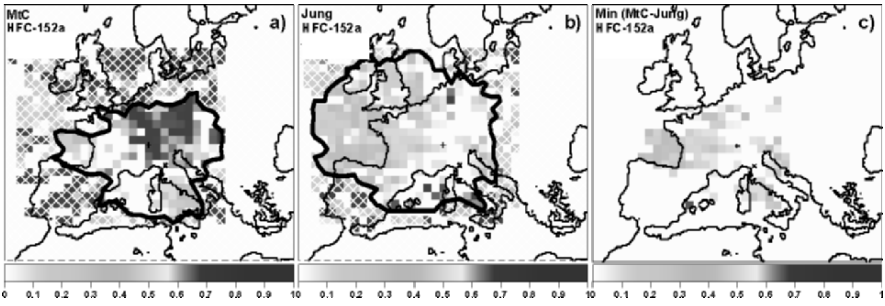

Figure 8. a) Map of conditional probability of potential sources of HFC-152a. The map is obtained using concentration data collected at Mt. Cimone. Continuous black line encloses grid cells whose PBL has been visited by at least 20 back-trajectories over the entire data set. (x) symbol refers to Mt. Cimone; (+) symbol refers to Jungfraujoch. b) As in a), but for data collected at Jungfraujoch. c) Map of conditional probability of potential sources for HFC-152a. The map is obtained considering for each cell the minimum P(i, j) value between that estimated by Mt. Cimone and Jungfraujoch; i.e., for each cell the minimum value between maps in Figure 2a) and Figure 2b). P(i, j) has been evaluated only for grid cells whose PBL has been visited by at least 20 back-trajectories for both Mt. Cimone and Jungfraujoch data (Source, Maione et al., submitted)

and Jungfraujoch, respectively. Map *c* is obtained considering for each cell the minimum value between that estimated by Mt. Cimone and Jungfraujoch. It can bee seen how this simple approach reduces the unrealistic localization of "ghost" source in the lee of real source and it is able to evidence localized area sources. The efficiency of the proposed method is a func tion of relative position of receptor sites and of emission sources, with the maximum efficiency obtained for source areas that are in between of the receptor sites. However, when estimating potential source regions for a compound such as methyl bromide, for which the Mediterranean area (ocean and agricultural activities) is the most important source region, two stations located to the North on the Mediterranean are redundant. In this case, a station located in the Southern Mediterranean (i.e. Northern Africa) should provide more useful information.

3. Conclusions

The analyses of the behavior of climate-altering trace gases concentrations recorded at Mt. Cimone can provide the opportunity to draw interesting conclusions concerning their behavior, and also help in attaining a better knowledge of transport phenomena. Moreover, a number of Saharan dust transport episodes with a high particulate concentration can be studied.

For this reason it is important to have continuous measurements at a baseline site which is representative of a large area of Europe and the Mediterranean Basin.

However, even if the station is considered to be representative of continental Europe as well as of the Mediterranean region, the latter can be monitored only marginally. As a matter of fact, in this region, atmospheric circulation frequently exhibits a meridional component facilitating the transport of tracers between Europe and North Africa. Many compounds exhibit a high meridional gradient of emission but the presently available stations do not have a proper spatial distribution allowing to show it.

For these reasons, a remote station in the southern side of the Mediterranean basin not only would provide useful information but also powerful synergies with other European stations.

4. Acknowledgments

The authors thank P. Cristofanelli, J. Arduini, F. Furlani and L. Belfiore for collaboration in the Mt. Cimone data analyses; the Italian Air Force Meteorological Service for support at the Mt. Cimone Station. Special thanks is due to P. Giambi, F. Calzolari and U. Bonafè for technical assistance at

"O. Vittori" Mt.Cimone station. Research activities have been supported by the EU Projects CARBOEUROPE, MINATROC, STACCATO, SOGE, and ACCENT.

5. References

Bian H. and Zender C. S., 2003, Mineral dust and global tropospheric chemistry: Relative role of photolysis and heterogeneous uptake, *J. Geophys. Res.*, **108** (D21):4672.

Bonasoni P., Stohl A., Cristofanelli P., Calzolari F., Colombo T., Evangelisti F., 2000, Background ozone variations at Mt. Cimone Station. *Atmos. Environ.* **34**:5183-5189.

Bonasoni P., Cristofanelli P., Calzolari F., Bonafè U., Evangelisti F., Stohl A., Zauli Sajani S., van Dingenen R., Colombo T., and Balkanski Y., 2004, Aerosol-ozone correlations during dust transport episodes, *Atmos. Chem. Phys.*, **4**:1201-1215.

Ciattaglia L., Cundari V., and Colombo T., 1987, Further measurements of atmospheric carbon dioxide at Mt. Cimone, Italy:1979-1985. *Tellus* **39B**:13-20.

Colombo T., Santaguida R., Capasso A., Calzolari F., Evangelisti F., and Bonasoni P., 2000, Biospheric influence on carbon dioxide measurements in Italy. *Atmos. Environ.* **34**:4963-4969.

Cristofanelli P., Bonasoni P., Carboni G., Calzolari F., Casarola L., Zauli Sajani S., Santaguida R., 2007, Anomalous high ozone concentrations recorded at a high mountain station in Italy in summer 2003. *Atmos. Environ.* **41**:1383-1394.

Dentener F. J., Carmichael G. R., Zhang Y., Lelieveld J., and Crutzen P. J.: The role of mineral aerosols as a reactive surface in the global troposphere, 1996, *J. Geophys. Res.*, **101**, 22 869-22 889.

Fischer H., Kormann R., Klupfel T., Gurk C., Konigstedt R., Parchatka U., Muhle J., Rhee T.S., Brenninkmeijer C.A.M., Bonasoni, P., Stohl A., 2003, Ozone production and trace gas correlations during the June 2000 MINATROC intensive measurement campaign at Mt. Cimone. *Atmos. Chem. Phys.* **3**:725-738.

Greally B. R., Manning A. J., Reimann S., McCulloch A., Huang J., Dunse B. L., Simmonds P. G., Prinn R. G., Fraser P. J., Cunnold D. M., O'Doherty S., Porter L. W., Sturrock G. A., Stemmler K., Vollmer M. K., Lunder C. R., Schmidbauer N., Hermansen O., Arduini J., Salameh P. K., Krummel P. B., Wang R. H. J., Folini D., Weiss R. F., Maione M., Nickless G., Stordal F., and Derwent R. G., 2007, Observation of 1,1-difluoroethane (HFC-152a) at AGAGE and SOGE monitoring stations 1994-2004 and derived Global and regional emission estimates. *J. Geophys. Res*, In Press.

Logan J. A., 1985, Tropospheric ozone: seasonal behaviour, trends and anthropogenic influence. *J. Geophys. Res.* **90**:10463-10482.

Maione M., Giostra U., Arduini J., Belfiore L., Furlani F., Geniali A., Mangani G., Vollmer M.K., Reimann S., Localization of potential sources of non-CO_2 greenhouse gases combining data collected at two European mountain Stations. Submitted to *Sci. of Tot. Environ.*

Maione M., Arduini J., Mangani G., Geniali A., 2004, Evaluation of an Automated Gas Chromatographic - Mass Spectrometric Instrumentation to be Used for Continuous Monitoring of Trace Anthropogenic Greenhouse Gases. *Intern. J. Environ. Anal. Chem.* **84**(4): 241-253.

Martin R. V., Jacob D. J., Logan J. A., et al., 2002, Interpretation of TOMS observations of tropical tropospheric ozone with a global model and in situ observation, *J. Geophys. Res.*, **107**(D18), 4351, doi:10.1029/2001JD001480.

O'Doherty S., Cunnold D. M., Manning A., Miller B. R., Wang R. H. J., Krummel P. B., Fraser P. J., Simmonds P. G., McCulloch A., Weiss R. F., Salameh P., Porter L. W., Prinn R. G., Huang J., Sturrock G., Ryall D., Derwent R. G., and Montzka S. A., 2004, Rapid growth of hydrofluorocarbon 134a and hydrochlorofluorocarbons 141b, 142b, and 22

from Advanced Global Atmospheric Experiment (AGAGE) observations at Cape Grim, Tasmania, and Mace Head, Ireland. *J. Geophys. Res.*, **109**, D06310, doi:38 10.1029/ 2003JD004277.

Prodi F. and Fea G., 1979, A case of transport and deposition of Sahara dust over the Italian Peninsula and Southern Europe, *J. Geophys. Res.*, **84C**: 6951-6960.

Reimann S., Schaub D., Stemmler K., Folini D., Hill M., Hofer P., Buchmann B., Simmonds P. G., Greally B., and O'Doherty S., 2004, Halogenated greenhouse gases at the Swiss High Alpine Site of Jungfraujoch (3580 m asl). Continuous measurements and their use for regional European source allocation. *J. Geophys. Res.* **109**, D05307, doi:10.1029/ 2003JD003923.

Santaguida R., Carboni G., di Sarra A.G., in press*, in WMO. 2006. 13th WMO/IAEA meeting of experts on carbon dioxide concentration and related tracers measurement techniques*. National Repor, Boulder (CO), USA, September 2005.

Schmitt R. and Schreiber B. 1998, Effect of long-range transport on atmospheric trace constituents at the baseline station Tenerife (Canary Islands). *J. Atmos. Chem.*, **1**:335-351.

Stohl A., Spichtinger-Rakowsky N., Bonasoni P., Feldmann H., Memmesheimer M., Scheel H. E., Trickl T., Hubener S., Ringer W., and Mandl M., 2000, The influence of stratospheric intrusions on alpine ozone concentrations. *Atmos. Environ*. **34**: 1323-1354.

Thoning K., Tans P. P., and Komhyr W. D., 1989, Atmospheric carbon dioxide at Mauna Loa observatory, 2: Analysis of the NOAA GMCC data, 1974-1985. *J. Geophys. Res.* **94**: 8549-8565.

Zhang Y., Sunwoo Y., Kotamarthi V., and Carmichael G. R., 1994, Photochemical oxidant pro-processes in the presence of dust: An evaluation of the impact of dust on particulate nitrate and processes ozone formation, *J. Appl. Met.*, **33**:813-824.

KEY PROCESSES FOR DUST EMISSIONS AND THEIR MODELING

GILLES BERGAMETTI*
LISA, Universities Paris7 and Paris12, UMR CNRS 7583, CMC, 61 avenue du Génaral de Gaulle, F 94010 Créteil, France

BEATRICE MARTICORENA
LISA, Universities Paris7 and Paris12, UMR CNRS 7583, CMC, 61 avenue du Génaral de Gaulle, F 94010 Créteil, France

BENOIT LAURENT
LISA, Universities Paris7 and Paris12, UMR CNRS 7583, CMC, 61 avenue du Génaral de Gaulle, F 94010 Créteil, France

Key Words: Dust emissions; erosion processes; threshold friction velocities; horizontalt flux; vertical flux**.**

1. Introduction

At the beginning of the nineties, many attempts have been made to simulate the desert dust cycle and its impacts at a global scale, mainly by using general circulation models (Joussaume, 1990, 1993; Genthon, 1992). However, these simulations generally failed in reproducing the present data or the information retrieved for the Last Glacial Maximum (Gaudichet et al., 1992; Grousset et al., 1992). According to the authors, deficiencies in the source parameterization accounted for a large part of the observed discrepancies. Generally, in those simulations, the dust production function was only dependent on the extent of the desert regions and on the wind velocity. Indeed, dust emissions were always defined as a continuous function of the wind velocity, whereas many experiments clearly indicate that the dust mobilization occurs only for wind velocities higher than a threshold value and that the production is not linearly dependent on the wind velocity (Bagnold, 1941; Gillette et al., 1982; Nickling and Gillies, 1989). The source regions were defined either like the present arid zones or according to the simulated mean aridity assuming that all the desert zones were emission areas of equal erodibility. In fact, it has been experimentally shown that the erodibility depends strongly on the soil texture, the soil type and the ground surface characteristics (vegetation cover, rocks, and pebbles) (Gillette,

* To whom correspondence should be addressed.

A. Mellouki and A.R. Ravishankara (eds.), Regional Climate Variability and its Impacts in the Mediterranean Area, 63–81.

1979; Marticorena and Bergametti, 1995; Marticorena et al., 1997a; Shao and Lu, 2000). The lack of such soil features dependence in the source parameterization may explain shortcomings in the simulations concerning the underestimation or overestimation of dust production for specific regions.

Indeed, these surface features control both the aeolian erosion thresholds and the intensity of the dust fluxes. As a result, dust emissions are sporadic and spatially heterogeneous, making difficult any assessment of their impacts. During the last ten years, physical dust emission schemes representing the influence of the wind velocity and the surface features on the dust production have been developed and validated during the last ten years (Marticorena and Bergametti, 1995; Marticorena et al., 1997a; Shao et al., 1996; Shao, 2001). This paper reviews the major dust emission processes and of the way by which they are presently accounted for into regional or global scale dust models.

2. Aeolian Threshold Friction Velocity

The force exerted on a grain by wind is the shear stress. This shear stress can be expressed as $\tau = \rho_a u^{*2}$ where ρ_a is the air density, u^* is the wind friction velocity defined in neutral conditions as $u_{(z)} = u^*/K \ln z/z_0$ where $u_{(z)}$ is the wind velocity at a height z above the surface, z_0 is the aerodynamic roughness height and K is the Von Karman's constant (≈0.4). Thus, the wind friction velocity can be considered as the relevant parameter to quantify the energy provided by wind to an erodible surface.

2.1. THRESHOLD FRICTION VELOCITY VERSUS SOIL PARTICLE SIZE

It can be easily observed that dust emissions do not occur for any wind velocity conditions: indeed, dust emissions only occur when the wind velocity (and thus the wind friction velocity) exceeds a certain value. This wind (friction) velocity value is called the threshold wind (friction) velocity. It is a key parameter in the modelling of wind erosion and dust emissions.

Experimental data from Bagnold (1941) and Chepil (1945) indicated that, for large grains, the threshold friction velocity, u_t^*, increases when the grain size increases (due to the gravity forces). However, they also revealed an increase of the threshold friction velocity values when the size grain decreases for the smallest particles mainly due to the existence of interparticles cohesive forces reinforcing the links between grains (Iversen et al., 1976; Iversen and White, 1982). These two effects lead to an optimum grain size (~80 μm) for which the threshold friction velocity is minimum (Figure 1).

At the threshold for aeolian erosion, the aerodynamic forces due to the fluid equal the particle weight and the interparticle cohesive forces. Based on a large set of measured threshold friction velocities obtained in wind

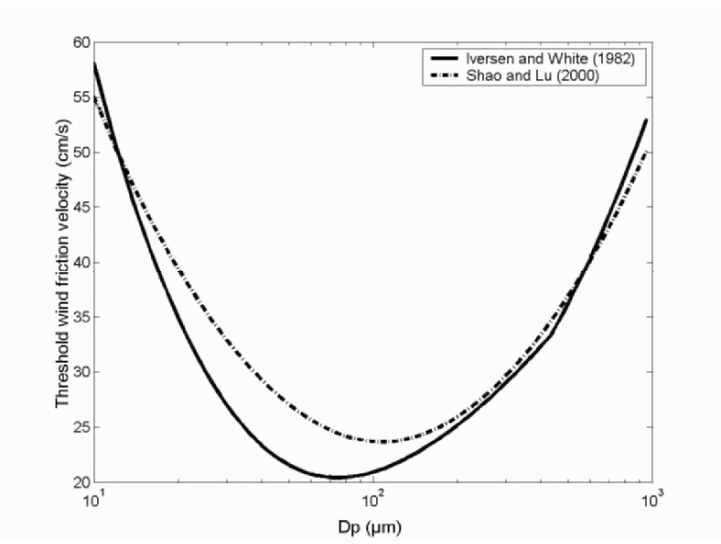

Figure 1. Parameterization of the threshold friction velocity (U_t^* in $cm.s^{-1}$) versus particle diameter (Dp in μm) for smooth surfaces according to Iversen and White (1982) and Shao and Lu (2000)

tunnels and involving various particle densities and diameters, Iversen and White (1982) established a semi-empirical formulation based on the equilibrium of the forces acting on a spherical loose particle at rest on a similar particle bed under an air flow stream. The difficulty in using their expression into models is that it requires iterative calculations to determine U_t^* versus the grain size and thus needs to be approximated (Marticorena and Bergametti, 1995). More recently, Shao and Lu (2000) proposed a more simple and effectt-ive expression based on the balance between the driving forces (aerodynamic drag and lift) and the retarding forces (cohesion and gravity) assuming that the cohesive force is proportional to the particle size.

In a natural soil, various soil grain sizes are simultaneously present. Since theses grains of different sizes have different threshold wind friction velocities, this implies to describe into models the in situ soil size distribution of grains and aggregates.

Existing soil maps generally classify soils according to the "well-known textural triangle" defined by the three size components: sand (2000 to 80 or 63 μm), silt (80 or 63 to 4 or 2 μm) and clay (<4 or 2 μm) (Chatenet et al., 1996; Ding et al., 1999). However, this classification is based on measurements performed by using wet sedimentation techniques (ultrasonic pretreatment, dissolution), which break the soil aggregates (Chatenet et al., 1996; Ding et al., 1999). As an example, such classification leads to relatively high amounts of loose clay particles that are generally not encountered in

the natural soils as loose particles. In natural soils, these particles generally form aggregates of larger size (>50-100 μm)As a result, such a classification cannot be directly used to characterize the in-situ size distributions of erodible soils. An alternative approach is to determine the soil size distribution using dry techniques that minimize, as much as possible, the breakage of the aggregates. Such an approach has been proposed by Chatenet et al. (1996) for the Saharan and Sahelian soils and applied to Chinese soil samples by Mei et al. (2004). In these works, the soil grain size is assumed to be log-normally distributed or to be the combination of 2 or 3 different log-normal distributions. However, the present data sets of such measurement remain relatively limited and not homogeneous in terms of analytical methods. Thus, there is a clear need for both standardized methods and sampling programs allowing a correct mapping of the in situ size distributions of desert erodible soils.

2.2. THRESHOLD FRICTION VELOCITY VERSUS SURFACE ROUGHNESS

A second factor that strongly affects the erosion threshold in natural situations is the presence on an erodible surface of non-erodible elements (pebble, stones, vegetation…). These non-erodible elements affect the erosion threshold by two ways. On one hand, the roughness elements cover a fraction of the surface and thus protect it from the aeolian erosion; on the other hand, they consume a part of the wind momentum that will not be available to initiate particle motion. This leads to a global decrease of the wind shear stress acting on the erodible surface and thus of the erosion efficiency. So, a physical scheme describing the drag partition between the roughness elements and the erodible surface is necessary to parameterize the threshold wind friction velocity in "rough" situations which are the most frequently encountered in arid and semi-arid areas.

Based on an approach proposed by Schlichting (1936), Marshall (1971) expressed the overall shear stress caused by wind passing over a roughened surface as being partitioned between stress on the roughness elements and stress on the non-covered surface:

$$\tau = \rho_a u^{*2} = \frac{W_R}{S} + \frac{S'}{S}\tau_S$$

where τ corresponds to the overall shear stress, S is the total surface; S' refers to the uncovered part of the surface; W_R is the force exerted on the roughness elements and τ_S is the shear stress acting on the uncovered surface.

The force exerted on the roughness elements and thus their momentum absorption is primarily controlled by their frontal surface. That is why the

description of the drag partition generally involves a roughness density, λ, which is defined by:

$$\lambda = \frac{nbh}{S}$$

where n is the number of roughness elements; b is the mean breadth of the roughness elements and h is the mean height of the roughness elements.

To investigate the relation between the drag partition and λ, Marshall (1971) has performed wind-tunnel measurements of the overall shear stress and of the forces acting on the roughness elements for a large range of roughness densities. Roughly, τ_S decreases as the roughness density increases and becomes negligible for a value of $\lambda = 0.03$. This provides an estimation of the critical value of the roughness density for which the decrease of the wind shear stress on the uncovered surface is such that it inhibits erosion.

The consequence of the drag partition on erosion is that erodible surfaces covered with roughness elements have higher apparent threshold wind friction velocities than surfaces with less roughness elements. For erosion to occur, the shear stress component acting on the erodible surface must at least equal ($\rho_a U_{ts}^{*2}$) which is the shear stress corresponding to the threshold wind friction velocity in a "smooth" situation. This explains why the threshold friction velocities U_t^* measured in situations with roughness elements are apparently higher than in smooth situations.

To determine predictive expressions for practical applications, Raupach (1992) proposed an analytical treatment of the drag partition on a rough surface based on a dimensional analysis and physical hypothesis. His expression gives the ratio of the overall shear stress to the shear stress on the uncovered surface as a function of λ. The predictions based on this equation agree well with Marshall (1971)'s data and other measurements performed in wind tunnel or for natural sites, and thus this formulation can be considered as the best available to retrieve the drag partition on a rough surface. One of the advantages of the expression was to be predictive and to be free of any adjustable constant; but when applied to real situations, this formulation requires the introduction of an empirical parameter called *m*. Raupach et al. (1993) indicates that this parameter could reflect the differences between the average substrate surface stress and the maximum stress on the surface at any point. The adjustment of this equation to erosion data has lead to the recommendation of two kinds of values for *m* according to the stabilization state of the particle bed; but no objective method to generalize these values exists and this coefficient does not refer to any measurable value. Indeed, the practical use of this equation as a predictive tool is not direct.

An alternative specification of the drag, using a more integrative parameter to represent the effect of the roughness elements, is that based on the

roughness height, z_0. Such an approach has been first developed by Arya (1975) to determine the wind stress on the Arctic pack ice.

As mentioned above, under adiabatic conditions the wind profile in the atmospheric boundary layer (ABL) is logarithmic (Priesley, 1959) and defined, for $z >> z_0$, as:

$$u_{(z)} = \frac{u_*}{K} ln \frac{z - D}{z_0}$$

where $u_{(z)}$ is the wind velocity at the height z; K the Von Karman's constant (≈0.4); U^* is the wind friction velocity, D is the displacement height and z_0 is the aerodynamic roughness height.

Then, for situations where roughness elements are not too closely spaced ($\lambda < 0.05$), Arya (1975) assumes that an internal boundary layer (IBL) grows behind the roughness elements. The development of this IBL is considered to be similar to the development of the IBL occurring after a sudden change in roughness, a problem thoroughly investigated both theoretically and experimentally. When the equilibrium with the new surface has been reached, Arya (1975) assumed that the wind profile in the IBL also follows a logarithmic law.

At the top of the IBL is a blending zone which represents the wake effect of a single element. Far downstream from the element, this effect becomes very weak and this transition zone is thin enough to be neglected. The height of the IBL δ can then be defined as the height where the two profiles intersect. Thus when the flow comes to equilibrium with the surface, the wind velocity at the height δ satisfies both the two logarithmic laws. Thus the ratio of local to total shear stress is defined by:

$$\frac{\tau_S}{\tau} = \left(\frac{U_S^*}{U^*} \right)^2 = \left(\frac{\ln\left(\frac{\delta}{Z_0} \right)}{\ln\left(\frac{\delta}{z_{0s}} \right)} \right)^2$$

For convenience, an efficient friction velocity ratio f_{eff} is defined as the ratio of local to total friction velocity:

$$f_{eff} = \frac{U_S^*}{U^*} = 1 - \left(\frac{\ln\left(\frac{Z_0}{Z_{0s}} \right)}{\ln\left(\frac{\delta}{z_{0s}} \right)} \right)$$

Marticorena and Bergametti (1995) adapted this expression to erosion threshold, especially by defining the value of δ and validated it by comparing predictions with Marshall, (1971)'s data. The final drag partition parameterization is expressed by:

$$f_{eff} = \frac{U_s^*}{U^*} = 1 - \left(\frac{ln\left(\frac{Z_0}{z_{0s}}\right)}{ln\left(0.35\left(\frac{10}{z_{0s}}\right)^{0.8}\right)} \right)$$

z_0 and z_{0s} having units of centimeters.

By combining the size-dependent equation established by Iversen and White (1982) and the efficient ratio previously defined, an expression of the threshold wind friction velocity in a rough situation and depending on the soil grain size is obtained:

$$U_t^*(D_p; Z_0; z_{0s}) = \frac{U_{ts}^*(D_p)}{f(Z_0, z_{0s})}$$

2.3. VALIDATION OF PARAMETERIZATION OF THE EROSION WIND FRICTION VELOCITY THRESHOLDS

The drag partition scheme has been applied to retrieve experimental measurements of erosion threshold wind friction velocity for natural soils. Measurements of the threshold wind friction velocities were obtained by Gillette et al. (1982) and Nickling and Gillies (1989), by using portable wind tunnels, on various erodible sites of the United States. Since such measurements involve a small fetch and are thought to be representative of the eroded surface, the required conditions for the determination of the roughness height are assumed to be fulfilled.

For both experiments, the roughness heights were determined from wind velocity profiles. The threshold wind friction velocities have been measured at the moment where particles motion was first visible and thus will correspond to particle size for which the movement is most easily initiated. A reference value of the threshold wind friction velocity ($U_t^*(D_p) \approx 21.7$ cm s^{-1}) is used to perform the computations; it corresponds to a range of a particle diameter of 120 μm, which is compatible with the available information on the grain size characteristics of the tested soils. Figure 2 shows that the

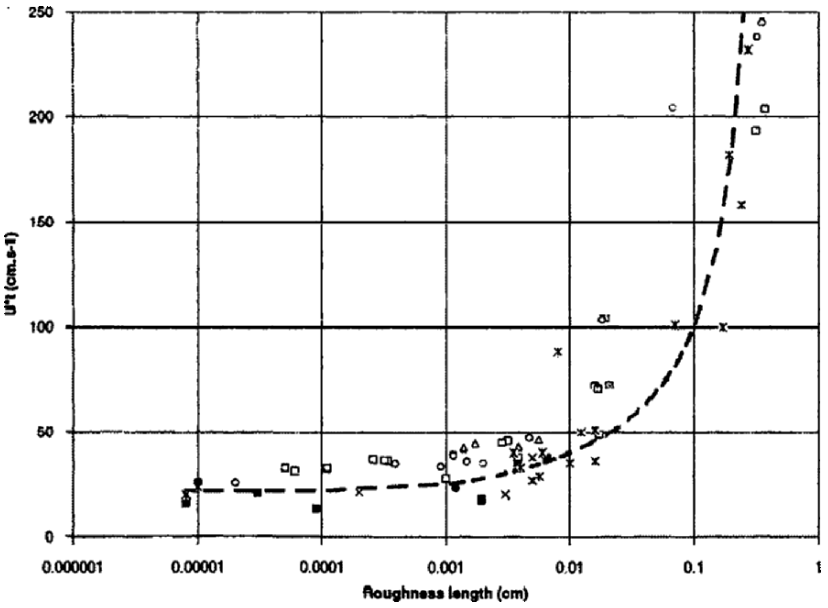

Figure 2. Comparison between computed and measured threshold wind friction velocities as a function of the roughness height (from Marticorena et al., 1997b)

model prediction matches the threshold wind friction velocities observed for various roughness heights. The discrepancies with (Gillette et al. (1982)'s measurements are generally lower than 30%, with a better agreement in the range of 20 to 60 cm s^{-1} (Marticorena et al., 1997b). The latter wind frictions velocities can be reached under reasonable wind conditions and thus correspond to situations where erosion could frequently occur. The agreement with the values reported by Nickling and Gillies (1989) remains quite satisfying, although larger discrepancies, probably due to the averaging of measurements, are observed.

When applied to regional and global scales dust models, such drag partition scheme induces a problem similar to that encountered for the mapping of the soil grain size distributions: how can we obtain a map of aeolian roughness heights over desert areas? A first method was developed for the Sahara desert by Marticorena et al. (1997a) and Callot et al. (2000). This approach, based of a geomorphologic approach, lead to satisfying results since simulations of dust emissions using these roughness heights compared satisfyingly with satellite observations (Marticorena et al., 1997a). However, this approach was very time consuming and its extension to others deserts was very dependent on the number and quality of the available geomorphologic information.

Thus, an alternative approach was to examine how satellite observations could provide a global mapping of the aeolian roughness height. Following the pioneer work performed by Greeley et al. (1997) who used the radar backscatter signal to retrieve the roughness heights over selected desert targets, Marticorena et al. (2004) investigated the possibility to retrieve the surface roughness of arid areas using the surface bi-directional reflectance products derived from the POLarization and Directionality of the Earth Reflectance (POLDER-1) space-borne. An empirical relationship between the aerodynamic roughness height and a protrusion coefficient (PC) derived from the POLDER-1 bi-directional reflectance distribution function in the visible range was established. Thus, maps of roughness height at a scale of 1/16° × 1/16° (Figure 3) were established for the Sahara and the Chinese deserts (Marticorena et al., 2004, Laurent et al., 2005). When applied over the Sahara and the Arabian Peninsula, this method leads to a good agreement between simulated dust event frequencies and those derived from Infrared METEOSAT Dust Index (IDDI) (Marticorena et al., 2004).

This approach was further extended to radar backscatter coefficient from high resolution ERS images based on situ measurements of aeolian roughness heights, performed in Tunisia (Marticorena et al., 2006). This new relationship provides an operational tool to derived surface roughness maps for local to regional applications.

Thus, most of the physical processes and input data required to correctly describe the effects of the roughness height on threshold wind friction velocities into dust models are available. These new parameterizations, combined with the new data sets of roughness heights, should allow to better account for the difference in erodability of desert surfaces in large scale models dealing with the dust transport.

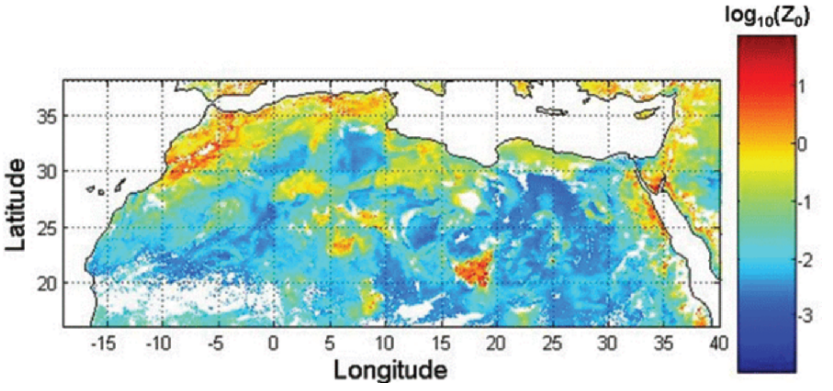

Figure 3. Map of the aeolian roughness heights for the Sahara desert as retrieved from the Polder BRDF measurements (adapted from Marticorena et al., 2004)

2.4. THRESHOLD FRICTION VELOCITY VERSUS SOIL MOISTURE

Another factor affecting the threshold wind friction velocities is the soil moisture. Briefly, the soil water reinforces the cohesive forces between the soil grains and thus increases the erosion thresholds. However, soil water retention consists of molecular adsorption on the soil grains surface and capillary forces between the grains (Mc Kenna and Nickling, 1989). Interparticle capillary forces are the main factor responsible for the increase of the wind erosion threshold observed when the soil moisture increases. Below a soil moisture content close to the maximum amount of adsorbed water, w', these capillary forces are considered as being not strong enough to significantly increase the erosion threshold. Since w' depends on the soil texture, the increase in erosion threshold is different for the same soil water content depending on the soil type.

A parameterization of the influence of the soil moisture (w) on the erosion threshold has been proposed by Fécan et al. (1999). It allows the computation of the increase of the erosion threshold in wet conditions by reference to dry conditions as a function of the soil moisture w and the residual soil moisture w' defined as a function of the soil clay content.

$$\frac{U^*_{tw}}{U^*_{td}} = \left[1 + 1.21\,(w - w')^{0.68}\right]^{0.5} \quad \text{for } w > w'$$

with $w' = 0.0014\ (\%\ clay)^2 + 0.17\ (\%\ clay)$.

This formulation is presently largely used, in connection with soil texture maps, in regional and global scale dust models to account for the effect of soil moisture on threshold wind friction velocities.

2.5. THRESHOLD FRICTION VELOCITY FOR AGRICULTURAL SOILS

Semi-arid areas are of special interest in terms of future dust emissions. Indeed, in these areas, the vegetation, which has a protective role for the surface, is clearly limited by the availability in water. Thus, any change in climate which affects the precipitation regime in these areas should lead to significant changes in both the dust sources location and strength. Moreover, in semi-arid areas, the growing of the population leads to an intense land use, especially for agricultural and pastoral activities. Even if the estimation of the importance of dust emissions related to anthropogenic activities significantly differs from one model to another (Mahowald and Luo, 2003; Tegen et al., 2004), their contribution should be included in any global dust emissions model.

A particular problem addresses by erodible anthropogenic surfaces is that of tilled surfaces. The presence of ridges on such surfaces can: 1 - affect the wind profile by modifying the surface aerodynamic roughness height, and 2 - affect the erosion flux by trapping a part of the saltating soil grains into the furrows. Obviously, these effects are highly dependent on the geometry of the ridges, i.e., mainly their height and spacing.

Recently, wind tunnel experiments were realized to determine the relationships linking both the roughness height and the erosion flux to the height and spacing for a variety of ridges (Kardous et al., 2005a; 2005b). Parameterizations for both the roughness height and the erosion flux was developed and validated against wind tunnel experiments and existing published data (Hagen and Armbrust, 1992). The interest of this work is mainly that these parameterizations are only based on the geometric characteristics of the ridges (height and spacing) and thus should be easily included into dust models, provided information on land use and agricultural practices.

3. Horizontal and Vertical Fluxes

In dust emissions modelling, there are two important fluxes to determine:

- The horizontal flux (also called saltation flux) which quantifies the soil material crossing a vertical plane perpendicular to the soil surface per unit time; this flux concerns all the material mobilized directly or indirectly by wind (i.e., particles from less than 1 μm to about 1000 μm);
- The vertical flux which quantifies the mass of fine particles passing through a horizontal unit area, parallel to the soil surface, per unit time.

The vertical flux is also called dust flux since it corresponds to the flux of particles having a size allowing medium or long-range transport (i.e., generally less than about 50 μm).

As we will see latter in more details, these two fluxes are directly linked, the vertical flux being both a part and a consequence of the horizontal flux.

3.1. HORIZONTAL FLUX

Assuming that, for wind above the wind erosion threshold, all the wind momentum is transferred to the surface by the saltating grains and based on dimensional arguments, Bagnold (1941) suggested that the horizontal flux is proportional to a third power of the wind friction velocity. Such dependence has been experimentally observed in natural situations or in wind tunnel, especially for large values of u_* (Gillette, 1974, 1979; Gillette and Stockton, 1989; Sörensen, 1985; Leys and Raupach, 1991; Shao et al.,

1993). Using a trench on a beach, Greeley et al. (1994) have performed horizontal flux measurements with a high confidence level (5% in mass) allowing the evaluation of the various equations proposed to retrieve the horizontal fluxes. These authors found that Bagnold (1941)'s model and White (1979)'s formulation most closely agree with the experimental data. But since only White's equation includes a threshold term and is supported by a dimensional analysis, we can consider this one as the best available formulation for the horizontal flux:

$$G = C\frac{\rho_a}{g}U^{*3}\left(1+\frac{U_t^*}{U^*}\right)\left(1-\frac{U_t^{*2}}{U^{*2}}\right)$$

with C a constant of proportionality with a value of 2.61 determined from wind tunnel experiments (White, 1979), this value being confirmed by the results of the Greeley et al.'s (1994) experiment.

Including in White (1979)'s equation, for an ideal case (i.e., all particles having the same diameter), the parameterization of the threshold wind friction velocity previously discussed (see 2.2) leads to express the horizontal flux as:

$$G(D_p) = E\,C\frac{\rho_a}{g}U^{*3}\left(1+R\right)\left(1-R^2\right)$$

where $R=\dfrac{U_t^*(D_p,Z_0)}{U^*}$ and E is the ratio of the erodible surface to the total surface.

The problem in applying this formulation to natural situations is, as mentioned above, that the soil grains are generally not characterized by a unique diameter. Thus, the relative contribution of each size range to the total flux is assumed to be proportional to the relative surface it occupies on the total surface. The surface covered by each grain is assimilated to its basal surface. The total horizontal flux is then computed by integrating the previous distribution on the studied range of particle diameters.

3.2. VERTICAL FLUX

The vertical flux is composed by the finest particles setting in suspension from the saltation layer and able to be long-range transported. The suspension-saltation boundary is controlled by the ratio of the threshold friction velocity

and the terminal velocity of the particles. The terminal velocity is defined by the equilibrium of the particle weight and the wind drag and so depends on the particle diameter and density. The value of the particle diameter for saltation-suspension boundary is about 50 μm (Greeley and Iversen, 1985). However, as mentioned above, particles with a diameter lower than this limit involve very high threshold friction velocities due to the strong cohesive forces linking them together (see Figure 1). Thus the movement of these fine particles is not initiated directly by the wind friction on the erodible surface but requires an intermediate process called "sandblasting" which corresponds to the bombardment of the aggregates present on the surface by the saltating grains. This phenomenon is responsible for the disruption of the aggregates and for the production of dust particles able to be set in suspension (Gillette, 1979, 1981; Gomes et al., 1990; Shao et al., 1993). Since the dust production implies saltation as an intermediate process, the vertical flux is generally derived from the horizontal one.

To investigate more thoroughly the relation between the horizontal and vertical fluxes, wind tunnel experiments of saltating sand grains on a loose dust bed were performed (Shao et al., 1993; Alfaro et al., 1997). These measurements show that both the total flux and the dust flux are proportional to a power 3 of the wind velocity. This result also confirms that the dust production corresponds to the rupturing of the interparticle bonds linking dust particles together or to the surface. When the saltating grains impact on the surface, their kinetic energy is used to disintegrate the aggregates and to produce fine dust particles. Thus, models have been elaborated by these authors (Alfaro et al., 1997; 1998; Lu and Shao, 1999; Alfaro and Gomes, 2001; Shao, 2001) to simulate this sandblasting process. Briefly, the model proposed by Alfaro et al. (1997; 1998), is based on the existence in aggregates of various binding energies depending on the size of the dust constituting the agregate. This implies that it exists different thresholds for the disruption of an aggregate and thus the dust size distribution should vary according to the kinetic energy of the saltating grains (and thus of their size and their velocity).

In contrast to energy based models, Lu and Shao (1999) estimated dust production on the basis of the volume removed by the saltating grains when they impact the surface. In this case, the saltation bombardment is considered as the main mechanism for dust production through the excavation of craters in the surface. The total volume of the grains ejected into the air is assumed to be equal to that of the crater created by the saltating grains. In 2001, Shao (2001) provided a more elaborated version of this model, including not only the saltation bombardment but also the aerodynamic entrainment and the aggregates disintegration.

When applied to large scale modelling of dust emissions, both sandblasting models have significant drawbacks. For energy based models, the values of

the binding energies is difficult to measure and thus they have been only indirectly determined by adjustment of their value to fit the size distributions of dust particles measured for different soils and different friction velocities (i.e., for different kinetic energy of the saltating grains). However, until these binding energies will be directly measured, they will remain quite uncertain and should require some adjustments to fit the experimental data sets (Gomes et al., 2003). For saltation bombardment models, the main problem is due to the value of the soil plastic pressure and that of a dimensionless coefficient c_y. However, both groups have recently provided new tests of their models (Alfaro et al., 2004; Shao, 2004) and their applicability at large scale could be considered in a next future. This is very important since only these types of physical schemes describing the processes involved in sandblasting can provide not the dust flux but also the dust size distribution.

4. Wind Velocity

Wind is obviously the driven force in aeolian processes. The accuracy of the wind velocity used in dust models is crucial. As mentioned above, the dust emissions have a highly non linear dependence to wind velocity: dust emission is a process involving a threshold and the strength of these emissions is a third power of the wind velocity. Due to that particular relation between wind and dust, limited errors on wind velocity could lead to large errors on dust emissions.

Figure 4 illustrates such a high sensitivity of the dust emissions to the accuracy in wind velocity. This figure reports the horizontal fluxes computed using the White (1979) equation for a surface exhibiting a threshold wind friction velocity equal to 30 cm s^{-1}. On this figure, the horizontal fluxes are normalized to the horizontal flux computed for u* = 35 cm s^{-1} which is assumed to be equal to 1.

For example, if we consider a wind friction velocity of 50 cm s^{-1} (for example, it corresponds to a 10 m high wind velocity of about 10 m s^{-1} for a surface having a roughness height of 0.35 cm) with an accuracy of +/– 5% (giving a range of wind friction velocities from 47.5 to 52.5 cm s^{-1}), we can observe that the difference in the computed horizontal fluxes is of the order of 1.5. This difference reaches a factor greater than 2 for accuracy of ±10%. This clearly points out that the dust emissions modelling is highly dependdent on the quality of the surface wind field used in the model.

Most of the dust model use wind fields provided by meteorological centres like National Centers for Environmental Predictions (NCEP) or European Centre for Medium Range Forecasts (ECMWF). Their spatial resolution is generally never better than about 1° × 1°. Other models, especially those treating feedbacks between dust and dynamics, use wind fields

computed on line by an atmospheric general circulation model. In this case, the resolution is generally lower (in the order of 2 to 5° × 2 to 5°). Such an "averaging" of the wind velocity over large areas tends to underestimate the wind velocity.

At least in certain locations (Tegen et al., 2002; Mahowald et al., 2002) and does not allow accounting for specific meteorological situations responsible for dust emissions (like squall lines). To limit these effects, some authors introduced additional parameterizations, mainly based on wind probability density functions, to account for the subgrid wind fluctuations (Westphal et al., 1988; Gillette and Passi, 1988; Cakmur et al., 2004).

If this type of approach is valuable for climatic simulations, the use of wind fields derived from well-resolved regional meteorological models (i.e., MM5 or RAMS) should be favoured for the simulations of specific events.

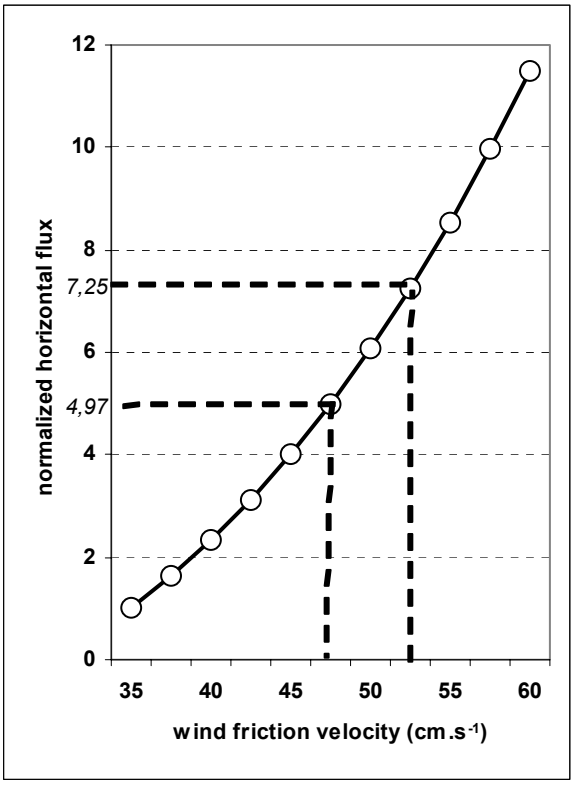

Figure 4. Horizontal fluxes computed using White (1979)'s formulation vs wind friction velocity (u*). Note that the horizontal fluxes are normalized to the horizontal flux for u* = 35 cm.s^{-1}. The dashed lines correspond to horizontal fluxes computed respectively for wind friction velocities equal to 47.5 and 52.5 cm.s^{-1} (see text for details)

5. Conclusion

This brief review of recent progresses performed in terms of dust emissions processes and modelling points out some key elements:

– During the last ten years, significant efforts have been made to develop dust emissions models based as much as possible on physical basis and allowing to better account for the heterogeneity of the surface features. This is a very important progress since a part of the spatial variability of the dust emissions is directly linked to differences existing between erodible surfaces in terms of grain size distributions, texture, roughness…
– At the same time, new techniques were developed, especially those derived from satellite observations, to provide the relevant surface data required by this type of models. A good example is the aeolian roughness height for which maps have been developed for Sahara and Asia and for which a global maps (i.e., for all arid desert areas) should be available very soon. In the same way, even if new data on the soil grain size distributions of desert areas remain necessary, the available data set has significantly growth, especially for Sahara and Asian deserts.
– Sandblasting models have been conceptually developed and should be operational very rapidly. This also should represent a significant progress since these models have the capability to simulate not only the dust flux but also the dust size distribution which is a key parameter to evaluate the log range transport and the impacts of dust.
– These recent developments have significantly reduced the uncertainties due to the parameterizations of dust processes and surface properties into dust models. However, a consequence of these progresses is that the uncertainty due to the accuracy of the surface wind velocity used in these models is becoming more and more evident. Thus, a large part of the future advances in dust modelling will probably result in our capability to provide better resolved and more accurate wind fields to these models.

6. References

Alfaro, S., Gaudichet, A., Gomes, L., and Maillé, M., 1997, Modeling the size distribution of a soil aerosol produced by sandblasting, *J. Geophys. Res.* **102:** 11,239-11,249.

Alfaro, S., Gaudichet, A., Gomes, L., and Maillé, M., 1998, Mineral aerosol production by wind erosion: aerosol particles size and binding energies, *Geophys. Res. Lett.* **25:** 991-994.

Alfaro, S. and Gomes, L., 2001, Modeling mineral aerosol production by wind erosion: emission intensities and aerosol size distributions in source areas, *J. Geophys. Res.* **106:** 18,075-18,084.

Alfaro, S., Rajot, J.L., and Nickling, W.G., 2004, Estimation of PM20 emissions by wind erosion: main sources of uncertainties, *Geomorphology*, **59:** 63-74.

Arya, S.P.S., 1975, A drag partition theory for determining the large-scale roughness parameter and wind stress on Arctic pack ice, *J. Geophys. Res.* **80:** 3447-3454.

Bagnold, R.A., 1941, *The Physics of Blown Sand and Desert Dunes,* Methuen, New York, 265 pp.

Cakmur, R.V., Miller, R.L., and Torres, O., 2004, Incorporating the effect of small-scale circulations upon dust emission in an atmospheric general circulation model, *J. Geophys. Res.* **109:** doi:10.1029/2003JD004067.

Callot, Y., Marticorena, B., and Bergametti, G., 2000, Geomorphologic approach for modelling the surface features of arid environments in a model of dust emissions: application to the Sahara desert, *Geodin. Acta* **13:** 245-270.

Chatenet, B., Marticorena, B., Gomes, L., and Bergametti, G., 1996, Assessing the microped size distributions of desert soils erodible by wind, *Sedimentology*, **43:** 901-911.

Chepil, W.S., 1945, Dynamics of wind erosion. *Soil Sci.* **60:** 305-320.

Ding, Z.L., Ren, J.Z., Yang, S.L., and Liu, T.S., 1999, Climate instability during the penultimate glaciation: evidence from two high resolution loess records, China, *J. Geophys. Res.* **104:** 20,123-20,132.

Fécan, F., Marticorena, B., and Bergametti, G., 1999, Parameterization of the increase of the aeolian erosion threshold wind friction due to soil moisture for semi arid areas, *Annales Geophys.* **17:** 149-157.

Gaudichet, A., De Angelis, M., Jousseaume, S., Petit, J.R., Korotkevitch, Y., and Petrov, V.N., 1992, Comments on the origin of dust in Antarctica for present and ice age conditions, *J. Atmos. Chem.* **14:** 129-142.

Genthon, C., 1992, Simulations of desert dust and sea salt aerosols in Antarctica with a general circulation model of the atmosphere, *Tellus B* **44:** 371-389.

Gillette, D.A., 1974, On the production of soil wind erosion aerosols having the potential for long range transport, *J. Rech. Atmos.*, **8:** 735-744.

Gillette, D.A., 1979, Environmental factors affecting dust emission by wind erosion in *Saharan Dust,* C. Morales, ed., John Wiley, New York, pp. 71-94.

Gillette, D.A., 1981, Production of dust that may be carried great distances: origin, characteristics and effect on man, *Spec. Pap. Geol. Soc. Am.* **186:** 11-26.

Gillette, D.A. and Passi, R., 1988, Modeling dust emission caused by wind erosion, *J. Geophys. Res.* **93:** 14,233-14,242.

Gillette, D.A. and Stockton, P. H., 1989, The effect of nonerodible particles on wind erosion of erodible surfaces, *J. Geophys. Res.* **94:** 12,885-12,893.

Gillette, D.A. Adams, J., Muhs, D.R., and Khil, R., 1982, Threshold friction velocities and rupture moduli for crusted desert soils for the input of soil particles into the air, *J. Geophys. Res.* **87:** 9003-9015.

Gomes, L., Bergametti, G., Coudé-Gaussen, G., and Rognon, P., 1990, Submicron desert dust: a sandblasting process, *J. Geophys. Res.* **95:** 13,927-13,935.

Gomes, L., Rajot, J.L., Alfaro, S.C., and Gaudichet, A., 2003, Validation of a dust production model from measurements performed in semi-arid agricultural areas of Spain and Niger, *Catena* **52:** 257-271.

Greeley, R., Blumberg, D.G., and Williams, S.H., 1994, Field measurements of active windblown sand, in *Abstract of the Workshop on Response of Eolian Processes to Global Change*, Desert Research Institute, ed., Occas. Pap. 2, Reno, USA.

Greeley, R. and Iversen, J.D., 1985, *Wind as a Geological Process on Earth, Mars, Venus and Titan,* Cambridge University Press, New York, pp. 333

Greeley, R., Blumberg, D.G., McHone, J., FDobrovolski, A., Iversen, J., Lancaster, N., Rasmussen, K.R., Wall, S., and White, B., 1997, Applications of spaceborne radar laboratory data to the study of aeolian processes, *J. Geophys. Res.* **102:** 10,971-10,983.

Grousset, F., Biscaye, P.E., Revel, M., Petit, J.R., Pye, K., Joussaume, S., and Jouzel, J., 1992, Antarctic (Dome C) ice-core dust at 18 Ky B.P.: Isotopic constraints on origins, *Earth Planet. Sci. Lett.* **111:** 175-182.

Hagen, L.J. and Armbrust, D.V., 1992, Aerodynamic roughness and saltation trapping efficiency of tillage ridges, *Trans. ASAE* **35:** 1179-1184.

Iversen, J.D., Pollack, J.B., Greeley, R., and White, B.R., 1976, Saltation threshold on Mars: the effect on interparticle force, surface roughness, and low atmospheric density, *Icarus* **29:** 381-393.

Iversen, J.D. and White, B.R., 1982, Saltation threshold on Earth, Mars and Venus, *Sedimentology* **29:** 111-119.

Joussaume, S., 1990, Three-dimensional simulations of the atmospheric cycle of desert dust particles using a general circulation model, *J. Geophys. Res.* **95:** 1909-1941.

Joussaume, S., 1993, Paleoclimatic tracers: an investigation using an atmospheric general circulation model under ice age conditions, 1. desert dust, *J. Geophys. Res.* **98:** 2767-2805.

Kardous, M., Bergametti, G., and Marticorena, B., 2005a, Aerodynamic roughness length related to tillage ridges of the semi-arid regions, *Annales Geophys.* **23:** 3187-3193.

Kardous, M., Bergametti, G., and Marticorena, B., 2005b, Wind tunnel experiments on the effects of tillage ridge features on wind erosion horizontal fluxes, Annales Geophys. **23:** 3195-3206.

Laurent, B., Marticorena, B., Bergametti, G., Chazette, P., Maignan, F., and Schmechtig, C., 2005, Simulation of the mineral dust emission frequencies from desert areas of China and Mongolia using an aerodynamic roughness length map derived from the POLDER/ ADEOS 1 surface products, J. Geophys. Res. 110: D18S04. doi:10.1029/2004JD005013.

Leys, J.F. and Raupach, M.R., 1991, Soil flux measurements with a portable wind erosion tunnel, *Aust. J. Soil Res.* **29:** 533-552.

Lu, H. and Shao, Y., 1999, A new model for dust emission by saltation bombardment, *J. Geophys. Res*. **104:** 16,827-16,842.

McKenna-Neuman, C. and Nickling, W.G., 1989, A theoretical and wind tunnel investigation of the effect of capillarity water on the entrainment of sediment by wind, *Can. J. Soil Sci.* **69:** 79-96.

Mahowald, N.M., Zender, C.S., Luo, C., Savoie, D., Torres, O., and del Corral, J., 2002, Understanding the 30-year Barbados desert dust record, *J. Geophys. Res*. **107:** doi: 10.1029/2002JD002097.

Mahowald, N.M. and Luo, C., 2003, A less dusty future?, *Geophys. Res. Lett*. **30:** doi:10.1029/2003GL017880.

Marshall, J.K., 1971, Drag measurements in roughness arrays of varying density and distribution, *Agric. Meteorol.* **8:** 269-292.

Marticorena, B. and Bergametti, G., 1995, Modeling the atmospheric dust cycle: 1-Design of a soil derived dust production scheme, *J. Geophys. Res.* **100:** 16415-16430.

Marticorena, B. Bergametti, G., Aumont, B., Callot, Y., N'Doumé, C., and Legrand, M., 1997a, Modeling the atmospheric dust cycle: 2-Simulation of Saharan sources, *J. Geophys. Res*. **102:** 4387-4404.

Marticorena, B., Bergametti, G., Gillette, D.A., and Belnap, J., 1997b, Factors controlling threshold friction velocities in semi-arid areas of the United States, *J. Geophys. Res.* **102:** 23277-23288.

Marticorena, B., Chazette, P., Bergametti, G., Dulac, F., and Legrand, M., 2004, Mapping the aerodynamic roughness length of desert surfaces from the POLDER/ADEOS bi-directional reflectance product, *Int. J. Remote Sens.* **25:** 603-626.

Marticorena, B., Kardous, M., Bergametti, G., Callot, Y., Chazette, P., Khatteli, H., Le Hégarat-Mascle, S., Maillé, M., Rajot, J.L., Vidal-Madjar, D., and Zribi, M., 2006, Aeolian geometric and aerodynamic surface roughness in arid and semi-arid areas and their relation with radar backscatter coefficient, *J. Geophys. Res.* **111:** doi:10.1029 /2006JF000462.

Mei, F., Zhang, X., Lu, H., Shen, Z., and Wang, Y., 2004, Characterization of MASDs of surface soils in north China and its influence on estimating dust emission, *Chin. Sci. Bull.* **49:** 2169-2176.

Nickling, W.G. and Gillies, J.A., 1989, Emission of fine-grained particulates from desert soils, in *Paleoclimatology and Paleometeorology: Modern and Past Patterns of Global Atmospheric Transport*, M. Leinen and M. Sarnthein, eds., Kluwer Academic, Norwell, Mass., pp. 133-165.

Priesley, C.H.B., 1959, *Turbulent Transfer in the Lower Atmosphere,* University of Chicago Press, Chicago, USA, 130 pp.

Raupach, M.R., 1992, Drag and drag partition on rough surfaces, *Bound. Layer Meteorol.* **60:** 375-395.

Raupach, M.R., Gillette, D.A., and Leys, J.F., 1993, The effect of roughness elements on wind erosion threshold, *J. Geophys. Res.* **8:** 3023-3029.

Schlichting, H., 1936, Experimentelle Untersuchungen zum Rauhigkeitsproblem, *Ingr. Arch.*, **7:** 1-34. (English Translation; *NASA Tech. Memo. 823*).

Shao, Y., 2001, A model for mineral dust emission, *J. Geophys. Res.* **106:** 20,239-20,254.

Shao, Y, 2004, Simplification of a dust emission scheme and comparison with data, *J. Geophys. Res.* **109:** doi:10.1029/2003JD004372.

Shao, Y., Raupach, M.R., and Findlater, P.A., 1993, Effect of saltation bombardment on the entrainment of dust by wind, *J. Geophys. Res.* **98:** 12,719-12,726.

Shao, Y., Raupach, M.R., and Leys, J. F., 1996, A model for predicting aeolian sand drift and dust entrainment on scales from paddock to region, *Aust. J. Soil Res.* 34: 309-342.

Shao, Y. and Lu, H., 2000, A simple expression for wind erosion threshold friction velocity, *J. Geophy. Res*. **105:** 22,437-22,443.

Sörensen, M., 1985, Estimation of some aeolian saltation transport parameters from transport rate profiles, in Proceedings of the International Workshop on the Physics of Blown Sand, O.E. Barndorff-Nielsen, Möller, J.T., Römer Rasmussen K., and Willets B.B., eds., University of Aarhus, Aarhus, Denmark, pp. 141-190.

Tegen, I., Harrison, S.P., Kohfeld, K., Prentice, I.C., Coe, M., and Heimann, M., 2002, Impact of vegetation and preferential source areas on global dust aerosol: Results from a model study, *J. Geophys. Res*. **107:** doi:10.1029/2001JD000963.

Tegen, I., Werner, M., Harrison, S.P., and Kohfeld, K.E., 2004, relative importance of climate and land use in determining present and future global soil emissions, *Geophys. Res. Lett*. **31:** doi:10.1029/2003GL019216.

Westphal, D.L., Toon, O.B., and Carlson, T.N., 1988, A case study of mobilization and transport of Saharan dust, *J. Atmos. Sci.* **45:** 2145-2175.

White, B.R., 1979, Soil transport by winds on Mars, *J. Geophys. Res.* **84:** 4643-4651.

MODELLING OF THE GLOBAL AND REGIONAL PHENOMENA

CLIMATE/WATER-CYCLE FEEDBACKS IN THE MEDITERRANEAN: THE ROLE OF LAND-USE CHANGES AND THE PROPAGATION OF PERTURBATIONS AT THE REGIONAL AND GLOBAL SCALE

MILLÁN M. MILLÁN*,
Fundación CEAM, Valencia, Spain

Key Words: Climate, Feedbacks, Water-Cycle, Drought, Land-Use Change, Mediterranean, Desertification.

Summary Around the Mediterranean sea, deserts and desert-like conditions can be found in close proximity to a very warm sea and thus to a marine airmass with a high moisture content, e.g., the coasts of Morocco, Algiers, Tunisia, Libya, and Almeria in Southeastern Spain. These regions were covered with vegetation in historical times, e.g., during the Roman Empire, and in the case of Almeria, just 150 years ago, before the forests were used to fuel lead mines. The question is: did forest removal cause them to run a feedback cycle towards desertification? The reanalysis of results from seventeen♦ EC research projects (**Section 5**) suggests that this could be the case.

This work shows that the hydrological system in this region is very sensitive to land-use changes and, more recently, to air pollution effects as well. Both of these can combine to exceed critical threshold levels, e.g., the height of the cloud condensation levels with respect to the height of the coastal mountain ranges. This results in the loss of summer storms and tips the regional climate towards desertification and drought. The non-precipitated water vapour returns and accumulates over the Western Mediterranean Basin to heights reaching over 5000 m, for periods lasting from 3 to 10 days in summer.

Moreover, changes and perturbations to the hydrological cycle in any part of the basin can propagate to the whole basin and adjacent regions, and ultimately to the global climate system, through other mechanisms. These involve: (1) an increase in Mediterranean cyclogenesis in autumn-winter through cumulative (greenhouse) heating of the sea surface by the water vapour and the pollutants (ozone) accumulated over the sea, (2) the export of the accumulated water vapour and pollutants to other regions at the end of

* To whom correspondence should be addressed.

A. Mellouki and A.R. Ravishankara (eds.), Regional Climate Variability and its Impacts in the Mediterranean Area, 83–101.

each 3-10 day accumulation-recirculation period, which can contribute to summer floods in Central-Eastern Europe and, in turn, (3) change in the evaporation-self-precipitation balance over the Mediterranean, which increases its salinity and drives the Atlantic-Mediterranean salinity valve.

Both the available data and the modelling results at regional scale indicate that these processes are already operating, and suggest that fundamental changes, and long-term perturbations to the water-cycle, are taking place right now. This information and the questions it raises are thus crucial for the water policies in the whole Mediterranean Region and in other European areas. Of particular importance is the question of their long term effects, since feedback processes on the hydrological cycle cannot be simulated properly in the Global Climate models used to assess future water scenarios in these regions.

1. How the System Works

The Western Mediterranean system consists of: (a) a deep sea totally surrounded by high mountains in the sub-tropical latitudes, (b) anticyclonic conditions prevailing for approximately seven months of the year (April to October), and (c) current surface properties around the WMB. In this set-up, the seabreezes develop and grow in a stepwise fashion (Salvador et al., 1997) by successively incorporating upslope wind cells into a circulation, i.e., a "combined breeze", stronger than the sum of its components (Mahrer and Pielke, 1977; Miao et al., 2003). As Figure 1 shows, orographic-convective injections (orographic chimneys) take place at the breeze's leading edge. These increase in height as the seabreeze progresses inland and their return flows produce layers aloft. Available experimental data and modelling results indicate that the coastal circulations have the following characteristics:

1. The combined breezes tend to become self-organised at the scale of the whole western Mediterranean basin (Figure 2), and form convergence lines located over the main mountain ranges surrounding the sea.
2. Field data show that the breezes can reach inland more than 100 km from the coast, and the modelling results show that the orographic chimneys at their leading edges reach up to 4 to 6 km by late afternoon (Figure 2).To maintain flow continuity, compensatory subsidence over the sea is generated during the whole process (Figure 2), which increases in intensity and extension during the morning and early afternoon.
3. The subsidence becomes fully generalised over the basin during the late morning and afternoon, and confines the boundary layers along the coasts to depths of less than ≈200-300 m, all the way from the coast to their orographic chimneys inland (Figure 3).

4. Thus, the volumes of air involved in these processes are bounded. Their lengths are the distances the breezes travel inland, i.e., 120-160 km, but their heights are confined to 200-300 m, per unit width along the coast, i.e., the displaced volumes are very long but very shallow.
5. These mechanisms generate vertical recirculations that accumulate pollutants (ozone) and water vapour (see below) in layers piled up to ≈5000 m over the sea.
6. Tracer experiments during the MECAPIP♦ project indicate that vertical recirculation times are of the order of two to three days (Millán et al., 1992).

2. The Climate Connection

From 1974 to 2004, the objective of most of the EC projects mentiones to was to determine the dynamics of pollutants in southern Europe, including (circa 1986) the circulations responsible for the high tropospheric ozone levels observed over the Mediterranean region. It was in 1993-94 when the EC inquired about using the newly acquired meso-meteorological knowledge to elucidate the observed loss of summer storms in the mountains surrounding the western Mediterranean sea (Millan et al., 2005a; 2005b). This task required a new assessment of the available data, including aspects not previously considered.

Perhaps the most important finding (points 4 and 5 above) is the vertically confined nature of the surface flows in the combined breezes. This discovery enables us to assume that the airmass of the breeze exchanges heat and moisture only with the surface, and that lateral exchanges take place with airmasses of similar characteristics. It follows then that aerological diagrams can be used to evaluate the role of surface exchanges, as illustrated in Figure 4 with climatological data from Castellón.

For example, when the marine airmass moves inland its water vapour content increases through evaporation from the surface. If the airmass accumulates enough moisture to reach its Cloud Condensation Level (CCL), storms can develop in the orographic chimneys at the leading edge of the combined breeze. When this occurs, a large fraction of the water vapour precipitates, while the released latent heat contributes to the development of deep convection. This results in the mixing of the breeze components (including the non-precipitated water vapour) within the troposphere, where the upper winds (i.e., at heights above ≈6000 m) can advect them out of the region. In this case the coastal circulations act like a small monsoon and can be considered to remain **"open"**.

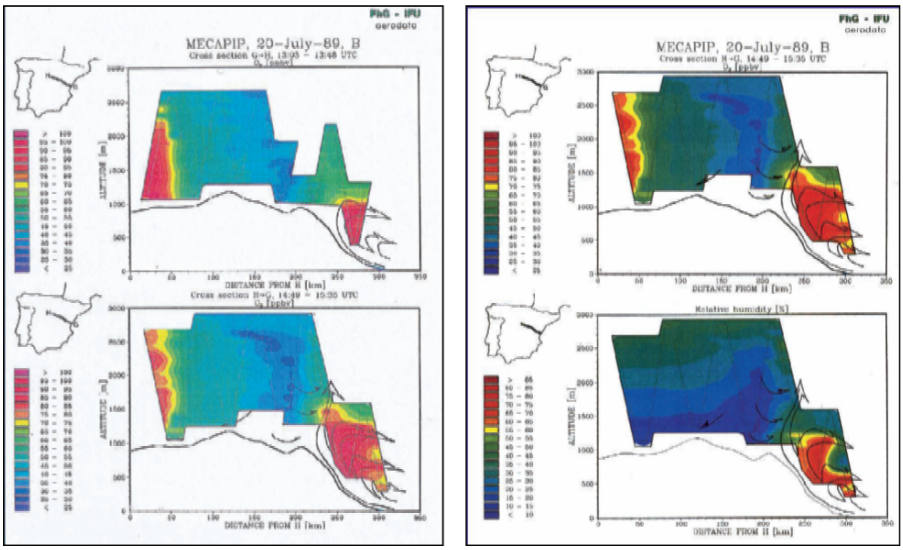

Figure 1. Left. Two stages in the development of the seabreeze on the Spanish East coast on 20 July 1989, documented by an aircraft instrumented to measure ozone during the EC MECAPIP project (1988-1991, Millán et al., 1991). The footprint of the flight track (H-G ≈350 km, from the Castellón coast to Guadalajara) is shown over the Iberian Peninsula at left. The figures show the seabreeze front and the return flows at 13:03-13:48 UTC, and at 80 (+) km from the coast. Modelling (Figure 2) shows that the orographic chimney reaches over ≈6000 m. Right. Ozone and relative humidity measurements at 14:49-15:35 UTC. They show that the water vapour follows the same path as the ozone into the return flows and the formation of layers over the sea. This figure shows that a satellite flying over the coastal mountains in the morning-early afternoon would look down the developing orographic chimneys at the leading edge of the combined breezes

If, on the contrary, the combined breeze does not accumulate enough moisture to compensate for the surface heating along its path, the CCL of the airmass will rise above the mountain ridges, and storms will either not develop or not reach maturity (Millán et al., 2005a; 2005b). In fact, it is precisely under these conditions that the convective-orographic injections at the leading edge of the combined breezes keep the surface winds directly connected to their return flows aloft (Figure 1), which, under the effect of compensatory subsidence, become stable and form the layers observed over the sea (Millán et al., 1997; 2002).

On the next day, the combined breeze brings the lower layers inland while: (1) the layer system over the sea sinks under compensatory subsidence (Figure 2), and (2) at the leading edges of the developing breezes newly injected airmasses begin to renovate the (older) layer system. These

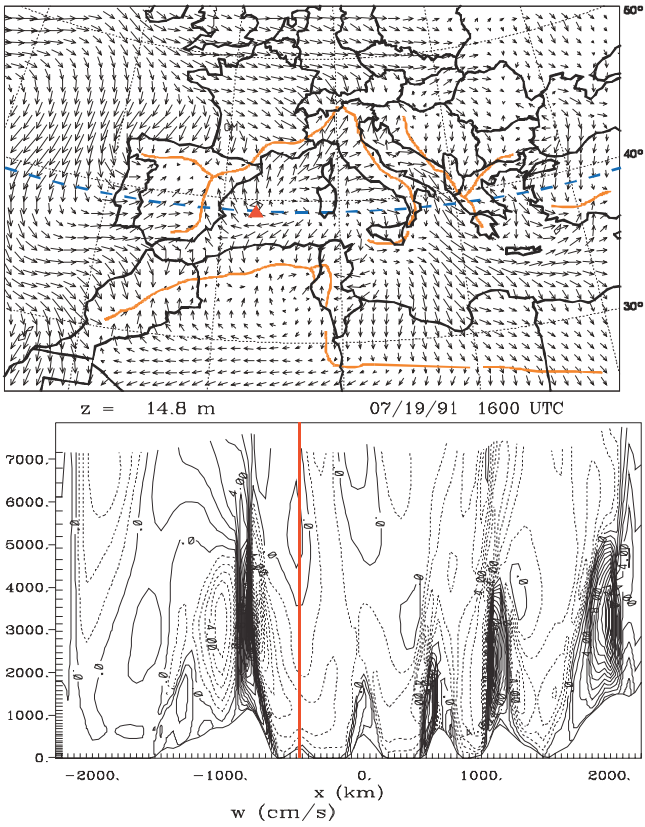

Figure 2. Simulated winds over the Mediterranean at 16:00 UTC on 19 July 1991. Top: The winds at 14.8 m originate near the centre of the basin, increase in speed, and turn anticyclonically (clockwise) as they flow towards convergence lines over the mountains surrounding the basin. Bottom: Vertical component of the wind on a surface following the 39.5 North Parallel (blue dashes above). It shows deep orographic/convective injections (upward solid lines) over Eastern Spain, Sardinia and the west-facing coasts of Italy, Greece and Turkey. To replace the surface air moving towards the coasts continuity requires subsidence (dotted lines) over the western Mediterranean basin, the Tyrrhenian, the Adriatic and the Aegean seas. At this time, with the sun at 60° West longitude, upward motions remain over the west-facing coasts of Turkey, Greece and Italy but are barely developed over the Atlantic coast of Portugal. This situation also illustrates the time lag and the inertia of the circulations

processes form part of a vertical recirculatory loop that takes several days to complete (see 7 above) and the coastal (re)circulations can be considered **“closed”**.

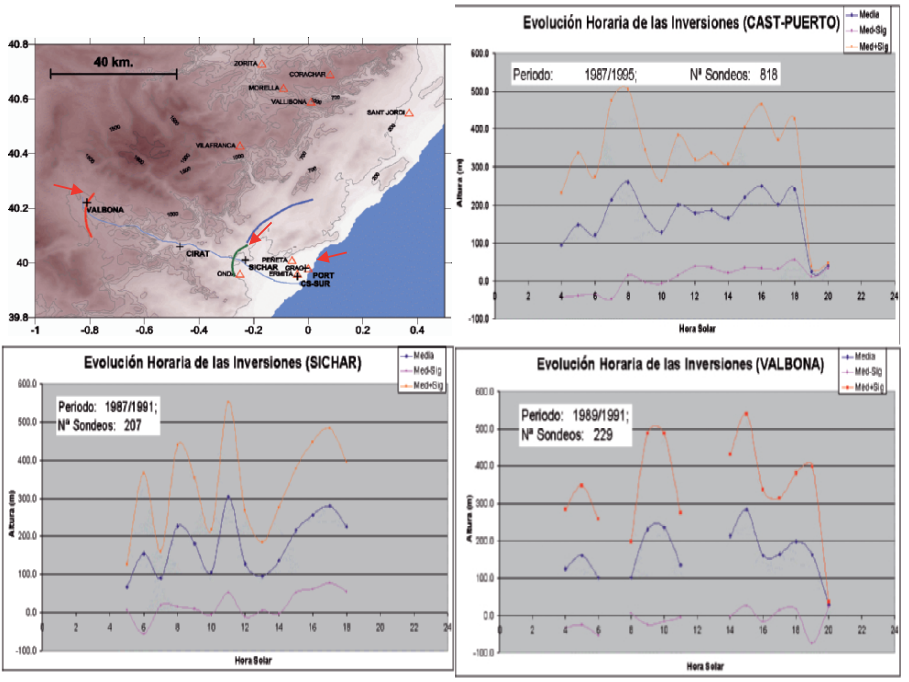

Figure 3. Boundary layer evolution at three sites on the Spanish east coast in summer (the last two weeks of July). Tethered balloons were used at the coast (PORT), at 17 km inland (SICHAR) and at 78 km inland (VALBONA). The years and the number of soundings are shown at the upper left of the figures, and the mixing height was defined by the base of the first temperature inversion. The average values are shown in blue, and the other lines mark ± one standard deviation. It was observed in 1986 that the mixing height at the coastal site (Puerto) grew rapidly during the morning and decreased during the afternoon (Millán et al., 1992); a similar process had been recorded previously in the Great Lakes in 1978 (Portelli et al., 1982). Subsequent analyses of all soundings for the three sites indicate that: (1) The average boundary layer height seldom exceeds 200 m in depth all the way from the coast to ≈80 km inland, (2) the depth of the layer oscillates during the day, and (3) the oscillations propagate inland. It is interesting to consider whether these oscillations are correlated to the wavy structure observed in the return flows aloft (see Figure 13)

The main conclusion from the data reanalysis is that the CCL of the local breeze with respect to the height of the mountain ridges is the **"critical threshold"** of the system. It determines whether storms develop and the coastal circulations become "open", or whether they remain "closed". Thus, the mechanisms for accumulating pollutants in layers over the sea, first observed in 1983, depend, in fact, on whether storms develop or not. And if

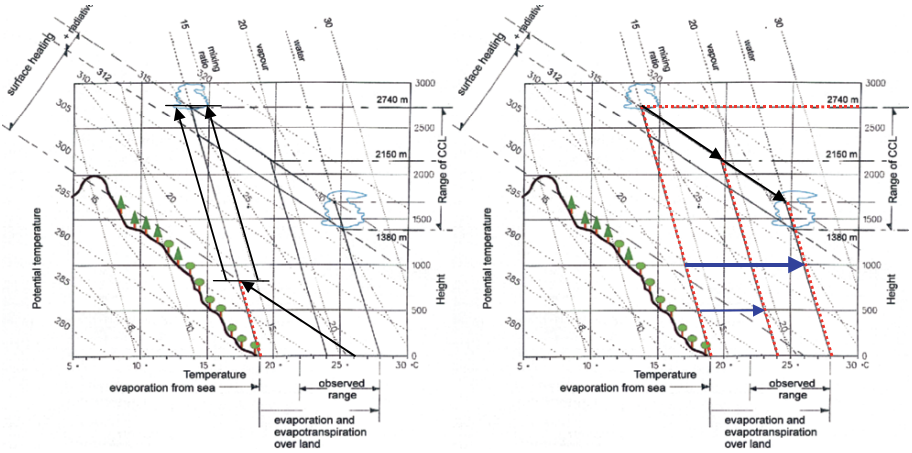

Figure 4. Emagram (Iribarne and Godson, 1981) showing the conditions controlling the Cloud Condensation level in Mediterranean seabreezes. Average climatological values for the water vapour mixing ratio in Castellón (Spain) during the summer are ≈14 g kg^{-1}, the average sea surface temperature is 26°C, and the CCL for natural ascent occurs at a height of ≈750 m. This agrees with the cloud base level of the stratocumulus observed towards the end of the seabreeze period. Field measurements also indicate that the air in the seabreeze gains 16°C after it travels 80 km inland (Figure 1). Under these conditions the CCL would rise to 2740 m, i.e., from ≈750 to 1000 m higher than the mountain ridges. For the CCL to drop to the height of the highest peaks (2020 m) the airmass needs to increase its water vapour mixing ratio to at least 20 g kg^{-1}, and for the CCL to drop below ≈1700 m the airmass must increase its water vapour mixing ratio to more than 25 g kg^{-1}. This suggests that the addition of water vapour to the seabreeze from evaporation from coastal marshes, irrigated land and natural vegetation is required to trigger a storm. Thus, land-use changes that alter (diminish) the evaporation along the breeze path will affect the local rain regime, i.e., the summer storms driven by the seabreeze

they do not develop, **the non-precipitated water vapour** will follow the return flows aloft (Figures 1, 14) to become stratified over the sea together with the pollutants.

3. Complementary Processes

The (now) obvious fact that the water vapour follows the return flows aloft when the circulations are “closed” has also become a paramount finding. It means that water vapour can be used as a tracer of opportunity of the recirculating airmasses (instead of just the ozone used previously in the EC projects), and that the available satellite data, with a quasi synoptic-like coverage, can be used to characterise process continuity within the whole

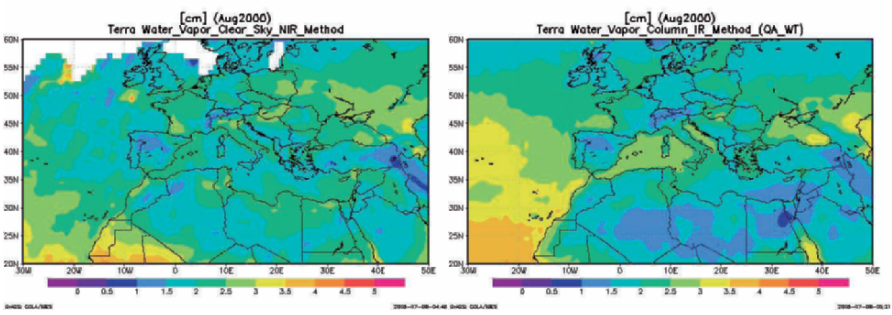

Figure 5. Monthly averages of the MODIS-Terra (King et al., 2003) water vapour vertical column measured for August 2000. The Day product (left), derived from the morning pass at 10:30 UTC, emphasises the Mediterranean coastal areas where the satellite looks down the developing orographic chimneys at the sea-breeze fronts (Figures 1-2). Available experimental evidence suggests that during the diurnal part of the cycle ≈1/3 (2/6) of the airmass (including the water vapour) accumulated over the sea on the previous day(s) sinks to maintain continuity with the coastal surface flows. The result is seen as lower water column values over the sea (see Figure 6 for more details). The Day + Night product shows the average of the satellite measurements at 10:30 UTC (morning pass) and at 22:30 UTC (night pass). Inland of the coastal areas this product shows roughly half of the morning (Day) values. Over the centre of the basin it shows the average of the morning value (≈4/6 of the total) plus the night value, i.e., closer to the total accumulated by the end of the day (6/6). The average is ≈5/6 of the total value accumulated, and it emphasises the area over which the accumulation occurs, i.e., the sea. A similar situation can be observed over the Adriatic and Black seas. These MODIS products yield the water vapour signal only; they eliminate the data in pixels where condensation is detected (cloud masking). This explains some of the low water vapour column values shown over regions where summer storms are frequent (e.g., Alps, Apennines and Atlantic Mid-Atlas)

Mediterranean Basin (and Black Sea), as shown in Figure 5. In this context, the points related to the workings of the system can be re-examined and expanded.

For example, in point 3 (above) it was stated; "To maintain flow continuity compensatory subsidence over the sea is generated during the whole process (Figure 2), which increases in intensity and extension during the morning and early afternoon". This can be observed in Figure 6.

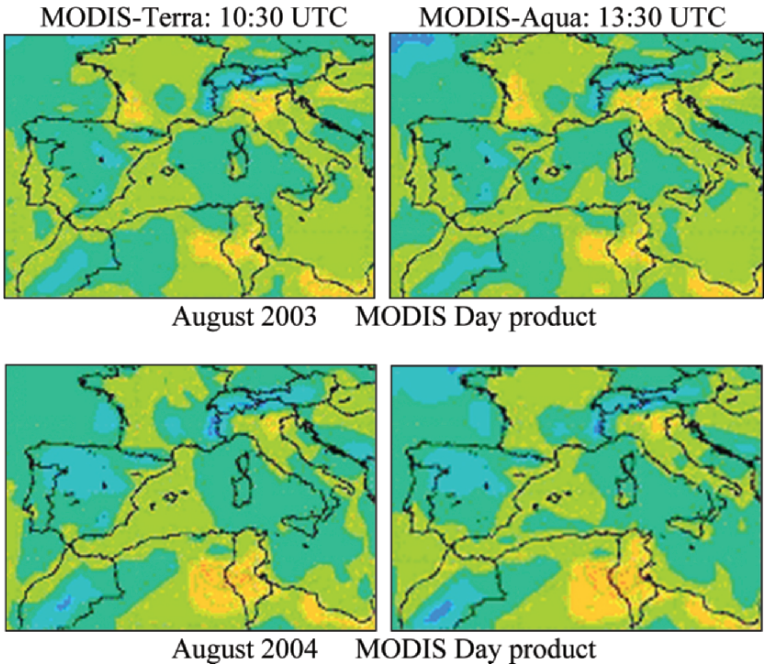

Figure 6. Detail of the water vapour column monthly averages for August 2003 and 2004. The images at left were obtained by the MODIS-Terra satellite with descending synchronous orbit and equatorial pass at 10:00 UTC. The images at right were obtained by the MODIS-Aqua satellite with ascending orbit and equatorial pass at 13:30 UTC. At the time of the Terra passes, the coastal circulations are one or two hours old and the compensatory subsidence over the centre of the basin is not fully developed. When the Aqua passes, after 13:30 UTC, the compensatory subsidence has been acting for a longer time. The time lag between the spreading of the surface air towards the coasts to feed the breezes, the compensatory sinking over the centre of the basin, and the replacement of the new layers aloft later in the afternoon, makes it possible to detect the effects of the compensatory subsidence. They appear as a lowering of the water column near the centre of the basin, accompanied by increasing values over the coastal areas surrounding the basin, and over the major islands, e.g., Sardinia, Sicily

The other points are:

7. In contrast with regions dominated by advection, pollutants and water vapour can accumulate over the sea in layers piled up to ≈5000 m. And without requiring the high evaporation rates of more tropical latitudes, these mechanisms can generate a very large, polluted, moist, and potentially unstable airmass after a few days (Figures 7 and 8).

8. The number and duration of the vertical recirculation/accumulation periods vary during the summer; the maximum number is registered in July (5 periods) with an average duration of 4 days, although the longest accumulation periods tend to occur in August (3 periods) with an average duration of 5-7 days.

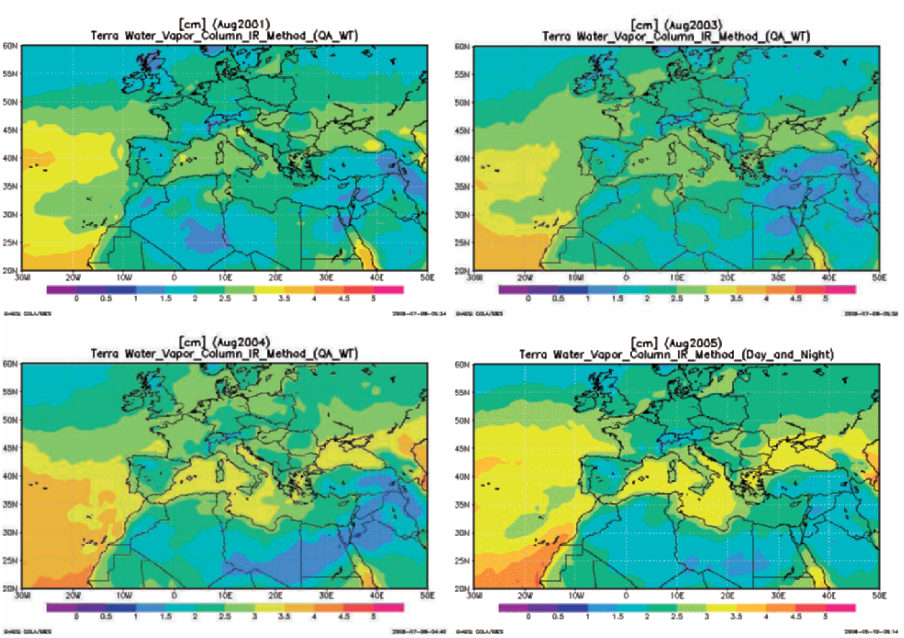

Figure 7. August monthly averages of the MODIS Day + Night product for the years 2001, 2003, 2004 and 2005. Together with the equivalent products for August 2000 (in Figure 5) and August 2002 (in Figure 11), these graphs illustrate the evolution in the average water vapour accumulated over the Mediterranean Basin by the coastal circulations in August for these years. They emphasise the "closed" nature of the coastal circulations at this time, with the result that water vapour accumulates over the sea instead of precipitating over the coastal mountain ranges. The accumulation is weaker over the eastern basin in summer, in spite of higher sea surface temperatures and more evaporation, because the flows there are dominated by advection (Millán et al., 1997)

Finally, during the accumulative periods it can be considered that the WMB acts as a large holding tank where the vertical recirculations increase the airmass residence times (Gangoiti et al., 2001). In these periods the surface inputs to the WMB below ≈1000 m come through the Carcassone gap and the Rhöne and Ebro valleys, while the surface outputs to the Atlantic occur directly through Gibraltar, or via the Sicilian straits, towards the Canary Islands, following the Southern Atlas corridor (Gangoiti et al., 2006). This had been indicated in a previous work (Millán et al., 1997, Figure 9), and can also be observed in Figure 10.

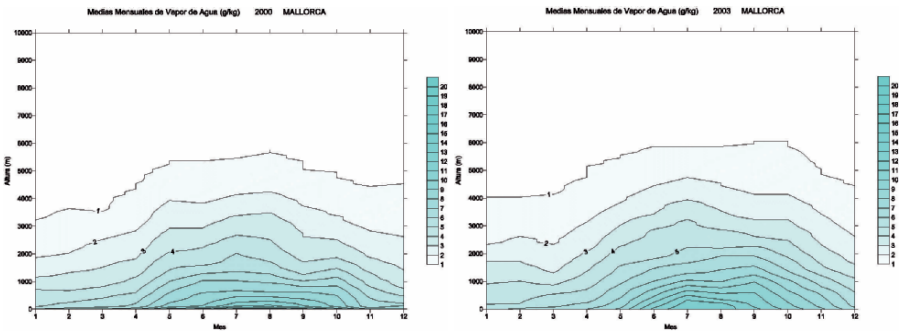

Figure 8. Yearly evolution of the monthly-averaged water vapour mixing ratio in g kg^{-1} over Mallorca for the years 2000 and 2003, obtained from Spanish Meteorological Service daily synoptic soundings. These graphs show that the build-up of moisture over the Western Mediterranean Basin basin starts in April. In 2000, the maximum build-up occurred in August and the 1g kg^{-1} isoline reached ≈5500 m. In 2003, the maximum values reached a higher altitude (≈6000 m) and were displaced to October. The graphs also show an increase in the average mixing ratio near the surface for July-August, from ≈11 g/kg^{-1} in 2000, to ≈12 g kg^{-1} in 2003. The point to consider is that the build-up of water vapour over the basin does not occur directly by evaporation from the sea surface to the upper layers, which would require deep convection over the sea, but rather by transport of the moisture from the sea surface to the upper layers following an overland path, i.e., the combined breezes and the deep orographic/convective injection at their leading edges. It is also important to note that this type of build-up, with the water vapour transported back over the Mediterranean with the return flows aloft, is favoured when storms do not mature over the coastal mountains

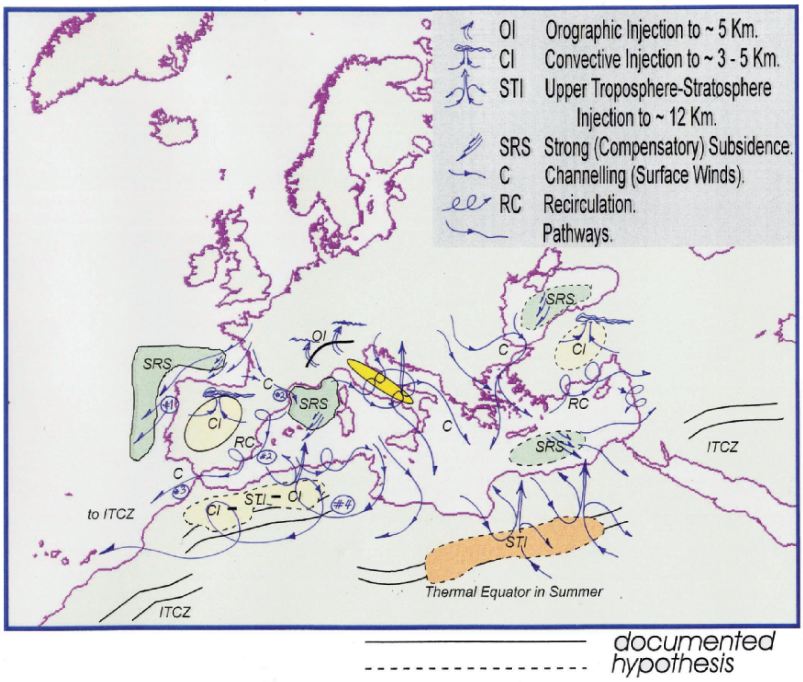

Figure 9. Conceptual model of atmospheric circulations in the Mediterranean Basin in summer, summarising the results from EC research projects to 1995 (Millán et al., 1997). These circulations have a marked diurnal cycle, and the graph is intended to illustrate their stage of development by mid-afternoon, and their spatial continuity. The flows include: (#1) the transport of aged airmasses along the coast of Portugal under strong subsidence during the day, (#2) the inflow of Atlantic air into the western Mediterranean via the Gulf of Lion followed by vertical recirculations along the Spanish East Coast and the Italian and African coasts, and (#3) the outflow of the aged airmasses through Gibraltar. The Italian case it includes the transition from combined sea-breezes and up-slope winds to storms along the Apennines in the afternoon. The effects of the Atlas Mountains may include upper tropospheric injections of airmasses aged within the Western Basin via path (#2) type, as well as transport towards the Canary Islands with vertical recirculations and lower stratospheric injection along the Southern Atlas (#4), and/or combinations of these (Gangoiti et al., 2006)

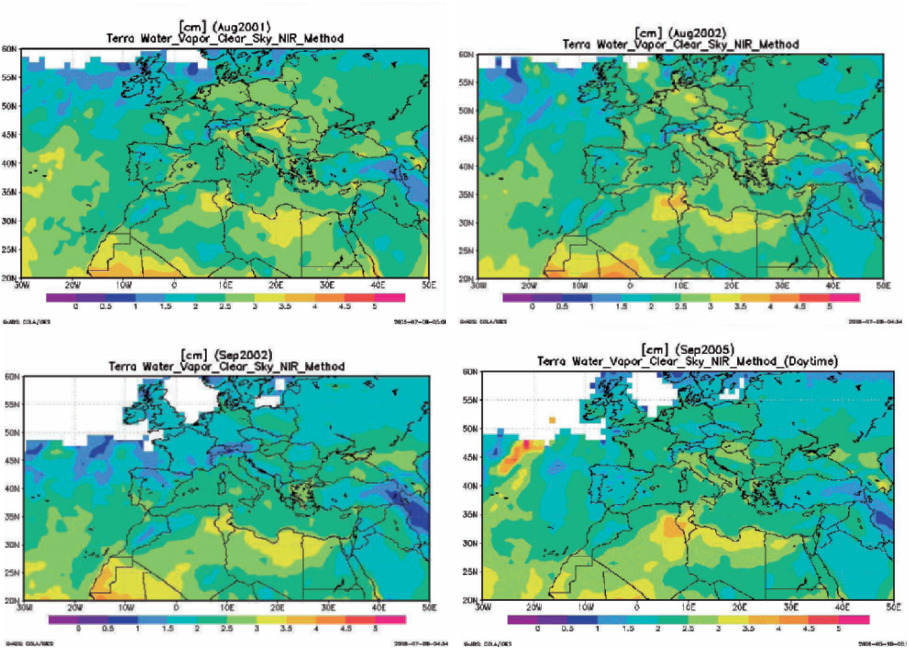

Figure 10. Monthly averages of the MODIS Terra Day product for August 2001, August 2002, September 2002, and September 2005. These graphs support some of the working hypotheses on the transport of Mediterranean air masses along the southern Atlas corridor (see #4 in the previous Figure). They also illustrate how much water vapour, together with air pollutants, is transported from the Mediterranean sea to the Atlantic ocean over the Sahara desert. At this time of year the transport occurs at the rear flows of the Azores anticyclone. This advected moisture could help in the formation of shallow clouds in any up-slope winds developing on the south-facing slopes of the Atlas mountains. Moreover, these shallow clouds could also provide the right environment for heterogeneous reactions involving Saharan dust and pollutants from the Mediterranean area

4. The Feedbacks

Figure 11 summarises the findings and presents a hypothetical framework linking Western Mediterranean Basin (WMB)-specific atmospheric-oceanic processes, and their possible feedbacks, to effects at the hemispheric (Ulbrich et al., 2003) and global scales (Savoie et al., 1992; 2002; Prospero and Lamb, 2003; Gangoiti et al., 2006). This framework describes some of the mechanisms behind one of Schellnhuber's "tipping points" in climate change, i.e., the Mediterranean-Atlantic salinity valve (Kemp, 2005).

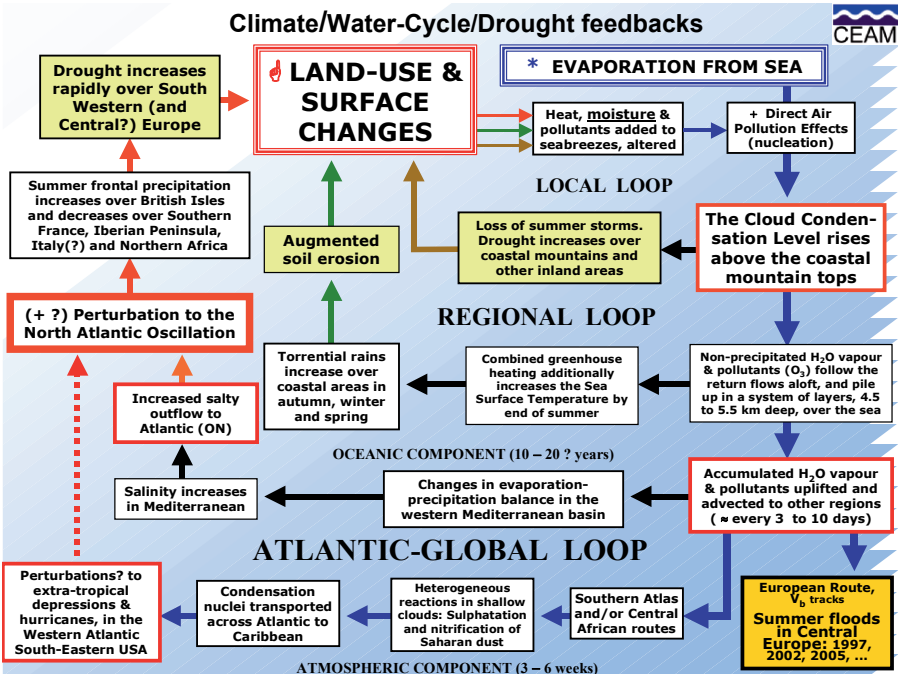

Figure 11. Feedback loops between land-use perturbations in the Western Mediterranean basin and the climatic-hydrological system from the local through the regional to the global scales. The path of the water vapour is marked by dark blue arrows, the directly related effects by black arrows, and the indirect effects by other colours. Critical thresholds are outlined in red

At this stage, land-use change appears to be the main driving factor determining whether the local atmospheric circulations become **"open"**, i.e., with the development of storms inland, or whether they remain **"closed"**, i.e., with no precipitation and continuing vertical recirculations. In turn, the loss of summer storms inland results in: drier soil, increased surface heating, higher CCL and, thus, the reinforcement of the **first feedback loop** towards desertification (Millán et al., 2005a).

This situation now prevails along the Mediterranean coasts of Northern Africa, the Iberian peninsula, southern France and southern Italy from late spring to early autumn, under current land-use conditions that could, in turn, be the result of feedbacks accumulated during the last 2000 years (Bolle, 2003). Another recent factor is the increase in atmospheric emissions, adding aerosols, ozone (Bastrup-Birk et al., 1997; Lelieveld et al., 2002) and other photo-oxidants to the returned water vapour, all with strong greenhouse properties. At this stage a working hypothesis is that their combined greenhouse effect could produce a 1-3°C increase in the temperature of the airmass below ≈2500 m, and that this concomitat additional rise of ≈100-300 m in

the airmass CCL could act as a "tipping point" in a climatic system already near its critical threshold.

The **second feedback loop** arises from the greenhouse effect of the components stacked over the sea (Figures 5, 7 and 8), i.e., the photo-oxidants and the non-precipitated water vapour, which would tend to increase the cumulative heating of the sea during summer. Higher Sea Surface Temperatures[1] (SSTs) increase torrential precipitation over the coastal areas in autumn-winter (Pastor et al., 2001). And because warm water pools move within the basin, they can feed torrential rains and flash floods anywhere in the basin. Thus, this **second feedback loop** would also tend to propagate the effects of land-use perturbations from one part of the basin, i.e., loss of summer storms, to other parts of the basin (in the form of torrential rains) with a three-to-six-month delay and in a random fashion.

The **third feedback loop** originates through the loss of the (non-precipitated) moisture accumulated over the sea when it becomes uplifted out of the region. The vented airmass can then follow either a European route (Figure 12 from Ulbrich et al., 2003) or an African route (Gangoiti et al., 2006). The loss of this moisture alters the balance between evaporation and self-precipitation in the WMB and would tend to increase the saline content of the deep water flowing through Gibraltar to the Atlantic (Figure 13, Kemp, 2005). How this saltier outflow could affect processes at the North Atlantic level, at what time scale it operates, and what critical thresholds (if any) could be exceeded are additional questions.

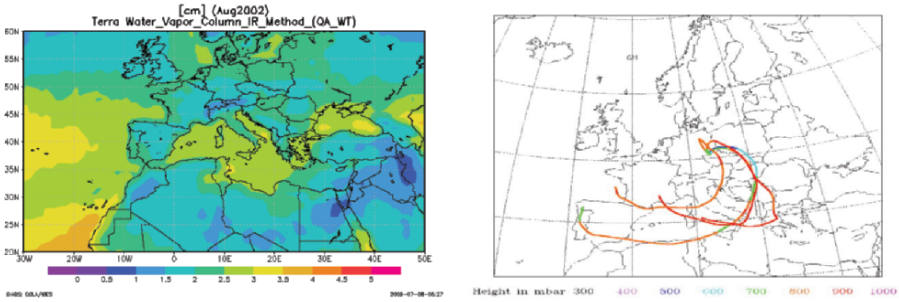

Figure 12. MODIS Day + Night product averaged for August 2002. It shows ≈5/6 of the average water vapour accumulated over the Mediterranean and available for advection to other regions. The right side shows the back trajectories (type V_b) that fed torrential rains in Germany and the Czech Republic on 11-13 August, 2002 (Ulbrich et al., 2003). These figures illustrate the evident interconnection between processes from the local to the regional scale in Southern Europe and, possibly, further to the global scale

[1] Higher SST by the end of summer yield more evaporation over the sea, but also reduce the land-sea temperature contrast that drives the seabreeze. How these effects combine to increase or reduce storm precipitation over the coastal areas, and how the possible effects evolve during the summer, are not yet known.

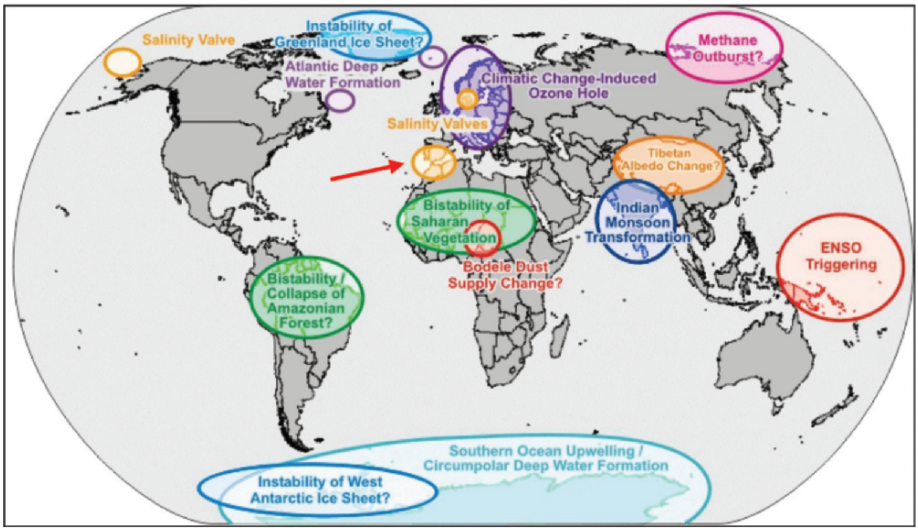

Figure 13. "Tipping points" in climate change from Prof. H. J. Schellnhuber, published in Nature, (437, 1238) by M. Kemp (Inventing an icon) on October 24, 2005. It includes the Atlantic-Mediterranean salinity valve resulting from changes in the evaporation-precipitation balance over the Mediterranean sea

Finally, when the accumulated airmass is vented along the Southern Atlas corridor, it can provide moisture (Figure 14) and pollutants that modify the physico-chemical characteristics of the Saharan dust transported across the Central Atlantic towards the Caribbean (Hamelin et al., 1989; Savoie et al., 1992; 2002; Gangoiti et al., 2006). For example, the upslope winds on the South-facing slopes of the Atlas also generate vertical recirculations whose added moisture would favour the formation of shallow clouds and provide the right environment for heterogeneous reactions. In this area dust layers of up to ≈7 km high have been already detected in the mont of March by NASA (Winker et al., 1996).

How the modified aerosols affect weather processes over the Caribbean and the US, and how they link the North Atlantic Oscillation to the conditions over Europe, are questions related to the **fourth feedback loop**. However, if the combined effects of the two components in the Atlantic-Global Loop influence the North Atlantic Oscillation positively, one could expect an increase in precipitations roughly north of the 45°N parallel (affecting Northern France and the British Isles), and a corresponding decrease south of it (affecting Southern France, the Iberian peninsula and Northern Africa).

♣ This work is a summary of the text:
Climate feedbacks in Europe: MODIS evidence of a water vapour accumulation mode in the Mediterranean, and its climatic implications.

Figure 14. Left. Waves in the return flows of the coastal circulations, photographed shortly before sunset at ≈80 km from the Mediterranean sea, looking Southeast in the direction of the coast. On this day the return flows could be visualised thanks to the shallow clouds formed at the front of the combined breezes (Millán et al., 1992) and the dust layers that remain after the droplets have re-evaporated. Right. Photo taken 15 minutes later looking West towards the mountains (background) where the orographic chimneys were located during the afternoon. After the breezes die out and the shallow clouds dissipate, all that is left to see are dust layers. Some of the particles result from heterogeneous reactions (wet-phase), at the droplet stage, between the components brought inland by the combined breeze. Similar processes can also occur when the moisture and pollutants vented out from the Western Mediterranean Basin follow the Southern Atlas corridor, joining and acting as a background airmass for the upslope winds and their recirculations of Saharan dust along the south-facing slopes of the Atlas, before reaching the Atlantic at the latitude of the Canary Islands by: Millán M. Millán[*], L. A. Alonso[#], Mª.J. Estrela[*], E. Mantilla[*], J.J. Dieguez[*], G. Perez-Landa[*], G. Gangoiti[#], M. Navazo[#] ([*]CEAM, [#]ETSII-UPV), for publication in the *Journal of Geophysical Research-Atmospheres*.

5. Acknowledgements

The MODIS images used in this study were acquired using the GES-DISC Interactive Online Visualisation and Analysis Infrastructure (Giovanni) as part of NASA Goddard Earth Sciences (GES) Data and Information Services Center (DISC). The satellite images were prepared by Prof. Lucio Alonso from the UPV/EHU and Figures 4 and 8 by Mr. Enrique Mantilla.

♦ The first experimental data used for this work were obtained during the European Commission Campaigns on Remote Sensing of Air Pollution in: **LACQ** (France, 1975), **TURBIGO** (Po Valley, Italy, in 1979) and **FOS-BERRE** (Marseille, France, 1983). Additional experimental and modelling results come from the European Commission research projects: **MECAPIP**

(MEso-meteorological Cycles of Air Pollution in the Iberian Peninsula, 1988-1991), **RECAPMA** (REgional Cycles of Air Pollution in the Western Mediterranean Area, 1990-1992), **SECAP** (South European Cycles of Air Pollution, 1992-1995), **T-TRAPEM** (Transport and TRansformation of Air Pollutants on East Mediterranean, 1992-1995), **MEDCAPHOT-TRACE** (The Mediterranean Campaign of Photochemical Tracers-Transport and Chemical Evolution, 1993-1995), **VOTALP I** (Vertical Ozone Transport in the Alps, 1995-1998), **VOTALP II** (Vertical Ozone Transport in the Alps, Phase II, 1995-1998), **BEMA I** (Biogenic Emissions in the Mediterranean Area, Phase I/ 1993-1995), and **BEMA II** (Phase II/ 1998-2000), **MEDEFLU** (Carbon and Water Fluxes of MEDiterranEan Forest and Impacts of Land Use/Cover Changes, 1998-2000), **RECAB** (REgional Assessment and Modelling of the CArbon Balance within Europe, 2000-2003), **ADIOS** (Atmospheric Deposition and Impact of pollutants, key elements and nutrients on the Open Mediterranean Sea, 2000-2003), **CARBOMONT** (Effects of Land Use Changes on Sources, Sinks and Fluxes of CARBOn in European MOuNTain Areas, 2001-2004), and **FUMAPEX** (Integrated Systems for Forecasting Urban Meteorology, Air Pollution and Population Exposure, 2001-2005).

This work is dedicated to the memory of both Dr. Heinrich (Heinz) Ott (†2004) for his initial support of this research in 1985 and his request in 1993 to search out the problems with summer storms, and Dr. Anver Ghazi (†2005) for his continued encouragement and support.

6. References

Bastrup-Birk, A., J. Brandt, Z. Zlatev, I. Uría,1997: Studying cumulative ozone exposures in Europe during a 7-year period. *J. Geophys. Res.*, **102, D20**, 23,917- 23,935.

Bolle, H.-J. (Ed.), 2003: Mediterranean Climate, Springer-Verlag, Berlin, New York, 372 pp.

Gangoiti, G., M. M. Millán, R. Salvador, E. Mantilla, 2001: Long-Range transport and re-circulation of pollutants in the Western Mediterranean during the RECAPMA Project. Atmos. Environ., 35, 6267-6276.

Gangoiti, G., L. Alonso, M. Navazo, J. A. García, M. M. Millán, 2006: North African soil dust and European pollution transport mechanisms to America during the warm season: Hidden links shown by a passive tracer simulation. J. Geophys. Res., 111, D10109, doi: 10.1029/ 2005JD005941.

Hamelin, B., F. E. Grouset, P. E. Biscaye, A. Zindler, J. M. Prospero, 1989: Lead isotopes in trade winds aerosols at Barbados: The influence of European emissions over the North Atlantic. J. Geophys. Res., 94, 16, 243-16,250.

Iribarne, J. V., W. L. Godson, 1981: Atmospheric Thermodynamics (2nd Ed.), D.Reidel Publishing Company, Dordrecht: Holland, 259 pp.

Kemp, M., 2005: (H. J. Schellnhuber's map of global "tipping points" in climate change), Inventing an icon, Nature, 437, 1238.

King, M. D., W. P. Menzel, Y. J. Kaufman, D. Tanré, B.-C. Gao, S. Platnick, S. A. Ackerman, L. A. Remer, R. Pincus, and P. A. Hubanks, 2003: Cloud and Aerosol Properties, Precipitable Water, and Profiles of Temperature and Water Vapor from MODIS. IEEE Transactions on Geoscience and Remote Sensing, 41, 442-458.

Lelieveld, J., H. Berresheim, S. Borrmann, P. J. Crutzen, & others, 2002: Science, 298, 794-799 Global Air Pollution Crossroads over the Mediterranean.

Mahrer, Y., R. A. Pielke, 1977: The effects of topography on the sea and land breezes in a two dimensional numerical model. Mon. Weather Rev. 105, 1151-1162.

Miao, J.-F., L. J. M. Kroon, J. Vilá-Guerau de Arellano, A. A. Holtslag, 2003: Impacts of Topography and Land Degradation on the Sea Breeze over Eastern Spain. Meteorology and Atmospheric Physics, 84, 157-170 (2003).

Millán, M. M., B. Artíñano, L. Alonso, M. Navazo, M. Castro, 1991: The effect of meso-scale flows on the regional and long-range atmospheric transport in the western Mediterranean area. Atmos. Environ. 25A, 949-963.

Millán, M. M., B. Artíñano, L. Alonso, M. Castro, R. Fernandez-Patier, J. Goberna, 1992: Meso-meteorological Cycles of Air Pollution in the Iberian Peninsula, (MECAPIP), Contract EV4V-0097-E, Air Pollution Research Report 44, (EUR Nº 14834) CEC-DG XII/E-1, Rue de la Loi, 200, B-1040, Brussels, 219 pp.

Millán, M. M., R. Salvador, E. Mantilla, G. J. Kallos, 1997: Photo-oxidant dynamics in the Western Mediterranean in Summer: Results from European Research Projects. J. Geophys. Res., 102, D7, 8811-8823.

Millán, M. M., 2002: Ozone Dynamics in the Mediterranean Basin: A collection of scientific papers resulting from the MECAPIP, RECAPMA and SECAP Projects. Air Pollution Research Report 78, European Commission, DG RTD I.2, LX 46 2/82, Rue de la Loi, 200, B-1040, Brussels, 287 pp.

Millán, M. M., Mª. J. Estrela, Mª. J. Sanz, E. Mantilla, & others, 2005a: Climatic Feedbacks and Desertification: The Mediterranean model. J. Climate, 18, 684-701.

Millán, M. M., Mª. J. Estrela, J. Miró, 2005b: Rainfall Components Variability and Spatial Distribution in a Mediterranean Area (Valencia Region). J. Climate, 18, 2682-2705.

Pastor, F., Mª. J. Estrela, D. Peñarrocha, M. M. Millán, 2001: Torrential Rains on the Spanish Mediterranean Coast: Modelling the Effects of the Sea Surface Temperature. J. Appl. Meteor., 40, 1180-1195.

Prospero, J. M., P. J. Lamb, 2003: African droughts and dust transport to the Caribbean: Climate change implications. Science, 302, 1024-1037 (2003).

Portelli, R. V., B. R. Kerman, R. E. Mickle, N. B. Trivett, R. M. Hoff, M. M. Millán, P. Fellin, K. S. Anlauf, H. A. Wiebe, P. K. Misra, R. Bell, O. Melo, 1982: The Nanticoke shoreline diffusion experiment, June 1978. Atmos. Environ. 16, 413-466.

Salvador, R., M. M. Millán, J. M. Baldasano, 1997: Mesoscale modelling of atmospheric processes over the western Mediterranean during summer. Int. J. Environment and Pollution. 8, 513-529.

Savoie, D. L., J. M. Prospero, S. J. Oltmans, W. C. Graustein, K. K. Turekian, J. T. Merrill, H. Levy, 1992: Source of nitrate and ozone in the marine boundary layer of the tropical North Atlantic. J. Geophys. Res., 97, 11,575-11,589.

Savoie, D. L., R. Akimoto, W. C. Keene, J. M. Prospero, R. A. Duce, J. N. Galloway, 2002: Marine biogenic and anthropogenic contributions to non-salt sulphate in the marine boundary layer over the North Atlantic Ocean. J. Geophys. Res., 107(D18), 4356, doi:10,1029/ 2001JD000970.

Ulbrich, U., T. A. Brücher, A. H. Fink, G. C. Leckebusch, A. Krüger, G. Pinto, 2003: The central European floods of August 2002: Part 2 - Synoptic causes and considerations with respect to climatic change. Weather, 58, 371-377.

Winker D. M., R. H. Couch, M. P. McCormick, 1996: An Overview of LITE: NASA's Lidar In-Space Technology Experiment. Proceedings of the IEEE, vol. 84, 164-180.

AEROSOLS DIRECT RADIATIVE FORCING ON DJOUGOU (NORTHERN BENIN) DURING THE AMMA DRY SEASON EXPERIMENT

M. MALLET, V. PONT, C. LIOUSSE,
A. MARISCAL, V. THOURET
Laboratoire of Aerologie, OMP, Toulouse

L. GOMES
CNRM, Meteo-France, Toulouse

J. PELON
Service of Aeronomie, University of Jussieu, Paris

S. OSBORNE, J. HAYWOOD
The Met Office, Bracknell, UK

P. DUBUISSON
LOCL/MREN, ELICO, Wimereux

J.C. ROGER
LAMP, OPGC, Clermont Ferrand

P. GOLOUB
Laboratoire of Optique Atmospherique, Lille

Key Words: AMMA experiment, aerosols microphysical and optical properties, direct radiative impact.

Abstract The purpose of this work is to investigate the direct radiative forcing of aerosols on the supersite of Djougou (Northern Benin) during the AMMA (African Monsoon Multidisciplinary Analyses) dry season experiment (January 2006). We focus our simulations on the Top Of Atmosphere (TOA), Bottom Of Atmosphere (BOA), and ATMosphere (ATM) radiative forcings. During the period, Sun-photometric measurements indicate a rather turbid atmosphere with a mean Aerosol Optical Depth (AOD), for the overall period, about 0.90 ± 0.01 at 440 nm. The aerosol absorption coefficient at the surface was comprised between 2 and 90 Mm^{-1}, with a mean value of 19.2 Mm^{-1}. In the same time, the scattering coefficient ranged between 50 and 400 Mm^{-1}, with an averaged of 160 Mm^{-1}. This leads to a Single Scattering Albedo (SSA) comprised between 0.75 and 0.95 with an average value of 0.90, indicating moderate absorbing aerosols.

A. Mellouki and A.R. Ravishankara (eds.), Regional Climate Variability and its Impacts in the Mediterranean Area, 103–111.

Differential mobility analyser measurements indicate a monomodal (nucleation mode) number size distribution, with a mean geometric diameter of 96.5 nm, associated with a geometric standard deviation of 1.87. The characteristics of the size distribution, associated with the refractive index of aerosols, have been used in the Mie theory for computing aerosol optical properties at different wavelengths. Associated with ground-based observations, the micro pulse lidar indicates the presence of two distinct aerosol layers, with a first one located between the surface and 500 m and a second one, characterized by aged biomass burning particles, located above (1500-3500 m). Based on surface and aircraft observations, sunphotometer measurements, Lidar profiles and MODIS sensor, an estimation of the daily direct radiative forcing has been estimated for the 17th to 24th January 2006 period, by using a discrete ordinate radiative transfer model. Simulations indicate that aerosols reduce significantly the solar energy reaching the surface (mean $\Delta F_{BOA} = -61.3$ Wm^{-2}) by reflection to space (mean $\Delta F_{TOA} = -19.0$ Wm^{-2}) but predominantly by absorption of the solar radiation into the atmosphere (mean $\Delta F_{ATM} = +42.3$ W.m^{-2}).

1. Introduction

Among all sources of atmospheric particles around the world, Western Africa is the world's largest source of biomass burning aerosols and mineral dust. Long past satellite observations indicate that these aerosol plumes, characterizing by high aerosol optical depths (often superior than one in the visible range) are the most widespread, persistent and dense observed at global scale. The effect of such plumes of dust and smoke aerosols on climate change represents one of the largest uncertainties in the Earth radiative budget. In a first time, atmospheric aerosols emitted in Western Africa can modify the radiative budget directly by absorption or scattering of solar radiations. Secondly, they can modify clouds properties and/or lifetimes when particles act as Cloud Condensation Nuclei. Furthermore, as dust and smoke particles are able to absorb solar radiations, the radiative heating due to aerosol layers can modify the atmospheric dynamic and suppress convection, resulting in evaporation of clouds. This effect, named "semi-direct" effect, can lead to a positive forcing by reducing cloud fractional cover and counterbalances the aerosol indirect effect.

Hence, dust and smoke particles coming from the West Africa region could strongly modify the regional or global climate as they have the potential to be exported over great distances by prevailing winds and atmospheric waves. A better representation of their climatic effects needs, in addition with modeling exercises and satellite observations, ground based and integrated-column measurements of their physical, chemical and optical properties,

associated with their vertical stratifications. This specific question represents one of the objectives of the AMMA (African Monsoon Multidisciplinary Analysis) project, as few data's characterizing optical properties of aerosols in the Western Africa region are available in the literature. In this work, we present results of our analysis of data's obtained during January 2006, in the frame of the SOP_0 (Special Observation Period_0) experiment, on the Djougou ground-based station (9.70N/1.68W, Northern Benin). Among all sites instrumented during AMMA, the measurements performed on Djougou represent a unique database for studying the microphysical and optical properties of aerosols over the region of fires, contrary to the other sites, more specifically deployed in the Sahelian dust transect, located northern of the main biomass burning areas. We focus our analysis during the dry season, as maximum emissions of anthropogenic biomass burning aerosols from the sub-Sahelian region of northern Africa occur during the December to February period.

2. Experimental Setup

During the AMMA dry season experiment, several sites, as Djougou (Benin), Niamey (Niger), Banizoumbou (Niger) and M'Bour (Senegal) were equipped with in situ and remote sensing instruments for characterizing dust and biomass burning aerosols microphysical and optical properties, their mixing, vertical repartition, transport and radiative forcings. These ground-based stations were completed by aircraft (BAe-146 from UKMO/NERC) and Ultra-light (LSCE/CNRS-CEA) measurements, as well as satellite observations. In this work, we used surface measurements performed on the station of Djougou (9.70 N, 1.68 W) located on the Northern Benin, which was administered by the Laboratoire of Aerologie (France, Toulouse). Concerning the aerosols, the ground-based instrumentation developed on Djougou was dedicated to characterize the chemical composition of particles, their physical (number size distribution) and optical (absorption and scattering) properties. In conjunction with the ground based instrumentation, a sunphotometer of the PHOTONS network (French part of the AErosol RObotic NETwork, AERONET) was also used to estimate aerosol microphysical and optical properties for the whole atmospheric column. Finally, over Djougou, the vertical stratification of particles has been estimated from an aerosol Micro Pulse Lidar (MPL) developped by CIMEL, which is a micropulse system operating at 532 nm.

3. Aerosol Optical Properties

3.1. AEROSOL OPTICAL DEPTH

Results of photometer measurements obtained during January 2006 are presented in the Figure 1. We present AOD at 440 nm (noted AOD_{440}), associated with uncertainty in AOD retrievals (~0.01– 0.02) (Holben et al., 1998). Although a much smaller amount of mineral dust has been observed during 2006, compared to previous years, the region of fires was rather turbid and AOD_{440} exceeds 0.5 for major days. The mean AOD_{440} during January 2006 is equals to 0.90, indicating a significant aerosol loading. We can observe very high AOD for the 17th and 18th January, with daily mean values of 1.5 and 1.1 (at 440 nm), respectively. These important values correspond to biomass burning particles produced from fires. From AOD measurements, we compute the Angström exponent, which represents the spectral variation of AOD. Over Djougou, the mean value of α is equals to 1, which is characterizing of fine aerosols.

3.2. AEROSOL ABSORBING COEFFICIENT

The dry absorption coefficient measured at 520 nm ($b_{abs(520)}$) ranged from 2 to 90 Mm^{-1}, with an average for the overall period of about 19.2 Mm^{-1}. Results indicate significant values of $b_{abs(520)}$ for the 17th-19th January period (~40 Mm^{-1}). The average and maximum values are comparable, or higher, to b_{abs} values obtained in regions influenced by anthropogenic emissions like

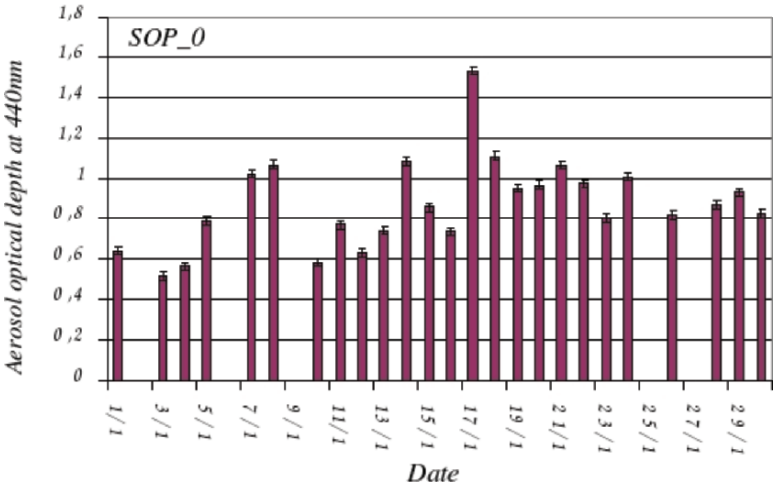

Figure 1. Aerosol Optical Depth (AOD) retrieved from SunPhotometer (PHOTON/ LOA) during the dry season (January 2006) over Djougou

the mid-Atlantic coast of the US during TARFOX (~3 Mm^{-1}), over the Indian Ocean during INDOEX (~16 Mm^{-1}), in the Asian outflow region during ACE-Asia (~8.6 Mm^{-1}), for anthropogenic pollution from Europe during ACE-2 (~8.9 Mm^{-1}).

3.3. AEROSOL SCATTERING COEFFICIENT

The dry scattering coefficient measured at 520 nm ($b_{scat(520)}$) ranged from 50 to 400 Mm^{-1}, with a mean value, for the overall period, of about 160 Mm^{-1}. For comparison, the values of b_{scat} observed over Djougou during the dry season are found to be significantly higher to b_{scat} values obtained during different field experiments, such as TARFOX (~44 Mm^{-1}), INDOEX (~62 Mm^{-1}), ACE-Asia (~55.3 Mm^{-1}), ACE-2 (~40 Mm^{-1}).

3.4. AEROSOL SINGLE SCATTERING ALBEDO

From nephelometer and aethalometer measurements, we computed the dry SSA at 520 nm and at the surface. We can observe values comprised between 0.75 and 0.99. The mean value, for the overall period, is 0.90, indicating moderate absorbing particles. Results indicates that aerosols are mostly absorbing (SSA ~ 0.85) during the 17^{th}-19^{th} period, corresponding to a bio-mass burning event, and mostly scattering (SSA ~ 0.95) for the 20^{th}-25^{th} period.

4. Methodology

4.1. RADIATIVE TRANSFER MODEL GAME

The GAME Radiative Transfer Model was used to compute the radiative fluxes at different altitudes. From these fluxes, we computed the aerosol clear-sky daily direct forcing at the Bottom Of Atmosphere (BOA), ΔF_{BOA}, and at the Top Of the Atmosphere (TOA, 70 km in this case), ΔF_{TOA}. The first one represents the effect of particles on the net short-wave radiation fluxes reaching the surface and the second one the radiation fluxes reflected back to space by aerosols. Finally, we compute the ATMospheric forcing, ΔF_{ATM}, as the difference between ΔF_{TOA} and ΔF_{BOA} which represents the possible absorption of solar radiations due to absorbing particles within the atmospheric layer.

4.2. AEROSOL VERTICAL STRATIFICATION

MicroPulse lidar measurements indicate that the Boundary Layer Height (BLH) is around 0.5 km and characterized by extinction coefficients of 0.1 km^{-1}.

Above 1 km, we can observe a second aerosol layer, with significant extinction coefficient ~0.3 km^{-1}, for altitudes comprised between 1500 and 3500 m, composed in majority by aged biomass burning aerosols. MPL measurements show the significant contribution of the BBL to the total AOD (around 75%) and the more negligible contribution of the BHL (around 15%).

For radiative transfer calculations, we have used in a first time the extinction vertical profiles retrieved from the MPL over Djougou, adjusted with AOD sunphotometer measurements at each wavelength. Associated with the aerosol extinction, the spectral variation of SSA and g computed at the surface are used for the BLH. Concerning the BBL, we used the SSA obtained onboard the BAe-146. Finally, for FT an ST, we used the spectral variation of aerosol optical properties coming from the free tropospheric and stratospheric aerosol models.

Concerning the thermodynamic parameters, the vertical profiles of RH and temperature used in GAME have been measured onboard BAe-146 aircraft for the 19th January and from Celiometer over Djougou. We completed the stratification by using Shadoz measurements for altitudes larger than 4 km. Concerning the ozone concentration profiles, we used ground-based measurements performed over Djougou for the BHL and we completed the vertical stratification with Shadoz measurements, carried out on the Southern Benin for the upper atmosphere.

As the estimation of radiative forcings has been performed over land, surface reflection is an issue. This property represents a critical parameter in the estimation of the Top Of Atmosphere (TOA) and ATMospheric (ATM) direct radiative forcings. The MODIS albedo provides the spectral dependence of surface albedo at seven wavelength bands. We can note a moderate value of 0.20 at 555 nm.

5. Results

5.1. BOTTOM OF ATMOSPHERE DIRECT RADIATIVE FORCING

As reported in the Figure 2, simulations indicate important radiative surface forcings for each days studied, with ΔF_{BOA} always negative (ΔF_{BOA} values are comprised between –48.7 and –84.5 Wm^{-2}). The averaged daily ΔF_{BOA} over Djougou during the period studied is about –61.3 Wm^{-2}. For comparison, the mean simulated daily radiative forcing over Djougou is found to be higher than those reported during experimental campaigns, characterizing anthropogenic aerosols, such as TARFOX (~ –26 Wm^{-2}) or INDOEX (~ –45 Wm^{-2}).

The difference is mainly due to higher AOD obtained over the region of fires during AMMA compared to previous campaigns. It is clear that such significant decrease of solar energy at the surface can strongly modify the surface energy budget. Indeed, under normal equilibrium conditions, surface reaching radiation flux is balanced by evaporation (latent heat fluxes) and sensible heat flux from the surface. In order to compensate for the reduction in surface reaching solar flux, any of them or both these heat fluxes released from the surface must decrease.

5.2. ATMOSPHERIC DIRECT RADIATIVE FORCING

Over Djougou, the association of moderate absorbing aerosols and surface reflectance leads to low ΔF_{TOA}, with a mean of –19.04 Wm^{-2}. The higher value of ΔF_{TOA} is obtained for the 22th January, corresponding to the higher SSA of particles (~0.98), which efficiently reflect solar radiations back to space. One of the most important results is that the mean ΔF_{TOA} is found to be 3 times lower than the mean ΔF_{BOA}, indicating a large atmospheric forcing over Djougou. Radiative computations estimate that atmospheric forcings occur for each days ($+27.2 < \Delta F_{ATM} < +65.2$ Wm^{-2}) but much more strongly for the 17th and 18th during the biomass burning event, with significant values about +63.4 Wm^{-2}. As mentioned for the surface forcings, this maximum in ΔF_{ATM} is obviously due to high AOD (~1.5), associated with low SSA (~0.85).

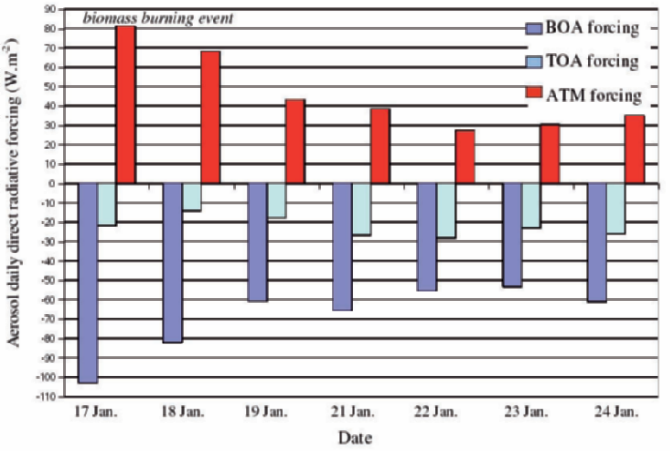

Figure 2. Clear-sky direct radiative forcing simulated over Djougou for the 17th-24th period

6. Conclusion

The purpose of this work is to investigate the clear-sky direct radiative forcing of aerosols over the ground-based station of Djougou, located in the Northern Benin, during the AMMA (African Monsoon Multidisciplinary Analyses) dry season experiment (January 2006). The methodology developed here is based, in a first time, on ground-based measurements for specifically estimating aerosol optical (scattering and absorption coefficients) and physical (number size distribution) properties. Additionally, we used aircraft, sun-photometer, Micro Pulse Lidar and MODIS observations for estimating, respectively, the vertical profiles of the thermodynamic parameters, the spectral variation of the Aerosol Optical Depth (AOD), the aerosol extinction vertical profiles and the surface albedo. Finally, all these informations have been used as input in the discrete ordinate radiative transfer model, for computing the direct radiative forcing of aerosols during the 17^{th}-23^{th} January period. We focus our simulations on the Top Of Atmosphere (TOA), Bottom Of Atmosphere (BOA), and ATMospheric (ATM) forcings.

During January 2006, sun-photometer measurements indicate a mean AOD of 0.90 ± 0.01 at 440 nm, indicating a significant aerosol loading over Djougou. The average aerosol absorption and scattering coefficients at the surface are 19.2 Mm^{-1} and 160 Mm^{-1} (at 520 nm), leading to a Single Scattering Albedo of 0.90 (moderate absorbing particles). The aerosol number size distribution measured over Djougou is clearly monomodal, with a nucleation mode, characterized by a mean geometric diameter of 96.5 nm and a geometric standard deviation of 1.87.

Associated with ground-based measurements, the vertical profile of the aerosol extinction coefficient has been investigated from a Micro Pulse Lidar (MPL). Results obtained over Djougou indicate a vertical structure characterized by the presence of two aerosol distinct layers, with a first one located between the surface and 1 km and a second one, characterized by aged biomass burning particles and located above (1.5–4.0 km). Micro Pulse Lidar profiles indicate also that the majority of the solar extinction is due to the BBL (~70% of the total AOD).

Our radiative simulations indicate that aerosols over Djougou lead to a significant diurnal average reduction of 61.3 Wm^{-2} in the surface solar radiation, an increase of 42.3 Wm^{-2} in the atmospheric solar absorption, and an increase of 19 Wm^{-2} in the reflected solar radiation at the top of atmosphere. Our simulations show also that the instantaneous surface forcing predicted by GAME can reach up to significant values of –240 Wm^{-2} for the 17^{th} january (AOD ~1.5) and for a solar zenith angle of 30°.

Changes in heating rates due to the presence of aerosols have been also investigated and discussed. The results we obtained indicate that the heating rates within the BHL and BBL are considerably enhanced, with a mean value of 1.48 and 1.90°K by day, respectively. In regards to such radiative forcings and changes in heating rate, future works are now clearly required for investigating the possible impact on the surface-atmosphere system during the dry season over the region of fires in West Africa.

CLIMATE AND REGIONAL AIR QUALITY

IMPACT OF CHANGING CLIMATE AND EMISSIONS ON SURFACE OZONE DISTRIBUTIONS AND EVOLUTION

HIROSHI TANIMOTO*, HITOSHI MUKAI, TOSHIMASA OHARA
National Institute for Environmental Studies Asian Environment Research Group Regional Atmospheric Modeling Section & Center for Global Environment Research, 16-2 Onogawa, Tsukuba, Ibaraki 305-8506, Japan

ITSUSHI UNO
Kyushu University

Key Words: Surface ozone; climate change; emissions; biomass burning; Asia.

Abstract Socio-economic activities are rapidly increasing in many countries of Asia due to a population explosion. It is also suggested that greenhouse gases alter regional climate, causing changes in meteorological factors such as atmospheric circulation, precipitation, heat balance, and monsoon. These factors have potential impact on chemical transformation and long-range transport of air pollutants. To detect current and future changes in air quality, systematic observational networks with wide spatial and temporal coverage are highly required. In this work, ground-based measurement data of ozone and its precursors at ~20 remote sites from multiple monitoring networks including operational programs and collaborative research projects in East Asia are integrated. The idea and basis is that in-situ data are more accurate than satellite and sounding data, though its spatial coverage is limited. The intercomparisons of reference scales in each network make ambient data comparable to each other, and the integration of such traceable data allows us to cover wide latitudinal zones ranging from subtropical to boreal regions in the western Pacific within ~2% uncertainties. The data are further utilized to test multi-year simulations by a regional chemistry transport model (CMAQ). Interestingly, there are sizable interannual variations (and latitudinal dependences), suggesting that changes in regional meteorology (e.g., transport paths, patterns, and efficiency) and/or enhanced precursor emissions from biomass burning may have large contribution. Trends for 7 years are not visible at boundary layer sites, but are substantial at mountainous sites during continental outflow seasons, possibly due to increasing NOx emissions from East Asia. Implications to Meditteranean region are discussed in terms of emissions from biomass burning in present and expanding human activities in future.

* To whom correspondence should be addressed.

A. Mellouki and A.R. Ravishankara (eds.), Regional Climate Variability and its Impacts in the Mediterranean Area, 113–127.

1. Introduction

Tropospheric ozone (O_3) plays a central role in controlling oxidizing capacity through generation of hydroxyl radicals (OH). As a major greenhouse gas, it is estimated to have made the third largest contribution to increases in direct radiative forcing since the pre-industrial era (Intergovernmental Panel on Climate Change (IPCC), 2001). While it was originally believed that the intrusion of stratospheric ozone into the troposphere dominated the abundance of tropospheric ozone, recent studies have demonstrated that the contribution of ozone photochemically produced in the lower atmosphere is also substantial (e.g., Lelieveld and Dentener, 2000; Wang et al., 1998). However, an unambiguous separation of the mechanisms that lead to the spatial and temporal variations of ozone has not been achieved, and understanding of distribution and evolution of tropospheric ozone is still a key aspect in atmospheric chemistry research (e.g., Monks, 2000). Recently it was reported that tropospheric ozone levels observed over Japan have been rising over the last three decades, likely as a consequence of increasing emissions of nitrogen oxides (NOx) from Asia (Naja and Akimoto, 2004). Emissions from Asia also have a potential impact on air quality over the United States, and on widespread ozone pollution in the Northern Hemisphere through intercontinental transport (Jacob et al., 1999; Jaffe et al., 1999; Wild and Akimoto, 2001).

2. Observational Data and Model Description

2.1. OBSERVATION SITES

Observational data used in this work were compiled from ongoing international monitoring programs operated mainly by the Ministry of the Environment of Japan as part of the Acid Deposition Monitoring Network in East Asia (EANET) program, and by the Japan Meteorological Agency as part of the Global Atmosphere Watch (GAW) programme of the World Meteorological Organization (JMA, 2005). In addition to these two programs, data from National Institute for Environmental Studies (NIES) and from the University of Tokyo/Chiba University (SKYNET) were used. We selected 18 remote boundary layer sites and mountainous sites, to investigate the broad features of low altitude ozone, and the influence of continental outflow as a function of latitude and longitude (Table 1). Data used for the analysis are hourly means over the period 1998 to 2004. Figure 1 shows the geographical locations of the 18 stations, ranging from 24°N to 45°N. All of these sites are away from major mega-city source regions of Asia, to minimize

TABLE 1. Data source, name, site code, and geographic information of ground-based stations used in this study. Station types are: CBL, continental rim boundary layer sites; OBL, open ocean boundary layer sites; MT, mountainous sites

Source	Name	Site Code	Latitude (ºN)	Longitude (ºE)	Altitude (m asl.)	Type
EANET	Rishiri	RIS	45.13	141.24	40	CBL
EANET	Tappi	TPI	41.25	140.35	106	CBL
EANET	Sado	SDO	38.25	138.40	110	CBL
EANET	Oki	OKI	36.28	133.18	90	CBL
EANET	Ogasawara	OGS	27.09	142.21	230	OBL
EANET	Okinawa	ONW	26.78	128.23	50	CBL
EANET	Tsushima	TSM	34.23	129.28	390	CBL
EANET	Happo	HPO	36.69	137.80	1850	MT
EANET	Nikko	NKO	36.78	139.52	1781	MT
EANET	Akagi	AKG	36.53	139.18	1500	MT
EANET	Tanzawa	TNZ	35.48	139.08	920	MT
NIES	Ochiishi	COI	43.16	145.50	45	CBL
NIES	Hateruma	HAT	24.05	123.81	30	CBL
JMA	Ryori	RYO	39.03	141.83	230	CBL
JMA	Yonagunijima	YON	24.47	123.02	30	CBL
JMA	Minamitorishima	MNM	24.30	153.97	8	OBL
SKYNET	Fukuejima	FKE	32.75	128.68	NA	CBL
SKYNET	Amami	AMA	28.40	129.70	NA	CBL

the impact of local and domestic pollution. Among these, sixteen stations are located in the boundary layer of the Eurasian continental rim, two stations are in open ocean marime boundary layer, and four stations are on mountains. Many of the data are intercompared and referenced to the Standard Reference Photometer (SRP) owned by NIES (Tanimoto et al., 2006).

Instruments for ozone and carbon monoxide measurement at Rishiri Island, which we will describe in detail later, have been described in detail in Tanimoto et al. (2000). Briefly, ozone and carbon monoxide were measured by a commercial UV absorption analyzer and a modified nondispersive infrared (NDIR) photometer instrument, respectively. Both ozone and carbon monoxide data were recorded on a personal computer via analog-to-digital boards. The instrument cycle for carbon monoxide was changed to consist of 40-min ambient measurement periods and 20-min zeroing periods each hour to obtain the precision for low carbon monoxide mixing ratio measurements. A standard addition calibration was made every 10 days using 1.8 ppmv carbon monoxide in air (Nippon Sanso). The detection limit of the ozone measurements is 1 ppbv, and the overall uncertainty is estimated

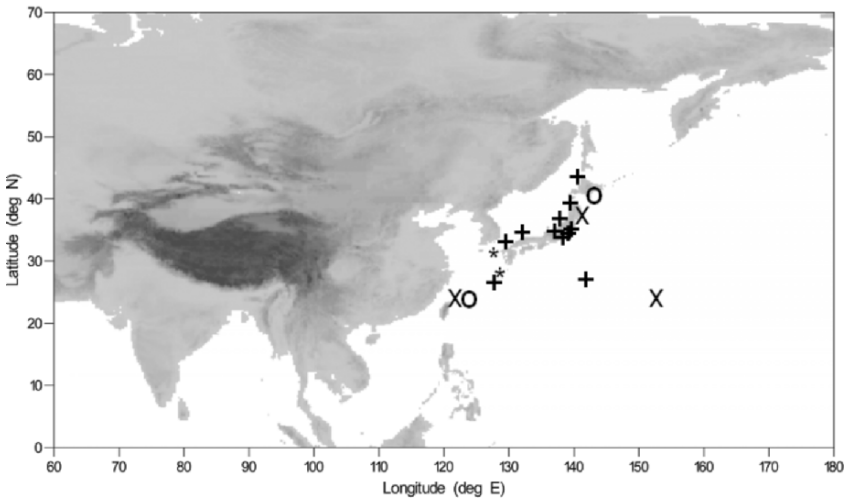

Figure 1. Geographical locations of ground-based stations in East Asia. Each station is marked with the following symbols: EANET (+), NIES (o), JMA (x), and SKYNET (*)

to be 5% at a mixing ratio of 20 ppbv. The detection limit of the hourly carbon monoxide measurements is 10 ppbv, based on 3 × standard deviations of baseline fluctuation. The overall uncertainty of the hourly average carbon monoxide data at a typical mixing ratio of 150 ppbv is estimated to be 7%, including contributions from the precision, flow controllers, and calibration gas.

2.2. CHEMICAL TRANSPORT MODEL

A three dimensional regional-scale chemical transport model used in this study has been developed jointly by Kyushu University and the National Institute for Environmental Studies (Uno et al., 2005) based on the Models-3 Community Multiscale Air Quality (CMAQ) modeling system released by the US EPA (Byun and Ching, 1999). Briefly, the model is driven by meteorological fields generated by the Regional Atmospheric Modeling System (RAMS) with initial and boundary conditions defined by NCEP reanalysis data. The horizontal and vertical resolutions are 80 km and 14 layers (up to 23 km), respectively. The SAPRC-99 scheme is applied for gas-phase chemistry. Emissions from anthropogenic and biomass burning sources are supplied according to Streets et al. (2003a, b). Lateral boundary conditions are provided by a global chemical transport model, CHASER (Sudo et al., 2002).

3. Interannual Variations and Recent Trends in Asia

3.1. INTERANNUAL VARIATIONS

Figure 2 shows surface ozone mixing ratios as a function of latitude and year from 1998 to 2003. The latitudinal dependence of surface ozone was constructed by observations at multiple ground-based stations distributed in wide range from subtropics to boreal latitudinal zones. Overall ozone mixing ratios range from ~20 ppbv to ~60 ppbv throughout the year. Day-to-day pollution episodes are observed as thin lines, suggesting that these pollutin events are large scale phenomena, which often occur with synoptic scale transport in East Asia. There are distinct seasonal cycles observed. Spring maxima, summer minima, and fall secondary peaks are commonly observed at all latitudinal regions. The existence of seconday peaks in fall is a characteristic phenomenon in East Asia (Pochanart et al., 2002; Tanimoto et al., 2002a, b). Mean seasonal cycles, particularly the sprimg maximum, are dependent of latitude, as reported in our previous paper (Tanimoto et al., 2005). Closer look at year-to-year variability reveals that there are slight interannual variations, as we discuss in more detail in the following sections.

Figure 3 shows time series of Multivariate ENSO Index (MEI) and fire spots detected by the ATSR satellite sensor over Siberia from 1998 to 2004. The MEI is known to be a good indicator to represent global scale El Nino – Southern Oscillation phenomena rather than regional ones. The numbers of fire spots are the sum of those detected over four regions in Siberia (western Siberia, eastern Siberia, far eastern Siberia, and Kamchatka peninsula). The

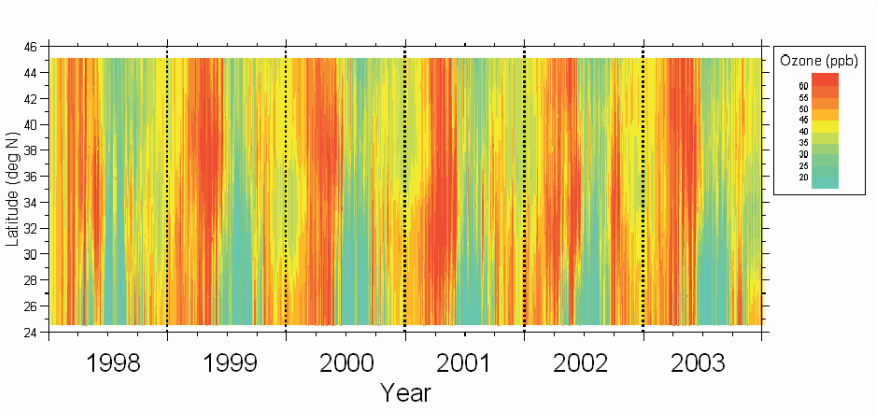

Figure 2. Observed latitudinal dependence of the surface ozone temporal variations in East Asia. The observed contour is constructed by bilinear interpolation of measurement data, followed by weighted smoothing

MEI shows positive index in earlier half of 1998, and from latter half of 2002 to whole period of 2003-2004. In contrast, the MEI indicates negative values from latter half of 1998 to earlier half of 2002. It is well known that strong El Nino occurred in 1997-1998, causing severe biomass burnings in Southeast Asia. It was also reported that extensive fires in boreal forests took place from summer to fall in 1998, releasing huge amount of trace gases including ozone precursors, as reported by measurements of carbon monoxide (e.g., Tanimoto et al., 2000; Zhou et al., 2002; Yurganov et al., 2004). This feature is clearly illustrated in fire spot data by ATSR. The ATSR data suggest that similar forest fires in Siberia occurred in 2002 and 2003. The enhanced carbon monoxide, and hence ozone levels due to Siberian forest fires were reported over western North America (Jaffe et al., 2004). In contrast, the numbers of fire spots in 1999, 2000, 2001, and 2004 are relatively small, indicating that Siberian forest fires were not so extensive compared to 1998, 2002, and 2003. It seems that the MEI and the numbers of fire counts well correlated with each other, recent paper suggests only weak correlation between ENSO and boreal forest fires in Siberia since Siberian fires are not mainly driven by climate factors such as lightning (Patra et al., 2005). Nevertheless, we believe that meteorological parameters including soil moisture, precipitation, and vegetation coverage are still important for accelerating or damping forest fires.

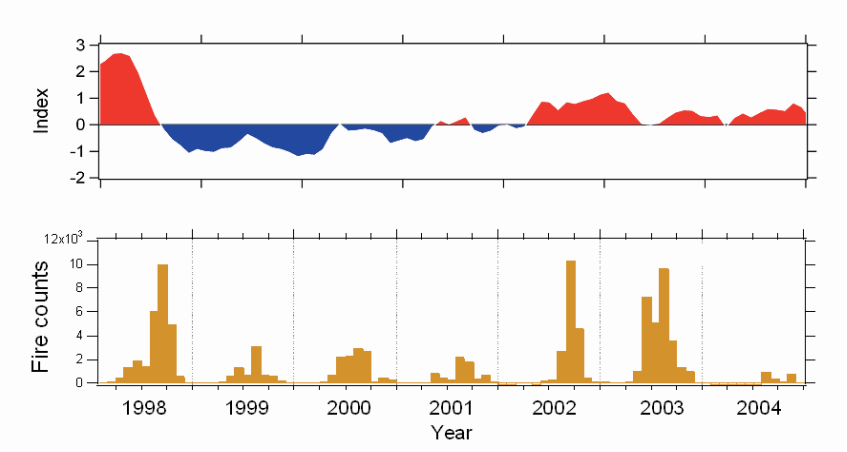

Figure 3. Trends in Multivariate ENSO Index (MEI) (upper panel) and fire spots detected by ATSR over Siberia from 1998 to 2004 (lower panel). MEI is taken from NOAA CIRES web page (http://www.cdc.noaa.gov/people/klaus.wolter/MEI/). The numbers of fire spots are taken from ATSR World Fire Atlas web site (http://dup.esrin.esa.int/ionia/wfa/index.asp), and are based on algorism 1 (3.7 μm > 312 K). The sum of those detected over four regions in Siberia as shown in Figure 4

Figure 4 shows distribution of ATSR fire spots over Siberia during July – September 1998. There were extensive and frequent fires in far eastern Siberia. Fires counts are much less in western and eastern Siberia, and Kamchatka peninsula in this summer season. However, location and frequency of fires largely depend on season and year (Kajii et al., 2002). Also shown in the figure is the location of Rishisi Island, where we have made continuous measurements of both ozone and carbon monoxide since 1998. The station is a remote site, located on the northern tip of Japan, close to the border to Russia. Our previous paper reported observation of very high (>1000 ppbv) carbon monoxide mixing ratios (as hourly means) at the site (Tanimoto et al., 2000). However, enhancement of ozone in the fire plume was not so high as that of carbon monoxide, likely due to short transport time from the emission source to the site, small amount of NOx emitted from the fires, or insufficient solar radiation due to sea fog, which is common in summer season around the site (Tanimoto et al., 2000).

Figure 5 shows anomalies in ozone and carbon monoxide observed at Rishiri Island in 1998. Both ozone and carbon monoxide clearly depict correlative anomalies, having large positive peaks in summer. Again, positive anomaly in carbon monoxide is due to emissions from forest fires in Siberia. This suggests that mean mixing ratios of ozone were substantially enhanced by the fires, as a consequence of photochemical production. The ozone build up due to forest fires was 4 ppbv, with enhancement of 60 ppbv for carbon monoxide. Northern part of Japan substantially receives air masses from the

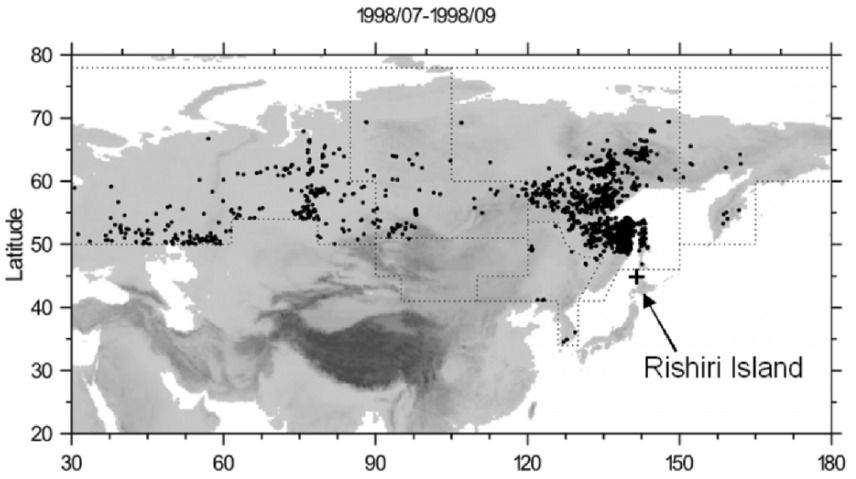

Figure 4. Distribution of fire spots detected by ATSR over Siberia during July – September 1998. Data are based on algorism 1 (3.7 μm > 312 K). Location of Rishiri Island is shown as +

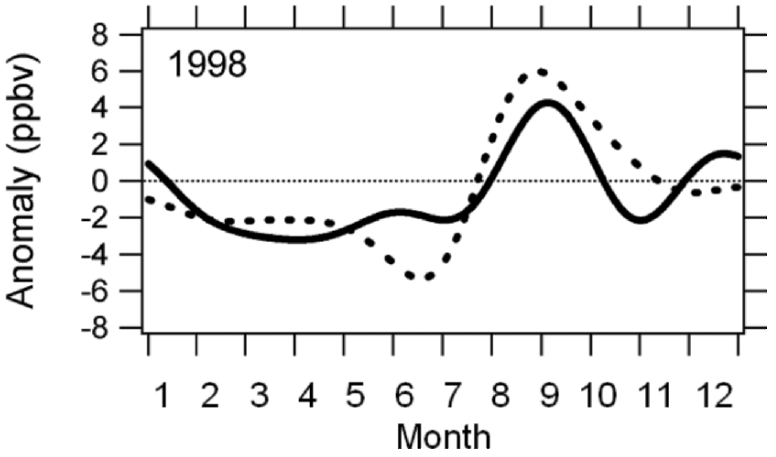

Figure 5. Anomalies in ozone (solid) and carbon monoxide (dashed, × 1/10) observed in 1998 at Rishiri Island, in northern Japan

high latitudes, for example, clean continental air masses from Siberia originating from the north, and high-latitude maritime air masses from the Bering Sea. These circulation patterns contribute to efficient transport of fire plumes to Rishiri site.

3.2. RECENT TRENDS

Figure 6 shows long-term trends in "bottom-up" NOx emissions from Europe, North America, and Asia over the past 30 years (Akimoto, 2003). In contrast to the emissions from Europe and North America, showing decreasing and stabilized trends, respectively, the emissions from Asia are rapidly increasing. The Asian emissions are now beyond the European emissions, and will be the largest source of NOx, one of the most important ozone precursors. East Asian emissions are ~50% of Asian emissions. Chinese emissions dominate ~75% of East Asian emissions, mainly because emissions from power plants and transportation sectors are growing. The estimate predicts a rapid increase from 1996 to 2003, with the increasing rate of +145%. This has potential impacts on the distribution and evolution of surface ozone not only in Asia but also in the northern hemisphere. Recent trends in surface ozone mixing ratios observed at remote boundary layer sites show negligible increase and those at mountainous sites show significant increasing tendency. However, our model including year-dependent emissions inventory did not reproduce observed features. Detailed description and possible reasons for the discrepancy between observation and model will be reported elsewhere (Tanimoto et al., manuscript in preparation, 2006).

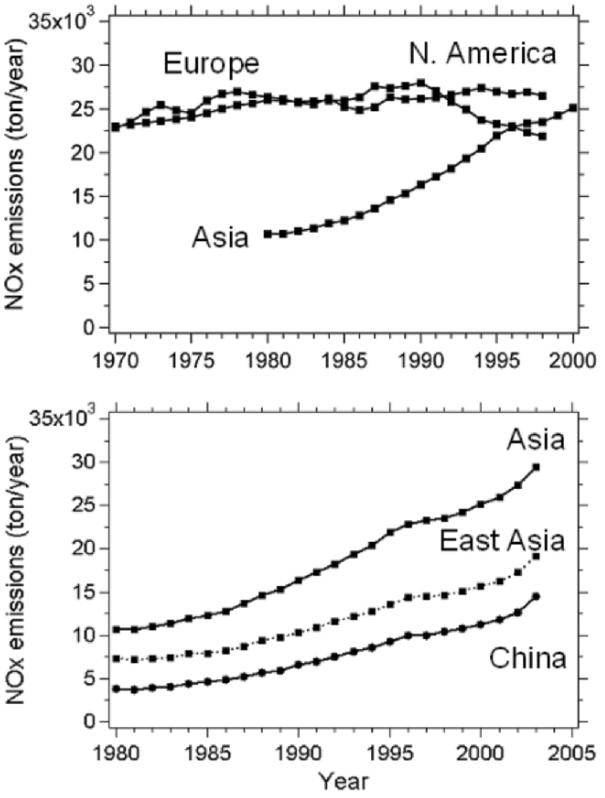

Figure 6. Long term trends in "bottom-up" NOx emissions from Europe, North America, and Asia (Akimoto, 2003) (upper panel). East Asian and Chinese emissions are further illustrated in detail (lower panel). Recent emission estimates are from REAS (Regional Emissions Inventory in ASia) by JAMSTEC/FRCGC (T. Ohara et al., in preparation, 2006)

4. Implication to Mediterranean Region

4.1. BIOMASS BURNING

Figure 7, 8, 9, 10, and 11 show distribution of fire spots detected by ATSR in Mediterranean region during summertime. Mediterranean region is nominally divided into four zones: North Africa, Europe, Middle East, and Western Siberia. Substantial amount of fires are often observed in every sector. In Europe, there are substantial fires over Portugal in every summer, likely due to forest fires driven by dry land surface. It is well known that forest fires frequently occurred in Europe in the summer of 2003. In 1998, fires are also

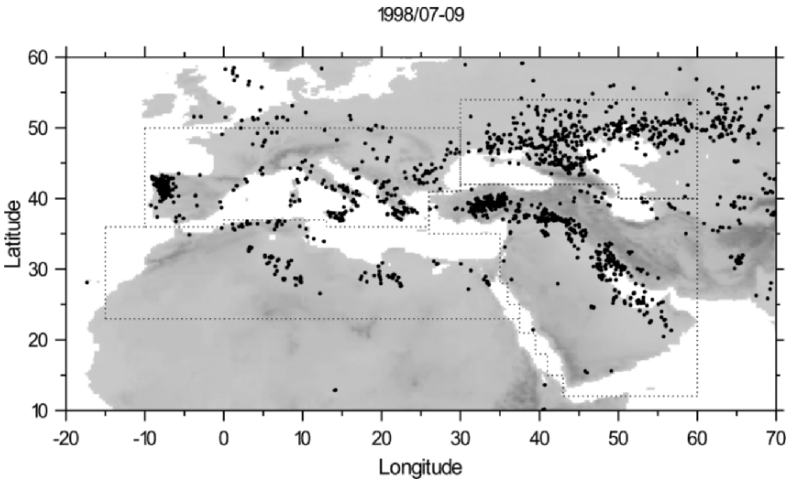

Figure 7. Distribution of fire spots detected by ATSR in Mediterranean region during July – September 1998. Data are based on algorism 1 (3.7 μm > 312 K)

observed over Turkey. Fires detected over North Africa and Middle East are likely due to agricultural burning or oil burning, respectively. It should be noted that extensive forest fires are observed over Western Siberia, particularly in 2001 and 2002.

Figure 12 summarizes time series of fire spots detected by ATSR in Mediterranean region from 1997 to 2005. The total count numbers are highest in

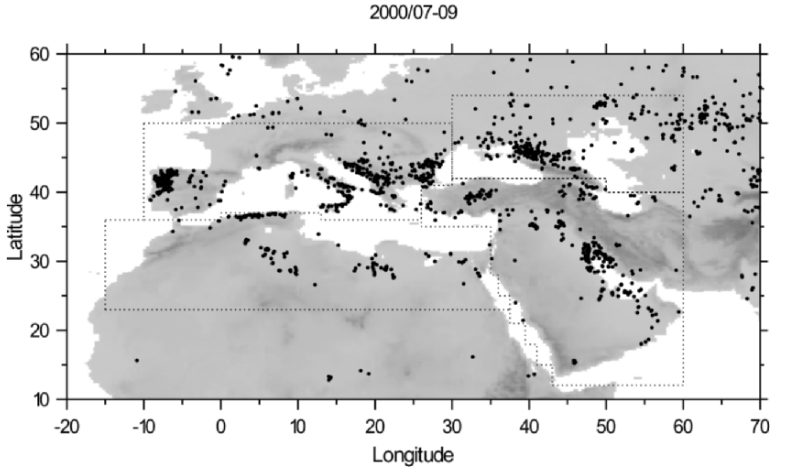

Figure 8. Same as Figure 7, but for 2000

Middle East, and those in other regions are comparably small. The high numbers in Middle East would be very likely because of oil burning activities. Interestingly, all regions show clear seasonal variations, having a distinct summer maximum and a winter minimum. This would be related to dry weather condition in summertime, which is typical to Mediterranean region. The fires in Western Siberia in 2001 and 2002 are again apparently overwhelming other years, and would have impacted on air quality in Mediterranean region during summer, depending on synoptic scale transport.

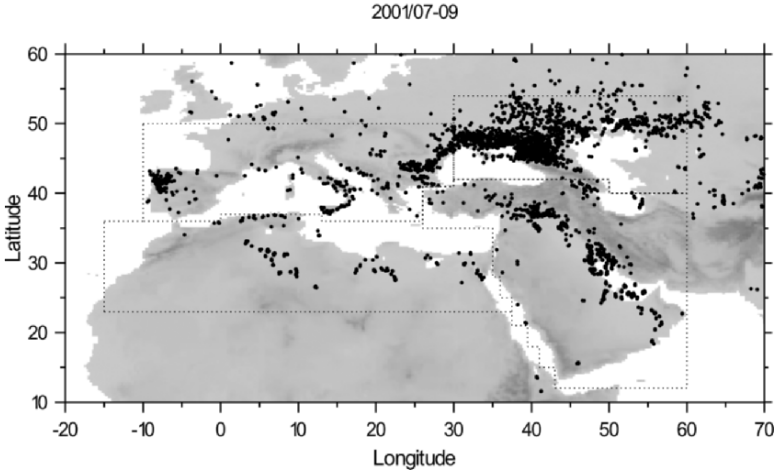

Figure 9. Same as Figure 7, but for 2001

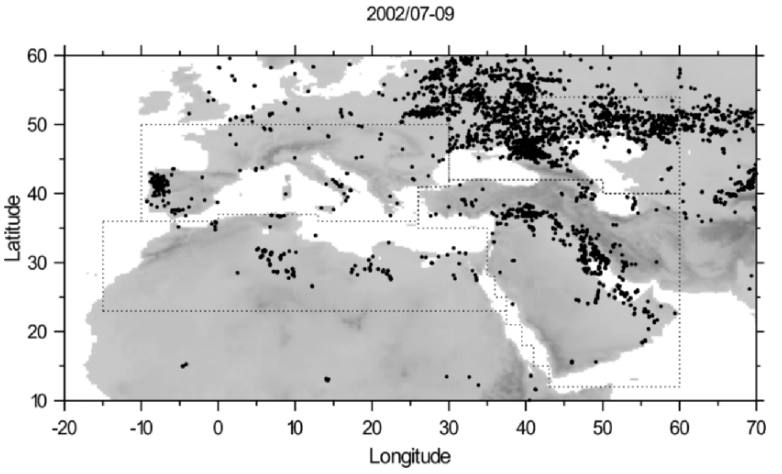

Figure 10. Same as Figure 7, but for 2002

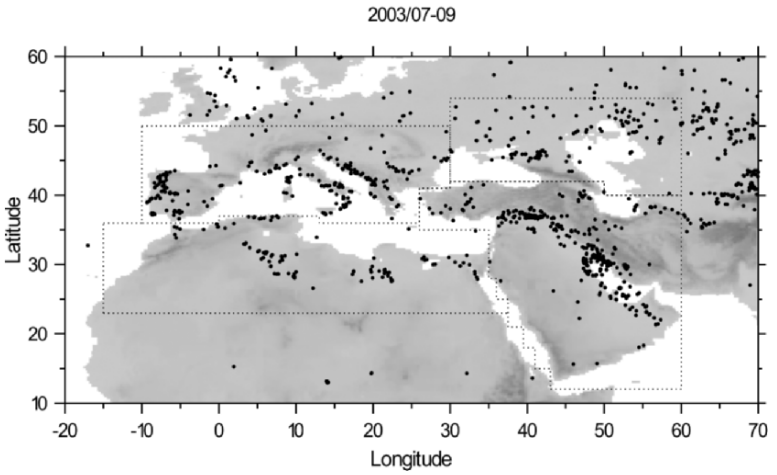

Figure 11. Same as Figure 7, but for 2003

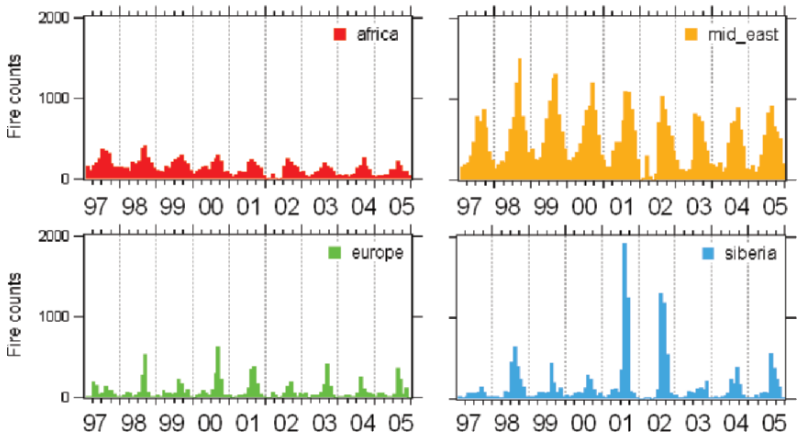

Figure 12. Time series of fire spots detected by ATSR in Mediterranean region from 1997 to 2005. Region are nominally classified into four sectors: (a) North Africa, (b) Europe, (c) Middle East, and (d) Western Siberia

4.2. FUTURE AIR QUALITY

Figure 13 illustrates monthly "surface" ozone increase for July during 2000-2100, based on the ensemble model simulation with the emission inventory of IPCC TAR A2 scenario. The chemical transport models predict that surface ozone levels will be enhanced throughout the world in future, particularly over Asia (e.g., China and India) where NOx emissions are estimated to

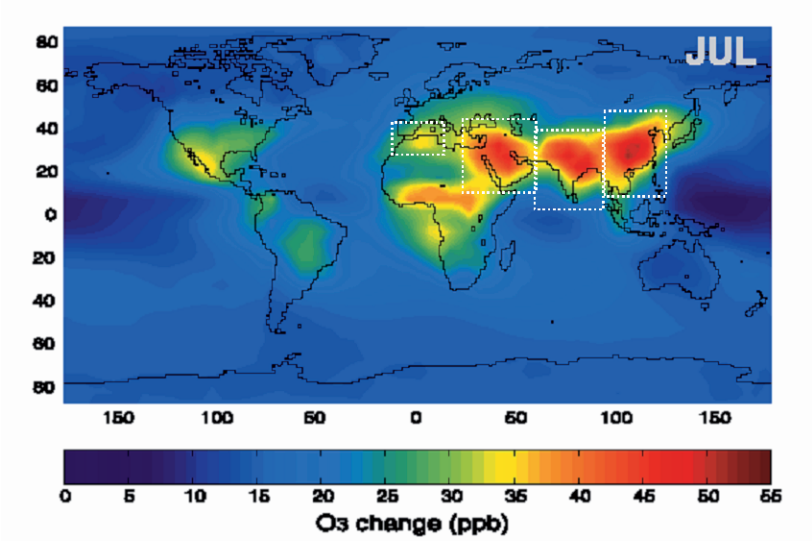

Figure 13. Model predicted monthly "surface" ozone increase for July during 2000-2100, based on IPCC TAR A2 emissions scenario (Prather et al., 2003). Highlighted regions are Middle East and North Africa as well as East and South Asia

increase most severely (Prather et al., 2003). Under these circumstances consideration of hemispheric and regional influences is crucial to design strategies to meet Air Quality Standards (AQS) in many countries in Asia, and likely in other countries in northern hemisphere. The heavily impacted regions are not only Asia. The models predict that air quality over Middle East and North Africa will also become severe, likely due to increase in population and socioeconomic activities. This greatly highlights the need of environmental strategies for air pollution abatement in Mediterranean region in near future.

5. Summary

To summarize,

- Boreal forest fires in Siberia play an important role in controlling inter-annual variability of surface ozone and carbon monoxide. Since emissions from forest fires have much larger uncertainties than those from anthropogenic sources, better quantification of emissions inventory from forest fires with high-time resolution is important. The question is how can we better convert fire spots to emissions inventory of chemical species?
- Bottom-up estimates in past and near-future predict large increase in NOx (and VOC) emissions from rapidly developing countries. The emissions may affect air quality not only regionally but also hemispherically.

More efforts can be made to improve year-dependent emissions inventtory by combination of ground-based, aircraft, and space-based measurements.

- Much larger uncertainties exist in VOCs than in NOx. More speciated inventory and more explicit treatment of VOC oxidation in chemical transport models are desired.
- In future, changes in land-use, agriculture style, and forest fires due to climate change have potential impact on air quality.

6. Acknowledgments

Multivariate ENSO Index dataset is taken from NOAA-CIRES web page. ATSR World Fire Atlas dataset is taken from the Data User Element of the European Space Agency. We thank Miori Ohno for figure preparation.

7. References

Akimoto, H., 2003, Global air quality and pollution, *Science* **302:** 1716-1719.

Byun, D.W. and Ching, J.K.S., 1999, *Science algorithms of the EPA Models-3 community multi-scale air quality (CMAQ) modeling system*, NERL, Research Triangle Park, NC.

Intergovernmental Panel on Climate Change (IPCC), 2001, *Climate Change 2001: The Scientific Basis*, edited by J. T. Houghton et al., Cambridge Univ. Press, New York.

Jacob, D.J., Logan, J.A., and Murti, P.P., 1999, Effect of rising Asian emissions on surface ozone in the United States, *Geophys. Res. Lett.* **26:** 2175-2178.

Jaffe, D.A., et al., 1999, Transport of Asian Air Pollution to North America, *Geophys. Res. Lett.* **26:** 711-714.

Jaffe, D., Bertschi, I., Jaegle, L., Novelli, P., Reid, J.S., Tanimoto, H., Vingarzan, R., and Westphal, D.L., 2004, Long-range transport of Siberian biomass burning emissions and impact on surface ozone in western North America, *Geophys. Res. Lett.* **31:** doi:10.1029/2004GL020093.

Japan Meteorological Agency (JMA), 2005, *Annual Report on Atmospheric and Marine Environment Monitoring No.5 (CD-ROM)*.

Kajii, Y., et al., 2002, Boreal forest fires in Siberia in 1998: Estimation of area burned and emissions of pollutants by advanced very high resolution radiometer satellite data, *J. Geophys. Res.* **107:** doi:10.1029/2001JD001078.

Lelieveld, J. and Dentener, F.J., 2000, What controls tropospheric ozone?, *J. Geophys. Res.* **105:** 3531-3551.

Monks, P.S., 2000, A review of the observations and origins of the spring ozone maximum, *Atmos. Environ.* **34:** 3545-3561.

Naja, M., and Akimoto, H., 2004, Contribution of regional pollution and long-range transport to the Asia-Pacific region: Analysis of long-term ozonesonde data over Japan, *J. Geophys. Res.* **109:** doi:10.1029/2004JD004687.

Patra, P.K., Ishizawa, M., Maksyutov, S., Nakazawa, T., Inoue, G., 2005, Role of biomass burning and climate anomalies for land-atmosphere carbon fluxes based on inverse modeling of atmospheric CO_2, *Global Biogeochem. Cycles* **19:** doi:10.1029/2004GB002258.

Prather, M., et al., 2003, Fresh air in the 21st Century?, *Geophys. Res. Lett.* **30:** doi:10.1029/2002GL016285.

Pochanart, P., Akimoto, H., Kinjo, Y., and Tanimoto, H., 2002, Surface ozone at four remote island sites and the preliminary assessment of the exceedances of its critical level in Japan, *Atmos. Environ.* **36:** 4235-4250.

Streets, D.G., et al., 2003a, An inventory of gaseous and primary aerosol emissions in Asia in the year 2000, *J. Geophys. Res.* **108:** doi: 10.1029/2002JD003093.

Streets, D.G., Yarber, K.F., Woo, J.-H., and Carmichael, G.R., 2003b, Biomass burning in Asia: Annual and seasonal estimates and atmospheric emissions, *Global Biogeochem. Cycles* **17:** doi:10.1029/2003GB002040.

Sudo, K., Takahashi, M., Kurokawa, J., and Akimoto, H., 2002, CHASER: A global chemical model of the troposphere: 1. Model description, *J. Geophys. Res.* **107:** doi:10.1029/2001JD001113.

Tanimoto, H., Kajii, Y., Hirokawa, J., Akimoto, H., and Minko, N.P., 2000, The atmospheric impact of boreal forest fires in far eastern Siberia on the seasonal variation of carbon monoxide: Observations at Rishiri, a northern remote island in Japan, *Geophys. Res. Lett.* **27:** 4073-4076.

Tanimoto, H., Furutani, H., Kato, S., Matsumoto, J., Makide, Y., and Akimoto, H., 2002a, Seasonal cycles of ozone and oxidized nitrogen species in Northeast Asia, 1, Impact of regional climatology and photochemistry observed during RISOTTO 1999-2000, *J. Geophys. Res.* **107:** doi:10.1029/2001JD001496.

Tanimoto, H., Wild, O., Kato, S., Furutani, H., Makide, Y., Komazaki, Y., Hashimoto, S., Tanaka, S., and Akimoto, H., 2002b, Seasonal cycles of ozone and oxidized nitrogen species in northeast Asia, 2, A model analysis of the roles of chemistry and transport, *J. Geophys. Res.* **107:** doi:10.1029/2001JD001497.

Tanimoto, H., Sawa, Y., Matsueda, H., Uno, I., Ohara, T., Yamaji, K., Kurokawa, J., and Yonemura, S., 2005, Significant latitudinal gradient in the surface ozone spring maximum over East Asia, *Geophys. Res. Lett.* **32:** doi:10.1029/2005GL023514.

Tanimoto, H., Mukai, H., Hashimoto, S., and Norris, J.E., 2006, Intercomparison of ultraviolet photometry and gas-phase titration techniques for ozone reference standards at ambient levels, *J. Geophys. Res.* **111:** doi:10.1029/2005JD006983.

Uno, I., et al., 2005, Development of RAMS/CMAQ Asian Scale Chemical Transport Modeling System, *J. Jpn. Soc. Atmos. Environ.*, **40:** 148-164.

Wang, Y.H., Logan, J.A., and Jacob, D.J., 1998, Global simulation of tropospheric O_3-NOx-hydrocarbon chemistry, 2. Model evaluation and global ozone budget, *J. Geophys. Res.* **103:** 10,727-10,756.

Wild, O. and Akimoto, H., 2001, Intercontinental transport of ozone and its precursors in a three-dimensional global CTM, *J. Geophys. Res.* **106:** 27,729-27,744.

Yurganov, L.N., et al., 2004, A quantitative assessment of the 1998 carbon monoxide emission anomaly in the Northern Hemisphere based on total column and surface concentration measurements, *J. Geophys. Res.* **109:** doi:10.1029/2004JD004559.

Zhao, Y., et al., 2002, Spectroscopic measurements of tropospheric CO, C_2H_6, C_2H_2, and HCN in northern Japan, *J. Geophys. Res.* **107:** doi:10.1029/2001JD000748.

SHORT AND LONG-TERM TRANSPORT OF CRUSTAL AND ANTHROPOGENIC INORGANIC COMPONENTS OF COARSE AND FINE AEROSOLS OVER BEIRUT, LEBANON

NAJAT A. SALIBA[1]*, HOVIG KOUYOUMDJIAN[1], GHADA AL KADAMANY[1] AND MOHAMMAD ROUMIE[2]
[1]*American University of Beirut, Chemistry Department*
[2]*National Council for Scientific Research, Ion Beam Analysis Laboratory, Beirut, Lebanon*

NAJAT A. SALIBA*, CORRESPONDING AUTHOR
American University of Beirut, Chemistry Department

Key Words: Dust, coarse and fine particles; Beirut; Lebanon; Eastern Mediterranean region; inorganic composition.

Abstract Beirut is an interesting experimental environmental chamber for its a cross road for several meteorological phenomena. Hence, measurements of fine and coarse particles were carried out during a whole year between February 2004 and January 2005 in a congested place (BH) in Beirut, Lebanon. The ionic and elemental compositions of PM collected in BH were determined using ion chromatography and PIXE analysis, respectively. Other PM10 mass concentrations and chemical speciation were conducted in several urban places in Beirut for comparison purposes. BH results showed that crustal elements mainly Ca, Ti, Mn and Fe, which were typical products of the calcite and basaltic rocks specific to Lebanon, were higher than most reported values in the eastern Mediterranean region and constituted the main component of the coarse particles. In addition, coarse nitrate and sulfate ions resulted from the respective reactions of nitric and sulfuric acids with a relatively high amount of dust, i.e., calcium carbonate. In the fine particles, ammonium sulfate predominated with higher amounts determined in the summer. While nitrate was mainly due to local heavy traffic, sulfates were due to local and long-range transport phenomena. Chlorine levels were high when the wind originated from the sea and low during sand storms. In addition to sea salt, elevated levels of chloride were also attributed to waste mass burning in proximity to the site. Variability of the different elements seemed to be strongly dependent upon meteorological and atmospheric stability conditions and, in particular, wind regimes. Anthropogenic elements

* To whom correspondence should be addressed.

A. Mellouki and A.R. Ravishankara (eds.), Regional Climate Variability and its Impacts in the Mediterranean Area, 129–142.

like Cu and Zn were generated from local industrial emission and vehicle exhausts whereas elevated levels of Pb were directly linked to a southerly wind originated from Egypt and Israel. The comparison of BH to other micro environmental sites in Beirut showed that high diurnal and seasonal variations in PM10 concentrations and ionic composition confirmed the dynamicity of the eastern Mediterranean environment. Nevertheless, higher PM10 levels seemed to correlate with congested areas. Considering the location in Beirut at the levant of the eastern Mediterranean region, its local atmospheric environment is highly affected by the regional pollution and the meteorological conditions.

1. Introduction

It has been well established that in the Eastern Mediterranean region, enhanced photochemical reactions due to pollutants originating from Eastern Europe, marine aerosols and dust coming from Africa produce high levels of secondary pollutants and other reactive species (Alpert et al., 1990; Dayan et al., 1991; Goudie and Middleton, 2001; Kouvarakis et al., 2000; Kubilay et al., 2000; Lelieveld et al., 2002). In fact, several studies in Greece, Turkey and Israel have confirmed the predicted high levels of ozone over the region, and have suggested that the Saharan deserts (S/SW) constitute the major source of mineral elements in the region (Kubilay et al., 2000). In addition to long-range transported pollutants, local emissions play an important role in increasing the levels of HNO_3, H_2SO_4 and NH_3 (Danalatos and Glavas, 1999; Erduran and Tuncel, 2001; Kassomenos et al., 1999). Beirut exhibits several sand storm episodes during the fall and spring seasons, high traffic density, and intense solar radiation in the summer. It is also a semi-island like city influenced by marine aerosols from three directions and bounded by high mountains from the East. Considered as an interesting experimental chamber, environmental emission levels and chemical composition of particulate matters measured in Beirut are used to assess the effect of local emissions on the regional concentrations of coarse and fine particles and their chemical transformations.

2. Experimental Procedure

2.1. SAMPLING

The yearly random sampling (every sixth day) between February, 2004 and January, 2005 was conducted in Bourj Hammoud (BH) (33º53′N, 35º32′E) street in Beirut. BH is a populated area with several commercial and industrial facilities (Figure 1). It is considered a good representation of urban

Beirut since it experiences high traffic density, sea spray, Beirut harbor operations, and some waste-mass burning activities. Sampling was performed at 3 m above the ground on the municipality building overlooking a busy street with heavy traffic. The sampling site is located one kilometer away from the Mediterranean coast at an elevation less than 10 m above sea-level. Coarse and fine particulate matters were drawn from the air stream by the use of a dichotomous sampler (Sierra-Anderson Dichotomous Model SA246B) (Shaka' and Saliba, 2004). The method of collection, conditioning and weighing of the filters is described in detail in Kouyoumdjian and Saliba (2006).

Seasonal sampling in other urban Beirut sites was conducted between June 2004 and March 2005. Sites distributed as shown in Figure 1 are: Ain el-mreiseh (*AM*), Ashrafieh (*Ash*), Borj El-Barajneh (*BB*), Borj Hammoud (*BH*), Dekweneh (*Dek*), Horsh Tabet (*HT*), Mallah (*Mal*), Salim Slem (*SS*), Tarik El-Matar (*TM*). At each location, three outdoor PM10 measurements were taken in summer and two in winter. Each PM10 measurement was conducted using the Mini-Partisol Air Sampler model 2100 (Rupprecht and Patashnick Co.). It consisted of a top-mounted bracket containing a particle inlet for PM_{10} and a single 47 mm filter holder, which was used for PM sampling. Each PM_{10} sample was collected on a PTFE Teflon filter for a 24-hour period at a sampling rate of 5 L/min. The Teflon filters used for PM10 collection were subjected to pre and post-sampling gravimetric analysis, which was carried out using a Metler-Toledo microgram analytical balance model UMX2. The filters were desiccated for 24 hours before each mass measurement.

2.2. CHEMICAL ANALYSIS

2.2.1. Ion Analysis

Collected filters and blanks were dissolved in water and then analyzed for their ion content (Kouyoumdjian and Saliba, 2006). In brief, ions were extracted from filters ultrasonically using 20ml of deionized water (18 $M\Omega\ cm^{-1}$) for 40 min. One set of coarse and fine filters collected on the same day, were dedicated for the analysis of anion (SO_4^{2-}, NO_3^-, Cl^-) concentrations and another set of filters for cation (Na^+, K^+, Ca^{2+}, Mg^{2+}, NH_4^+) concentrations using ion Chromatography (IC, model AllTech). Ion concentrations were determined in relative to calibration curves with a regression range (r^2) of 0.993 and 0.999. The relative standard deviation for each ion was less than 0.71 and the sensitivity of the detector was 0.01 μS.

2.2.2. Sampling Artifact

Filter based aerosol sampling for an extended period of time is accompanied with positive or negative artifacts (Sloss and Smith, 2000). Artifacts are

reduced due to the use of hydrophobic Teflon filters for sampling. Unlike quartz or glass fiber filters, Teflon is known for its inertness and low tendency for SO_2 absorption (Artaxo et al., 2005; Tsai and Perng, 1998).

2.2.3. PIXE Analysis

The elemental composition (Si, S, Cl, K, Ca, Ti, V, Cr, Mn, Fe, Ni, Cu, Zn and Pb) of the aerosol samples was measured using in vacuum Proton Induced X-ray Emission (PIXE), using the accelerator facility at the Lebanese Atomic Energy Commission (Kouyoumdjian and Saliba, 2006).

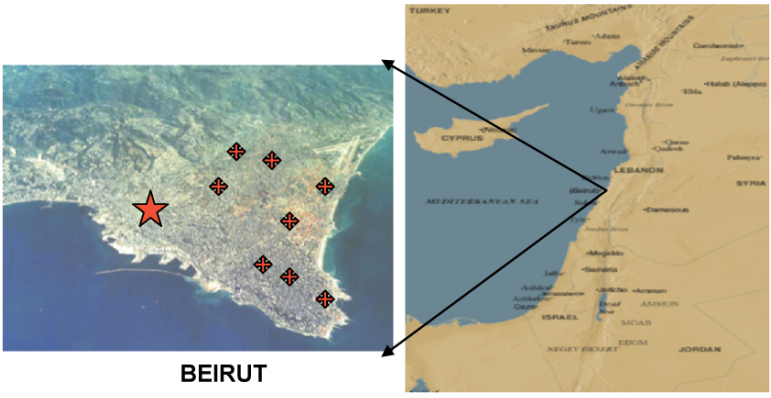

Figure 1. Different urban sites measured in the city of Beirut. The star shows the BH location where annual averages of PM mass concentrations and chemical compositions are reported and the crosses indicate other urban sites where only three measurements were conducted in the summer and two in the winter

3. Results and Discussions

3.1. ANNUAL PM10-2.5 AND PM2.5 MASS CONCENTRATIONS AND COMPOSITION

Annual averages of PM10-2.5 and PM2.5 concentrations at BH were 53 ± 20 and 31 ± 9 μg m^{-3}, respectively. The highest PM concentrations were recorded in dust storms occurring in the fall and spring seasons. Other coastal Mediterranean regions reported a similar behavior (Dayan et al., 1991; Goudie and Middleton, 2001; Gullu et al., 2000; Kubilay et al., 2000; Rodríguez et al., 2002). Figure 2 represents the inorganic normalized ionic composi tion of coarse and fine particles based on ion chromatography analysis. In the coarse mode (Figure 2A), an overall average of 6.66 ± 1.1% of Ca in mass of PM with little monthly variation was determined. This was attributed to the calcitic nature of the rocks in Lebanon (Abdel-Rahman and Nader, 2002). Sodium also showed a constant variation during the days sampled between

April and December with lower concentrations determined in the days sampled in February, March, and January due to wind originating from dry lands. Potassium, magnesium and ammonium were at much lower concentration in the coarse mode, and hence their variational analysis is omitted. The chloride concentration originated from sea salt and defined as 1.174 the concentration of Na^+, constituted only a small percentage of the total concentration of chloride in the coarse particles. The lowest value of chloride observed in November was assigned to sea-salt chloride. Higher values determined during other sampling days, were attributed to the emission of HCl from the waste mass burning activities located at 450 m away from the sampling site. High Cl^- concentration usually indicates that the sea salt reaction with acids leading to nitrated and sulfated salts and gaseous HCl is limited (Kerminen et al., 1997; Kocak et al., 2004; Niemi et al., 2005; Pathak et al., 2004; Zhuang et al., 1999) whereas the reactions of $CaCO_3$ (main component of mineral dust) with HNO_3 and H_2SO_4 is predominant (Evans et al., 2004; Laskin et al., 2005). In the fine mode, both ammonium and sulfate exhibited the highest concentrations in the summer due to the enhancement of fermentation and photooxidation reactions, respectively. A strong correlation ($r^2 > 0.97$) between NH_4^+ and SO_4^{2-} indicated that the predominant salt present in the fine particles is $(NH_4)_2SO_4$. Also, the high correlation ($r^2 = 0.65$) identified between Cl^- and Na^+ suggested the presence of NaCl. The sum of the micro-equivalent anions (Cl^-, NO_3^-, and SO_4^{2-}) in the fine particles was found to be highly correlated to the sum of all the micro-equivalent cations (Na^+, K^+, NH_4^+, Mg^{2+} and Ca^{2+}). In addition, the median cation/anion ratio was 0.98 suggesting that an ammonium poor medium was prevalent and anions were balanced by their counter ions to give neutrality to the aerosols (Trebs et al., 2005).

Other inorganic elements present in the PM samples collected in BH were determined using PIXE analysis. Figure 3 shows the normalized concentrations of elements like Si, S, K, Ca, Ti, Mn, Fe, Cl, Ni, Cu, Zn and Pb. The sum of all detected elements amounted to approximately 17% of the total PM10 concentration, 21% of PM10-2.5 and 8.5% of PM2.5. In the coarse fractions, crustal components, namely Ca, Si and Fe, predominated and constituted around 82% of their total elemental composition. This percentage decreased to 35% in the fine particles, with S being the most abundant element. It constituted almost 52% of the total elemental composition of the fine filter. Elevated crustal markers determined on February 27, September 29 and October 15, 2004 correlated with a southerly wind coming from Africa and the Arabian Peninsula as shown by the air trajectory HYSPLIT model (Figure 4). Sulfur was more prominent in the summer and showed elevated levels on June 17, July 27 and August 02, 2004. In addition to local sources, sulfur determined in the coarse and fine aerosols seemed to

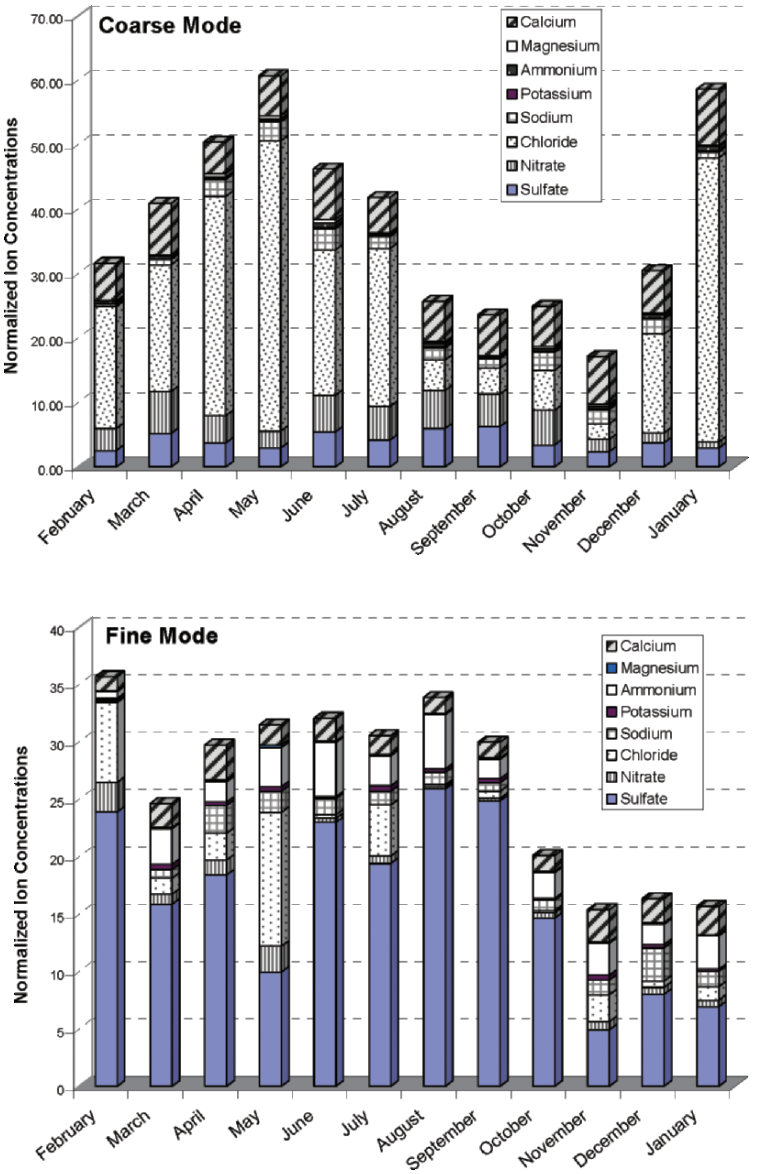

Figure 2. Normalized cationic and anionic concentrations of coarse and fine particles sampled over a whole year in BH between February 2004 and January 2005

have long-range transported contributions as reported by several other investigators in the area (Ganor et al., 2000; Luria et al., 1996; Sciare et al., 2003; Tsitouridou et al., 2003; Zerefos et al., 2000). Alternatively, emission

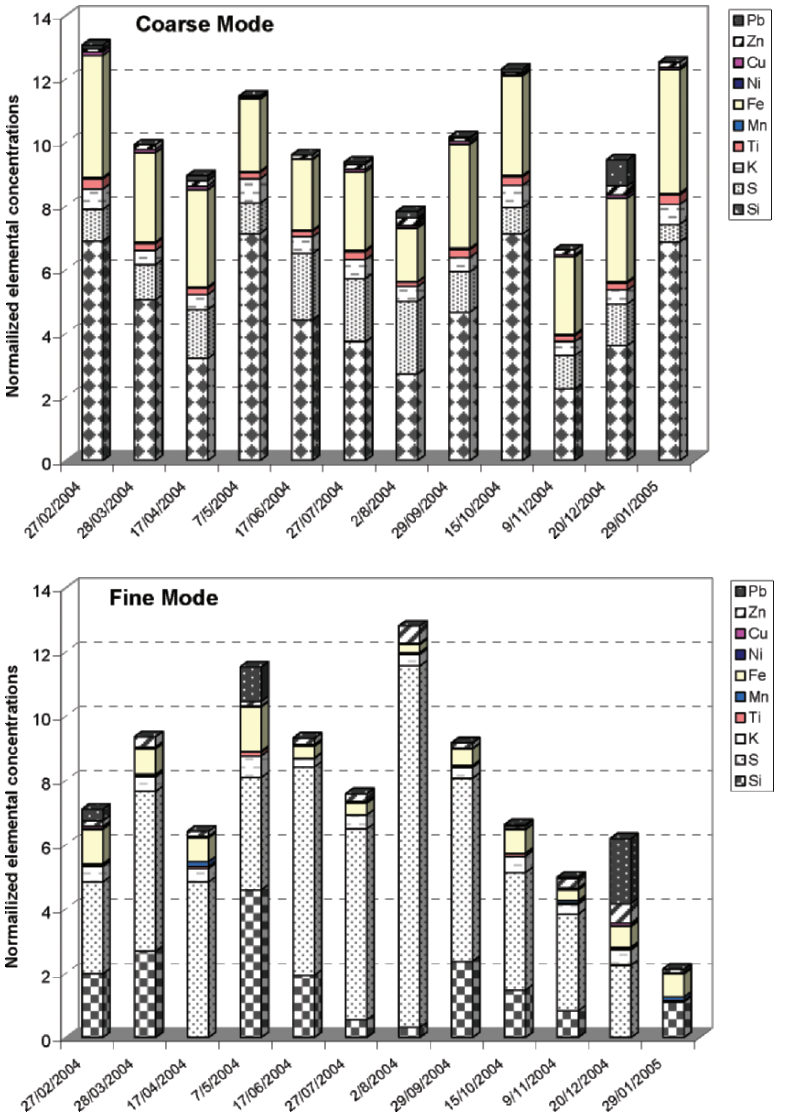

Figure 3. Normalized elemental concentrations of coarse and fine particles sampled over a whole year in BH between February 2004 and January 2005

of elements like Cu and Zn were attributed to local industries and vehicle exhausts as Zn is considered a marker of gasoline and diesel fuel (Chow et al., 1996). Zn and Cu have been also shown to generate from worn brakes and vehicles tires and higher levels are a good indication of sites heavily populated with a high traffic density as it is the case at the BH site. Lead, on the other hand, showed high levels on February 27 (357 ng m^{-3}), May 7 (302 ng m^{-3}), and December 20, 2004 (1082 ng m^{-3}); dates associated with wind

coming directly from Egypt as determined by the air trajectory HYSPLIT model (one day example is shown in Figure 4).

3.2. MICRO VERSUS MACRO ENVIRONMENTS

In an attempt to compare the BH location to other micro environmental sites in Beirut, PM10 samples and ionic analysis was conducted in several sites in the city. Measured high diurnal and seasonal variations in PM10 concentrations was in accordance with a study conducted in Erdemli, located at the Turkish coast of the eastern Mediterranean, where a dynamic environment was suggested to induce high PM variability in space and time (Kocak et al., 2004; Kubilay et al., 2000). Nevertheless, high PM10 levels seemed to be correlated with congested areas (Table 1), given that the ratio between the mean concentration during workdays and that on weekends was greater than one (1.27). The PM10 mean concentrations measured in specific sites of Beirut, in the past few years showed that the mass concentration varied from 44 to 110$\mu g/m^3$ (Kouyoumdjian and Saliba, 2006; Saliba et al., 2006; Shaka' and Saliba, 2004). PM10 mean concentrations in other western European cities were reported to be significantly lower (~20$\mu g/m^3$) (Eleftheriadis et al., 1998; Kubilay et al., 2000; Roosli, 2001).

The normalized summer and winter ionic concentrations, represented by the mass concentration of each ion divided by the total PM10 mass concentration are plotted in Figure 5A & B. Even though the overall nitrate summer average was 2.12 ± 0.83 $\mu g/m^3$, high spatial variability over the nine sampling sites resulted from the marked differences in the concentration of the precursor substance, NO_2, between the sites and the dynamic nature of the Mediterranean atmosphere. Higher values correlated with sites exhibiting high traffic density, and the measured nitrate concentrations over Beirut were higher than the average particulate nitrates over the eastern Mediterranean area (1 ± 0.5 $\mu g/m^3$) (Danalatos and Glavas, 1999), suggesting thereby that local anthropogenic activities have a higher contribution than the air masses originating from neighboring places (Alper-Siman Tov et al., 1997; Ganor et al., 1998). On the other hand, the average value for particulate SO_4^{2-} was 9.51 ± 4.94 $\mu g/m^3$, again with higher values correlating with highly dense area, but the mean sulfate concentration was consistent with previous studies performed in Beirut, and in the Mediterranean region (Eleftheriadis et al., 1998; Foner and Ganor, 1992; Kouyoumdjian and Saliba, 2006; Seter et al., 1996). These results supported the fact that sulfate originated mainly from long range transport phenomena (Ganor et al., 1998; Ganor et al., 2000). As for the cations, low NH_4^+ levels detected in summer were attributed to the insignificance of NH_3 sources. Other cationic levels did not show any noticeable site-to-site variation. K^+ and Mg^{2+} were found

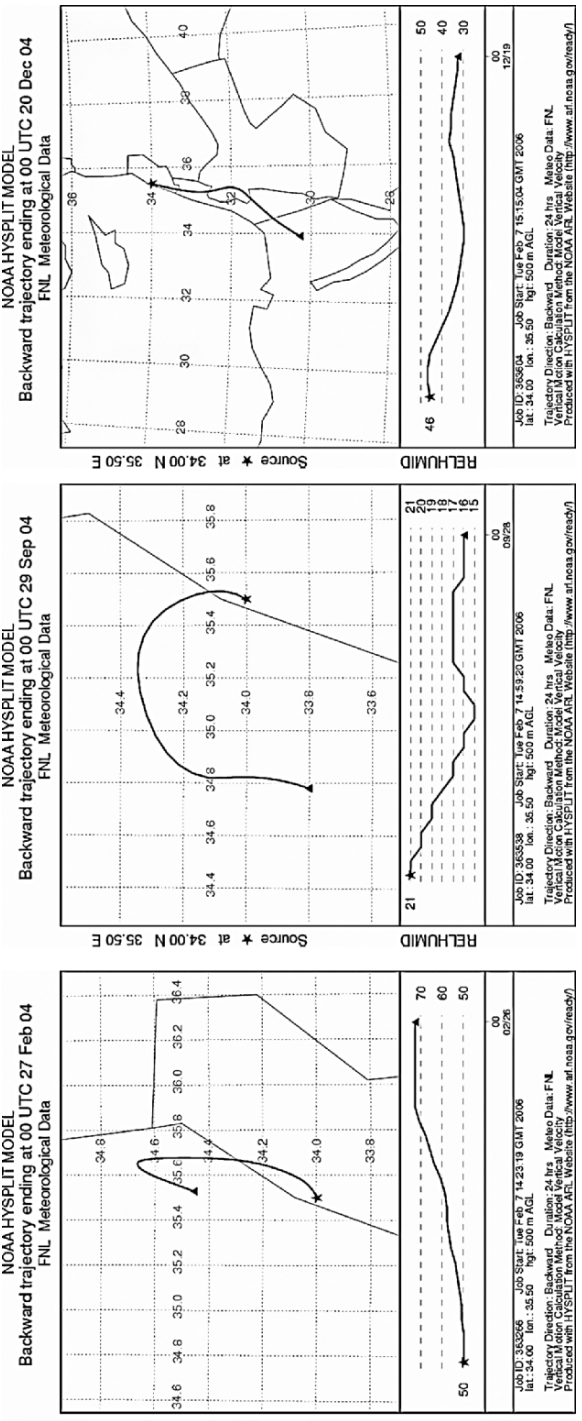

Figure 4. HYSPLIT backward air trajectories of the days that showed high correlation between elevated crustal (ca, Ti, Mn, and Fe) and Pb elemental concentration and the wind direction

at low concentrations while Ca^{2+} and Na^{+} were the main constituents with Ca^{2+} being the most predominant. Both K^{+} and Mg^{2+} did not seem to originate from the sea since the ion-to-sodium ratios were found to be higher than the corresponding values for sea water. Additionally, calcium levels (overall average of 4.7 $\mu g/m^3$) were found to be much higher than those detected in countries like Crete (1.51 $\mu g/m^3$) (Bardouki et al., 2003) or Switzerland (0.72 $\mu g/m^3$) (Roosli, 2001) but were more comparable to

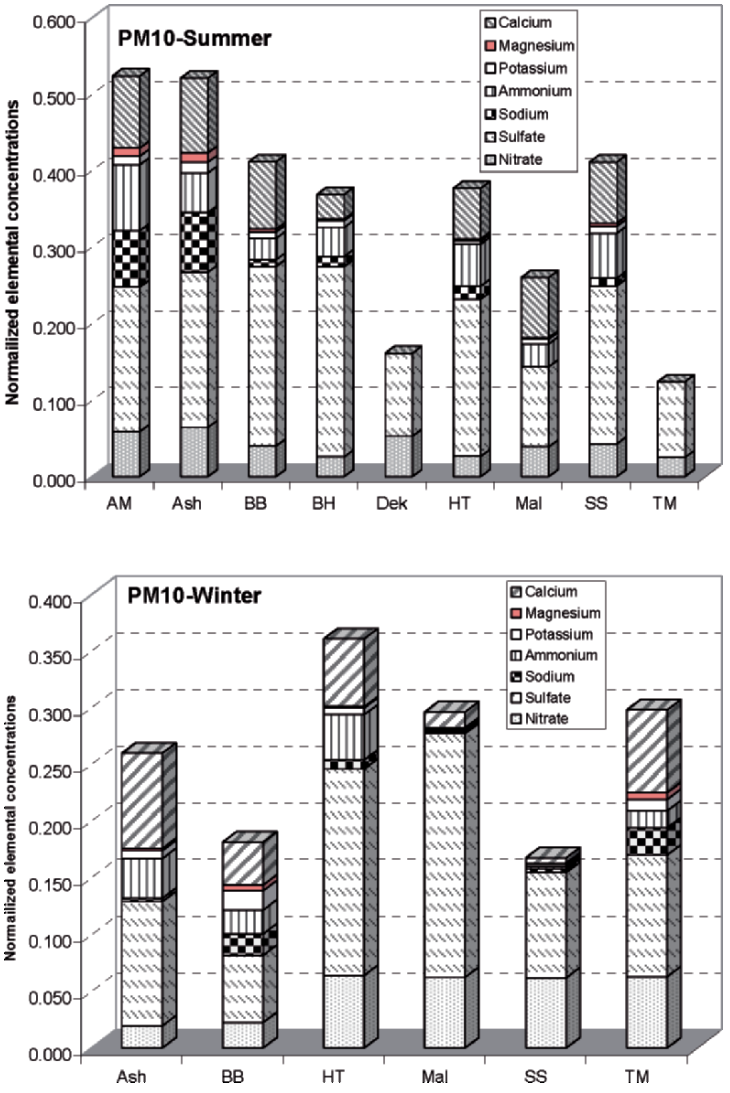

Figure 5. Normalized cationic and anionic concentrations of PM10 sampled in different urban sites in Beirut

values detected in Israel (Ganor et al., 2000). They are lower than those found in Athens, Greece (7 μg/m^3) (Eleftheriadis et al., 1998). Such high levels are characteristic to regions rich in calcitic and basaltic rocks (Abdel-Rahman and Nader, 2002). In winter, the normalized average cation and sulfate concentrations, were lower than summer while nitrate levels were 1.5 times higher. This indicated that nitrate concentrations, which were more locally produced, were enhanced due to the formation of the inversion layer and/or heterogeneous reactions in winter. On the other hand, the emission of particulate sulfate which was reduced almost by half during winter due to the decrease in the concentrations of oxidizing species (5.68 ± 1.85 μg/m^3) was in agreement with other winter average values reported in the eastern Mediterranean area (Bardouki et al., 2003; Danalatos and Glavas, 1999; Erduran and Tuncel, 2001; Kocak et al., 2004), and was comparable to NSSS indicating the insignificance of both the local and marine sources on SO_2 emission in the region (Bardouki et al., 2003; Ganor et al., 1998; Ganor et al., 2000; Levin et al., 2003; Mihalopoulos et al., 1997).

TABLE 1. Detailed description of the urban sites sampled in Beirut

Location	busy road	Summer		Winter	
		Average	Std Dev	Average	Std Dev
AM	No	49.35	16.09	–	–
Ash	No	38.54	4.34	69.08	27.21
HT	No	57.3	6.52	37.26	9.143
BB	Yes	48.90	14.38	24.31	26.21
Dek	Yes	56.08	2.14	–	–
SS	Yes	66.87	5.03	40.58	11.17
BH	Yes	54.59	43.17	–	–
TM	Yes	54.04	20.47	39.20	18.27
Mal	Yes	69.71	12.36	23.28	9.59

4. Summary and Conclusions

Annual averages of PM10, PM10-2.5 and PM2.5 concentrations at BH were higher than the U.S. Environmental Protection Agency (EPA) limits. The main water-soluble ions in the coarse particles were Na^+, Ca^{2+}, Cl^-, SO_4^{2-} and NO_3^-, and in the fine particles NH_4^+, Ca^{2+} Na^+ and SO_4^{2-} were determined. High chloride concentrations indicated that limited losses due to the formation of HCl from the NaCl and HNO_3 and/or H_2SO_4 reactions occurred. Rather, the reactions of $CaCO_3$ with HNO_3 and/or H_2SO_4 reactions to produce calcium nitrate and sulfate salts, respectively, are enhanced. In the fine particles, the ammonium concentration was the highest with relatively higher levels in the summer. A strong correlation with SO_4^{2-} indicated that $(NH_4)_2SO_4$ predominated. Elemental analysis of PM2.5 and PM10-2.5

particles using PIXE analysis showed that elevated concentrations of crustal elements (Si, Ca, Fe, Ti, and Mn), mostly present in the coarse particles, were associated with desert storms coming from the Saharan desert and Africa. However, non-crustal elements like Cu and Zn originated mainly from vehicles emission, worn tires and brakes. Sulfur was abundant in fine particles, and the increase in its concentration correlated well with the summer season and high solar radiations. Pb, on the other hand, was detected at higher levels when transported from Egypt and/or Israel. The comparison between BH and other urban sites in Beirut showed that high temporal variation were attributed to the location of Beirut on the Eastern Mediterranean coast, where long range transported particulate species are carried out by dynamic air masses passing over the region. Nevertheless high PM10 nitrate and sulfate concentrations seemed to also be correlated to sites with higher local emission sources.

5. Acknowledgments

The author would like to thank the University Research Board at the American University of Beirut for funding the project.

6. References

Abdel-Rahman, A.-F. M. and Nader, F. H., 2002, Characterization of the Lebanese Jurassic-Cretaceous carbonate stratigraphic sequence: a geochemical approach. *Geol J*, **37**: 69-91.

Alper-Siman Tov, C., Peleg, M., Matveev, V., Mahrer, Y., Seter, I. and Luria, M., 1997, Recirculation of polluted air masses over the East Mediterranean cost. *Atmos Environ*, **31**(10): 1441-1448.

Alpert, P., Neeman, B. U. and Shay-El, Y., 1990, Intermonthly variability of cyclone tracks in the Mediterranean. *J climate*, **3**: 1474-1478.

Artaxo, P., Slanina, J., Andreae, M. O., Trebs, I., Metzger, S., Meixner, F. X., Helas, G., Hoffer, A., Rudich, Y., Falkovich, A. H., Moura, M. A. L. and da Silva, R. S., 2005, The NH_4^+-NO_3^--Cl^--SO_4^{2-}-H_2O aerosol system and its gas phase precursors at a pasture site in the Amazon Basin: How relevent are mineral cations and soluble organic acids? *J Geophys Res*, **110**: (D07303).

Bardouki, H., Liakakou, H., Economou, C., Sciare, J., Smolik, J., Zdimal, V., Eleftheriadis, K., Lazaridis, M., Dye, C. and Mihalopoulos, N., 2003, Chemical composition of size resolved atmospheric aerosols in the Eastern Mediterranean during summer and winter. *Atmos Environ*, **37**: 195-208.

Chow, J. C., Watson, J. G., Lu, Z., Lowenthal, D. H., Frazier, C. A., Solomon, P. A., Thuillier, R. H. and Magliano, K., 1996, Descriptive analysis of PM2.5 AND PM10 at regionally representative locations during SJVAQS/AUSPEX. *Atmos Environ*, **30**(12): 2079-2112.

Danalatos, D. and Glavas, S., 1999, Gas phase nitric acid, ammonia and related particulate matter at a Mediterranean coastal site, Patras, Greece. *Atmos Environ*, **33**: 3417-3425.

Dayan, U., Heffter, J., Miller, J. and Gutman, G., 1991, Dust intrusion events into the Mediterranean basin. *J Appl Meteorol*, **30**: 1185-1199.

Eleftheriadis, K., Ballis, D., Ziomas, I. C., Colbeck, I. and Manalis, N., 1998, Atmospheric aerosol and gaseous species in Athens, Greece. *Atmos Environ*, **32**: 2183-2191.

Erduran, M. S. and Tuncel, S. G., 2001, Gaseous and particulate air pollutants in the Northeastern Mediterranean Coast. *Sci Total Environ*, **281**: 205-215.

Evans, M. C., Campbell, S. W., Bhethanabotla, V. and Poor, N. D., 2004, Effect of sea salt and calcium carbonate interactions with nitric acid on the direct dry deposition of nitrogen to Tampa Bay, Florida. *Atmos Environ*, **38**: 4847-4858.

Foner, H. A. and Ganor, E., 1992, The chemical and mineralogical composition of some urban aerosols in Israel. *Atmos Environ*, **26B**: 125-133.

Ganor, E., Levin, Z. and Van Grieken, R., 1998, Composition of individual aerosol particles above the Israelian mediterranean coast during the summer time. *Atmos Environ*, **32**: 1631-1642.

Ganor, E., Foner, H. A., Bingemer, H. G., Udisti, R. and Setter, I., 2000, Biogenic sulphate generation in the Mediterranean Sea and its contribution to the sulphate anomaly in the aerosol over Israel and the Eastern Mediterranean. *Atmos Environ*, **34**: 3453-3462.

Goudie, A. S. and Middleton, N. J., 2001, Saharan dust storms: nature and consequences. *Earth-Sci Rev*, **56**: 179-204.

Gullu, G. H., Olmez, I. and Tuncel, G., 2000, Temporal variability of atmospheric trace element concentrations over the Eastern Mediterranean Sea. *Spectrochim Acta part B*, **55**: 1135-1150.

Kassomenos, P. A., Skouloudis, A. N., Lykoudis, S. and Flocas, H. A., 1999, "Air-quality indicators" for uniform indexing of atmospheric pollution over large metropolitan areas. *Atmos Environ*, **33**: 1861-1879.

Kerminen, V. M., Pakkanen, T. A. and Hillamo, R. E., 1997, Interactions between inorganic trace gases and supermicrometer particles at a coastal site. *Atmos Environ*, **31**: 2753-2765.

Kocak, M., Kubilay, N. and Mihalopoulos, N., 2004, Ionic composition of lower tropospheric aerosols at a Northeastern Mediterranean site: implications regarding sources and long-range transport. *Atmos Environ*, **38**: 2067-2077.

Kouvarakis, G., Tsigaridis, K., Kanakidou, M. and Mihalopoulos, N., 2000, Temporal variations of surface regional background ozone over Crete Island in the southeast Mediterranean. *J Geophys Res*, **105**(D4): 4399-4407.

Kouyoumdjian, H. and Saliba, N. A., 2006, Mass Concentration and Ion Composition of Coarse and Fine Particles in an Urban Area in Beirut: Effect of Calcium Carbonate on the Absorption of Nitric and Sulfuric Acids and the Depletion of Chloride. *Atmos Chem Phys*, **6**: 1865-1877.

Kubilay, N., Nickovic, S., Moulin, C. and Dulac, F., 2000, An illustration of the transport and deposition of mineral dust onto the eastern Mediterranean. *Atmos Environ*, **34**: 1293-1303.

Laskin, A., Iedema, M. J., Ichkovich, A., Graber, E. R., Taraniuk, I. and Rudich, Y., 2005, Direct observation of completely processed calcium carbonate dust particles. *Faraday Discuss*, **130**: 453-468.

Lelieveld, J., Berresheim, H., Borrmann, S., Crutzen, P. J., Dentener, F. J., Fischer, J., Flatau, P. J., Heland, J., Holzinger, R., Korrmann, R., Lawrence, M. G., Levin, Z., Markowicz, K. M., Mihalopoulos, N., Minikin, A., Ramanathan, V., De Reus, M., Roelofs, G. J., Scheeren, H. A., Sciare, J., Schlager, H., Schultz, M., Seigmund, P., Steil, B., Stephanou, E. G., Steir, P., Traub, M., Warneke, C., Williams, J. and Ziereis, H., 2002, Global air pollution crossroads over the Mediterranean. *Science*, **298**: 794-799.

Levin, Z., Teller, A., Ganor, E., Graham, B., Andreae, M. O., Maenhaut, W., Falkovich, A. H. and Rudich, Y., 2003, Role of aerosol size and composition in nucleation scavenging within clouds in a shallow cold front. *J Geophys Res*, **108**(D22): doi:10.1029/2003JD003647.

Luria, M., Peleg, M., Sharf, G., Siman Tov-Alper, D., Spitz, N., Ben Ami, Y., Gawii, Z., Lifschitz, B., Yitzchaki, A. and Seter, I., 1996, Atmospheric sulfur over the Eastern Mediterranean region. *J Geophys Res*, **101**: 25917-25930.

Mihalopoulos, N., Stephanou, E., Kanakidou, M., Pilitsis, S. and Bousguet, P., 1997, Tropospheric aerosol ionic composition in the Eastern Mediterranean region. *Tellus*, **49B**: 314-326.

Niemi, J. V., Tervahattu, H., Virkkulad, A., Hillamod, R., Teinil7d, K., Koponene, I. K. and Kulmala, M., 2005, Continental impact on marine boundary layer coarse particles over the Atlantic ocean between Europe and Antarctica. *Atmos Res*, **75**: 301-321.

Pathak, R. K., Louie, P. K. K. and Chan, C. K., 2004, Characteristics of aerosol acidity in Hong Kong. *Atmos Environ*, **38**: 2965-2974.

Rodríguez, S., Querol, X., Alastuey, A. and Mantilla, E., 2002, Origin of high summer PM10 and TSP concentrations at rural sites in Eastern Spain. *Atmos Environ*, **36**: 3101-3112.

Roosli, M. T., G., Kunzli, N., Staehelin, J., Mathys, P., Oglesby, L., Camenzind, M., Braun-Fahrlander, Ch., 2001, Temporal and spatial variation of the chemical composition of PM10 at urban and rural sites in the Basel area, Switzerland. *Atmos Chem*, **35**: 3701-3713.

Saliba, N. A., Moussa, S., Salame, H. and El-Fadel, M., 2006, Variation of selected air quality indicators over the city of Beirut, Lebanon: Assessment of emission sources. *Atmos Environ*, **40**: 3263-3268.

Sciare, J., Bardouki, H., Moulin, C. and Mihalopoulos, N., 2003, Aerosol sources and their contribution to the chemical composition of aerosols in the Eastern Mediterranean Sea during summertime. *Atmos Chem Phys*, **3**: 291-302.

Seter, L. M., Peleg, M., Sharf, G., Siman Tov-Alper, D., Spitz, N., Ben ami, Y., Gawii, Z., Lifschitz, B. and Yitzchaki, A., 1996, Atmospheric sulfur over the eastern mediterranean region. *J Geophys Res*, **101**: 25917-25930.

Shaka', H. and Saliba, N. A., 2004, Concentration measurements and chemical composition of PM10-2.5 and PM2.5 at a coastal site in Beirut, Lebanon. *Atmos Environ*, **38**: 523-531.

Sloss, L. L. and Smith, I. M., 2000, PM10 and PM2.5: an international perspective. *Fuel Process Technol*, **65-66**: 127-141.

Trebs, I., Metzger, S., Meixner, F., Helas, G., Hoffer, A., Rudich, Y., Falkovich, A. H., Moura, M. A. L., da Silva Jr., R. S., Artaxo, P., Slania, J. and Andreae, M. O., 2005, The NH_4^+-NO_3^--Cl^--SO_4^{2-}-H_2O aerosol system and its gas phase precursors at a pasture site in the Amazon Basin: How relevant are mineral cations and soluble organic acids. *J. Geophys Res*, **110**: doi: 10.1029/2004JD005478.

Tsai, C. J. and Perng, S. N., 1998, Artifacts of ionic species for Hi-vol PM10 and PM10 dichotomous samplers. *Atmos Environ*, **32**: 1605-1613.

Tsitouridou, R., Voutsa, D. and Kouimtzis, T., 2003, Ionic composition of PM10 in the area of Thessaloniki, Greece. *Chemosphere*, **52**: 883-891.

Zerefos, C., Ganev, K., Kourtidis, K., Tzortsiou, M., Vasaras, A. and Syrakov, E., 2000, On the origin of SO_2 above Northern Greece. *Geophys Res Lett*, **27**: 365-368.

Zhuang, H., Chan, C. K., Fang, M. and Wexler, A. S., 1999, Formation of nitrate and non-sea-salt sulfate on coarse particles. *Atmos Environ*, **33**: 4223-4233.

DETAILS OF CHEMICAL AND AEROSOLS PROCESSES

AEROSOLS IN GLOBAL MODELS – FOCUS ON EUROPE

MARIA KANAKIDOU
Environmental Chemical Processes Laboratory, Dept. of Chemistry, University of Crete, P.O. Box 2208, 71003 Heraklion, Greece, mariak@chemistry.uoc.gr

Key Words: Aerosol; climate; global modeling; secondary organic aerosol; aerosol components; Europe; uncertainties; biogenic emissions; future; anthropogenic impact.

Abstract Aerosols are chemically complex constituents of the troposphere. They affect human health, visibility, tropospheric chemistry, ecosystems and climate. They exert an opposite to greenhouse gases effect on the global atmospheric temperature by decelerating the warming of the climate. Global 3-dimensional models have to account for the atmospheric processes that affect aerosols in the atmosphere, namely emissions, nucleation, condensation, evaporation, coagulation, cloud processing, atmospheric transport, dry and wet deposition and chemistry/climate feedback mechanisms. To describe this complex atmospheric system, simplifications are requested that result in differences in the model simulations of the budgets and the properties of the tropospheric aerosols and of their climatic impact. Such differences are documented in the frame of the international aerosol model intercomparison exercise AEROCOM (AEROsol model inter COMparison project). A major factor of uncertainty in the model simulations is related to the water associated to the particulate phase that can equal or even exceed the dry aerosol mass. Secondary organic aerosols (SOA), chemically formed in the atmosphere, are another major source of uncertainties in the models. SOA modelling is in its infancy and is actually based on oversimplifications due to the gaps in our understanding of the SOA occurrence and fate in the atmosphere. European aerosol budgets and the contribution of the various aerosol components over the Mediterranean to the total aerosol mass have been computed by the 3-dimensional global chemistry-transport model TM in the frame of the EU funded project PHOENICS (Particles of Human Origin Extinguish Natural solar Irradiance in the Climate System). Natural contributions of dust, sea-salt and SOA to the total aerosol mass are shown to be significant over the Mediterranean. Biogenic SOA are computed to be more important during summer and are expected to increase more in the future atmosphere. Challenges for future research and chemistry/climate model development are highlighted.

A. Mellouki and A.R. Ravishankara (eds.), Regional Climate Variability and its Impacts in the Mediterranean Area, 143–154.

1. Environmental Significance of Aerosols

Aerosol particles influence the global atmospheric radiation budget directly by scattering and absorption of light in the visible and infrared spectrum. They also indirectly influence climate by modifying cloud properties and the hydrological cycle. Aerosols exert an opposite to greenhouse gases effect on the global atmospheric temperature by decelerating the warming of the climate (IPCC, 2001; 2007). Consideration of aerosol direct and indirect climate effect in coupled atmosphere/ocean climate model is providing better agreement between model simulations and observations of atmospheric temperature changes (Figure 1). Finally, aerosols influence ozone levels because heterogeneous reactions take place on the aerosol surface and in liquid aerosol particles.

Aerosols are complex ensembles of particles of varying composition and size that also affect human and ecosystem health and visibility. It is only in the last two decades that our understanding of aerosol has sufficiently advanced to successfully integrate all information on aerosol emission, formation, transport and removal processes in global atmospheric chemistry transport and general circulation models (Kanakidou et al., 2005a).

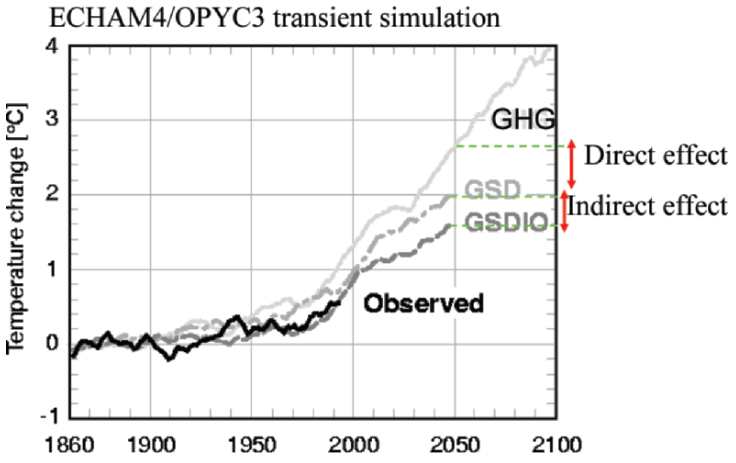

Figure 1. Temperature changes simulated by a coupled atmosphere/ocean climate model and comparison with observations (solid line). Simulations are performed by considering only the climate impact of green house gases (GHG), the GHG effect and the aerosol direct climate effect (GSD) and in addition to these two earlier effects the aerosol indirect climate effect (GSDIO). The figure is adopted from Roeckner et al. (1999)

Observations show that the mixing state and size distribution of the global aerosol system are highly variable, with both externally and internally mixed contributions and varying ratios among constituents. Aerosol removal processes and climate impacts are greatly influenced by the size-distribution. Moreover, anthropogenic emissions favour the transformation of insoluble to mixed particles by coating them with secondary products formed in the atmosphere. This increases the number of cloud condensation nuclei affecting the microphysical properties of aerosol with impacts on aerosol lifetimes, global distributions and radiative properties.

The concept of radiative forcing by aerosol applied in IPCC (2001) is therefore challenged, since linear additivity of the forcing by aerosol components (e.g., separate estimates of forcing for soot and sulphate) is not necessarily valid (Stier et al., 2006; Kanakidou et al., 2005a). Sector-based aerosol (precursor) emission reduction strategies further emphasize the need for a better understanding of the complex chemical and microphysical feedbacks between aerosol and its long range transport.

The present study first discusses uncertainties in global 3-dimensional simulations of aerosol budget terms as documented by the AEROCOM (AEROsol model inter COMparison Project; *http://nansen.ipsl.jussieu.fr/AEROCOM/data.html*; Dentener et al., 2006; Textor et al., 2006; Kinne et al., 2006; Schulz et al., 2006) exercise. Limitations in the 3-d global modeling of the secondary organic aerosol component (SOA) are discussed. Projections of future SOA tropospheric burden are computed and the sensitivity of the results to the future biogenic emission scenarios is discussed. Finally, focusing on Europe, the aerosol budget terms are derived and the anthropogenic component is clearly distinguished from the natural one.

2. Aerosols in Global Models

Most of the modelling studies of the global aerosol system have simulated the aerosol mass of individual aerosol components; the so-called bulk approach. These studies represented aerosol either by an external mixture, in which each particle is made of solely one compound, or by an internal mixture, in which each particle consists of a uniform aggregate of all the individual components. They also assumed a constant aerosol size-distribution. Up-to date global aerosol models include some parameterization of the aerosol size-distribution.

These models have been recently compared in the frame of the international exercise AEROCOM. AEROCOM demonstrated for the first time that ensembles of global aerosol models can provide an averaged model (combining several model results) that correlates better than individual

models to observed satellite observations. Interannual variability is a source of discrepancy when comparing to data obtained during a restricted time period, and General Circulation Models operating in climate mode perform significantly worse than models constrained by observed meteorology. Inter-model differences seem to be more important than inter-annual variability (Textor et al., 2006; Kinne et al., 2006). Comparison of Aerosol Optical Depth (AOD) of models participating in modeling exercise AEROCOM versus AERONET sunphotometers (AErosol RObotic NETwork) and satellite derived aerosol products revealed agreement for the globally averaged AOD. However, the models significantly differ with respect to the spatial distribution of AOD from different aerosol species. Figure 2 reveals a reasonable correspondence of global aerosol optical depth from most models and a composite of measurements.

Aerosol removal processes and climate impacts are highly sensitive to aerosol number and mass and therefore to the size-distribution. Important differences in the simulated wet aerosol composition are demonstrated in Figure 3 that shows the chemical composition of global aerosol as simulated by the 16 state-of-the-art global aerosol models that contributed to the AEROCOM model intercomparison exercise.

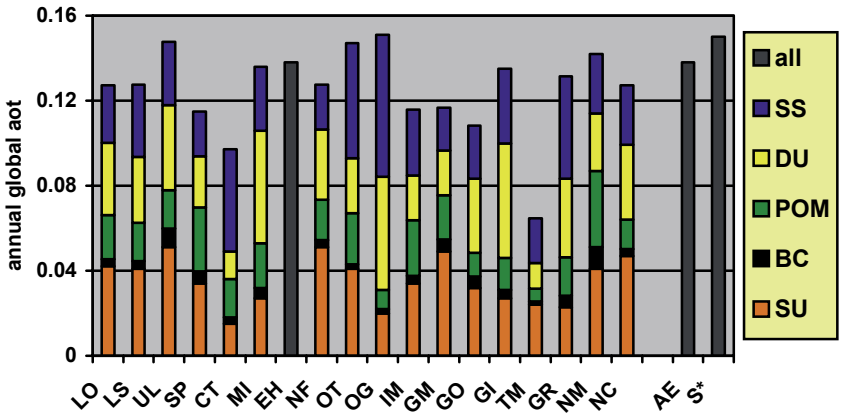

Figure 2. Individual contributions of the five aerosol components (SS-seasalt, DU-dust, POM-particulate organic matter, BC-black carbon, SU-sulphate) to the annual global aerosol optical depth (at 550nm). For comparison, two "quality" AOD data references from remote sensing are provided: ground data from AERONET (AE) and a satellite-composite (S*) based on MODIS (ocean) and MISR (land) data. (No apportioning is possible for the model "EH", due to consideration of inter-component mixing). Figure adopted from Kinne et al. (2006) and Kanakidou et al. (2005a)

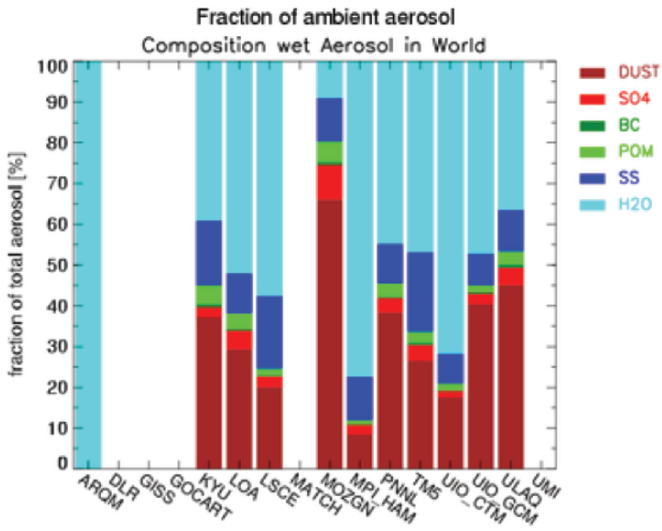

Figure 3. Composition differences between different aerosol models. H_2O: Aerosol water; SS: Sea salt; BC: black carbon; POM: particulate organic matter. Fractions are mass fractions of global aerosol mass (figure adopted from Textor et al., 2006)

AEROCOM has also shown that large uncertainties associated with calculations of radiative forcing estimates concern:

- The black carbon optical depth
- The loads of the natural aerosols sea-salt and dust.
- The organic aerosol oceanic source
- The natural secondary organic aerosol
- The water associated to aerosols

3. Water Associated to Aerosol

Water is an important component of aerosol; however experimentally the amount of aerosol water is difficult to determine, and no routine measurements are available. Under humid conditions hygroscopic aerosol particles - due to the uptake of water - can considerably reduce atmospheric visibility. Maritime air is often much more hazy than continental air and at high relative humidity the air becomes foggy. The extent of atmospheric visibility reduction depends on the total aerosol load and the relative humidity, as well as on the composition of the atmospheric aerosols. For instance, an aerosol that includes sea salt compounds is usually associated with a larger water fraction than e.g., mineral dust or organics that are partly hydrophobic. The aerosol composition determines not only the water uptake of the aerosol but

also the mass, size and optical properties of the aerosol particles. The water uptake in turn determines whether the aerosol phase is solid or liquid. The role of the aerosol associated water mass with respect to the Earth's climate and the hydrological cycle in the context of direct aerosol effects has been investigated by the PHOENICS models (Kanakidou et al., 2005a). The amount of water associated to aerosols varies spatially and can regionally strongly exceed the dry aerosol mass (Metzger et al., 2002).

4. Secondary Organic Component of Aerosols

The organic component of aerosols (OA) can be emitted directly as primary aerosol or formed by chemical reactions (secondary aerosol - SOA). Organic aerosol mass can contribute with 30-70% to the total aerosol mass, yet the exact formation processes and composition are poorly understood. Due to the chemical complexity of the organic components of OA there is an urgent need of simplified representations in global chemistry climate models of the volatility, solubility, hygroscopicity, chemical reactivity and the physical and optical properties of OA. Ideally, the net effect of a complex mixture of OA is described by only a limited number of representative compounds or mixtures.

An important fraction of organic aerosol that is only recently considered in global models is the secondary organic aerosol. The state of the art of our understanding of SOA formation in the atmosphere has been recently reviewed by Kanakidou et al. (2005b) and Fuzzi et al. (2006). SOA is relevant on local to global scales. The global formation of SOA is estimated to range from 2.5-70 Tg yr^{-1} with a central estimate of about 30 Tg yr^{-1} (Kanakidou et al., 2005b). Among the investigated sources of uncertainties in SOA modelling, the largest are the emissions of the precursors (intensity and chemical speciation) and of the primary carbonaceous particles, the volatility of the semi-volatile secondary precursors and their solubility, and the impact of multiphase chemistry on the modification of the organic component of aerosols. The contribution of SOA to aerosol optical density (AOD) is estimated to be larger than that of primary organic aerosol (POA) or black carbon (BC) (Tsigaridis et al., 2006). This contribution is likely to increase as (1) current SOA models significantly underestimate SOA production (e.g., de Gouw et al., 2005; Volkamer et al., 2006), (2) current regulations are likely to result into a reduced contribution of sulphate in the future, while (3) SOA precursor emissions could continue increase (Tsigaridis and Kanakidou, 2006).

The SOA is predominantly from biogenic precursors, with the anthropogenic SOA being about a factor of 10 smaller (Tsigaridis and Kanakidou, 2003). Despite the large uncertainties associated with the current modelling estimates of SOA formation in the global atmosphere, there is consensus that the major precursors of SOA are biogenic volatile organic compounds (BVOC).

C are very reactive and in the presence of NOx and light can form ozone (Crutzen, 1995). Both O_3 and SOA are radiatively active constituents of the troposphere. O_3 is a greenhouse gas and contributes to the global warming of the atmosphere, SOA are scattering solar radiation and can also act as cloud condensation nuclei affecting cloud properties and the hydrological cycle in the atmosphere (Kanakidou et al., 2005b). Therefore, BVOC emitted by vegetation via procedures that are driven by climate (temperature and light) and vegetation type (Guenther et al., 1995), form oxidation products that, in turn, affect climate. This feedback can be more intensive than earlier thought, since recent findings have demonstrated the key role played by isoprene, the major single compound emitted by vegetation, and producing SOA (Henze and Seinfeld, 2005). The natural variability of SOA production is evaluated to be about 10% and is as large as the SOA formation from anthropogenic precursors. Significant positive and negative feedback mechanisms in the atmosphere are responsible for the non-linear relationship between emissions of biogenic VOC and SOA burden (Tsigaridis et al., 2005). It is an open question how this biosphere-climate-chemistry feedback (iLEAPS, 2005) will evolve in the future and, in particular, what the SOA composition will be, and how important will SOA be relative to the major anthropogenic aerosol component (sulfate).

The SOA response to changes in BVOC emissions in the future atmosphere and the SOA importance relative to the major anthropogenic aerosol component (sulfate) have been investigated with the global 3-d TM model in which emission estimates of biogenic VOC and anthropogenic gases and particles from the literature for the year 2100 have been adopted.

According to these global simulations the future SOA burden is calculated to change from 1 Tg at present to 2.3 Tg in the future, driven by changes in emissions, oxidant levels and pre-existing particles. In 2100, SOA burden is calculated to exceed that of sulfate, indicating that SOA might become more important than nowadays (Tsigaridis and Kanakidou, 2007). These results are subject to high uncertainty in the biogenic emissions due to the insufficient knowledge on plant response to carbon dioxide changes. Nevertheless, they clearly indicate that the change in oxidants and primary aerosol caused by human activities is the major contributor to the increase of the biogenic SOA production in the future atmosphere. The computed

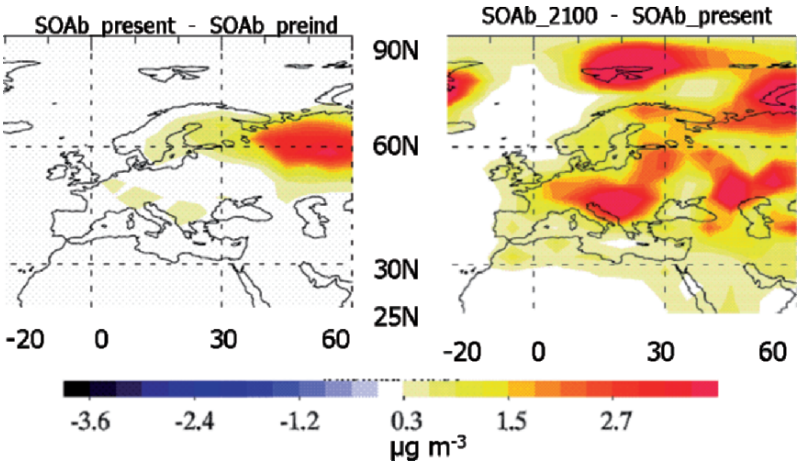

Figure 4. SOAb changes over Europe as simulated by the TM3 model. SOAb increase since pre-industrial period and are expected to further increase in the future

changes in the SOA produced by BVOC oxidation (SOAb) over Europe since pre-industrial times and in the future are depicted in Figure 4.

5. The European Aerosol Budget

Figure 5 shows a schematic representation of the budget of all major components of aerosols over Europe. Dust and sea-salt are mainly of natural origin, while BC, POM, SO_4 and NO_3 are mainly anthropogenic. The high precursor emissions of NO and NH_3 and the meteorological conditions over Europe (e.g., compared to Asia) promote the formation of nitrate aerosol. The high resolution 1° × 1° TM5 model has calculated a net import in Europe of sea-salt aerosol (from the west) and dust aerosol (from the south) of 11.8 Tg yr^{-1} and 20.4 Tg yr^{-1}, respectively. The export of anthropogenic aerosols from Europe wais calculated as 0.23 Tg yr^{-1} BC, 0.53 Tg yr^{-1} POM, 4.1 Tg sulphate yr^{-1}, and 0.4 Tg nitrate yr^{-1}, in total 5.3 Tg yr^{-1}. These numbers can be compared with European anthropogenic aerosol (and aerosol precursor) emissions of 14.4 Tg yr^{-1}, consisting of 0.55 Tg yr^{-1} BC, 1.72 Tg yr^{-1} POM, 10.6 Tg yr^{-1} $SO_4^{=}$ (mostly from oxidation of SO_2), and 1.8 Tg yr^{-1} NO_3^{-}. Thus almost 40% of European aerosol is transported to neighbour regions. This number would be higher if the transport of gaseous SO_2 out of Europe would also be taken into account. The fractions of BC and sulphate transported out of Europe are highest at 41% and 48%, respectively. In perspective, off all anthropogenic sulphur emissions (mainly as SO_2) 18% is transported out of Europe.

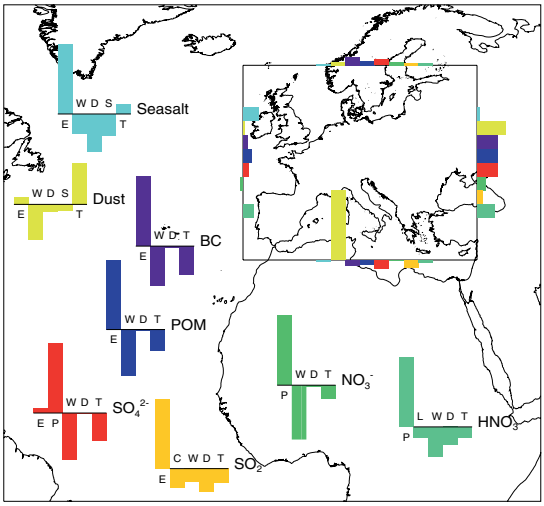

Figure 5. The aerosol budget over Europe. Bar-graphs denote the European production and destruction fluxes, scaled according to the maximum fluxes which are Sea-salt: 87.2 Tg yr^{-1}; Dust: 34.2 Tg yr^{-1}; BC: 0.55 Tg yr^{-1}; 1.72 Tg POM yr^{-1}; 10.6 Tg SO_4 yr^{-1}; 1.81 Tg NO_3 yr^{-1}, 22.8 Tg SO_2 yr^{-1}, 1.61 Tg HNO_3 yr^{-1}. E = emission, W = total wet deposition, D = dry deposition, S = sedimentation, T = total transport in/out Europe, P = chemical production, L = chemical loss

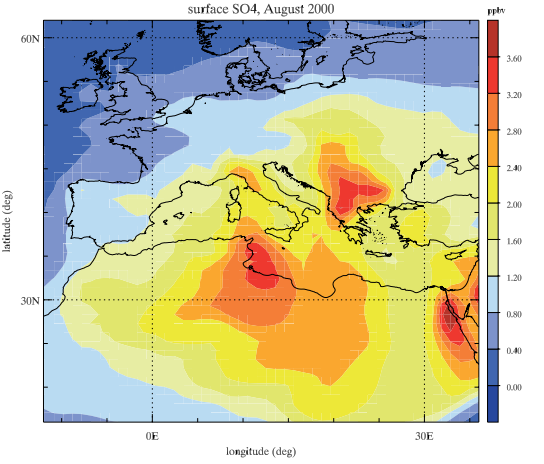

Figure 6. Surface field of sulphate calculated for August 2000 (TM5 model – Krol and coworkers model results, figure adopted from Kanakidou et al., 2005a)

Focusing on Figure 6 that depicts the surface sulphate levels computed by the model for August, a clear displacement of the European plume towards northern Africa is observed that is caused by a combination of transport and atmospheric oxidation of precursor SO_2. On the whole, Europe contributes

significantly to the global aerosol budget. It remains an open question how these aerosol budgets will change when moving to a warmer and drier climate resulting from a global warming of our planet that is expected to strongly affect the Mediterranean. Coupled earth system models considering both GHG and internally mixed size segregated aerosols are the appropriate tools to address this question.

6. Conclusions

To simulate the distribution of aerosols and their climate impacts global 3-dimensional models have to account for the atmospheric processes that affect aerosols in the atmosphere, namely emissions, nucleation, condensation, evaporation, coagulation, cloud processing, atmospheric transport, dry and wet deposition and chemistry/climate feedback mechanisms. In addition, they have to be able to parameterise the size segregated mass and its time evolution. To describe this complex atmospheric system, simplifications are requested that result in differences in the model simulations of the budgets and the properties of the tropospheric aerosols and of their climatic impact as are documented by the AEROCOM model inter comparison exercise. A major factor of uncertainty in the model simulations is related to the water associated to the particulate phase that can equal or even exceed the dry aerosol mass to SOA and to natural aerosol components like sea-salt and dust. Europe is subject to import of significant amounts of dust from the south and sea-salt from the west and export of dust and anthropogenic aerosols mainly to the east. Natural contributions of dust, sea-salt and SOA to the total aerosol mass are shown to be significant over the Mediterranean. Biogenic SOA are computed to be more important during summer and are expected to increase more in the future atmosphere. These aerosol budgets are expected to change in a warmer and drier climate resulting from a global warming of our planet that will strongly affect the Mediterranean. Due to the significant feedback mechanisms that are involved, such changes can be accurately evaluated only by using coupled earth system models considering both GHG and internally mixed size segregated aerosols.

7. Aknowledgments

This work has been supported by the EU project PHOENICS (2002-2005) and by a research and education PYTHAGORAS II grant co-funded by the Greek Ministry of Education (25%) and the European Social Fund (75%) (2005-2007).

8. References

Crutzen, P. J., 1995, Ozone in the troposphere, in H. B. Singh (ed.), Composition, Chemistry, and Climate of the Atmosphere, Van Nostrand Reinold Publications, New York, pp. 349-393.

de Gouw, J. A., Middlebrook, A. M., Warneke, C., Goldan, P. D., Kuster, W. C., Roberts, J. M., Fehsenfeld, F. C., Worsnop, D. R., Canagaratna, M. R., Pszenny, A. A. P., Keene, W. C., Marchewka, M., Bertman, S. B. and Bates, T. S., 2005, Budget of organic carbon in a polluted atmosphere: Results from the New England Air Quality Study in 2002, *Journal of Geophysical Research*, **110**, D16305, doi:10.1029/2004JD005623.

Dentener, F., Kinne, S., Bond, T., Boucher, O., Cofala, J., Generoso, S., Ginoux, P., Gong, S., Hoelzemann, J. J., Ito, A., Marelli, L., Penner, J. E., Putaud, J. P., Textor, C., Schulz, M., van der Werf, G. R. and Wilson, J., 2006, Emissions of primary aerosol and precursor gases in the years 2000 and 1750, prescribed data-sets for aerocom. *Atmospheric Chemistry and Physics*, **6**, 4321-4344.

Heald, C. L., Jacob, D. J., Park, R.J, Russell, L. M., Huebert, B. J., Seinfeld, J. H., Liao, H. and Weber, R. J., 2005, A large organic aerosol source in the free troposphere missing from current models, *Geophys. Res. Lett.,* **32**, L18809, doi:10.1029/2005GL023831.

Henze, D. K., and Seinfeld, J. H., 2006, Global secondary organic aerosol from isoprene oxidation, *Geophys. Res. Lett*., **33**, L09812, doi:10.1029/2006GL025976.

Guenther, A., Hewitt, C. N., Erickson, D., Fall, R., Geron, C., Graedel, T., Harley, P., Klinger, L., Lerdau, M., McKay, W. A., Pierce, T., Scholes, B., Steinbrecher, R., Tallamraju, R., Taylor, J. and Zimmerman, P., 1995, A global model of natural volatile organic compound emissions, *Journal of Geophysical Research*, **100**, 8873-8892.

iLEAPS, 2005, *Science plan and implementation strategy, IGBP report 54*, IGBP Secretariat, Stockholm, 52pp., http://www.atm.helsinki.fi/ILEAPS/downloads/ iLEAPS_SP.pdf.

IPCC, 2001, *Climate change: The scientific basis.* Cambridge University Press, UK.

IPCC, 2007, *Climate change: The scientific basis, Summary for policy makers.* http://ipcc-wg1.ucar.edu/wg1/docs/WG1AR4_SPM_Approved_05Feb.pdf

Kanakidou, M., et al., 2005a, *Particles of Human Origin Extinguish Natural solar Irradiance in the Climate System (PHOENICS) Synthesis and Integration Report,* ISBN, 960-88712-0-4, e-media, University of Crete.

Kanakidou, M., Seinfeld, J. H., Pandis, S. N., Barnes, I., Dentener, F. J., Facchini, M. C., van Dingenen, R., Ervens, B., Nenes, A., Nielsen, C. J., Swietlicki, E., Putaud, J. P., Balkanski, Y., Fuzzi, S., Horth, J., Moortgat, G. K., Winterhalter, R., Myhre, C. E. L., Tsigaridis, K., Vignati, E. Stephanou, E. G., And Wilson, J., 2005b, Organic aerosol and global climate modelling: A review, *Atmos. Chem. Phys.*, **5**, 1053-1123. SRef-ID: 1680-7324/acp/2005-5-1053.

Kinne, S., C. Textor, M., and Schulz, et al., 2006, An AeroCom initial assessment – optical properties in aerosol component modules of global models, *Atmos. Chem. Phys*., **6**, 1815-1834.

Metzger, S., Dentener, F., Pandis, S. and Lelieveld, J., 2002, Gas/aerosol partitioning: 1. A computationally efficient model. *Journal of Geophysical Research-Atmospheres*, **107**, doi:10.1029/2001JD001102.

Putaud, J. P. et al., 2004a, A European aerosol phenomenology—1: physical characteristics of particulate matter at kerbside, urban, rural and background sites in Europe, *Atmos. Environ.*, **38**, 2561-2577.

Putaud, J. P. et al., 2004b, A European aerosol phenomenology—2:physical characteristics of particulate matter at kerbside, urban, rural and background sites in Europe, *Atmos. Environ.*, **3**, 2579-2595.

Roeckner, E., Bengtsson, L., Feichter, J., Lelieveld, J., and Rodhe, H. 1999, Transient climate change simulations with a coupled atmosphere-ocean GCM including the tropospheric sulfur cycle. *J. Climate*. **12**, 3004-3032.

Simpson D., Yttri, K.E., Klimont, Z., Kupiainen, K., Caseiro, A., Gelencser, A., Pio, C., Puxbaum, H., and Legrand, M., 2007, Modelling Carbonaceous Aerosol over Europe. Analysis of the CARBOSOL and EMEP EC/OC campaigns. *J. Geophys. Res. special issue CARBOSOL*. accepted.

Stier, P., Feichter, J., Vignati, E., Wilson, J., Schulz, M., Ganzeveld, L., Werner, M., Tegen, I., Boucher, O., Kinne, S., and Kloster, S., 2005, The Aerosol-Climate Model ECHAM5-HAM, *Atmos. Chem. Phys*., **5,** 1125-1156. SRef-ID 1680-7324/acp/2005-5-1125.

Textor, C., M. Schulz, S., Guibert, et al., 2006, Analysis and quantification of the diversities of aerosol life cycles within AEROCOM, *Atmos. Chem. Phys*., **6**, 1777-1813.

Tsigaridis K., Kanakidou M., 2003, Global modelling of secondary organic aerosol in the troposphere: A sensitivity analysis, *Atmos. Chem. Phys.*, **3**, 1849-1869, SRef-ID: 1680-7324/acp/2003-3-1849.

Tsigaridis, K., Lathiere, J., Kanakidou, M., and Hauglustaine, D., 2005, Naturally driven variability in the global secondary organic aerosol over a decade, *Atmos. Chem. Phys*., **5**, 1891-1904, 2005, SRef-ID: 1680-7324/acp/2005-5-1891. www.atmos-chem-phys.org/acp/5/1891/

Tsigaridis K., Krol, M., Dentener, F. J., Balkanski, Y., Lathière, J., Metzger, S., Hauglustaine, D. A., and Kanakidou, M., 2006, Change in global aerosol composition since preindustrial times, *Atmos. Chem. Phys*., **6,** 5143–5162, www.atmos-chem-phys.net/6/5143/2006/

Tsigaridis K. and M., Kanakidou, 2007, Secondary organic aerosol importance in the future atmosphere, submitted to *Atmos. Environ.*

Vignati E., Wilson, J., and Stier, P., 2004, M7: an efficient size resolved aerosol microphysics module for large-scale aerosol transport models, *J. Geophys. Res.*, **109**, D22, 22202, doi:10.1029/ 2003JD004485.

Volkamer, R., Jimenez, J. L., San Martini, F., Dzepina, K., Zhang, Q., Salcedo, D., Molina, L. T., Worsnop, D. R. and Molina, M. J., 2006, Secondary organic aerosol formation from anthropogenic air pollution: Rapid and higher than expected, *Geophysical Research Letters*, **33**, L17811, doi:10.1029/2006GL026899.

MEASUREMENTS OF OZONE, BLACK CARBON AND PARTICLE SIZE DISTRIBUTIONS ALONG A MEDITERRANEAN CRUISE TRACK DURING THE PERIOD: OCTOBER 2005-OCTOBER 2006

K. VELCHEV, J. HJORTH*, E. VIGNATI, A. DELL'ACQUA,
S. MARTINS DOS SANTOS, F. DENTENER, F. RAES
European Commission, JRC, Institute for Environment and Sustainability, TP 290, I-21020 Ispra (VA)

Key Words: Mediterranean; climate change; air pollution; ozone; black carbon; particles.

Abstract High levels of ozone as well as particles, including Black Carbon (BC), have been observed at sites around the Mediterranean Sea, and several studies have shown very high aerosol radiative forcing in the area, but systematical, long term observations are scarce. A collaboration between the JRC and the Italian company 'Costa Crociere' has allowed to install a monitoring station on board the cruise liner 'Costa Fortuna' that performs cruises on the Mediterranean, with regular weekly tracks in the Western Mediterranean during spring, summer and autumn, and in the Eastern Mediterranean during winter. Measurements of ozone, Black Carbon (aethalometer) and particle size distributions (optical particle sizer) have been performed, starting from the autumn of 2005; this activity will continue for several years. The measured ozone concentrations are compared to those obtained by simulations in a recent model intercomparison (ACCENT-PHOTOCOM); the initial measurements are in the higher end of the range of modeled values in the winter and in the lower end during the summer. Measured concentrations of ozone and BC in 2006 are compared to model simulations for previous years and the results are discussed.

1. Introduction

Although it is well-recognized that the Mediterranean basin is exposed to relatively high levels of air pollution, the network of monitoring stations in the area is considerably weaker than in Central and Northern Europe, and data over the sea surface are obviously particularly scarce (Figure 1). In order to provide more such observational data, useful for describing the climatology of air pollution in the area and understanding its causes, a monitoring

* To whom correspondence should be addressed.

A. Mellouki and A.R. Ravishankara (eds.), Regional Climate Variability and its Impacts in the Mediterranean Area, 155–165.

station was set up on a Mediterranean cruise ship as a result of a collaboration agreements between the Costa Crociera company and the JRC. Ozone, Black Carbon (BC) and particle size distributions were measured continuously along regular cruise tracks in the Central and Eastern Mediterranean (winter) and in the Central Western Mediterranean (spring, summer and autumn). These pollutants are of particular relevance both because of their climate impacts and their potential impacts on human health and (in the case of ozone) vegetation.

Air pollution in the Mediterranean Basin is influenced by local emissions, breeze circulation as well as long range transport, mainly from the north. Northerly flows are particularly important in the summer period where the pressure gradient between the Azores. High and the low pressure area associated with the South West Asian Monsoon appears to bring air pollution across them Mediterranean to North Africa (Lelieveld et al., 2002, Duncam and Bey, 2004). Model simulations with the TM5 global atmospheric chemical transport model suggest that the yearly average ozone concentrations over the Mediterranean Sea is higher than most of the surrounding land-surfaces because the lifetime of ozone over the sea is longer than over the continent. The levels of ozone are obviously higher in summer than in winter because of its photochemical origin, however simulations with the TM5 also indicate that the levels of BC in the summer are highest in winter in both the Eastern and the Western Mediterranean, which can be explained by the characteristic pattern of transport of pollutants by the predominantly Northernly winds (Duncan and Bey, 2004). A field study (Lazaridis et al., 2006) confirms that the Eastern Mediterranean basin is moderately to highly polluted during summer and relatively unpolluted during winter

Many observations, ground based as well as remote sensing show that transport Saharan dust particles have an important influence on aerosol concentration in the Mediterranean basin. An analysis of satellite data from the year 2001 (Barnaba and Gobbi, 2004) showed that the maximum dust impacts in spring is found in the Eastern and Central Mediterranean while in summer and autumn a shift to the Central and Western Mediterranean is observed, in the winter the impact of desert dust in the area is relatively small.

2. Experimental

2.1. MEASUREMENTS

The instruments are placed in a cabin at the front of the ship, 47 m above sea-level; a comparison between this point and a measuring point at the tip

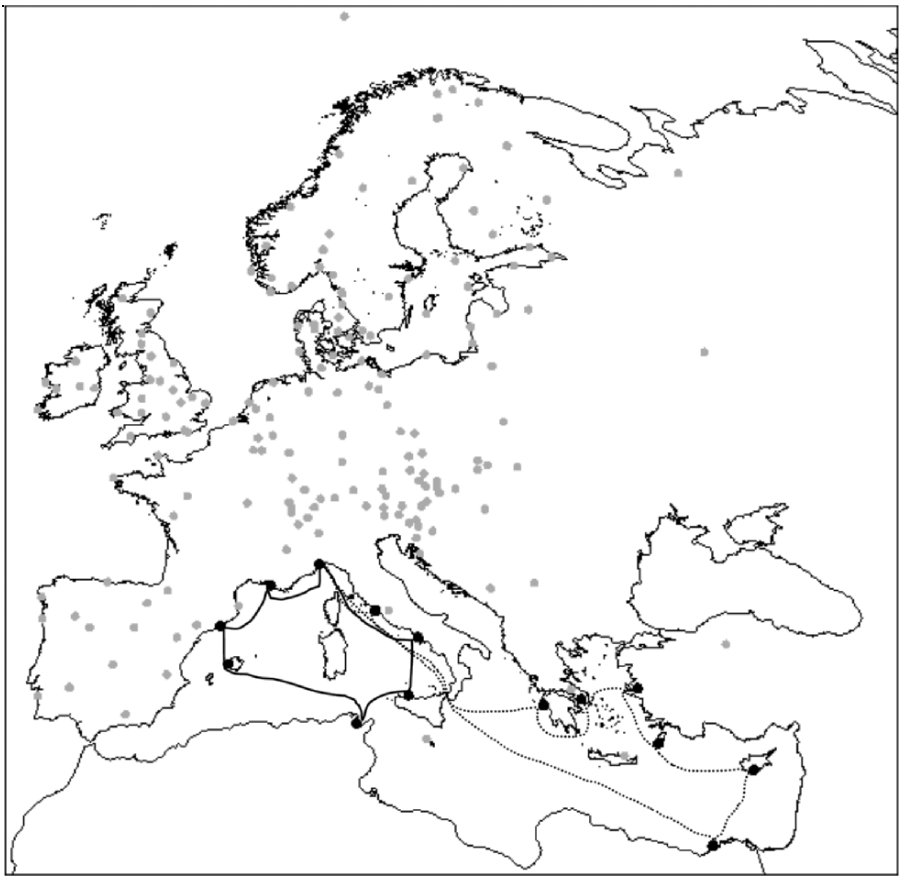

Figure 1. The regular cruise tracks of Costa Fortuna in the: Eastern Mediterranean, Savona-Civitavecchia-Alexandria-Limassol-Rhodes-Izmir-Piraeus-Katakolo-avona, (November 2005 - April 2006, 10 cruises) and in the Western Mediterranean, Savona-Napoli-Palermo-Tunis-Palma-Barcelona-Marseille-Savona (April 2006 - October 2006, 31 cruises). The positions of the stations of the main European network for monitoring of regional air pollution, EMEP, are shown in grey color

of the bow of the ship were found to provide the same values of the measured parameters. Ozone is measured by a Thermo C49 ozone analyzer, equivalent BC was measured by a 2-wavelength Aethalometer from Magee Scientific (model AE 21). Particle size distributions were measured by a Grimm optical particle analyzer. The inlet to the ozone analyzer and the Aethalometer had

a cut-off at 1 μm while the inlet to the optical particle sizer had a cut-off at 10 μm. Meteorological data were provided from the automatic measurement station on the ship and also information on the position, speed and direction of the ship were available, thus allowing to identify situations where contamination from the emissions of the ship itself might interfere with the measurements.

Particle samples were collected on quarts filters (47 mm diameter, flow rate 2.3 m^3/hour) during the week 9-16 July 2006 with a double purpose: To compare Aethalometer measurements of BC to measurements done with an independent method and to provide information on ions and on organic carbon (OC) content of the particles. BC and OC were determined using a thermo-optical method (Birch and Carry, 1996 and Mader et al., 2001) which provided and independent estimate of the BC concentration. The comparison between BC estimated by this procedure to the estimate provided by the two-wavelengths Aethalometer showed a good correlation ($R^2 = 0.95$) with the thermo-optical method providing 30-40% lower values than the Aethalometer.

The duration of the winter-cruises on the Eastern Mediterranean is ten days, while the summer cruises in the Western Mediterranean take only seven days. Costa Fortuna is mostly sailing during the evening/night and stays in harbors during the day, exceptions are the long tracks Tunis-Palma and Alexandria-Messina, where both day and night hours are included. Observations from Malta and Crete (personal communications) show relatively small (less than ± 5 ppbV around average) monthly averaged diurnal variations, suggesting that ozone-levels depend on transport more than local formation.

2.2. THE TM5 MODEL

TM5 model has been used for the simulations in the present work. It is an off-line global transport chemistry model (Krol et al., 2005) that uses the meteorological data calculated by the ECMWF model. It has a spatial global resolution of 6° × 4° and a two-way zooming algorithm that allows resolving regions (e.g., Europe, N. America, Africa and Asia) with a finer resolution of 1° × 1°. The vertical structure has 25 layers, defined in a hybrid sigma-pressure coordinate system.

Yearly averaged data of fossil fuel and biofuel BC emissions of antropogenic origin are based on Bond et al. (2004) emission inventories. Monthly emissions of large-scale biomass burning of black carbon are based on the

Global Fire Emission Database (GFED) inventory (van der Werf et al., 2003). Emission data for the full chemistry simulation are from EDGAR 3.2, 1995 data-base (Olivier et al., 2002).

In an intercomparison of simulations of the yearly variation of surface ozone over land in the Mediterranean area by 25 different models, TM5 was found to give concentrations approximately in the middle of the range of simulations (Ellingsen, 2007).

TM5 simulations for the year 2006 were not available when this work was prepared, so the analysis of the data of this year is based only on comparisons to simulations of previous years.

3. Observations

3.1. OZONE

Examples of ozone-observations from the track in the Central-Eastern Mediterranean in the winter and in the Western Mediterranean in the summer are shown in Figure 2. The influence of harbours and big cities is seen, mainly as a local titration effect causing lower ozone concentrations due to the reaction between ozone and NO from combustion sources. However, also evidence of enhancement of ozone levels in urban plumes, particularly downwind of the Marseille area, is seen.

A comparison between the simulations with the TM5 model and the observations made in October, November and December 2005 was made: Measurements of ozone and Black Carbon (aethalometer, optical measurement) have been compared to TM5 model predictions for 2005 (October-November-December) for selected points. The concentrations at the point locations are sampled in the model with linear interpolation using the neighbourhood grid concentrations.

The results of this comparison are shown in Figure 3 for ozone. The comparison was only made for the cases where the measured values did not show significant variations within a time interval of two hours around the point where the comparison was made because the resolution of the model does not allow it to simulate variations on shorter time scales. The measured concentrations tend to be somewhat higher than the modelled ones, the average deviation being 3.5 ppbV.

For the year 2006, comparisons with model simulations of previous years were made for the “open sea” trajectories Tunis-Palma and, when going from Civittavecchia to Alexandria, the trajectory between Sicily and Egypt.

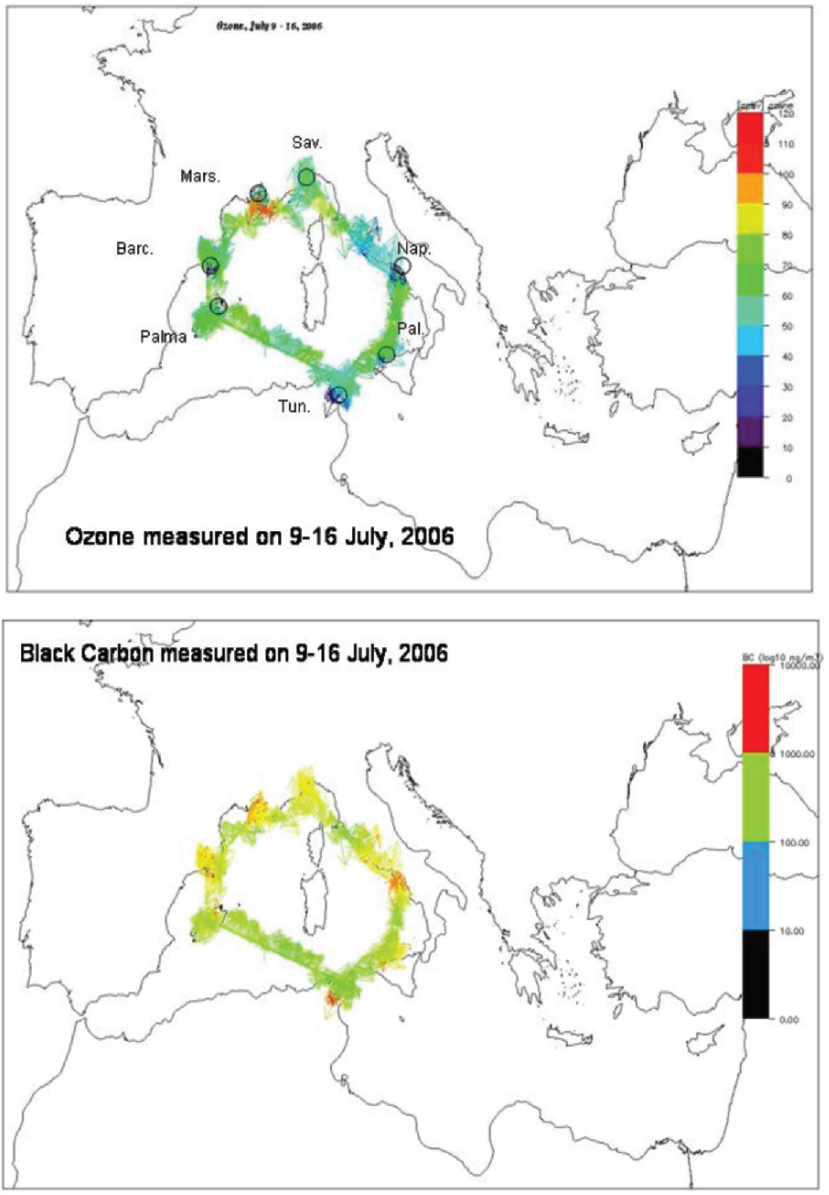

Figure 2. The concentrations of ozone and Black Carbon measured during one of the cruises on the Western Mediterranean. The color scales show ozone in ppbV (linear) and BC in ng/m^3 (logaritmic). The arrows show the direction of the wind, the length is proportional to wind speed (highest wind speed during this cruise was 42 km/hour)

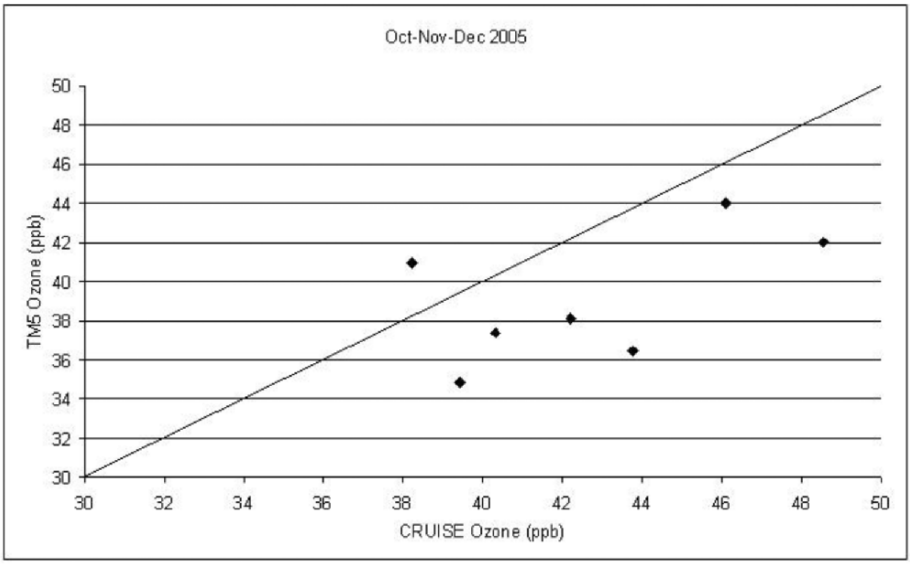

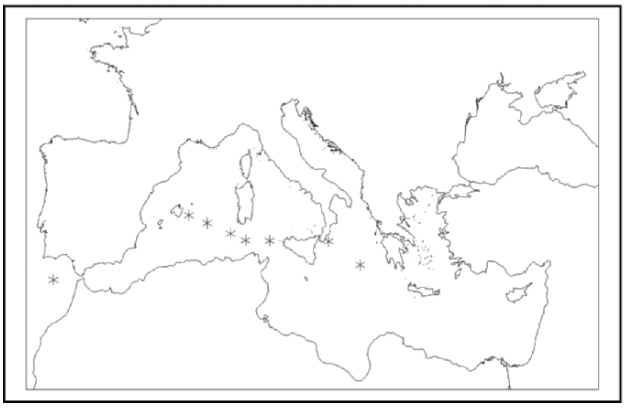

Figure 3. Comparison of measured ozone concentrations to those predicted by the TM5 model, as discussed in the text

The comparisons show that ozone levels in May-October of 2006 in the Western Mediterranean tend to be somewhat below the model simulations for 2000-2003, while the same comparison for the Eastern Mediterranean in January-March show somewhat higher measured than observed values. However, in the case of ozone, the observed differences are not dramatical and may be explained by year-to-year variations in the meteorological conditions.

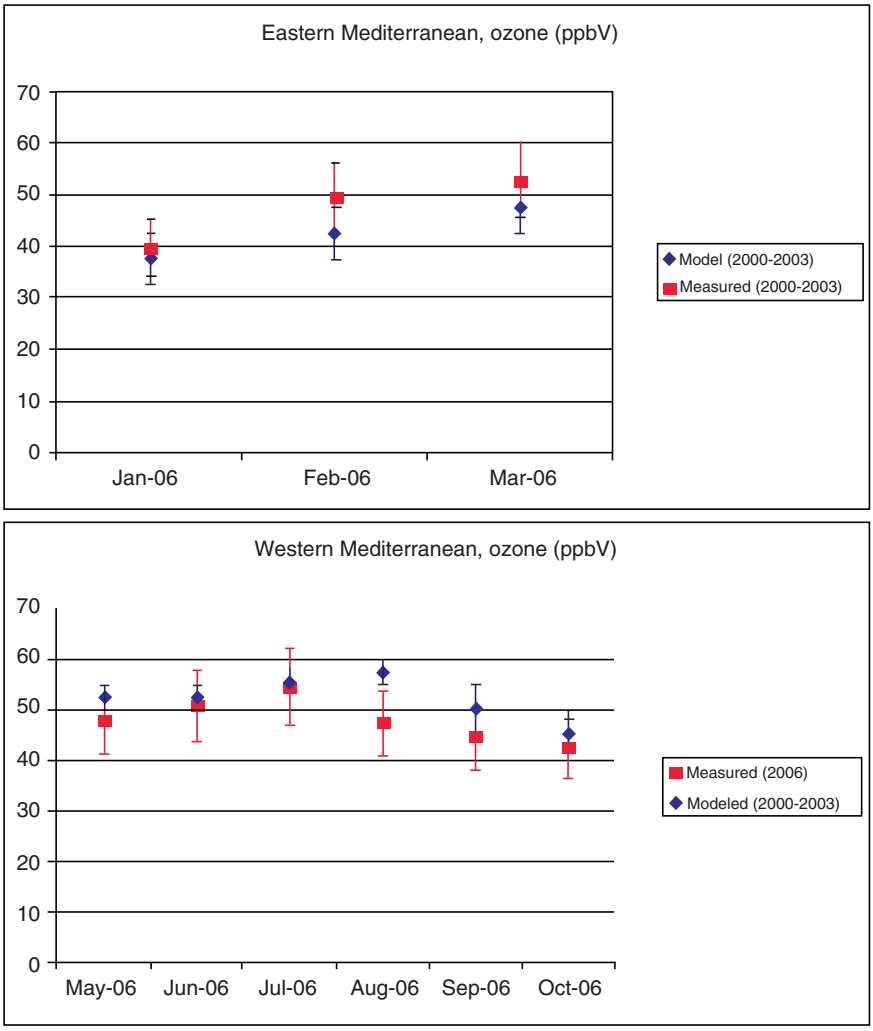

Figure 4. Comparison between monthly mean ozone concentrations measured over the open sea in 2006 and those simulated by the TM5 model for the years 2000-2003, as described in text. Error bars correspond to one standard deviation, comparing measurements on different cruises and monthly means for different years

3.2. BLACK CARBON

Measured values of BC were compared to model predictions (Figure 5) in the same way as for ozone. In the case of October–December 2005 the measurements at selected points were compared to values from the model output, calculated by interpolation of neighbouring grids, exactly like in the case of ozone. In this case the differences between observations and model output

are much larger than in the case of ozone. In order to test the influence of the choice of emission inventory, two different inventories were tested, as shown in the figure; however, the influence on the simulated concentrations was relatively small.

Some trajectory analysis has been carried out, using the HYSPLIT facility, available on a web-site (NOAA, 2007). The largest disagreements were found in the cases where the 72 hours trajectories passed over the area around Tunis; this may be explained by an underestimation of BC emissions from this area, but also, for instance, by an artifact in the BC measurements caused by the influence of dust from this area.

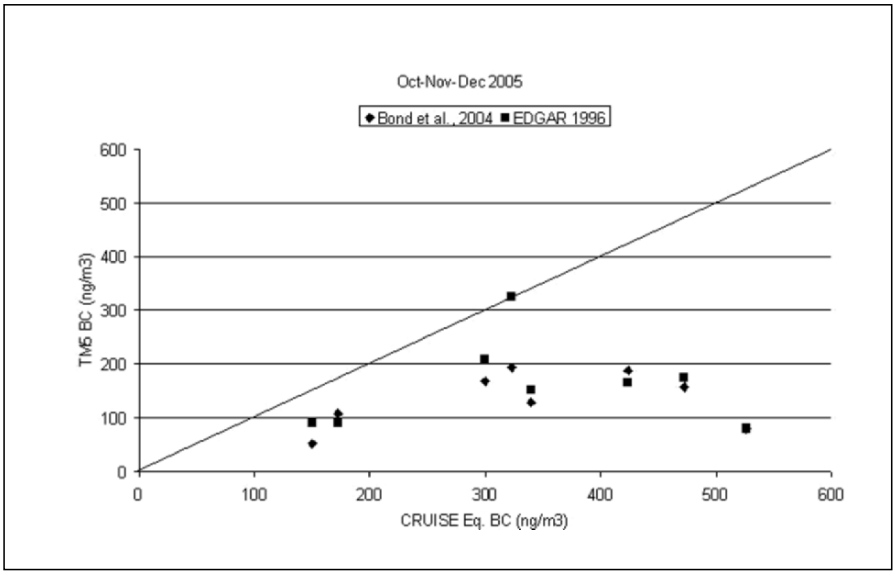

Figure 5. Comparison measurements-TM5 model as in Fig. 3, but here for Black Carbon. Two different emission inventories have been tested (Bond 2004, Edgar 1996)

Also for BC, the values measured in 2006 were compared to the average for the years 2000-2003 (Figure 6). The January-March measurements of BC concentrations in the Eastern Mediterranean as well as the October measurements in the Western Mediterranean give values that are at least a factor of two higher than the model-average of the previous years, but because of the large variations on the BC measurements between different cruises within the same month (relative standard deviation 47%) there is some overlap between the error bars. A detailed analysis of the meteorological conditions is needed to understand if the differences between measurments in 2006 and model simulations for previous years can be explained by particular caracteristics of this year.

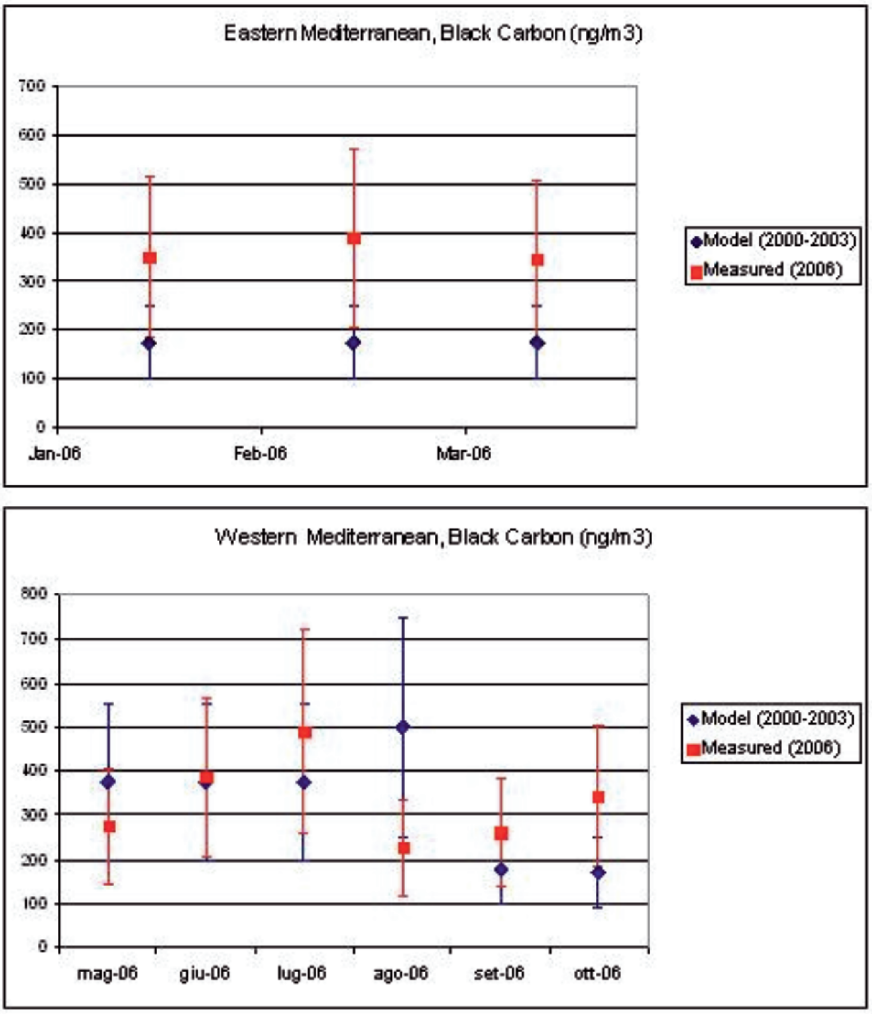

Figure 6. Comparison between monthly mean Black Carbon concentrations measured over the open sea in 2006 and those simulated by the TM5 model for the years 2000-2003, as described in text. Error bars correspond to one standard deviation, comparing measurements on different cruises and monthly means for different years

The trend for the summer months is not evident, measured BC values are not systematically higher or lower than modeled ones.

3.3. CHEMICAL ANALYSES OF PARTICLES

A striking feature of the outcome of the chemical analysis of the PM10 filter samples obtained in July 2006 is the very low content of sea salt (2-3% sodium) in all samples collected over the open sea; however, a recent

measurement series has shown that under more windy conditions, sea salt becomes a more important aerosol component, as expected. The PM10 samples collected over sea during this cruise show relatively high concentrations of sulfate. A comparison between the PM10 samples collected over the sea and average values determined for urban conditions in Barcelona and Marseille shows significantly higher values of the ratio SO_4^{--}/BC over the sea. Also the ratio Organic Matter/BC is significatly higher over the sea.

Further analyses of these data are underway.

4. References

Barnaba, F. and Gobbi, G. P., 2004, Aerosol seasonal variability over the Mediterranean region and relative impact of maritime, continental and Saharan dust particles over the basin from MODIS data in the year 2001, *Atmos. Chem. Phys.* **4:** 2367-2391.

Birch, M. E. and Cary, R. A., 1992, Elemental carbon-based method for monitoring occupational exposures to particulate diesel exhaust *Aerosol Sci. and Technol.* **26:** 221-241.

Bond, T., Streets, D., Yarber, K., Nelson, S., Wo, J.-H. and Klimont, Z., 2004, A technology-based global inventory of black and organic carbon emissions from combustion *J. Geophys. Res.* **109:** D14203, doi:10.1029/2003JD003697.

Duncan, B. N and Bey, I., 2004, A modeling study of the export pathways of pollution from Europe: Seasonal and interannual variations (1987–1997), *J. Geophys. Res.* **109:** D08301, doi:10.1029/2003JD004079.

Ellingsen, K., 2007, Manuscript in preparation.

Krol1, M., Houweling, S., Bregman, B., van den Broek, M., Segers, A., van Velthoven, P., Peters, W., Dentener, F. and Bergamaschi, P., 2005, The two-way nested global chemistry-transport zoom model TM5: algorithm and applications, *Atmos. Chem. Phys*. **5:** 417-432

Lazaridis, M., Eleftheriadis, K., Smolik, J., Colbeck, I., Kallos, G., Drossinos, Y., Zdimal, V., Vecerag, Z., Mihalopoulos, N., Mikuskag, P., Bryant, C., Housiadas, C., Spyridakia, A., Astithae, M. and Havranek, V., 2006, Dynamics of fine particles and photo-oxidants in the Eastern Mediterranean (SUB-AERO), *Atmospheric Environment* **40:** 6214-6228.

Lelieveld, J. et al. (30 authors), 2002, Global Air Pollution Crossroads over the Mediterranean, *Science* **298:** 794-799.

Mader, B. T., Flagan, R. C. and Seinfeld, J. H., 2001, Sampling atmospheric carbonaceous aerosols using a particle trap impactor/denuder sampler *Environ. Sci. Technol.* **35:** (2001), 4857-4867.

NOAA, 2007, http://www.arl.noaa.gov/ready/hysplit4.html

Olivier, J., Berdowski, J., Peters, J., Bakker, J., Visschedijk, A. and Bloos, J., 2002, Applications of EDGAR Including a Description of EDGAR V3.0: Reference Database with Trend Data for 1970–1995, NRP Report, 410200 051, RIVM, Bilthoven, The Netherlands. 2002.

van der Werf, G. R., Randerson, J. T., Collatz, G. J., and Giglio, L., 2003, Carbon emissions from fires in tropical and subtropical ecosystems *Global Change Biology* **9(4):** 547-562.

CONCENTRATION AND CHEMICAL COMPOSITION OF $PM_{2.5}$ AND $PM_{10\text{-}2.5}$ IN THE NORTHEASTERN MEDITERRANEAN

NILGÜN KUBILAY*
Institute of Marine Sciences-Middle East Technical University, P.O. Box 28, Erdemli-Mersin 33731, Turkey

MUSTAFA KOÇAK
Institute of Marine Sciences-Middle East Technical University, P.O. Box 28, Erdemli-Mersin 33731, Turkey

NIKOS MIHALOPOULOS
Environmental Chemical Process Laboratory, Depart. Of Chemistry, University of Crete, P.O. Box 2208, Gr-71003 Voutes, Heraklion, Greece

Key Words: $PM_{2.5}$; PM_{10}; air quality; Saharan dust; eastern Mediterranean; Turkey.

Abstract Two stage aerosol samples ($PM_{10–2.5}$ and $PM_{2.5}$) were collected at a rural site (Erdemli) located on the coast of the Northeastern Mediterranean, between April 2001 and April 2002. A total of 581 aerosol samples were analysed for trace elements (Fe, Ti, Mn, Ca, V, Ni, Zn, Cr) and water soluble ions (Na^+, NH_4^+, K^+, Mg^{2+}, Ca^{2+}, Cl^-, Br^-, NO_3^-, SO_4^{2-}, $C_2O_4^{2-}$ and MS^-). The annual mean PM_{10} and $PM_{2.5}$ levels were 36.4 ± 27.8 μg m^{-3} and 9.7 ± 5.9, respectively. The highest levels of PM_{10} were observed during the transition period (March, April and May) due to mineral dust transported from North Africa and during winter due to sea spray generation. However, $PM_{2.5}$ levels exhibited higher concentrations during summer resulting from an enhanced production of secondary aerosols. PM_{10}, crustal elements, sea salt aerosols and NO_3^- were mainly associated with the coarse mode whereas $nssSO_4^{2-}$, $C_2O_4^{2-}$, MS^-, NH_4^+, Cr and Ni were found predominantly in the fine fraction. Ionic balance analysis performed in the coarse and fine aerosol fractions indicated anion and cation deficiency due to CO_3^{2-} and H^+, respectively. A relationship between $nssSO_4^{2-}$ and NH_4^+ denoted that sulphate particles were partially neutralized (70%) by ammonium. Excess-K/BC presented two distinct ratios for winter and summer, indicating two different sources: Fossil fuel burning in winter and biomass burning in summer.

1. Introduction

Aerosols physically affect the heat balance of the Earth, both directly by reflecting and absorbing solar radiation, and by absorbing and emitting

A. Mellouki and A.R. Ravishankara (eds.), Regional Climate Variability and its Impacts in the Mediterranean Area, 167–180.

some terrestrial infrared radiation and indirectly by influencing the properties and cloud processes and, possibly, by changing the heterogeneous chemistry of reactive greenhouse gases (e.g., O_3; IPCC, 2001 and references therein). The global radiative forcing due to aerosols is roughly 1.6 ± 1.3 Wm^{-2}, which nearly compensates for the mean global radiative forcing of 2.4 ± 0.3 Wm^{-2} due to greenhouse gases warming. Recently, Vrekoussis et al., (2005) investigated aerosol optical properties in the Eastern Mediterranean and estimated radiative forcing at the top of the atmosphere ranging from –12.6 to –2.3 W m^2 for summer and winter, respectively. Their estimated radiative forcing values are up to five times higher than that induced by greenhouse gases but opposite in sign. The large range of uncertainty associated with aerosol forcing estimates reflects the poor state of knowledge regarding the sources, distributions, and properties of atmospheric aerosols.

The need for an increased effort in characterizing tropospheric aerosols in order to reduce the uncertainty in the aerosol forcing estimate has been stressed (Ramanathan et al., 2001; Kaufman et al., 2002). Recent model studies reproduced satellite observations and demonstrated the role of three major components of aerosols in surrounding regions of the Mediterranean basin (sulfate, black carbon and dust), having very high direct radiative forcing for aerosols at the top of the atmosphere (Jacobson, 2001). Knowledge of the spatial and temporal variability of aerosol concentrations, their physical, chemical and radiative properties are very important since they can directly and indirectly influence planetary albedo (climate).

2. Material and Methods

A Gent type PM_{10} stacked filter unit (SFU) sampler was used in order to collect atmospheric particles in two size ranges namely, $PM_{10–2.5}$ (coarse) and $PM_{2.5}$ (fine) at a rural site located on the coast of the Eastern Mediterranean, Erdemli (36°N and 34°E), Turkey (for more details see Kubilay and Saydam, 1995; Kubilay et al., 2002; Koçak et al., 2004a, 2004b).

Sampling commenced in April 2001 and ended in April 2002. During this period a total of 562 aerosol filter samples were collected with a temporal resolution of 24 hours. After collection of aerosol filters, $PM_{10–2.5}$ and $PM_{2.5}$ concentrations were determined gravimetrically (PM_{10} refers to the sum of $PM_{10–2.5}$ and $PM_{2.5}$ concentrations). Water soluble ions were measured by ion chromatography (IC) at ECPL (Environmental Chemical Processes Laboratory), University of Crete following the method described in details by Bardouki et al. (2003). Concentrations of the elements (Fe, Ti, Ca, Mn, K, Cr, V, Zn, Cl, S) were obtained using 2 cm^2 of the filter sample applying Proton Induced X-ray Emission (PIXE) at ATOMKI (Institute of Nuclear Research of the Hungarian Academy of Sciences, Debrecen, Hungary).

During the experiments the aerosol samples were irradiated by a 2 MeV proton beam, which was supplied by the 5 MV Van de Graaff Accelerator of ATOMKI (for more details see Borbely-Kiss et al., 1999). Black Carbon (BC) content in 46 fine aerosol filter samples collected during winter and summer was determined using a Smoke Stain Reflectometer (SSR).

3. Results and Discussion

3.1. GENERAL CHARACTERISTICS OF THE DATA

The largest portion of the atmospheric particle mass (PM_{10}) is associated with coarse particles and contributes 73.4% to the observed particle mass., and the fine fraction contributes only 26.6% of the particle mass. Crust originated trace metals, water-soluble ions Na^+, Cl^-, Mg^{2+}, Ca^{2+}, Br^- and NO_3^- are associated mainly with coarse particles (more than 75%). The above observations are expected for trace metal and ions known to arise from sea salt (Na^+, Cl^-, Mg^{2+}, Br^-) and crustal material (Fe, Ti, Mn, Ca^{2+}), respectively. On average about 85% of particulate nitrate (NO_3^-) was associated with coarse particles, which would strongly indicate that it combines mostly with alkaline ion species. The most likely formation pathway for particulate nitrate (NO_3^-) is the reaction of gaseous nitric acid or some other nitrogen compounds with sea salt particles and mineral dust particles. The mass concentration of oxalate ($C_2O_4^{2-}$) and non-sea salt sulfate ($nssSO_4^{2-}$) was mainly found in the fine mode (60% and 80%, respectively). On the other hand, ammonium (NH_4^+) and methane sulfonic acid (MS^-) mass concentrations were exclusively found in the fine size fraction. Trace metals V and Zn displayed almost half of their mass concentrations in the coarse fraction while about 40% and 30% of the mass concentrations of Ni and Cr were found in coarse fraction, respectively.

Figure 1 illustrates the regression analysis between $nss\text{-}SO_4^{2-}$ and NH_4^+ in fine aerosol particles during the observation period. The slope of the regression line is 0.68 ($NH_4^+/nssSO_4^{2-}$ equivalent ratio, r = 0.96), which indicates that partial neutralization of $nss\text{-}SO_4^{2-}$ by NH_4^+ occurs. Taking into the account the slope of the regression, it can be proposed primarily that $(NH_4)_{1.4}.(H)_{0.6}.(SO_4)$ is produced instead of $(NH_4)_2SO_4$ in the reaction between ammonium and non sea salt sulfate.

Relationships between black carbon (BC) and other species were also investigated in 46 fine aerosol filter samples. Black carbon and excess potassium indicated strong correlation in summer and winter. Therefore, except excess potassium, BC did not indicate strong correlations with water soluble ions and elements in the dataset. Figure 2 presents the relationship between

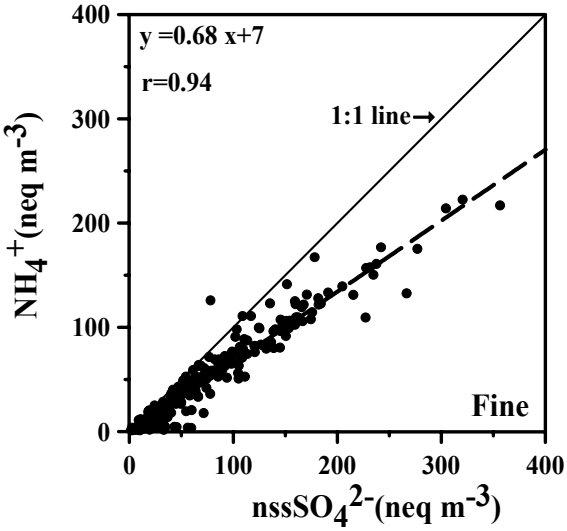

Figure 1. Observed relationship between $nssSO_4^{2-}$ and NH_4^+ (neq m^{-3})

BC and excess potassium. BC is emitted uniquely from combustion processes, including fossil fuel and biomass burning, while combustion of fossil fuel seems to produce a small amount of excess potassium. As a result, Andreae (1983) suggested that the mass ratio of excess potassium to BC may provide information enabling the distinction between the K that would be produced by biomass burning and combustion sources. As can be inferred from Figure 2 the excess potassium to BC ratio indicates two distinct ratios. The slope of the regression line in summer was found to be ~0.366 and close to the values generally measured in aerosols dominated by biomass burning (0.21 to 0.46; Andreae, 1983). Therefore, the observed ratio implies that biomass burning makes an important contribution to fine black carbon in the summer. However, the slope of the regression line in winter was about (0.062), 5 times lower than that found in summer and is similar to those found in an urban atmosphere dominated by fossil fuel burning (K/BC = 0.025-0.09, Yang et al., 2005). Hence an excess K to BC ratio suggests that fossil fuel burning predominant the source of fine black carbon particles during winter. Sciare et al., (2003) collected a total of 56 aerosol samples during summer at Finokalia (Central Mediterranean, from 26 July to 18 August 2001) and showed a nssK/BC ratio of ~0.044 (R^2 = 0.58) which was similar to the winter excess K/BC ratio observed at Erdemli. Therefore, their observed ratio suggests that potassium and BC is mainly influenced by fossil fuel burning during summer.

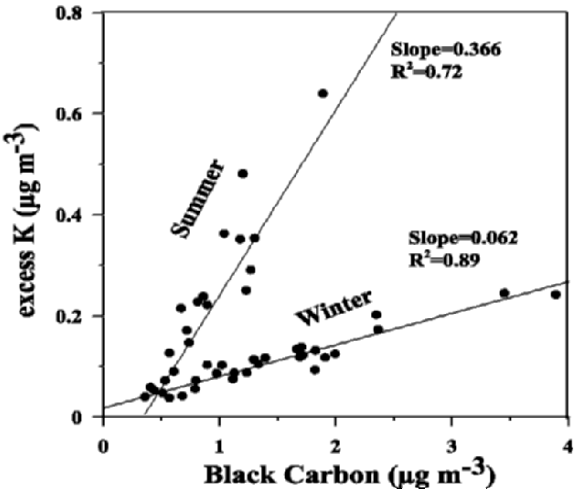

Figure 2. Relationship between excess potassium and black carbon in summer and winter

3.2. ABSOLUTE PRINCIPAL FACTOR ANALYSIS

In order to identify sources, factor analysis (FA), which is one of the multivariate statistical techniques, was carried out. Factor analysis is commonly used in environmental studies to deduce sources from data. The principal application of factor analysis is to reduce the number of variables. Therefore, factor analysis can be applied as a data reduction method. The results of varimax-rotated factor analysis are presented in Table 1a and Table 1b for atmospheric coarse and fine particles, respectively.

(A) Coarse Particles: The data can be interpreted on the basis of four common factors accounting for 87.8% of the total variance of the system. The first factor has high loadings of Ti, Fe, Mn and Ca^{2+} and moderate loadings of Zn and V. Since Factor-1 is heavily influenced by the concentrations of Ti, Fe, Mn and Ca^{2+} it may be attributed to the crustal component of the coarse aerosol population. For that reason, this factor is ascribed as the crustal factor, explaining 37.0% of the total variance. The second factor explains 28.1% of the total variance in the system, and can be identified as a marine factor, since it consists of high loadings of Na^{+}, Cl^{-}, Mg^{2+}, Br^{-} and high loadings of SO_4^{2-} and K^{+} as well. Factor-3 is highly loaded in Ni and V and moderately loaded in Zn. Therefore, this factor is attributed to residual oil combustion, and explains 12.4% of the total variance. The fourth factor explains a further 10.3% of the variance and can be identified as photochemical sources, since it is highly loaded with NO_3^{-} and $C_2O_4^{2-}$.

TABLE 1a. Varimax rotated factor matrix and corresponding probable source type for the coarse aerosol data set

Variable	Factor1	Factor2	Factor3	Factor4	Communalities
Ti	**0.96**	0.13	0.17	0.16	0.99
Fe	**0.95**	0.16	0.19	0.13	0.99
Mn	**0.93**	0.11	0.12	0.14	0.98
Ca^{2+}	**0.84**	0.34	0.31	0.13	0.94
K	**0.82**	0.51	0.16	0.08	0.98
Zn	0.49	0.06	**0.62**	0.26	0.98
V	0.48	0.02	**0.80**	0.02	0.65
Ni	0.14	0.12	**0.93**	–0.03	0.80
Cr	0.16	-0.03	0.15	0.07	0.71
Cl^-	0.11	**0.99**	0.04	–0.08	0.99
Mg^{2+}	0.12	**0.97**	0.02	–0.05	0.98
Na^+	0.20	**0.97**	0.03	–0.03	0.99
Br^-	0.11	**0.96**	0.07	–0.08	0.96
SO_4^{2-}	0.37	**0.89**	0.12	0.16	0.96
$C_2O_4^{2-}$	0.26	0.04	0.09	**0.89**	0.68
NO_3^-	0.19	–0.15	–0.01	**0.91**	0.66
Eigen Value	6.7	5.1	2.2	1.9	
Variance, %	37.0	28.1	12.4	10.3	
Probable Source	Crustal	Marine	Residual Oil	Photochem.	

(B) Fine Particles: The variables of chemical species in the fine fraction may be explained on the basis of four common factors, elucidating 857% of the total system variance. The first factor has high loadings of SO_4^{2-}, NH_4^+, MS^-, $C_2O_4^{2-}$, Zn and moderate loading of K^+ and explains 28.1% of the total variance. Therefore, this factor can be ascribed to secondary aerosols as it has high loadings of sulfate, ammonium, methane-sulfonate and oxalate. Factor-2 consists of high loadings of Ti, Fe, Mn and Ca^{2+} and clarifies a further 28.1% of the total variance. Since Factor-2 is heavily affected by concentrations of Ti, Fe, Mn and Ca^{2+}, may be attributed to a crustal factor. The third factor is highly loaded in Na^+ and Mg^{2+} and explains 11.0% of the total variance in the system and may be ascribed to a marine factor. Factor-4 has high loadings of NO_3^-, V and Ni and accounts for 12.5% of the total variance of the system, and hence may be attributed to residual oil combustion.

Absolute principal factor analysis (APFA) was applied to quantify the contributions of the different sources to the concentrations of the measures species. For each coarse and fine aerosol component identified, the factor score was computed for each sample. Mass loadings for the samples were

TABLE 1b. Varimax rotated factor matrix and corresponding probable source type for the fine aerosol data set

Variable	Factor1	Factor2	Factor3	Factor4	Communalities
SO_4^{2-}	**0.96**	0.04	0.14	0.04	0.96
NH_4^+	**0.95**	–0.03	–0.01	0.16	0.95
$C_2O_4^{2-}$	**0.88**	0.11	0.28	0.20	0.88
MS^-	**0.80**	0.15	0.25	–0.11	0.72
K^+	0.62	0.04	0.10	0.24	0.52
Mg^{2+}	0.25	0.29	**0.85**	–0.04	0.73
Na^+	0.24	0.01	**0.90**	0.05	0.70
NO_3^-	0.06	0.04	0.21	**0.86**	0.43
V	0.47	0.18	–0.20	**0.77**	0.87
Ni	0.41	0.40	–0.21	**0.70**	0.86
Zn	0.79	0.22	0.03	0.29	0.70
Ti	0.09	**0.97**	0.04	0.03	0.98
Fe	0.09	**0.96**	0.08	0.07	0.99
Mn	0.17	**0.91**	0.03	0.13	0.86
Ca^{2+}	0.02	**0.87**	0.13	0.20	0.79
Cr	0.05	0.13	0.01	0.06	0.81
Eigen Value	4.8	4.8	1.9	2.1	
Variance, %	28.1	28.1	11.0	12.5	
Probable Source	Secondary	Crustal	Marine	Residual Oil	

then regressed on the AFCS (Absolute Factor Component Scores). The resultant regression coefficients were then applied to convert the daily absolute factors scores to estimate the mass contributions.

(A) Coarse Particulate Mass: The results in Figure 3a indicate estimated contributions from each of the identified sources in the coarse samples. Of the coarse fraction, the largest portion is attributable to the sea salt related source (59% of the coarse mass). In addition, a crustal component would explain 36% of the observed coarse fraction. Therefore, these naturally derived aerosol components explain 95% of coarse fraction. However, photochemistry and residual oil combustion contributes 3% and 2% of the detected coarse fraction.

(B) Fine Particulate Mass: The estimated contribution from identified sources is shown in Figure 3b. Secondary aerosol components make the largest contribution to the fine fraction (59%). Residual oil combustion related component explains a further 12.7% of the fine fraction. In addition, crust and sea salt explain 6.8% and 4.7% of measured fine fraction, respectively.

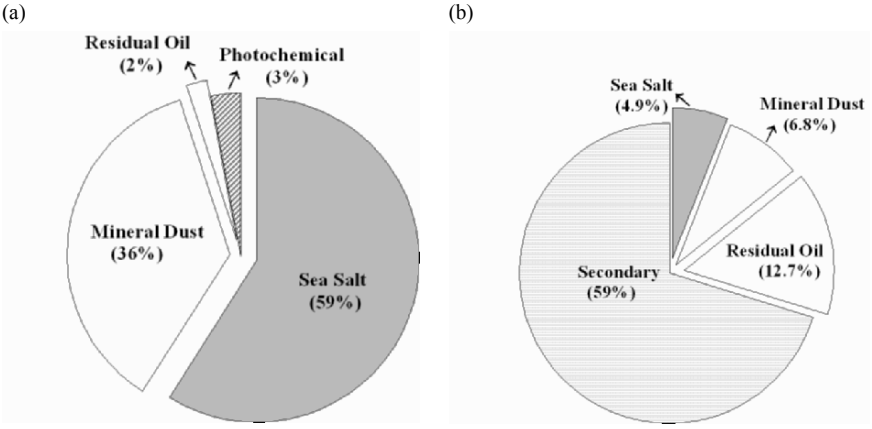

Figure 3. Estimated contribution from each source profile to particulate matter mass. (a) Coarse particulate matter mass and (b) Fine particulate matter mass

3.3. ORIGIN OF THE EXCEEDED PM_{10} LEVELS OF THE EUROPEAN DAILY LIMIT VALUE

Legislation of the PM_{10} limit values has been established by the European Commission for PM monitoring (EC/30/1999). The daily PM_{10} value has been limited to 50 μg m^{-3}, which may only be exceeded 35 days/year in 2005 (Phase I) and 7 days/year in 2010 (Phase II). A number of studies have focused on the origin of exceeded PM_{10} levels in the Western Mediterranean region (Artinano et al., 2001; Rodriguez et al., 2001). These studies have shown that exceedences of PM_{10} limit values may not always be caused by anthropogenic sources. This can be illustrated by using Spain as an example (various rural, urban and industrial sites, including the Canary Islands), where the studies indicated differences in PM_{10} chemical compositions (Rodriguez et al., 2001, 2002; Alastuey et al., 2005). These authors showed that PM_{10} concentrations are highly influenced by the occurrence of African dust. For example, more than half of the exceedences of PM_{10} at rural sites were attributed to the occurrence of African dust whereas approximately 20% of the exceedences of PM_{10} at urban and industrialized sites were originated from African dust transport. Therefore, at rural sites dust contributions might be considered to be an important contributor to the number of exceeded values of the EU daily limit value.

Figure 4 shows monthly arithmetic mean concentrations of PM_{10} at the Erdemli site. The seasonality of PM_{10} has been reported in rural, urban, and industrialized sites of the Western Mediterranean (Rodriguez et al., 2002) and the highest monthly PM levels are recorded in summer. In contrast, PM_{10} did not indicate a clear seasonal variability at Erdemli. However,

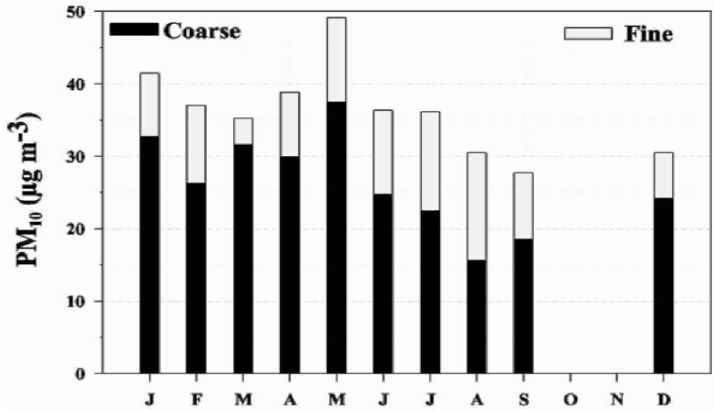

Figure 4. Monthly mean concentrations of PM_{10}

relative contributions of the fine fraction increased from winter to summer. For example, in August the relative contribution of fine fraction accounted for 50% of the PM_{10} mass. This might be attributed to the enhancement of secondary aerosol (such as sulphate) generation during summer in the Mediterranean region (Kubilay et al., 2002; Koçak et al., 2004b).

At the Erdemli site annual PM_{10} mass concentration is about 36.4 μg m^{-3} with high daily variability ranging between 1.5 and 326.0 μg m^{-3}. During the sampling period 28 events exceeded legislation of PM_{10} limit values established by the European Commission for PM monitoring. In order to clarify the source (natural or anthropogenic) of the exceedences of the forthcoming EU daily limit values, air mass back trajectories, concentrations of Fe (Ti and nssCa^{2+}; indicator of crustal material), Na^{+} (indicator of sea spray), pollution indicators nssSO_4^{2-} and NO_3^{-} and TOMS aerosol absorbing index were used.

Figure 5a shows an example of the source apportionment of the PM_{10} limit value due to Saharan air mass transport which occurred on the 6th of April 2002. On April 6th, the back trajectories at all four levels (see Figure 6a) indicate air mass flow arriving at Erdemli from North Africa. The TOMS image also shows an intense dust cloud over the North Africa and the northeastern Mediterranean (see Figure 6b). During this event the dust concentration was found to be around 85 μg m^{-3}. Dust contribution accounted for 78% of the PM_{10} level while sea salt explained 12% of PM_{10}. In addition, nssSO_4^{2-} and NO_3^{-} together accounted for 7% of PM_{10}.

On the 17th of December 2001, PM_{10} was found around 60 μg m^{-3} due to maritime air mass transport at 1000 hPa and 850 hPa. During this event sea salt concentrations were found to be high (47 μg m^{-3}) and the sea salt origin was also confirmed by the source apportionment analysis (see Figure 5b).

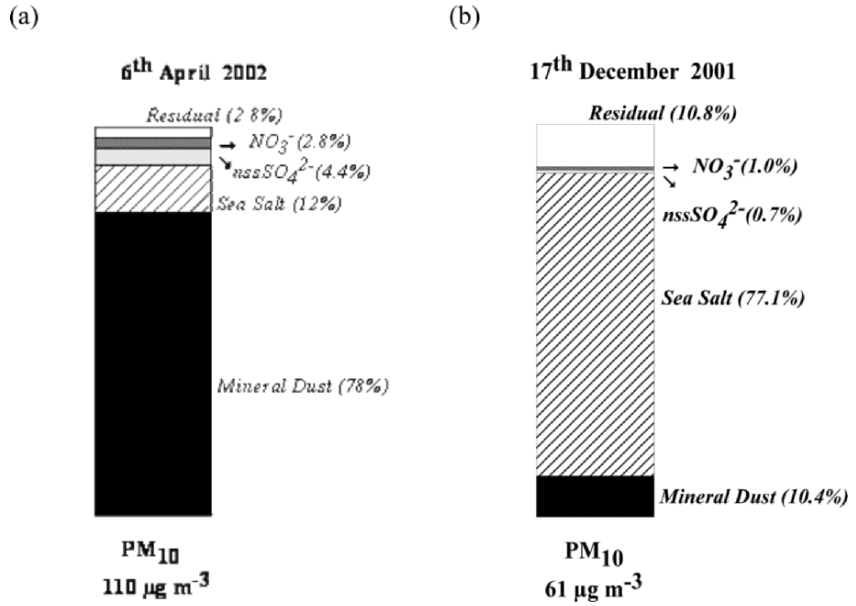

Figure 5. Source apportionment analysis for PM_{10} (a) during the Saharan dust event on the 6th of April 2002; (b) during the sea salt event on the 17th of December 2001

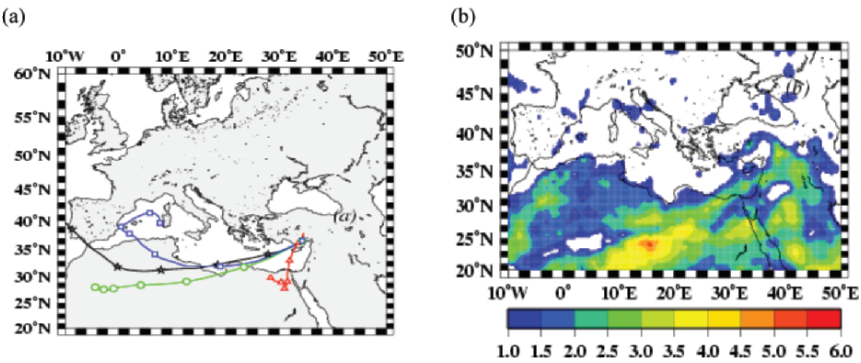

Figure 6. Saharan dust transport observed on 6th of April 2002 (a) Air mass back trajectories (b) TOMS Aerosol Absorbing Index

The source apportionment showed that sea salt accounted for 77.1% of the PM_{10} level while dust contribution explained for 10.4% of the PM_{10}. In addition, $nssSO_4^{2-}$ and NO_3^- together explained a small fraction (1.7%) of the PM_{10}.

3.4. AEROSOL IONIC BALANCE

Ion balance means the sum of the negative ions (anions) equals the sum of the positive ions (cations) when expressed as equivalents. An ion balance can be a useful tool to determine any possible parameters missing for the ionic balance. For this purpose, an ion balance was performed both in the coarse fine fractions of the aerosol particles. Plot of total cations equivalents against total anions equivalents for each size class are presented in Figures 7a and 7b, respectively. The slope of the regression line for coarse particles indicates value higher than unity (slope = 1.14, r = 0.97), which may be due to the existence of CO_3^{2-} in this size fraction which has not been measured using IC. In contrast, the slope of the regression line for the fine fraction is lower than unity (slope = 0.70, r = 0.97), which may be attributed to be presence of H^+ (not measured) in the aerosol samples. If this is the case, CO_3^{2-} is expected to associate with Ca^{2+} and H^+ is expected to react with SO_4^{2-} in the coarse and fine fractions, respectively (Figure 8a, b). A statistically significant correlation was found when Ca^{2+} concentrations were plotted against the anion deficit, defined as an excess of positive charge, indicating that CO_3^{2-} is most probably the missing anion in the coarse aerosol fraction. A significant correlation was also found between SO_4^{2-} and the cationic deficit in the fine fraction, that the cation deficit, defined as an excess of negative charge, is possibly due to H^+ associated with SO_4^{2-}.

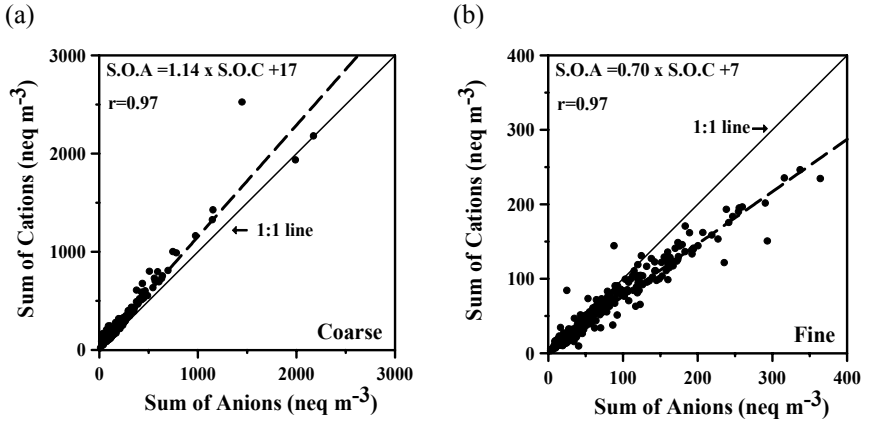

Figure 7. Sum of the anions *vs* sum of the cations: (a) Regression analysis in coarse samples, (b) Regression analysis in fine samples

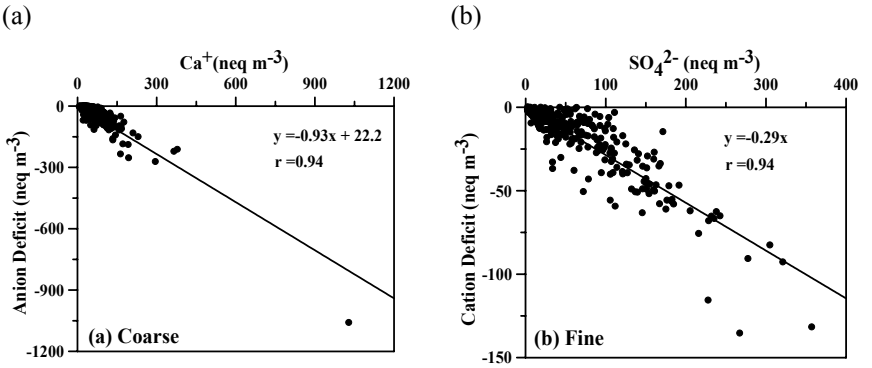

Figure 8. (a) Variation of anion deficit versus the Ca^{2+} concentrations in coarse samples, (b) Variation of cation deficit versus the SO_4^{2-} concentrations in fine samples.

4. Conclusions

$PM_{2.5–10}$, $PM_{2.5}$ and PM_{10} concentrations, factors controlling their levels and the origin and chemical composition of their exceedences have been identified at rural site located on the coast of the Eastern Mediterranean. From these findings the following conclusions may be made:

Annual mean concentrations of PM_{10} and $PM_{2.5}$ at Erdemli were 36.4 ± 27.8 μg m^{-3} 9.7 ± 5.9 μg m^{-3}, respectively, while concentrations indicated orders of magnitude change from day to day (PM_{10} = 2 to 326 μg m^{-3}; $PM_{2.5}$ = 0.5 to 28 μg m^{-3}). PM_{10} exhibited higher concentrations particularly during transition period due to mineral dust transported from North Africa and during winter owing to sea spray generation. $PM_{2.5}$ shows higher concentration mainly during summer as a result of an enhanced production of secondary aerosols.

PM_{10} mass is dominated by coarse fraction which accounts to about 75% of the total PM_{10} concentration. Crust (Fe, Ti, Mn, Ca), sea salt (Na^+, Cl^-, Mg^{2+}, Br^-) originated species and NO_3^- are associated mainly with coarse particles (>75%) whilst trace elements Cr and Ni and water soluble ions $nssSO_4^{2-}$, $C_2O_4^{2-}$, MS^- and NH_4^+ are primarily found in the fine fraction (>60%). V and Zn are found equally distributed between coarse and fine particles.

Investigation of the relationship between $nssSO_4^{2-}$ and NH_4^+ indicates that sulphate particles are not sufficiently neutralized by basic NH_4^+. Equivalent ratio ($NH_4^+/nssSO_4^{2-}$ = 0.68) exhibits that about 70% of the $nssSO_4^{2-}$ is neutralized by NH_4^+. Excess-K/BC presents two distinct ratios for winter (0.066) and summer (0.366), indicating two contrasting BC sources in the area.

These ratios suggest that in the winter BC is mainly originated from fossil fuel burning whilst it is predominantly emitted from biomass burning in the summer.

Aerosol ionic balance analyses imply that coarse and fine particles show basic and acidic character. Basic and acidic character for coarse and fine fraction might be attributed to the presence of CO_3^{2-} and H^+ in the aerosols, respectively.

5. Acknowledgements

This study was funded in part by the Middle East Technical University (AFP-2001-07-01-01) and WMO (through special service agreements of 5.115/A/CNS and 18.637/A/CNS). The authors would like to thank the NASA/GSFC/TOMS group for the use of TOMS Aerosols Index data, and Emin Özsoy for making available the ECMWF trajectory analysis through collaboration with the Turkish State Meteorological Office. Mustafa Koçak benefited from the research fellowship of the International Atomic Energy Agency (TUR/0/006) and RICAMERE project.

6. References

Alastuey, A., Querol, X., Castillo, S., Escudero, M., Avila, A., Cuevas, E., Torres, C., Romero P. M., Exposito, F. and García, O., 2005, Characterisation of TSP and PM2.5 at Izaña and Sta. Cruz de Tenerife (Canary Islands, Spain) during a Saharan Dust Episode (July 2002), *Atmos. Environ.*, **39:** 4715-4728.

Andreae, M. O., 1983, Soot carbon and excess fine potassium: long-range transport of combustion derived aerosols, *Science* **220:** 1148-1151.

Artinano, B., Querol, X., Salvador, P., Rodriguez, S., Alonso, D.G. and Alastuey A., 2001, Assessment of airborne particulate levels in Spain in relation to the new EU-directive, *Atmos. Env.* **35:** 43-53.

Bardouki, H., Liakakou, H., Economou, C., Sciare, J., Smolik, J., Zdimal, V., Eleftheriadis, K., Lazaridis, M., Dye, C. and Mihalopoulos, N., 2003, Chemical composition of size resolved atmospheric aerosols in the eastern Mediterranean during summer and winter, *Atmos. Environ.* **37:** 195-208.

Borbely-Kiss, I., Koltay, E., Szabo, Gy., Bozo, L. and Tar, K., 1999, Composition and sources of urban and rural atmospheric aerosol in Eastern Hungary, *Journal of Aerosol Scence* **30:** 369–391.

IPCC, 2001, Climate Change 2001, Intergovernmental Panel on Climate Change, *Cambridge University Press*, London.

Jacobson, M. Z., 2001, Global direct radiative forcing due to multicomponent anthropogenic and natural aerosols, *J. Geophys. Res.* **106:** 1551-1568.

Kaufman, Y. Tanre, J. D. and Boucher, O., 2002, A satellite view of aerosols in the climate system, *Nature* **419:** 215-223.

Koçak M., Nimmo, M., Kubilay, N. and Herut, B., 2004a, Spatio-temporal aerosol trace metal concentrations and sources in the Leventine Basin of the Eastern Mediterranean, *Atmos. Environ.* **38:** 2133-2144.

Koçak, M., Kubilay, N. and Mihalopoulos, N., 2004b, Ionic composition of lower tropospheric aerosols at a Northeastern Mediterranean site: implications regarding sources and long-range transport, *Atmos. Environ.* **38:** 2067-2077.

Kubilay, N. and Saydam, C., 1995, Trace elements in atmospheric particulates over the Eastern Mediterranean: concentration, sources and temporal variability, *Atmos. Environ*. **29:** 2289-2300.

Kubilay, N., Koçak, M., Çokacar, T., Oğuz, T., Kouvarakis, G. and Mihalopoulos, N. 2002, Influence of Black Sea and local biogenic activity on the seasonal variation of aerosol sulfur species in the eastern Mediterranean atmosphere, *Global Biogeochemical Cycles* **16(4):** 1079, doi:10.1029/2002GB001880.

Ramanathan, V., Crutzen, P. J., Kiehl, J. T. and Rosenfeld, D., 2001, Aerosols, climate, and the hydrological cycle, *Science* **294:** 2119-2124.

Rodriguez, S., Querol, X., Alastuey. A., Kallos, G. and Kakaliagou, O., 2001, Saharan dust contributions to PM10 and TSP levels in Southern and Eastern Spain, *Atmos. Environ*. **35:** 2433-2447.

Rodriguez, S., Querol, X., Alastuey, A. and Plana, F., 2002, Sources and processes affecting levels and composition of atmospheric aerosol in the western Mediterranean, *J. Geophys. Res.* **107 (D24):** 4777, doi:10.1029/2001JD001488.

Sciare, J., Cachier, H., Oikonomou, K., Ausset, P., Sarda-Estève, R. and Mihalopoulos, N., 2003, Characterization of Carbonaceous Aerosols during the MINOS campaign in Crete, July-August 2001, *Atmos. Chem. Phys.* **3:** 1743-1757.

Vrekoussis, M., Liakakou, E., Koçak, M., Kubilay, N., Oikonomou, K., Sciare, J. and Mihalopoulos, N., 2005, Seasonal variability of optical properties of aerosols in the eastern Mediterranean, *Atmos. Environ.* **39:** 7083-7094.

Yang, F., He, K., Ye, B., Chen, X., Cha, L., Cadle, S. H., Chan, T. and Mulawa, P. A., 2005, One-year record of organic and elemental carbon in fine particles in downtown Beijing and Shanghai, *Atmos. Chem. Phys*. **5:** 217-241.

NON-METHANE VOLATILE ORGANIC COMPOUND MEASUREMENTS IN THE CITY CENTRE OF WROCLAW, POLAND

A. NIEDOJADLO*, K. H. BECKER, Y. ELSHORBANY, R. KURTENBACH, P. WIESEN
Laboratory of Physical Chemistry, Department of Chemistry, University of Wuppertal
Gaußstr. 20, 42097 Wuppertal, Germany

A. SCHADY, A. ZWOZDZIAK, J. ZWOZDZIAK
Institute of Environment Protection Engineering, Wroclaw University of Technology
Wybrzeze Wyspianskiego 27, 50-370 Wroclaw, Poland

Key Words: NMVOCs; hydrocarbons; oxygenated compounds; emission profiles; traffic emission, industrial emission.

Abstract During the measurement campaign performed in August/ September 2005 non-methane volatile organic compounds (NMVOCs) were studied at different locations in the city of Wroclaw, Poland. The measurements covered NMVOCs in the range of C_1-C_{10}. Samples were collected using Carbotrap and Carbosieve SIII solid adsorption tubes and analysed off-line by thermal desorption and GC-FID analysis. Measurements were performed on purpose to assess the contribution of different emission categories to the observed NMVOC concentrations by using chemical mass balance modelling.

Profiles of volatile organic compounds for traffic emission were measured in a downtown intersection and during driving through the city. Solvent emission profiles for industrial sources were measured in the vicinity of different factories in Wroclaw. To obtain the ambient NMVOC concentrations sampling were performed at different points located in Wroclaw. The sampling sites represented residential, industrial, mixed settings and an area down-wind from the city centre.

All measured traffic profiles were found to be very similar. The same distribution could be observed for an intersection and street driving. Obtained industrial profiles differed significantly from factory to factory. Delivered emission fingerprints were characteristic for particular solvent factories and agreed well with their emission inventory.

* To whom correspondence should be addressed.

A. Mellouki and A.R. Ravishankara (eds.), Regional Climate Variability and its Impacts in the Mediterranean Area, 181–196.

1. Introduction

Among the species emitted to the atmosphere, the group of non-methane volatile organic compounds (NMVOCs) plays a very important role in affecting air quality, human health, plants and materials. Typical total NMVOC concentrations range in heavy polluted urban areas from 500 to 1500 $\mu g/m^3$, in suburban areas from 100 to 250 $\mu g/m^3$ and from 30 to 200 $\mu g/m^3$ in forest, rural and remote areas (Ciccioli et al., 1999).

NMVOCs are important precursors for the photochemical production of ground-level ozone in the presence of NO_x (NO_x: NO + NO_2). It is known, that volatile organic compounds together with NO_x under the influence of sunlight undergo a series of photochemical reactions leading to formation of secondary pollutants with ozone (O_3) as a major product, peroxyacetylnitrate (PAN), hydrogen peroxide, organic peroxides, organic acids and many other oxidizing species (Le Bras, 1997; Wayne, 2000). Besides tropospheric ozone formation, NMVOCs contribute also to the formation of secondary organic aerosols (SOA). This process involves again oxidation of the volatile precursors by OH, O_3 and NO_3 to form semi-volatile products and eventually particles (Odum et al., 1996; Seinfeld and Pandis, 1998; Dusek, 2000). In addition to their activity in photochemical air pollution processes, some NMVOCs are also found to have a direct negative impact on human health, e.g., benzene, 1,3-butadiene, styrene, formaldehyde, acetaldehyde and polycyclic aromatic hydrocarbons (PAHs) are toxic or even carcinogenic or mutagenic.

Due to the complexity of tropospheric formation of photo-oxidants and secondary organic aerosols the detailed knowledge about the degradation pathways of individual NMVOCs and their atmospheric concentrations and emissions of particular precursors is of paramount importance for the development of effective abatement strategies.

NMVOCs are emitted to the atmosphere from both natural and anthropogenic sources. The annual global NMVOC flux is estimated at about 1500 Tg (Gunther et al., 1995; Middelton, 1995; Ehhalt, 1999). The biogenic contribution to the NMVOC emission is difficult to evaluate because of the great variability of plant types, complexity of the emission processes and the strong dependence on meteorological conditions, landcover and geographical regions (Steinbrecher and Smiatek, 2004). Nevertheless, the total global biogenic NMVOC emission has been estimated to be about 1300 Tg per year (Gunther et al., 1995; Fall, 1999) and exceeds by far those of anthropogenic sources. Human activity is responsible for about 10% of the total NMVOC emission on a global scale and is estimated at about 150 Tg per year (Piccot et al., 1992; Middelton, 1995). But on the different scales,

the proportions between natural and man-made emission vary significantly. In the USA the contribution of anthropogenic emissions amounts to about 40%, in Europe to more than 50% and in Germany to more than 70% (Simpson et al., 1999; EPA, 2000; Schnitzler et al., 2002; UBA, 2002; EEA, 2003c).

The list of processes from which anthropogenic NMVOCs are emitted is very long; however, in Europe road traffic and solvent use are by far the most important emission sources of anthropogenic NMVOCs.

In the frame of presented study the investigation of the composition of the city air of Wroclaw, Poland has been undertaken. The atmospheric concentrations of a large number of NMVOCs emitted by different anthropogenic sources including aliphatic and aromatic hydrocarbons as well as oxygennated species like alcohols, esters and ketones have been analyzed. In particular, road traffic and industrial solvent emissions have been investigated in order to create typical, real world NMVOC source profiles of these source categories and to provide input data for the source apportion analysis with the Chemical Mass Balance (CMB) technique, which will be performed in the future.

2. Measurement Technique

The measurements of hydrocarbons and oxygenated species were performed with the following analytical procedure:

- ambient air collection by active sampling on glass tubes packed with adsorption materials,
- thermal desorption of the sampled tubes,
- sample pre-concentration with a cryo-trap,
- gas chromatography-flame ionisation detection analysis.

NMVOC samples were collected using Carbotrap and Carbosieve III solid adsorption tubes, stored and analyzed off-line in the laboratory (Niedojadlo et al., 2007). Measurements covered hydrocarbons in the range of C_3-C_{10} and oxygenated compounds in the range of C_1-C_6.

Measurements were carried out by a car equipped with an automatic sampling system for NMVOCs. To obtain a better characterization of the city air of Wroclaw also some other atmospheric compounds were investigated. The measurement car was additionally equipped with automatic analyzers for the detection of carbon monoxide, carbon dioxide, ozone, nitrogen oxides, sulphur hexafluoride and meteorological parameters. Figure 1 presents a view of the measurement car used in Wroclaw.

Figure 1. View of the car installed with instruments used for the measurements carried out in Wroclaw, Poland

3. Measurement Sites

The NMVOC measurements were performed in August/September 2005 in Wroclaw, Poland. Wroclaw is the fourth largest city in Poland with a total population of 634,000 inhabitants and a total area of 292.8 km^2. The city is located in South western Poland, 160 km from the German border and 120 km from the border with the Czech Republic.

The air quality in the city is determined by a large number of emission sources. The most important sources are road traffic and industry. Wroclaw is a major transportation hub with a junction of three international roads, two river ports and an international airport. The traffic density in the city is very high with a dramatic frequency of severe traffic jams.

Wroclaw's major industries include the automotive industry, household goods, electrical engineering, medical industry, food industry and chemical industry. The industrial emissions of NMVOCs in the city originate mainly from coating processes in automotive and household goods industry and from manufacturing of paints and coatings. NMVOCs are also emitted from production processes of insulation materials and from printing industry.

During the measurement campaign sampling was performed at various sites representing different city areas and different emission sources. Particular attention was paid to road traffic emission and emissions connected with industrial use and manufacturing of solvents.

3.1. TRAFFIC EMISSION MEASUREMENTS

In order to characterise traffic emission, measurements were performed at a large downtown street intersection (Plac Legionow) and during drives in the city centre and on the roads around the centre of Wroclaw.

3.1.1. Street Intersection

For the investigation of the traffic emission by "stop and go" driving conditions a larger street intersection located in the centre of Wroclaw was chosen. Samples were collected at the Plac Legionow, a few meters from the intersection. The position of the sampling port is presented in Figure 2. The yellow T point on the air map shows the exact positioning of the measurement van.

Figure 2. View of the car installed with instruments used for the measurements carried out in Wroclaw, Poland

3.1.2. Driving

To characterize the traffic emission, samples were also collected during drives in the city centre of Wroclaw and on the roads around the city. The sampling port was located outside the van, at about 1.5 m above the road.

3.2. SOLVENT EMISSION MEASUREMENTS

To obtain the characteristic of NMVOC solvent emission from industrial sources measurements were performed in the neighbourhood of various factories in Wroclaw. The following factories were selected:

- Polifarb Cieszyn-Wroclaw S.A.
- Volvo Sp.z o.o.
- Styropol Wroclaw Sp.z o.o.

Due to the fact that the emission from industrial factories is not limited only to point sources and is more likely spread over a larger area the emission studies of particular factories were performed down-wind of the source and in the background. Additionally, for better identification of the contaminated

plume coming from the investigated source, tracer experiments were performed with sulphur hexafluoride, used as a tracer, which was emitted up-wind from the source and measured down-wind.

3.2.1. Polifarb Cieszyn-Wroclaw S.A.

The Polifarb branch in Wroclaw is one of the biggest Polish producers of paints and coatings for private and industrial use. The NMVOC emissions in the factory originate from manufacturing and filling processes of different kind of paints.

During the measurements the sampling points were selected according to the actual wind direction. One sampling point was located up-wind and one down-wind from the factory. The measurements on the up-wind and down-wind site were performed in parallel. Additional NMVOCs measurements were also performed in the direct neighborhood of the production hall inside the factory area.

The locations of sampling points around the Polifarb company and the wind direction during the measurements are presented in Figure 3.

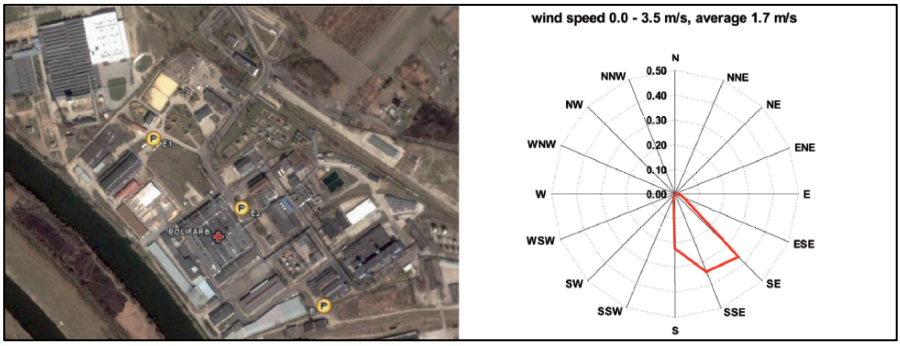

Figure 3. Location of sampling points around the Polifarb factory (P_B: background measurements up-wind from the factory, P_{E1}: emission measurements down-wind from the factory, P_{E2}: emission measurements in the direct neighbourhood of a production hall) and wind direction during the experiment

3.2.2. Volvo Sp.z o.o.

The Volvo factory in Wroclaw produces buses. The NMVOC emissions in the factory originate mainly from bus body coating processes. NMVOCs are also emitted during carpet gluing and during starting and testing of bus engines.

The measurement points around the Volvo factory were located according to the wind direction. One sampling point was located up-wind and one down-wind from the factory. The measurements at both points were performed in parallel.

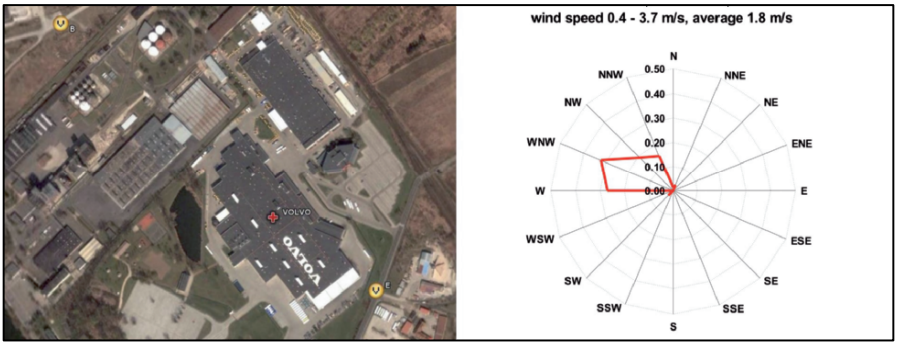

Figure 4. Location of sampling points around the Volvo factory (V_B: background measurements up-wind from the factory, V_E: emission measurements down-wind from the factory) and wind direction during the experiment

3.2.3. Styropol Wroclaw Sp.z o.o.

The products of the Styropol factory in Wroclaw are insulation materials and thermal and acoustic wall insulations. The source of NMVOC emissions of the factory is mainly the styrofoam production process.

To characterize the emission of Styropol, NMVOCs were measured parallel up-wind and down-wind from the factory. The measurement points were located according to the wind direction.

The location of the sampling points around Styropol and the wind direction during the measurements are presented in Figure 5.

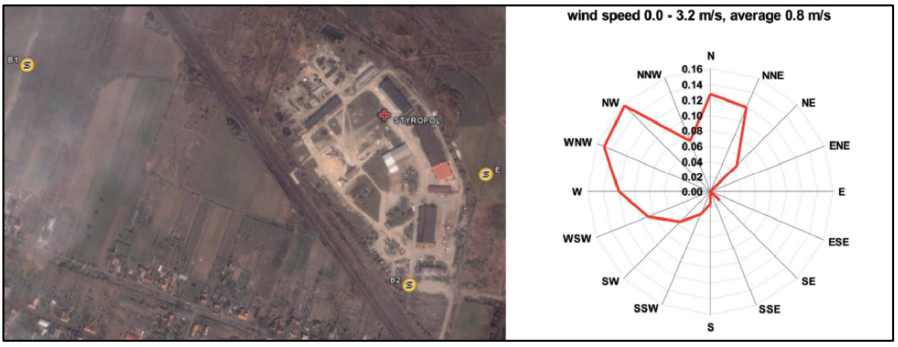

Figure 5. Location of sampling points around the Styropol factory (S_{B1}: background measurements up-wind from the factory, S_{B2}: background measurements, S_E: emission measurements down-wind from the factory) and wind direction during the experiment

3.3 AMBIENT AIR MEASUREMENTS

In order to obtain the ambient NMVOC concentrations sampling were performed at different points located in Wroclaw. The sampling sites represented residential, industrial, downtown, mixed settings and areas downwind from the city centre.

4. Results

The total NMVOC mixing ratios calculated as a sum of 23 measured alkanes, 28 alkenes and alkynes, 14 aromatic hydrocarbons and 17 oxygenated compounds varied during the measurements from 7.46 to 133.48 ppbV, with the average value of 37.059 ppbV.

From the NMVOC profiles (ppbC/ppbC benzene) the average percentage composition of the hydrocarbons mix for all measurement points from Wroclaw was calculated. The results are presented in table 1, which also shows a comparison with other studies.

TABLE 1. Percentage composition of NMVOC-mix in wt% of the city air of Wroclaw in comparison with other cities

	NMVOC composition (%)			
	alkanes	**alkenes and alkynes**	**aromatic hydrocarbons**	**oxygenated compounds**
Wroclaw 2005[a]	37	22	27	14[1]
Wuppertal 2001-2003[b]	32	16	37	15[1]
Wuppertal 1998[c]	46	9	42	3[2]
Wuppertal 1995[d]	56	15	29	n. m.
Berlin (residential)[e]	46	10	26	18[3]
Berlin (street site)[e]	45	12	33	10[3]
Hamburg[f]	42	12	47	n. m.
Vienna[g]	42	11	47	n. m.
Rome[h]	35	7	33	23[4]
Milan[i]	30	5	44	15[4]
Madrid[j]	34	8	35	20[4]
Athens[k]	30	4	66	n. m.
Krakow[l]	36	19	44	n. m.

[1] alcohols, ketones, esters; [2] phenols, cresols, aldehydes; [3] carbonyls; [4] alcohols, aldehydes, ketones, free acids; n.m. – not measured

[a] This study; [b] Niedojadlo, 2005; [c] Kurtenbach et al., 2002; [d] Schmitz et al., 1997; [e] Thijsse et al., 1999; [f] Bruckmann et al., 1988; [g] Lanzerstorfer and Puxbaum, 1990; [h] Brocco et al., 1997; [i] Ciccioli, 1993; [j] Ciccioli et al., 1999; [k] Moschonas and Glavas, 1996; [l] Juszkiewicz et al., 1997

As the Table 1 shows, the highest contribution comes from the alkanes and the second highest from the aromatic hydrocarbons. The composition of the hydrocarbons mix from the present study is in agreement with the results from other urban studies.

From the concentration profiles measured at traffic sites and close to the investigated factories emission profiles were calculated. Traffic profiles were built from the results of the measurements performed at a downtown street intersection and during the city drives. It has been assumed, that the concentration profiles measured at these sites are determined only by traffic emissions. All measured profiles were found to be very similar and were used to create an average traffic emission profile for Wroclaw. The traffic fingerprint is presented in Figure 6.

As observed in Figure 6, the traffic profiles shows the dominance of toluene, xylenes, benzene, 1-butene, i-butene and significantly high contribution from 2,2-dimethylbutane.

In case of the investigated factories emission profiles were obtained from concentration profiles measured down-wind after correction for the background concentrations measured up-wind.

The average emission profile for Polifarb was obtained from up-wind and down-wind measurements and from the measurements performed in the direct neighbourhood of production hall. The Polifarb fingerprint is presented in Figure 7.

To proof the measurement pertinence, the obtained profile was compared with the emission profile which is available from emission inventory (Marshal Office Wroclaw, 2004; City Office Wroclaw, 2004), which is also presented in Figure 7. Good agreement has been obtained. The high importance of xylenes, ethylbenzene, toluene, n-decane and some oxygenated compounds such as acetone and butyl acetate was observed.

The averaged emission profile for Volvo was obtained from measurements performed up-wind and down-wind from the factory. The obtained profile was compared with the emission profile delivered from emission inventory (Marshal Office Wroclaw, 2004; City Office Wroclaw, 2004). Both profiles are presented in Figure 8.

As observed in Figure 8, a reasonable agreement between the measured and reported emissions was obtained. The profiles show the high importance of toluene, alkanes like cyclohexane, 2,2-dimethylpentane, n-hexane, 2-methylpentane, 3-methylpentane, methylcyclopentane and of oxygenated compounds such as ethanol, acetone and ethyl acetate.

For Styropol the average emission profile was obtained from measurements performed up-wind and down-wind from the factory. The result is presented in Figure 9. Similar as for Polifarb and Volvo the measured

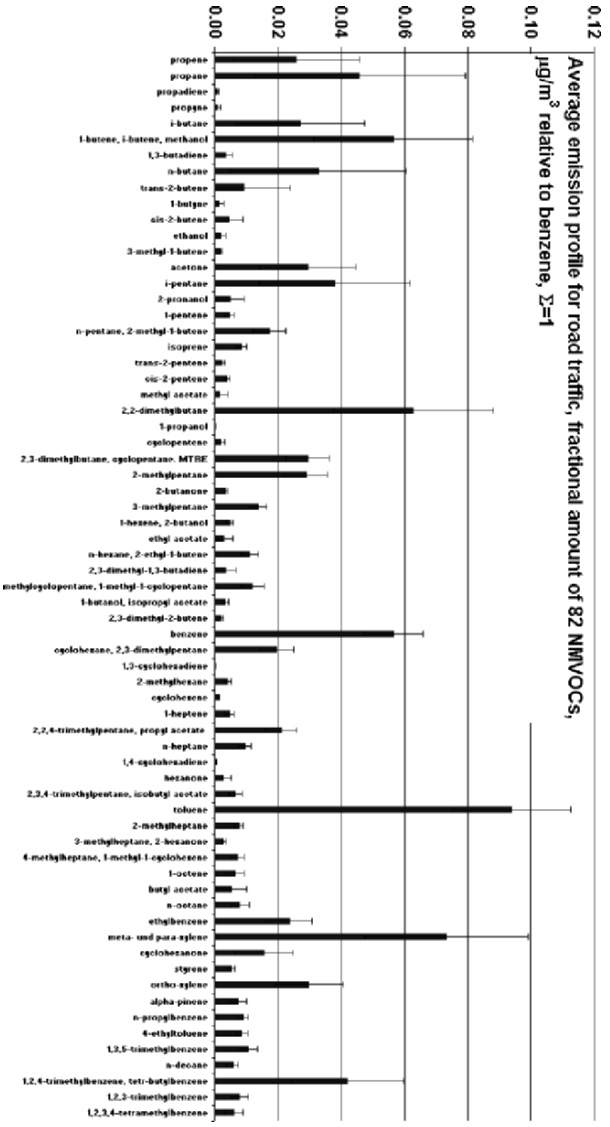

Figure 6. Average traffic emission profile for Wroclaw, Poland

emission profile was compared with the profile calculated from emission inventtory delivered from the factory. The comparison is presented in Figure 9. As observed in figure 9, an excellent agreement between measured and reported emissions was observed. Profiles show almost exclusively the emission of pentane

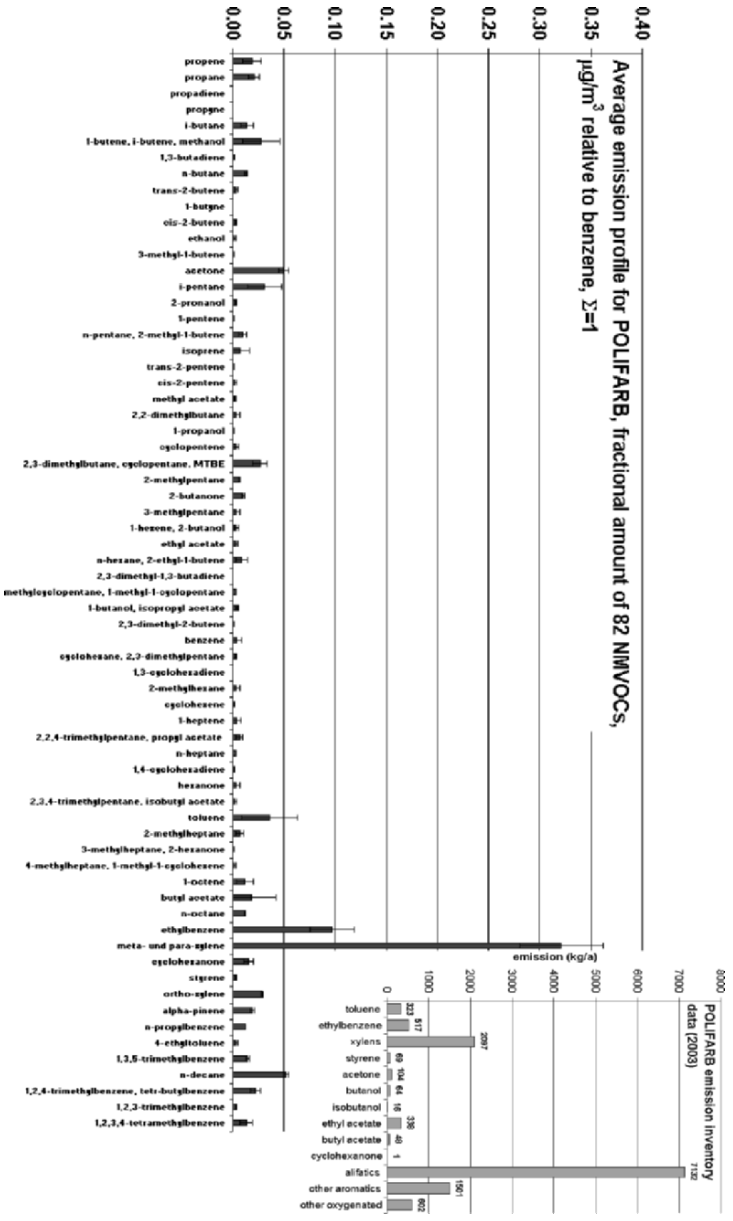

Figure 7. Averaged measured Polifarb emission profile and the emission inventory for the factory for the reference year 2003 for comparison (Marshal Office Wroclaw, 2004; City Office Wroclaw, 2004)

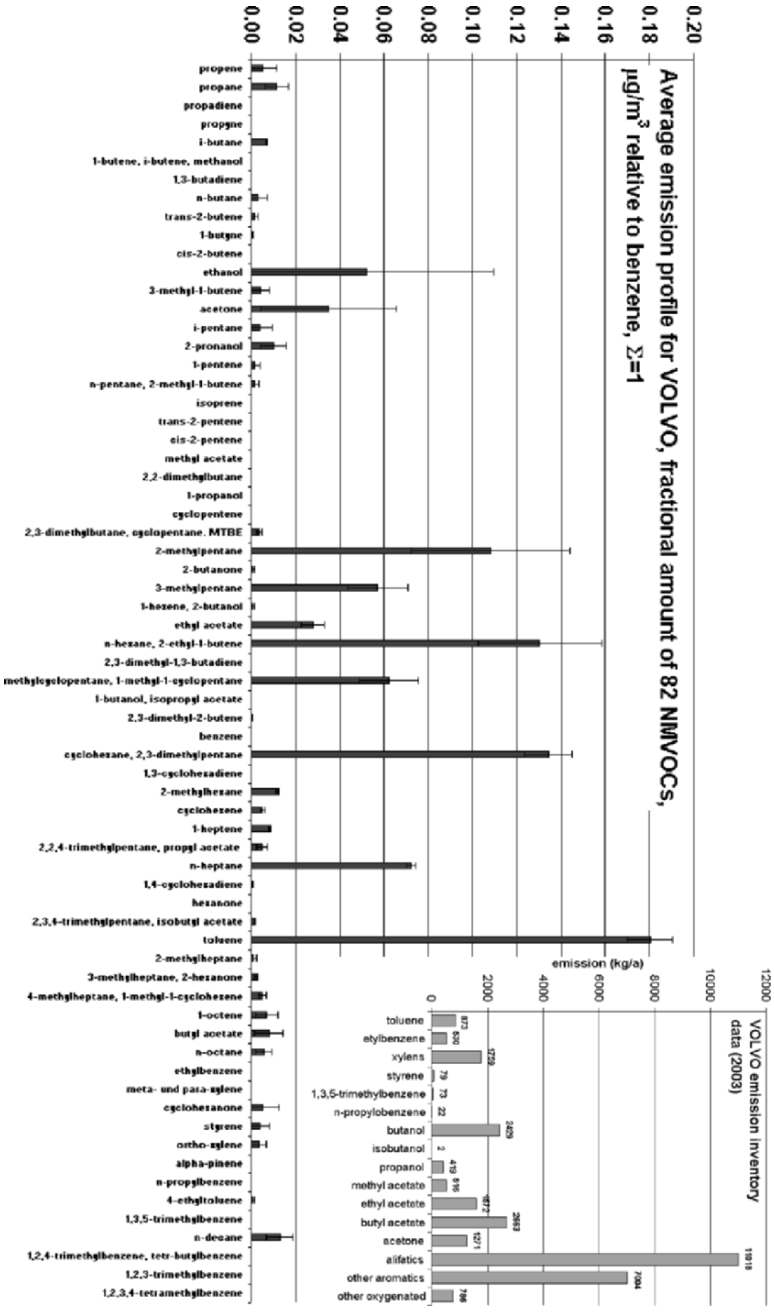

Figure 8. Averaged measured Volvo emission profile and the emission inventory for the factory in the reference year 2003 for comparison (Marshal Office Wroclaw, 2004; City Office Wroclaw, 2004)

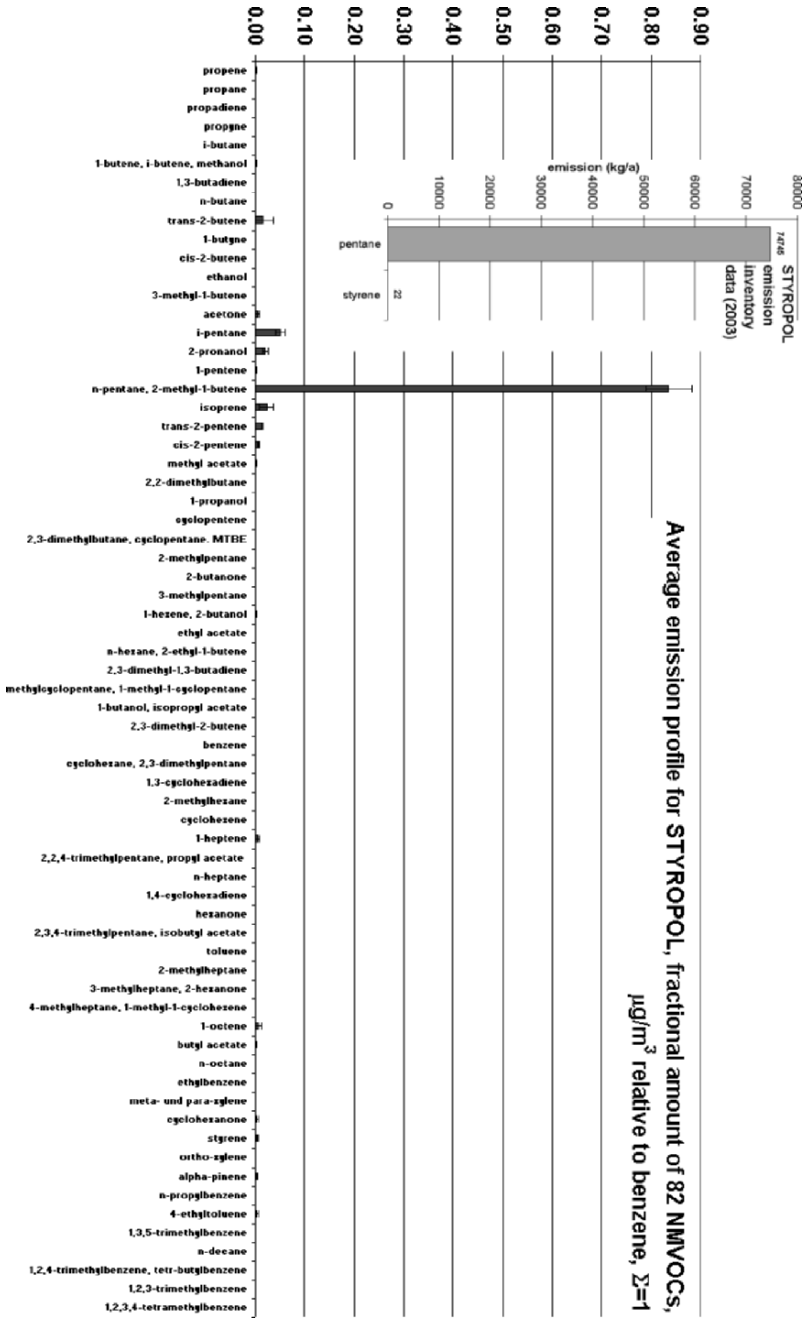

Figure 9. Averaged measured Styropol emission profile and the emission inventory for the factory in the reference year 2003 for comparison (Marshal Office Wroclaw, 2004; City Office Wroclaw, 2004)

5. Conclusions

The objective of this study was to measure the NMVOC concentrations in the city air of Wroclaw, Poland and to characterise the emission from road traffic and from some industrial solvent sources. All measured concentration profiles measured at traffic sites were found to be very similar. The same distribution was observed for a street intersection and street drives. The profiles obtained from the measurements performed in the direct neighbourhood of industrial sources differed significantly from factory to factory. Delivered emission fingerprints were characteristic for particular factories and reflected their individual emission patterns.

The comparisons between measured emission profiles for Polifarb, Volvo and Styropol and profiles calculated from the emission data show a very good agreement and confirm the suitability of the applied analytical method and measurement technique.

The obtained emission profiles for traffic and industrial sources and concentration profiles measured at different sites in Wroclaw will be used for source apportionment analysis with chemical mass balance (CMB) technique in the future.

6. Acknowledgements

The financial support by the Deutsche Bundesstiftung Umwelt (German Environment Foundation – DBU, contract no. 21518) is gratefully acknowledged.

7. References

Brocco, D., Fratarcangeli, R., Lepore, L., Petricca, M., Ventrone, I., 1997, Determination of aromatic hydrocarbons in urban air of Rome, *Atmos. Environ*., **31**:557-566.

Bruckmann, P., Kersten, W., Funcke, W., Balfanz, E., Konig, J., Theisen, J., Ball, M., Papke, O., 1988, The occurrence of chlorinated and other organic trace compounds in urban air, *Chemosphere*, **17**:2363-2380.

Ciccioli, P., Brancaleoni, E., Frattoni, M., 1999, Reactive hydrocarbons in atmosphere at urban and regional scale, in: Hewitt, C. N. (ed.): Reactive Hydrocarbons in the Atmosphere, Academic Press, San Diego, pp. 160-201.

Ciccioli, P., 1993, VOCs and air pollution, in: Bloemen, H. J. Th. and Burn, J. (ed.): Chemistry and Analysis of Volatile Organic Compounds in the Environment, Blackie Academic and Professional, London, pp. 92-174.

City Office Wroclaw, 2004, Data on NMVOC emissions from industrial factories in Wroclaw, personal communications.

Dusek, U., 2000, Secondary organic aerosols-formation mechanisms and source contributions in Europe, International Institute for Applied Systems Analysis, Interim Report IR-00-066, Laxenburg.

European Environmental Agency, 2003, Emission Inventory Guidebook, 3rd Edition, http://reports.eea.eu.int/EMEPCORINAIR4/en, Copenhagen.

Ehhalt, D. H., 1999, Gas phase chemistry of the atmosphere, in: Zellner, R. (ed.) Global Aspects of Atmospheric Chemistry, Steinkopff Verlag, Darmstadt, pp. 21-109.

Environmental Protection Agency, 2000, National Air Pollutants Emission Trends 1900-1998, Office of Air Quality Planning and Standards, EPA-454/R-00-02.

Fall, R., 1999, Biogenic emission of volatile organic compounds from higher plants, in: Hewitt, C. N. (ed.) Reactive Hydrocarbons in the Atmosphere, Academic Press, San Diego, pp. 43-96.

Guenther, A., Hewitt, N. C., Erickson, D., Fall, R., Geron, C., Graedel, T., Harley, P., Klinger, L., Lerdau, M., McKay, W. A., Pierce, T., Scholes, B., Steinbrecher, R., Tallamraju, R., Taylor, J., Zimmerman, P. A., 1995, Global model of natural volatile organic compound emissions, *J. Geophys. Res*., **100**:8873-8892.

Juszkiewicz, A., Kijak, B., Choczynski, M., 1997, Zanieczyszczenie powietrza atmosferycznego weglodorami w poblizu arterii komunikacyjnych o duzym natezeniu ruchu, *Ochrona Powietrza*, **182**:186-190.

Kurtenbach, R., Ackerman, R., Becker, K. H., Geyer, A., Gomes, J. A. G., Lörzer, J. C., Platt, U., Wiesen, P., 2002, Verification of the contribution of vehicular traffic to the total NMVOC emissions in Germany and the importance of the NO_3 chemistry in the city air, *J. Atmos. Chem*., **42**:395-411.

Lanzerstorfer, Ch., Puxbaum, H., 1990, Volatile hydrocarbons in and around Vienna, Austria, *Water Air Soil Pollut*., **51**:345-355.

LeBras, G. (ed.), 1997, Chemical Processes in Atmospheric Oxidation, Springer Verlag, Berlin.

Marshal Office Wroclaw, 2004, Data on NMVOC emissions from industrial factories in Wroclaw, personal communications.

Middelton, P., 1995, Sources of Air Pollutants, in Singh H. B. (ed.) Composition, Chemistry and Climate of the Atmosphere, Van Nostrand Reinhold, New York, pp. 88-119.

Moschonas, N., Glavas, S., 1996, C3-C10 hydrocarbons in the atmosphere of Athens, Greece; *Atmos. Environ*., **30**:2773-2778.

Niedojadlo, A., Becker, K. H., Kurtenbach, R., Wiesen, W., 2007, The contribution of traffic and solvent use to the total NMVOC emissions in a German city delivered from measurements and CMB modelling, *Atmos. Environ*., submitted.

Niedojadlo, A., 2005, The Impact of NMVOC Emissions from traffic and Solvent Use on Urban Air in Wuppertal, An Experimental Study, Dissertation of the University in Wuppertal, Wuppertal.

Odum, J. R., Hoffmann, T. P. W., Bowman, F., Collins, D., Flagan, R. C., Seinfeld, J. H., 1996, Gas/particle partitioning and secondary organic aerosols yields, *Environ. Sci. Technolog*., **30**:2580-2585.

Piccot, S. D., Watson, J. J., Jones, J. W., 1992, A global inventory of volatile organic compounds emissions from anthropogenic sources, *J. Geophys. Res*., **97**:9897-9912.

Schmitz, Th., Klemp, D., Kley, D., 1997, Messungen der Immissionskonzentrationen verschiedener Ozonvorläufersubstanzen in Ballungsgebieten und Autobahnen – Charakterisierung der Emissionsverhältnisse des Straßenverkehrs unter verschiedenen Verkehrssituationen durch Messungen in Quellnähe, Berichte des Forschungszentrum Jülich JÜL-3457, ISSN 0944-2952, Jülich.

Schnitzler, J. P., Baunknecht, N., Brüggemann, N., Enig, W., Forkel, R., Hampp, R., Heiden, A. C., Heizmann, U., Hoffmann, T., Holzke, C., Jaeger, L., Klauer, M., Komeda, M., Koppmann, R., Kreuzweiser, J., Mayer, K., Rennenberg, H., Smiatek, G., Steinbrecher, R., Wildt, J., Zimmer, W., 2002, Emission of biogenic volatile organic compounds: An overview of field, laboratory and modelling studies performed during the 'Tropospheric Research Program' (TFS) 1997-2000, *J. Atmos. Chem*., **42**:159-177.

Seinfeld, J. H., Pandis, S. N., 1998, Atmospheric Chemistry and Physics; From Air Pollution to Climate Change, John Wiley & Sons Inc., New York.

Simpson, D., Winiwarter, W., Börjesson, G., Cinderby, S., Ferreiro, A., Guenther, A., Hewitt, C. N., Janson, R., Khalil, M. A. K., Owen, S., Pierce, T. E., Puxbaum, H., Shearer, M., Skiba, U., Steinbrecher, R., Tarasson, L., Öquist, M. G., 1999, Inventoring emissions from nature in Europe, *J. Geophys. Res*., **104**(D7):8113-8152.

Steinbrecher, R., Smiatek, G., 2004, VOC emissions from biogenic sources, in: Friedrich, R., Reis, S. (ed.) Emission of Air Pollutants: Measurements, Calculations and Uncertainties, Springer-Verlag, Berlin, pp. 16-24.

Thijsse, Th. R., van Oss, R. F., Lenschow, P., 1999, Determination of source contribution to ambient volatile organic compound concentration in Berlin, *J. Air Waste Manage. Assoc*., **49**:1394-1404.

UBA, 2002, Environmental Data Germany 2002, Umweltbundesamt, Berlin.

Wayne, R. P., 2000, Chemistry of Atmospheres, Oxford University Press, New York.

NON-METHANE HYDROCARBONS ($NMHC_S$) VARIABILITY IN THE EASTERN MEDITERRANEAN

CECILIA ARSENE [1,2*]
AIKATERINI BOUGIATIOTI [1] AND NIKOLAOS MIHALOPOULOS [1]
[1] *University of Crete, Department of Chemistry, Voutes 71003, Heraklion, Greece, carsene@chemistry.uoc.gr*
[2] *"Al.I. Cuza" University of Iasi, Faculty of Chemistry, 700506 Iasi, Romania*

Key Words: Atmosphere; Hydrocarbons; $NMHC_S$; Variability; Mixing Ratios; Radicals; Eastern Mediterranean.

Abstract Non-methane hydrocarbons ($NMHC_S$) are important constituents of the atmosphere that contribute both to the oxidation capacity of the atmosphere and to the formation of the secondary organic aerosol. In Europe, over the last decades, many efforts have been devoted to the assignment of NMHCs sources and although $NMHC_S$ role is well established large uncertainties in their emissions still exist.

Measurements of $NMHC_S$ in the atmosphere of the Eastern Mediterranean are very scarce in the literature and, therefore, the present work is willing to provide an assessment of individual $NMHC_S$ sources on both spatial and temporal basis in the Eastern Mediterranean. Intensive campaigns of several days took place each month by in situ continuous hourly measurements of $NMHC_S$ from C_2 to C_8 in different locations on the island of Crete, Greece (marine, rural and urban areas). All samples were analysed for 45 $HMHC_S$ with a gas chromatographic (GC) system equipped with a flame ionisation detector (FID).

A simple statistical analysis of the relationship between various hydrocarbon pairs indicates influences from common sources. The average measured hydrocarbon concentrations show seasonal variations in agreement with previous published measurements. Evidence for both chemical processing and source dominating the variability of $NMHC_S$ mixing ratios were obtained. Chlorine atom concentrations were indirectly derived from changes in the patterns of the measured $NMHC_S$. The result of the present study suggests that the Cl-atom induced reaction may be as well of considerable importance in the troposphere of the region.

* To whom correspondence should be addressed.

A. Mellouki and A.R. Ravishankara (eds.), Regional Climate Variability and its Impacts in the Mediterranean Area, 197–206.

1. Introduction

Most of the non-methane hydrocarbons ($NMHC_S$) are recognized as trace atmospheric gases that still play a central role in the photochemistry of the atmosphere or in determining the concentration of species like hydroxyl (OH) or hydro-peroxy (HO_2) radicals in the troposphere. Under favourable conditions, including solar radiation and oxides of nitrogen, $NMHC_S$ oxidation may lead to the production of ozone, significantly contributing to the enhancement of the oxidation capacity of the troposphere.

Many of the known $NMHC_S$ are involved in the process of aerosol formation especially through rapid reactions with atmospheric oxidants such as O_3, OH, NO_3 (Atkinson and Arey, 2003a). As some of them have a potentially toxic-harmful effect on human health (benzene, 1,3-butadiene) the necessity of their continuous monitoring is still an important present day task. Up to now $NMHC_S$ ambient concentrations have been reported for many sites around the world, see for instance (Arriaga-Colina et al., 2004; Hopkins et al., 2005; Durana et al., 2006; Colomb et al., 2006).

As the reports for the $NMHC_S$ measurements in the atmosphere of the Eastern Mediterranean are very scarce in the literature, the present work is willing to provide an assessment of individual $NMHC_S$ sources on both spatial and temporal basis in this area. Evidence was found also for the existence of high OH radical and Cl atom concentrations in the troposphere of the investigated area. The importance of these findings in terms of atmospheric impact will be also presented.

2. Experimental

Measurements have been undertaken at three different sites corresponding to urban, rural and marine areas. Due to the geographical location of the island, at any of the investigated site there is the possibility to experience events like emission plumes, photo-smog and dust which will have an important effect on the photo-chemistry of the area. General characteris tics of the investigated sites indicate temperature above 5^oC in winter and 25^oC in summer with wind direction prevalence from N-NW during the dry season, i.e., summer, and S – SW during the wet season, i.e., winter. A number of 45 $NMHC_S$ from C_2 up to C_8 were analysed by using a GC Varian Star 3400 Gas Chromatograph equipped with an FID detector. The applied sampling technique was in *on line* mode and measurements have been undertaken with a resolution of 1 hour. Details on the area and the meteorological conditions encountered year-round are given by Mihalopoulos et al. (1997).

3. Results and Discussions

In Figures 1a,b the changes in the pattern of some long (1a) and short (1b) lived trace gases measured during summer in a marine area are presented. In Figure 1a two distinct periods characterised by high ethane and propane mixing ratios are observed. The changes in the pattern of these two compounds reveal mainly the importance of the long range transport processes.

Beside ethane and propane mixing ratios profiles, Figure 1a presents the variation of O_3 and Rn during the studied period. Combination of O_3 levels and Rn activities allow us to distinguish two periods: the first (27-31/07) with polluted air masses and relative small continental influence and a second one with less polluted air masses but with more important continental influence (01-04/08).

As Figure 1b shows among short time lived trace gases isoprene presents a clear diurnal cycle. Parameters as temperature, solar radiation intensity or wind speed/direction might be responsible on this pattern. The inset in this figure makes obvious the cycle showed by isoprene especially in the days with high wind speed. A very good agreement has been observed between the maximum in the diurnal cycle of the isoprene and that showed by the solar radiation intensity (maximum at 15:00 summer local time). Isoprene is considered to be the most important and abundant biogenic compound with a lifetime of about 3 h for an OH radical concentration abundance of 10^6 molecule cm^{-3}. However, during the investigated period relative low concentration with value as high as 9.51 + 3.81 pptv has been determined for isoprene abundance in the atmosphere of the marine area.

Still, depending both on the abundance and the factors controlling their variability in the atmosphere, other measured NMHC$_S$ may present interesting pattern (higher alkanes or alkenes, especially 2-methyl-pentane, 3-me-pentane and i-butene (Figure 1c)). The diurnal variability showed by different hydrocarbons could be used in order to estimate the concentration of some radical species (OH) and concentration as high as 3.0-5.0E + 06 radicals cm^{-3} were derived for the OH species for July and August. In a work performed by Vrekousis (2005), OH radical concentration of about 3.6E + 06 radicals cm^{-3} has been reported for July at the same site (marine area).

The average hydrocarbons mixing ratios measured at a rural site from February till October 2006 indicate seasonal variations in agreement with previous published data. Species as i-butane, n-butane (Figure 2a), ethane or propane (Figure 2b) show a distinct minimum during the warm season, minimum which is mainly due to the chemical destruction by OH radicals that is expected to present a maximum in summer. For the hydrocarbons of biogenic origin, i.e., mainly isoprene, the seasonal distribution showed a

maximum in summer, observation which is in good agreement with the studies reporting higher emission rates by the vegetation during the warm season (Kesselmeier and Staudt, 1999).

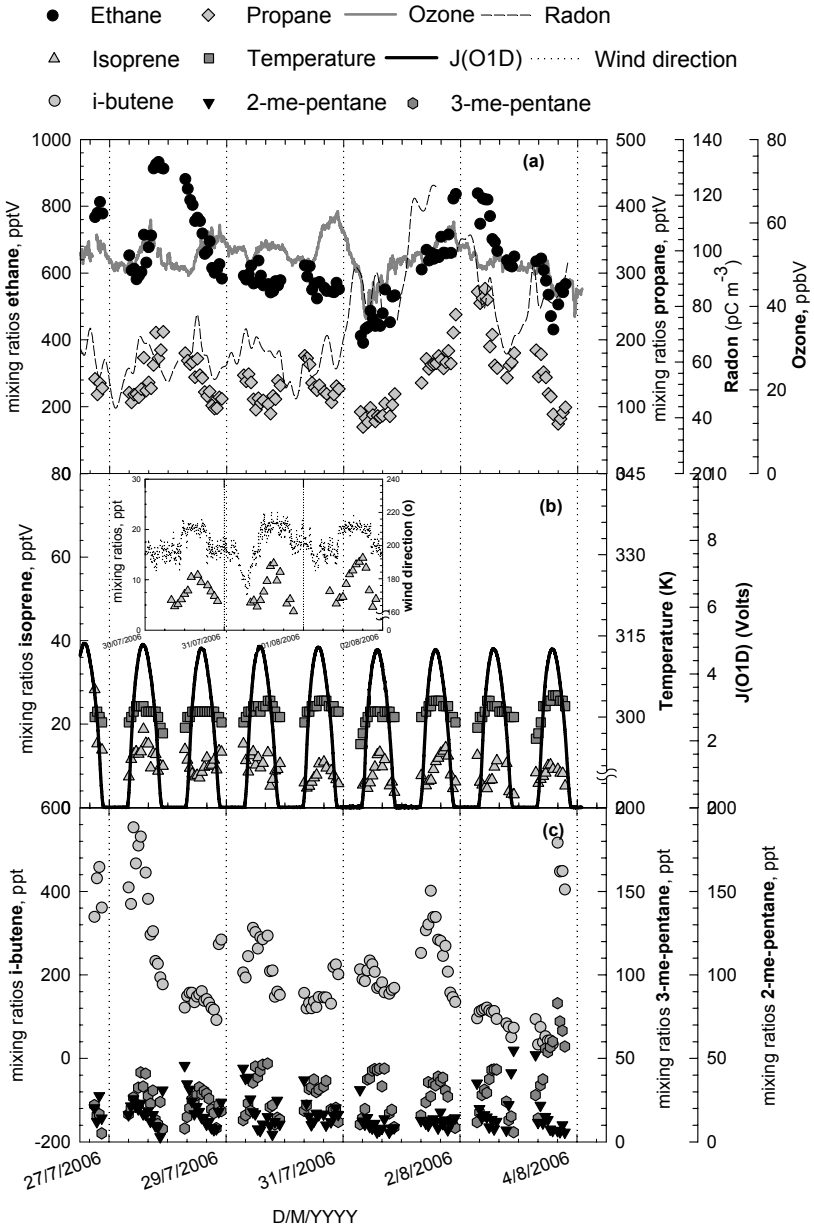

Figure 1. Patterns showed by long-and short- lived term $NMHC_S$

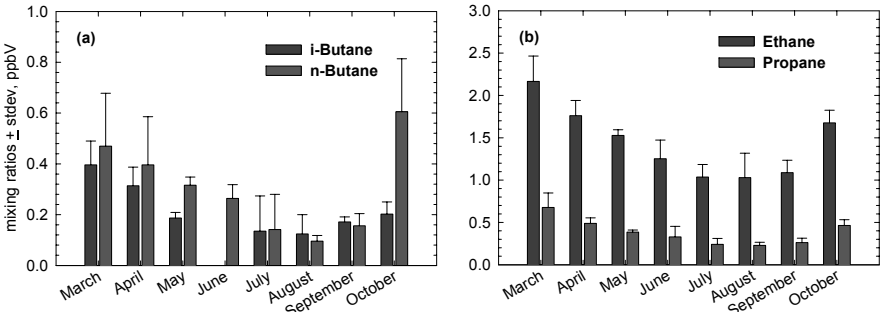

Figure 2. Seasonal variability of some measured NMHC$_S$

The regression analysis process was applied to different hydrocarbon pairs in order to obtain first indication for a possible source apportionment. For those measurements undertaken at the rural or urban areas very good correlations have been observed between pairs like n-butane, n-pentane, i-pentane and acetylene or ethene/propene. In the linear regression analysis all available measurements were used, regardless of where (rural or urban) and when (day or night) those measurements were performed (all intensive campaigns yielding more than 250 points) (example shown in Figure 3).

The high regression coefficients between various hydrocarbon pairs would indicate influences from common sources. For example, the correlation between ethane and propane (r = 0.94) would suggest leakages from natural gases and/or liquefied petroleum gases meanwhile the correlation of the pair n-butane/n-pentane with r = 0.96 would suggest emission from stationary sources (combustion boilers and industrial installations).

Principal Component Analysis (PCA) was applied to the available data sets to extract more meaningful information for a possible source appor tionment. This procedure gives the possibility to extract various groups of

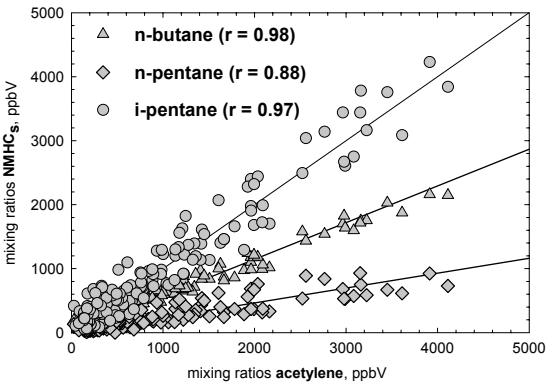

Figure 3. Correlation between various pairs of measured NMHC$_S$

chemicals with possibly the same source. The total explained variance accounts for about 92% at the rural and urban site meanwhile at the marine area accounts only for about 75%. A plot of the preponderance of selected extracted factors after rotation-varimax normalisation is presented in Figure 4. In this instance, for example, F1 is mainly related with emissions from stationary sources and combustion sources (acetylene, n-butane, butane, pentane, pentene), F2 to automotive exhaust (ethene, propene, benzene, toluene) meanwhile F4 indicate the existence of leaks from natural gas or liquefied petroleum gas (ethane and propane). Again, much different is the situation at the marine area where, generally, the large scatter in the hydrocarbons selected within various factors would indicate a more complex situation.

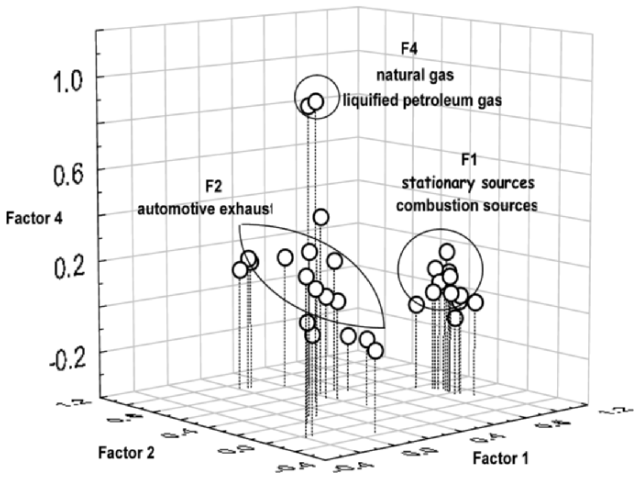

Figure 4. Tri-dimensional dependency between various factors extracted by PCA

In order to better differentiate between chemical processing and influence of the source strength cold/warm (October/June) ratios were plotted versus OH reactivity for measurements performed at a rural site (Figure 5). Actually a good correlation between these variables indicates that for aged air, seasonal variations in concentrations can be attributed to chemical processing via OH radicals. However, this figure reveals the existence of three distinct linear dependencies with compounds falling in one of the regression line depending on their reactivity toward OH radicals. We do observe as well that the slope changes from the less reactive (with circle $NMHC_S$ like ethane, propane) to the most reactive identified trace gases (with triangles higher alkenes, 1,3-butadiene and isoprene).

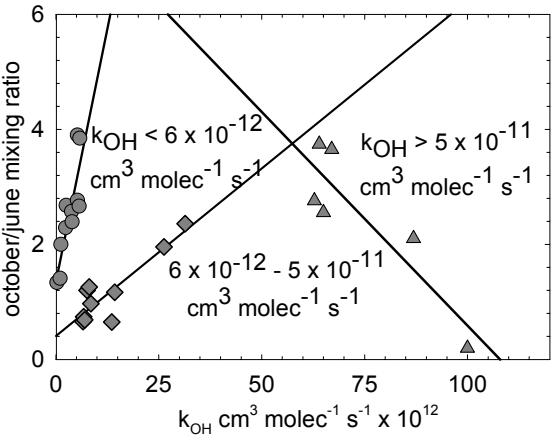

Figure 5. Variation of cold/warm ratio vs. OH reactivity

Investigations were also made in order to understand how the variability of the measured NMHC$_S$, at a specific site, can be related both to their sources and sinks processes. The variability concept based on the correlation between the hydrocarbon concentration and OH reactivity (Karl et al., 2001; Hopkins et al., 2005) was applied to all our measurements. The relationship is in the form $Sln(x_i) = A\tau_i^{-b}$ where $Sln(x_i)$ is the variance of the natural log of a time series concentration of hydrocarbon i, τ_i is the lifetime of the compound with respect to OH removal and A and b are empirical fitting parameters. Only those hydrocarbons with available rate constants were included in the processing of this approach. For the analysis the relative rate constants given by Atkinson and Arey (2003b) were used. It was also assumed that the OH radical is the only significant sink of these compounds.

The relationship between the variability and the lifetime of the measured NMHC$_S$ at the rural site is presented in Figure 6 where again the identified compounds are falling on the regression line depending on their reactivity toward OH radicals (the left side of the diagram includes all measured NMHC$_S$ with rate constants higher than 5.0E-11 cm^3 $molec^{-1}$ s^{-1}). In this figure ethane and propane appear to behave mainly as a kind of outliers and this might be due to the fact that their variability is not only due to the reactivity toward OH radicals but also to some other unaccounted processes. The results of the regression analysis lead to a value of 0.49 for parameter b and 0.24 for A, the value of the parameter b at this site suggesting that a combination between chemical processing and source strength dictates the variability of the measured NMHC$_S$.

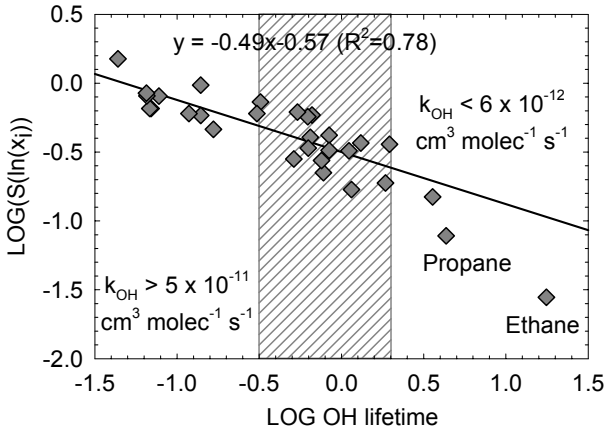

Figure 6. Log variance of natural logarithm of concentration vs. Log of OH lifetime

As there are suggestions that halogen atoms may be of considerable importance for the chemistry of the troposphere and also that they can contribute to the enhancement of the oxidizing capacity of the atmosphere, an attempt has been made to investigate the importance of these reactive species in the atmosphere of the investigated area. Presently no method that would allow the direct measurement of Cl-atoms in the atmosphere is available so, the indirect evidence for the existence of relevant levels of Cl atoms in the troposphere is a suitable tool to perform this kind of investigation. Normally plots of logarithmic ratios of NMHCs concentration can be used to gain an insight into their removal reactions and atmospheric mixing processes.

The approach described in Rudolph et al., 1997 was used in processing the data at the marine site. However, in applying this approach suitable log-log plots should be selected. In order to show how the model works, whenever applied to our data we have selected the pair ln(n-butane/benzene) *vs.* ln (n-pentane/benzene) (Figure 7) investigated also in Rudolph et al. (1997) study. For this dependency in the case only the OH radical reaction would be involved, a slope of 0.44 is expected. In the case there would be only Cl atom reaction involved, the slope is expected to be 0.80. However, the slope of the linear square fit obtained in the present work for afore log/log experimental pair is 0.65 which is not far from the value of 0.58 given by Rudolph et al. (1997).

With the former slope value, the derived ratio [Cl]/[OH] is estimated to be of about 1.20E-02 quite comparable to the value of 1.49E-02 reported by Rudolph et al. (1997). Assuming levels of OH radicals of the order of 10^6

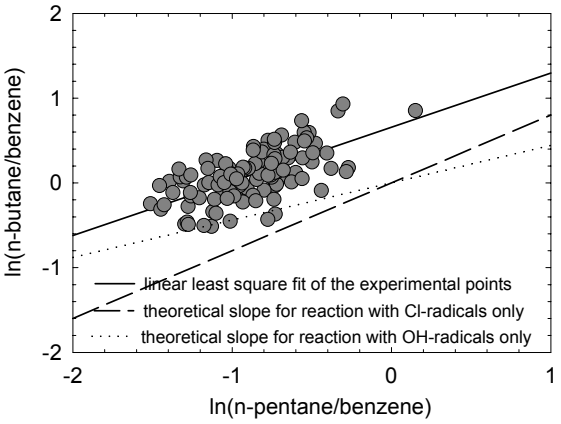

Figure 7. Plots of ln(n-butane/benzene) vs. ln(n-pentane/benzene)

radical cm^{-3}, the above ratio implies concentrations in Cl atoms of about 10^4 atoms cm^{-3}. Under such Cl levels, the Cl atom initiated reaction would be competing with the reactions initiated by OH radicals for various NMHC$_S$.

4. General Observations

The present study reports on measurements of organic trace gases such as alkanes, alkenes, dienes and aromatics in the lower troposphere of the Eastern Mediterranean. Anthropogenic or biogenic emission sources account mainly for their abundance in the investigated area and the intensity of the chemical processing, source strength or the combination of these will depend upon the characteristics of the investigated site (remote clean or polluted areas). The variability showed by some NMHC$_S$ can be used in the estimation either of the OH radical or of the Cl atom concentrations. The obtained data proves as well that in the case reliable NMHC$_S$ measurements are achieved they can be seen as a tool in assigning the oxidation capacity of the atmosphere.

5. Acknowledgments

Cecilia Arsene gratefully acknowledges the financial support of the Postdoctoral Fellow stay at the University of Crete, Greece, by the Marie Curie Intra-European Fellowship Action with the project MEIF-CT-2005-009578. The authors are grateful to Christos Donoussis for providing the OH concentration modelled data.

6. References

Arriaga-Colina, J.L., West, J.J., Sosa, G., Escalona, S.S., Ordunez, R.M., and Cervantes, A.D.M., 2004, Measurements of VOC_S in Mexico City (1992-2001) and evaluation of VOC_S and CO in the emissions inventory, *Atm. Env.* **38**:2523-2533.

Atkinson, R., and Arey, J., 2003a, Gas-phase tropospheric chemistry of biogenic volatile organic compounds: a review, *Atm. Env.* **37**:197-219.

Atkinson, R., and Arey, J., 2003b, Atmospheric degradation of volatile organic compounds, *Chem. Rev.* **103**:4605-4638.

Colomb, A., Williams, J., Crowley, J., Gros, V., Hofmann, R., Salisbury, G., Klufel, T., Kormann, R., Stickler, A., Forstewr, C., and Lelieveld, J., 2006, Airborne measurements of trace organic species in the upper troposphere over Europe: The impact of deep convection, *Environ. Chem.* **3**:244-259.

Durana, N., Navazo, M., Gomez, M.C., Alonso, L., Garcia, J.A., Ilardia, J.L., Gangoiti, G., and Iza, J., Long term hourly measurement of 62 non-methane hydrocarbons in an urban area: Main results and contribution of non-traffic sources, *Atm. Env.* **40**:2860-2872.

Hopkins, J.R., Lewis, A.C., and Seakins, P.W., 2005, Analysis and applications of measurement of source dominated hydrocarbon concentrations from the PUMA campaigns in June/July 1999 and January/February 2000 at an urban background site in Birmingham, UK, *Atm. Env.*, **39**:535-548.

Karl, T., Crutzen, P.J., Mandl, M., Staudinger, M., Guenther, A., Jordan, A., Falle, R., and Lindingerd, W., 2001, Variability-lifetime relationship of VOCs observed at the Sonnblick Observatory 1999. Estimation of HO-densities., *Atm. Env.* **35**:5287-5300.

Kesselmeier, J., and Staudt, M., 1999, Biogenic volatile organic compounds (VOC): An overview on Emission, Physiology and Ecology, *J. Atm. Chem.*, **33**:23-88.

Mihalopoulos, N., Stephanou, E., Kanakidou, M., Pilitsidis, S., and Bousquet, P., 1997, Tropospheric aerosol ionic composition above the Eastern Mediterranean Area, *Tellus* **B**: 314-326.

Rudolph, J., Ramacher, B., Plass-Dulmer, C., Muller, K.P., and Koppmann, R., 1997, The indirect determination of chlorine atom concentration in the troposphere from changes in the patterns of non-methane hydrocarbons, *Tellus*, **49B**:592-601.

Vrekousis, M., 2005, PhD Thesis, University of Crete, Greece.

REPRESENTATION OF CHEMICAL DETAIL IN ATMOSPHERIC MODELS

M. J. PILLING
School of Chemistry, University of Leeds, Leeds LS2 9JT, UK

Key Words: Tropospheric oxidation; ozone formation; chemical mechanisms; global chemistry; regional chemistry.

Abstract The master chemical mechanism (MCM) is an almost explicit mechanism describing the atmospheric oxidation of 135 primary emitted volatile organic compounds (VOCs). The basis of the protocols used for constructing the MCM is described, together with the website used for dissemination. A number of applications is briefly discussed, including policy development, support for field measurements and the formation of secondary organic aerosol. Heterogeneous uptake has been incorporated into the MCM and the difficulties involved are summarized. Finally, an aqueous phase mechanism, CAPRAM is outlined.

1. Introduction

The tropospheric oxidation of methane, carbon monoxide, hydrogen and volatile organic compounds (VOCs) plays a central role in a number of of important issues.

- Climate change, through its influence on the lifetime of methane, the concentration of ozone and the formation of secondary aerosol.
- Long range transport of pollution, e.g. through the intercontinental transport of ozone precursors.
- Air quality and the formation of ozone and other components of photochemical smog on a regional scale.

Modeling of all of these processes requires a representation of the chemistry involved, which is achieved using a chemical mechanism. The mechanism is used to construct a set of coupled ordinary differential equations (odes) for each of species. In a Eulerian model, the need to solve these odes at each grid point presents a serious computational overhead and there is a conflict between the chemical detail that can be incorporated and

A. Mellouki and A.R. Ravishankara (eds.), Regional Climate Variability and its Impacts in the Mediterranean Area, 207–218.

the computational feasibility. As a result, many of the chemical mechanisms that are used in global and regional models are *lumped*, and use representative species and chemistry, rather than explicit chemistry. As result, there is only limited, direct connection between the model chemistry and the chemistry studied in the laboratory.

Mechanisms that incorporate explicit chemistry can be used in models with less detailed atmospheric dynamics and provide a direct link with laboratory measurements. Such mechanisms can also provide a benchmark against which lumped mechanisms can be evaluated. They can also be reduced and lumped, to provide a mechanism dimension that is more compatible with the requirements of a dynamical model.

The master chemical mechanism (MCM) is an explicit (or almost explicit) mechanism that was developed to model surface ozone formation in Europe and the UK, for air quality policy purposes. It has also been used to interpret field experiments and as a benchmark for testing lumped mechanisms. This article briefly reviews the basis and the testing of the MCM and some of its applications. The MCM is a purely gas phase mechanism, but multiphase chemistry is also important the troposposphere. Sections 6 and 7 provide a brief discussion of representations of heterogeneous and condensed phase chemistry.

2. The Master Chemical Mechanism (MCM)

The MCM was constructed using protocols (Jenkins et al. (2003), Saunders et al. (2003)) that define the chemistry in the oxidation of a given VOC, via a series of reactions to the ultimate products, CO_2 and H_2O. The reaction types are:

(i) Initiation reactions involving reaction of the VOC with OH, NO_3, O_3 and, for compounds with absorption spectra in the actinic region, photolysis constitute the first step in the oxidation of a VOC. The reactions generate a radical, e.g., from CH_4 the radical produced from its reaction with OH is CH_3.

(ii) The organic radical reacts with O_2 to form a peroxy radical, RO_2. This reaction generally occurs very rapidly under atmospheric conditions.

(iii) The RO_2 intermediate the reacts with NO and NO_2, or with other peroxy radicals, HO_2 and R'O2. The reaction of a peroxy radical with NO form NO_2, which can then be photolysed to form O + NO. The oxygen atom reacts rapidly with O_2 to form O_3. This is the route to ozone formation in the troposphere.

(iv) The main product of the reaction of RO_2 with NO is an oxy radical, RO, which reacts with O_2, decomposes or isomerises. The general result, perhaps after one or two intermediate steps, is the formation of a

carbonyl compound, e.g., R'CHO, and HO_2; the latter reacts with NO to form NO_2, and hence ozone via photolysis, and OH, which can then go on and react with a VOC, recommencing the cycle of reactions.

(v) R'CHO is an intermediate in the reaction sequence; it is longer-lived than the radicals such as OH and HO_2, which have atmospheric lifetimes of a few seconds and ~1 minute respectively. The lifetime of R'CHO is several hours, or even longer. It undergoes the initiation reactions described in (i), primarily reaction with OH and photolysis. The sequence of reactions (i) – (iv) can be thought of as first generation reactions, if the VOC is a directly emitted species. Reaction of R'CHO initiates the second generation reactions, which will form another oxygenated intermediate, with fewer carbon atoms than R'CHO. Subsequent generations of reactions continue to degrade the carbon containing compounds until eventually CO_2 and water are formed.

(vi) The reaction sequences are components of a chain reaction and are termed propagation reactions. Each propagation reaction involves a radical reactant and forms a radical as a product, so that the total concentration of all radicals is not changed through such reactions. The chains are terminated by reactions that lead to net removal of radicals. Under high NO_x conditions, one of the main reaction is OH + NO_2 to form nitric acid, HNO_3, which is removed from the atmosphere in rain, for example. Under clean conditions, when the NO_2 concentration is small, radical removal involves reactions of peroxy radicals with other peroxy radicals, e.g., HO_2 + RO_2, which forms a hydroperoxide, ROOH, which is quite long-lived.

These reactions are incorporated in the MCM explicitly. It describes the oxidation of 135 different VOCs, based on the UK emissions inventory for anthropogenic species. It includes four biogenic compounds, isoprene, α and β pinene and methylbutenol. The MCM also contains the appropriate chemistry to describe the oxidation of CH_4, CO and H_2 and the inorganic chemistry involving, for example, the nitrogen oxides. Each VOC is degraded to CO_2 and H_2O. Some simplifications are made, through, for example, the neglect of reaction channels that make a small contribution, and the treatment of peroxy radicals, RO_2, with other peroxy radicals, $R'O_2$. The total number of species in the MCM is ~5 900 and there are ~13 500 reactions.

Each reaction has a rate constant associated with it, which is a function of temperature and, for some reactions, pressure. The rate constants for the simpler species are based on laboratory measurements; evaluations of rate data by, for example the IUPAC group (*http://www.iupac-kinetic.ch.cam.ac.uk/*) are used wherever possible. A database for the oxygenated compounds is under construction (*http://www.era-orleans.org/eradb/index.php*) and

will provide a valuable resource. For the bulk of the reactions, however, the rate constants are based on structure activity relations (SARs) that are derived from measurements of reactions for members of certain classes of reaction, that are then extended to the whole class. Photolysis reactions require measurements of absorption spectra and of quantum yields for formation of products. There are currently experimental parameters for 35 photolysis reactions in the MCM. Parameters for other photolysis reactions are based on analogy. The experimental database for the MCM, and the SARs derived from that database, are currently under review by an international panel assembled by the ACCENT programme.

3. The MCM Website

The MCM is mounted on a website (http://mcm.leeds.ac.uk/MCM/) from which the mechanisms for any chosen set of VOCs, or for the whole set of 135 VOCs, can be extracted. The mechanism is set up to be used with the FACSIMILE integrator, which is a commercial software package. The compounds are identified by trivial names that are constrained by the strings that FACSIMILE will accept, but each compound is also uniquely identified by a SMILES string, and a chemical structure is also provided, to facilitate compound identification when browsing the details of the mechanisms. In addition, the mechanisms can be output in formats compatible with the user's own FORTRAN codes, and with KPP, an integrator that is freely available. XML output is also available. The website is currently under further development to provide direct transfer of data from the IUPAC evaluated database, and to develop new tools to facilitate its use.

4. Testing the MCM

The MCM has been extensively tested, and its component mechanisms further developed against chamber data. For example, Pinho et al. (2006) used environmental chamber data from the Statewide Air Pollution Research Center (SAPRC) at the University of California to test mechanisms for the photo-oxidation of ethene, propene, 1-butene and 1-hexene in the presence of NOx. They found that, under the chamber conditions they had to include reactions of ground state oxygen atoms ($O(^3P)$) with the alkenes, even though these reactions are not significant in the atmosphere. They also found some deficiencies in the MCM.

The oxidation of toluene provides a further example (Bloss et al. (2005). Aromatics are key VOCs in ozone formation in polluted regions. Their oxidation differs from the norm, because the peroxy radical formed following addition of OH to the aromatic ring is very short lived. It does not react with NO, but either decomposes back to regenerate the reactants, or

reacts to form either a phenol + HO_2 or, through a sequence of reactions, ring opened products, e.g., glyoxal ($(CHO)_2$) and a C_5 dicarbonyl compound in the case of toluene. This channel is key in the formation of ozone, because the products are very photolabile. Figure 1 shows a comparison between simulations based on the latest version of the MCM (v3.1) and measurements made at the EUPHORE chamber in Valencia. There are three major failings of the mechanism:

(i) The measured toluene decays more rapidly than that modelled. Toluene is primarily removed by reaction with OH, so the measurements indicate that there is an OH source that is not recognised in the mechanism.
(ii) The modelled ozone substantially exceeds the measured ozone at later times; it is difficult to rationalise this failing with that in (i) and indicates that any radical source must not include NO_2 formation from NO, otherwise ozone would be further increased.
(iii) NO and NO_2 are poorly represented, reacting more rapidly than the model predicts.

Bloss et al. (2005) modified the mechanism in a number of ways in an attempt to improve the agreement between model and measurement, but were unable to reproduce the experimental behaviour using recognised chemistry. It is

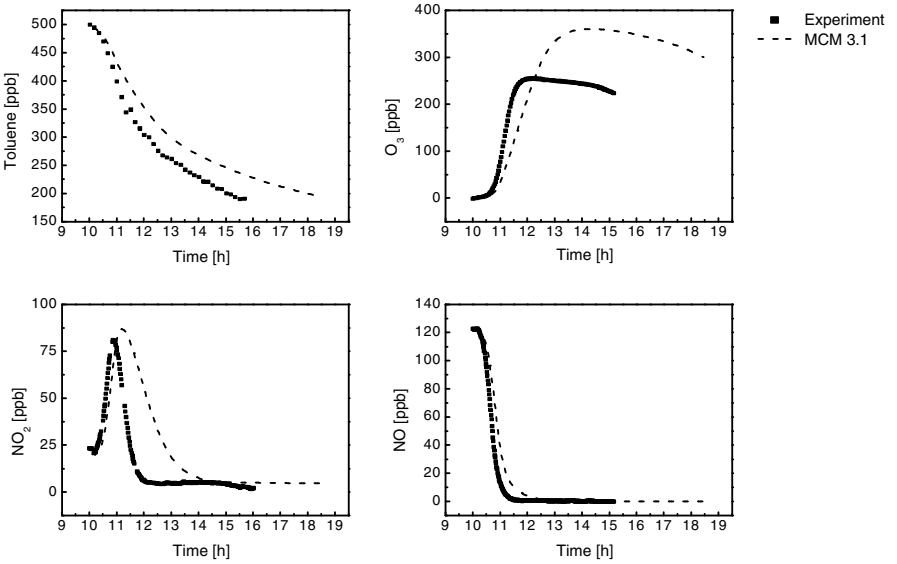

Figure 1. Comparison of experimental measurements of toluene, O_3, NO_2 and NO with predictions of MCM v3.1 in experiments on toluene oxidation at the EUPHORE chamber in Valencia. ■ experiment, ---, MCM 3.1

clear that fundamental aspects of the mechanism are not represented. This work has served to focus the need for further experimental and theoretical work on the elementary reactions involved.

5. Applications of the MCM

The MCM has been used in a range of applications. Examples include:

(i) Its first application was in 5 day trajectory calculations for an air mass passing over Europe under anticyclonic calculations, and reaching the west of Great Britain (Derwent et al. (1998). The calculations were used to assess the photochemical ozone creation potentials (POCPs) of 120 different VOCs, for policy applications by the UK Government.

(ii) Comparisons have been made, in field studies of OH and HO_2 radicals using the FAGE technique, between radical measurements and those modeled using a box model based on the MCM. A wide range of environments have been studied, from baseline conditions at Cape Grim in Tasmania, to polluted conditions in Birmingham in the UK (Heard and Pilling (2003), Sommariva et al. (2006)).

(iii) Lewis et al. (2005) made measurements of oxygenated VOCs at Mace Head in Western Ireland. They found that, under clean westerly conditions, the combination of oxygenated VOCs (acetone, methanol and acetaldehyde) contributed up to 85% of the total mass of measured non methane organics in air and up to 80% of the OH radical organic sink, when compared with the sum of all other organic compounds including non-methane hydrocarbons, DMS and OH-reactive halocarbons. They used a simple trajectory model, based on the MCM, to demonstrate in situ formation during air mass transport was on timescales longer than the atmospheric lifetime of precursor hydrocarbons or primary emission. The period over which this process was significant was similar to that of air mass motion on intercontinental scales, and formation via this route may reproduce that of a widespread diffuse source. The model indicated that continued short chain OVOC formation occurs many days from the point of emission, via longer lived intermediates of oxidation such as organic peroxides and long chain alcohols. Figure 2 shows the calculated profile for acetaldehyde, assuming initial VOC concentrations typical of those found in the Eastern US. The rise time reflects the decay time of acetaldehyde, which is only a few hours. The slow decay reflects the lifetime of its original precursors and of the precursor intermediates formed in the air mass. Its ultimate precursors consisted of $C_2 - C_6$ hydrocarbons.

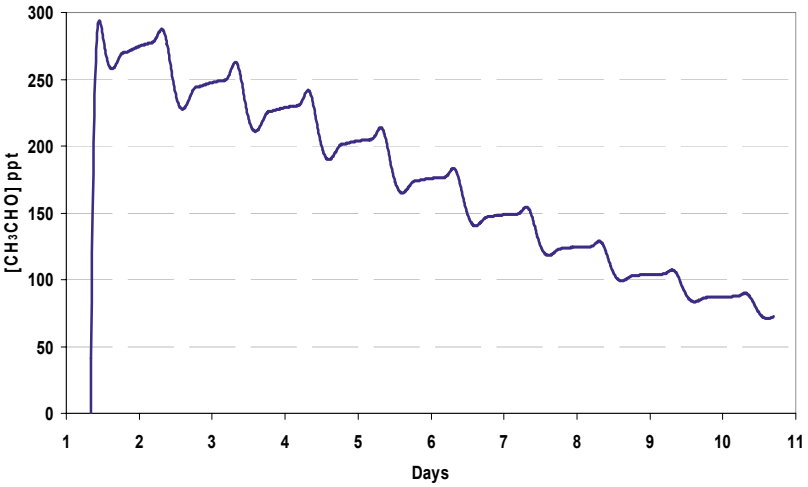

Figure 2. Box model calculation of acetaldehyde for a 10 day trajectory over the Atlantic, for an air mass initialised with background organic and inorganic content representative of fresh emissions leaving a continental landmass but with no subsequent sources

(iv) Johnson et al. (2006) used MCM v3.1 to simulate the formation of secondary organic aerosol (SOA) made by semi- and non-volatile products of VOC oxidation, in comparisons with measurements from a field campaign in SE England The formation of SOA by gas-to-aerosol transfer of lower volatility oxidation products was simulated successfully, but provided good agreement with observations only if all the partitioning coefficients were increased by a species-independent factor of 500. This scaling is indicative of the occurrence of chemical processes (e.g., oligomerisation) within the aerosol which allow the oxidised organic species to react by association and/or accretion reactions which generate even lower volatility products, leading to a persistent, non-volatile secondary organic aerosol.

6. Lumping and Reducing the MCM

The MCM is far too large for use in Eulerian models incorporating realis tic atmospheric transport on a global or regional scale. Such models use mechanisms with much more concise representations of the chemistry, in which single representative species are used for a range of similar species

(e.g., alkanes), and in which the oxidation steps are much more schematic. The problem with such mechanisms is that they are less closely linked to laboratory measurements than is the MCM. The MCM can be used to evaluate the performance of such mechanisms, but it can also be directly reduced and/or lumped.

Pöschl et al. (2000) developed a much reduced and lumped mechanism for isoprene oxidation, using the MCM as a benchmark, both in the construction of the original mechanism and in the evaluation of its accuracy for a range of atmospheric conditions. The aim was to generate a mechanism that could be used in global chemistry transport models. They used a single intermediate to represent classes of compound. For example methacrolein, methylvinylketone and other C_4 ketones are formed as first generation oxygenated intermediates. These were all represented by a single species, MACR. They generated a mechanism containing 16 species and 44 reactions, a substantial reduction from the original mechanism.

Jenkin et al. (2002) constructed a "common representative intermediates" (CRI) mechanism, based on MCM v2, which treats the degradation of methane and 120 VOC using ca. 570 reactions of ca. 250 species (i.e., the emitted VOC plus an average of about one additional species per VOC). It thus contains only ca. 5% of the number of reactions and ca. 7% of the number of chemical species in MCM v2, providing a computationally economical alternative. The CRI mechanism contains a series of generic intermediate radicals and products, which mediate the breakdown of larger VOC into smaller fragments (e.g., formaldehyde), the chemistry of which is treated explicitly. A key assumption in the mechanism construction methodology is that the potential for ozone formation from a given VOC is related to the number of reactive (i.e., C–C and C–H) bonds it contains, and it is this quantity which forms the basis of the generic intermediate groupings. Following a small degree of optimisation, the CRI mechanism was shown to generate concentrations of ozone, OH, peroxy radicals, NO and NO2 in excellent agreement with those calculated using MCM v2, in simulations using a photochemical trajectory model applied previously to the determination of POCPs. Figure 3 shows a schematic representation of the form of the CRI mechanism. Smaller oxidised intermediates, e.g., HCHO and CH_3CHO are represented directly, while generic radicals and carbonyls are given indices (e.g., 19 in RN19O2 and 11 in CARB11, for radicals and carbonyls respectively), that represent the number of NO to NO_2 conversions which can result from the subsequent complete degradation. Jenkin has subsequently improved the CRI mechanism, with some increase in size, but with a more accurate representation of the chemistry.

Whitehouse et al. (2004a,b) used a more formal and mathematical approach to produce a reduced and lumped scheme, again based on MCMv2, for 120 primary VOCs. They used sensitivity analysis to eliminate species and

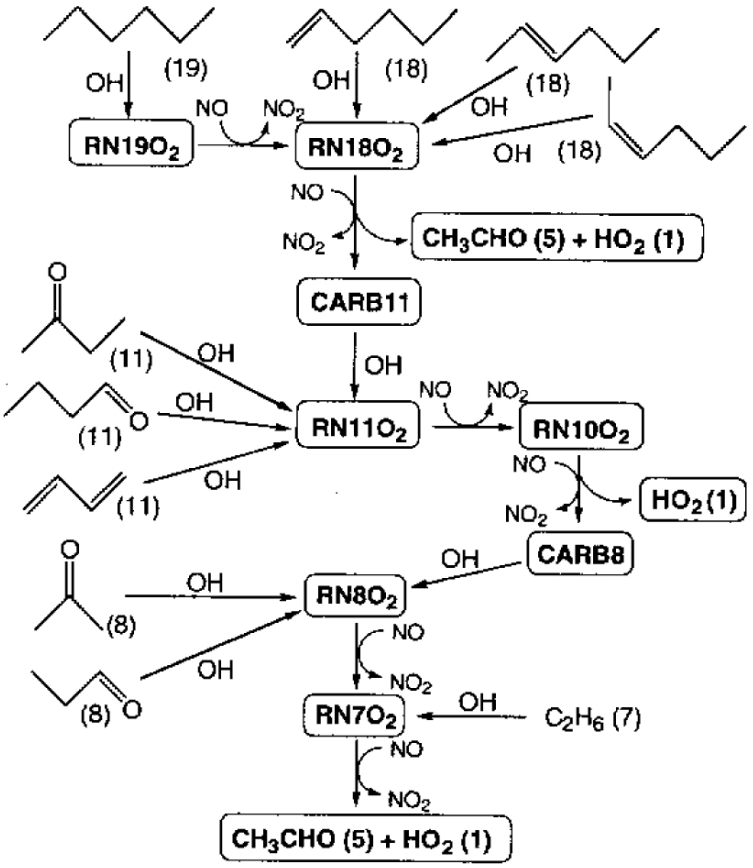

Figure 3. Partial degradation of species in the Common Representatitve Intermediates (CRI) mechanism, showing the involvement of lumped carbonyl (CARB) and radical (RN) intermediates in the oxidation of several different precursors. The numbers in the CARB and RN species refer to the number of potential NO to NO_2 conversions that can be generated from the complete oxidation of the compound

reactions that were not essential to the accurate representation of specified *important* species: O_3, NO, NO_2, HNO_3, NO_3, HONO, HNO_3, HO_2NO, HCHO, OH and the sum of all peroxy acyl nitrate (PAN) species, examined as total PAN. The use of the quasi-steady state approximation (QSSA) proved to be an extremely successful method of removing the fast timescales within the system. A method based on grouping species with reference to their chemical lifetimes and reactivity structures was used to provide lumps for the representation of groups of species. A method for determining the forward and reverse transformations between individual

and lumped compounds, thus providing a mapping between the MCM nd the lumped mechanism, was developed. The overall reduction was to 35% of the original species and 40% of the original reactions.

The crucial issue is the number of species, since this determines the number of ordinary differential equations that must be solved at each grid point in an Eulerian model. Both the CRI Mechanism and objective reduction/ lumping, and especially the latter, lead to mechanisms that are too large for use, for example, in global models. A combination of approaches may provide a way forward.

7. Heterogeneous Chemistry

Loss of species on aerosol is important for many species, and especially for HO_2 and N_2O_5. The loss is defined *via* an uptake coefficient, γ, and is described using a series of steps involving gas and aerosol phase diffusion, accommodation at the surface, equilibration between the aerosol and gas phases, and reaction in the aerosol phase. Uptake of HO_2 has been invoked in models using the MCM to partly explain differences between modelled and measured HO_2 concentrations in field campaigns (e.g., Sommariva et al. (2006)). The uptake is, however, very complex. Thornton and Abbatt (2005) showed uptake on aqueous aerosols depends on the concentration of oxidising agents in the aerosol phase. In the absence of such species, uptake depends on the condensed phase reaction of HO_2 with its conjugate base, O_2^- and it is therefore second order in dissolved HO_2 and depends on pH. This means that γ_{HO2} can vary by several orders of magnitude depending on $[HO_2]$, aerosol size and pH and the temperature. A full assessment of these effects is urgently needed.

8. Aqueous Phase Chemistry

The MCM is a purely gas phase mechanism, although, as discussed above, it has been used in models investigating secondary organic aerosol formation and heterogeneous uptake has been incorporated. It has not, however, been used in conjunction with aqueous phase chemistry. The most detailed aqueous phase model is the CAPRAM 3.0 mechanism (Herrmann et al. (2005)) that incorporates the oxidation mechanisms for 34 chemical species (5 alcohols, 10 carbonyl compounds, 13 mono- and dicarboxylic acids, 1 ester, 4 polyfunctional compounds and 1 heterocyclic compound). The mechanism is primarily based on $C_1 - C_4$ chemistry, but does include some larger species. The aqueous chemistry was coupled to the gas phase mechanism RACM (regional atmospheric chemistry model) (Stockwell et al. (1997)). Simulations of a remote environment showed a significant

decrease in the concentrations OH and NO_3 and that the gas phase and taqueous phase oxidations of aldehydes and ketones led to the formation of mono- and dicarboxylic acids which accumulate in the aqueous phase. The oxidation of acetone provides an interesting illustration of the importance of aqueous phase chemistry. It is primarily formed in the gas phase, and transferred to the liquid phase, with little direct production occurring in that phase. Its OH initiated oxidation generates hydroxyacetone and methyl glyoxal, the latter being the main source of pyruvic acid, $CH_3C(O)COOH$. Combining the MCM and CAPRAM would be very beneficial, but it would be necessary to find some way of compressing the large number of MCM species with significant uptake rates into the much smaller CAPRAM mechanism.

9. Acknowledgements

I am grateful to me colleagues M E Jenkin, R G Derwent, C Bloss, S Pascoe, A R Rickard, S M Saunders, R Sommariva, J E Stanton, A S Tomlin and L E Whitehouse for their considerable contributions to this work. Funding from the UK Department of Environment, Food and Rural Affairs, the European Union and the UK Natioanl Centre for Atmospheric Science is gratefully acknowledged.

10. References

Bloss, C., Wagner, V., Bonzanini, A., Jenkin, M.E., Wirtz, K., Martin-Reviejo, M., Pilling, M.J., 2005, Evaluation of detailed aromatic mechanisms (MCMv3 and MCMv3.1) against environmental chamber data, *Atmospheric Chemistry and Physics*, **5**: 623-639.

Derwent, R.G., Jenkin, M.E., Saunders, S.M., Pilling, M.J., 1998, Photochemical ozone creation potentials for organic compounds in north west Europe calculated with a master chemical mechanism, Atmospheric Environment, **32**: 2429-2441.

Heard, D.E., and Pilling, M.J., 2003, Measurement of OH and HO_2 in the troposphere, *Chem. Rev*., **103**: 63-5198.

Herrmann, H., Tilgner, A., Barzaghi, P., Majdik, Z., Gligorovski, S., Poulain, L., Monod, A., 2005, Towards a more detailed description of tropospheric aqueous phase organic chemistry: CAPRAM 3.0, *Atmospheric Environment* **39**: 4351.

Jenkin, M. E., Saunders, S. M., Derwent, R. G., Pilling, M.J., 2002, Development of a reduced speciated VOC degradation mechanism for use in ozone models, *Atmospheric Environment*, **36**: 4725-4734.

Jenkin, M.E., Saunders, S.M., Wagner, V., Pilling, M.J., 2003, Protocol for the development of the Master Chemical Mechanism, MCM v3 (Part B): tropospheric degradation of aromatic volatile organic compounds, *Atmospheric Chemistry & Physics*, **3**: 181-193.

Johnson, D., Utembe, S.R., Jenkin, M.E., Derwent, R.G., Hayman, G.D., Alfarra M.R., Coe H., McFiggans, G., 2006, Simulating regional scale secondary organic aerosol formation during the TORCH 2003 campaign in southern England. *Atmospheric Chemistry and Physics*, **6**: 403-418.

Lewis, A.C., Hopkins, J.R., Carpenter, L.J., Stanton, J., Read, K.A., Pilling, M.J., 2005, Sources and sinks of acetone, methanol, and acetaldehyde in North Atlantic marine air, *Atmospheric Chemistry and Physics*, **5**: 1963-1974.

Pinho, P.G., Pio, C.A., Carter, W.P.L., Jenkin, M.E., 2006, Evaluation of alkene degradation in the detailed tropospheric chemistry mechanism, MCM v3, using environmental chamber data, Journal of Atmospheric Chemistry, **55**: 55-79.

Poschl, U., von Kuhlmann, R., Poisson, N., Crutzen, P.J., 2000, Development and intercomparison of condensed isoprene oxidation mechanisms for global atmospheric modelling, *Journal of Atmospheric Chemistry*, **37**: 29-52 .

Saunders, S.M., Jenkin, M.E., Derwent, R.G., Pilling, M.J., 2003, Protocol for the development of the Master Chemical Mechanism, MCM v3 (Part A): tropospheric degradation of non-aromatic volatile organic compounds, , *Atmospheric Chemistry and Physics*, **3**: 161-180.

Sommariva, R., Bloss, W.J., Brough, N., Carslaw, N., Flynn, M., Haggerstone, A.-L., Hopkins, J.R., Lee, J.D., Lewis, A.C., McFiggans, G., Monks, P.S., Penkett, S.A., Pilling, M.J., Plane, J.M.C., Read, K.A., Saiz-Lopez, A., Rickard, A.R., Williams, P.I., 2006, OH and HO_2 chemistry during NAMBLEX: roles of oxygenates, halogen oxides and heterogeneous uptake, *Atmospheric Chemistry and Physics*, **6**: 1135-1153.

Stockwell, W.R., Kirchner, F., Kuhn, M., Seefeld, S., 1997, A new mechanism for regional atmospheric chemistry modelling, *Journal of Geophysical Research—Atmospheres* **102**: 25847-25879.

Thornton, J. and Abbatt, J.P.D., 2005, Mesaurements of HO_2 uptake to aqueous aerosol: mass accommodation coefficients and net reactive loss, *Journal of Geophysical Research – Atmospheres,* **110**: D08309.

Whitehouse, L., Tomlin, A. S., Pilling, M.J., 2004, Systematic Reduction of Complex Tropospheric Chemical Mechanisms, Part I: Sensitivity and Time-Scale Analysis, *Atmospheric Chemistry and Physics*, **4**: 2025 – 2056.

Whitehouse, L., Tomlin, A. S., Pilling, M.J., 2004, Systematic Reduction of complex tropospheric chemical mechanism, Part II: Lumping using a time-scale based approach, *Atmospheric Chemistry and Physics*, **4**: 2057-2081.

PHOTOENHANCED UPTAKE OF NO_2 ON MINERAL DUST

CHRISTIAN GEORGE(*), MARIEME NDOUR
IRCELYON, Institut de recherches sur la catalyse et l'environnement de Lyon, 2 avenue Albert Einstein, Villeurbanne, F-69626 cedex, France ; CNRS, UMR5256, Villeurbanne F-69626, France ; Université de Lyon, Villeurbanne, F-69626, France ; Université Lyon 1, Villeurbanne, F-69626, France ; Université Claude Bernard Lyon 1, Villeurbanne, F-69626, France.

YVES BALKANSKI
Laboratoire des Sciences du Climat et l'Environnement (CEA-CNRS), F-91191 Gif-sur-Yvette Cedex2

OUMAR KA
Université Cheikh Anta Diop-Faculté des Sciences et Techniques- Dakar-Fann Senegal.

Key Words: List all your keywords; do not exceed more than three lines; keywords are separated by a comma.

Abstract Dust events are commonly observed every year and have been shown to strongly impact on the tropospheric ozone budget. This impact arises from the uptake of different gases, such as NO_y (mainly as HNO_3 or N_2O_5), on the solid surfaces exhibited by the uplifted minerals. While such "dark" processes have been deeply studied over the last years, dust particles contain a series of oxides that may be initiate photochemical process that have not been considered so far. In fact, in addition to quartz, illite, montmorillonite, and calcite, mineral dusts are heterogeneous mixtures of mineral oxides containing small levels of TiO_2. In order to mimic the properties that these oxides confer to mineral Saharan dust, TiO_2 and SiO_2 were mixed and their heterogeneous reactions with NO_2 studied using a horizontal wall flow tube. In addition, experiments were performed with real Arizona test dust in order to assess the importance of photochemical reactions under realistic atmospheric conditions. The effect of light (in the 380-700 nm range), temperature (in the 288-303 K range) and relative humidity have been determined. The uptake coefficient on TiO_2 mixing in SiO_2 increases with temperature and decreases with relative humidity. We found that despite its very low abundance, titanium dioxide (TiO_2) will strongly favour the photo-conversion of NO_2 on mineral dust, nitrogen dioxide being otherwise quite unreactive on

* To whom correspondence should be addressed.

A. Mellouki and A.R. Ravishankara (eds.), Regional Climate Variability and its Impacts in the Mediterranean Area, 219–233.

these minerals. This photoenhanced uptake of gases will in turn impact on the ozone and/or HO_x budget during a dust event. In addition, such photo-enhanced process will affect the nitrate content of the dust particles, impacting on the optical properties of the aerosols and their associated climatic impact. We therefore exemplified, on mineral dust, that photochemical conversion on solid surfaces encountered in the troposphere needs to be considered an important process of wide impact due to the ubiquitous presence of minerals in our environment as it will change the level of photo-oxidant and aerosol optical properties.

1. Introduction

For any given year, between 1600 and 2000 Tg of mineral aerosol are predicted to be uplifted into the atmosphere (Ginoux et al., 2001). The diameter of the particles injected into the atmosphere spans at least 4 order of magnitudes from 0.1 to 100 μm. Particles smaller than 10 μm have atmospheric lifetimes of up to of several days whereas larger particles settle in a matter of hours (Prospero et al., 1999). The fraction of these particles with diameter from 0.1 to 10 μm can be transported over thousands of kilometres and hence be detected by mean of passive remote sensing far away from their sources (Husar et al., 2001).

The impact of mineral dust on the Earth's atmosphere is manifold. Dust particles are believed to have a direct effect on the radiation budget of the atmosphere and therefore are expected to have an impact on the climate (Diaz et al., 1998a). Mineral aerosols have been shown to increase solar reflectivity of the atmosphere i.e., leading to negative radiative forcing in the shortwave spectrum. The heating due to the longwave part of the spectrum and due to mineral oxides in the shortwave is thought to counterbalance this cooling over bright arid surfaces, hence dust warms up the atmospheric column over deserts. The overall climatic effect of dust is still under discussion for the time being due to the complexity to treat the climate effects of an internal mixture of minerals. Both the direct and indirect effects of these particles are currently pointed to as one of the greatest uncertainties in global climate models.

In addition to the recent interest in studying recent dust events (due to their impact on climate and more generally on the atmospheric composition), past records of dust deposition have shown that during glacial time the atmospheric load and the deposition of these aerosols far exceeded what is found at present. An example is given by the occurrence of dust events have identified even in deep ice core samples (Petit et al., 1999).

The huge amounts of mineral dust uplifted each year into the atmosphere constitute ubiquitous surfaces for gases to react. These particles act, beside their climatic impact, as a substrate for the conversion or scavenging of acidic gases and their precursors. Over the last years many uptake and or

reactive uptake of trace gases have been studied using a variety of experimental approaches. For instance, the uptake kinetics of HNO_3, N_2O_5, NO_2 and SO_2 were investigated on mineral dust and proxies like aluminium oxide. Indeed, studying the chemistry of dust particles is complicated by the complex chemical nature of these particles.

In fact, as dust particles are mobilised by strong winds and therefore eroded from the ground, their composition is somehow reflecting the chemical composition of crustal materials from which they are produced. As the Earth's crust is dominated by silicon and aluminium oxides, the latter are also dominantly present in uplifted particles. Indeed, several studies focusing on the chemical (elemental) composition of dust originating from various locations around the world demonstrated that mineral dust is approximately 60% SiO_2 and 10-15% Al_2O_3. Beside these major elements, some other oxides are found. The percentages of these other oxides, namely Fe_2O_3, MgO, and CaO, are slightly more varied and dependent on source location.

Finally, also some traces of titanium and titanium dioxide are found in dust particles at mass mixing ratios ranging from 0.1 to 10% which are highly dependent on the exact location from where the particles were uplifted.

Titanium dioxide, also known as titania is the naturally occurring oxide of titanium, chemical formula TiO_2. This compound is ubiquitous is most natural (at trace level see above) but also man-made material (such as paint, printing ink, plastics, paper, cosmetics…). However, TiO_2 has some particular properties (depending on its exact crystalline structure) as it acts as a photocatalyst for the decomposition (for both oxidation and reduction) once irradiated by light with wavelengths below 440 nm. The photocatalytic activity is the ability of a material to create an electron hole pair as a result of exposure to ultraviolet radiation. The resulting free-radicals are very efficient oxidizers of organic and inorganic matter. Photocatalytic activity in TiO_2 has been extensively studied because of its potential use in technical processes such as sterilization, sanitation, and remediation applications.

In this study, we were wondering if the traces of TiO_2 naturally present in dust particles could not have an effect on the reactivity of dust particles in presence of light. Especially, it is known that nitrogen dioxide in not reacting on dust particles in the dark, but nothing is known about dust photochemistry and its potential impact.

Especially, in this preliminary study, we decided to study if traces of TiO_2 have the potential to reduce nitrogen dioxide and from traces of nitrous acid. Indeed, nitrous acid (HONO) is an important precursor for OH radicals in the polluted troposphere but the heterogeneous conversion of NO_2 to HONO is currently not well understood.

Since the initial detection of nitrous acid in the atmosphere (Perner et al., 1979), many studies have shown that nitrous acid may accumulate during night time before undergoing photolysis in the early morning:

$$HONO + h\nu \rightarrow NO + OH \quad (1)$$

This creates an important morning OH radical burst (Harris et al., 1982, Harrisson et al., 1996). In recent studies (Zhou et al., 2002), a significant contribution of the HONO photolysis to the integrated OH yield of up to 60% was calculated.

While the night time formation of HONO in the atmosphere may be reasonably well explained by direct emissions and heterogeneous conversion of NO_2 on ground surfaces with the different mechanisms mentioned above, measured concentrations significantly exceeded modelled values during the day[9]. Accordingly, a strong daytime source was postulated in recent studies to explain daytime concentrations of HONO over snow e.g., (Zhou, et al., 2001), ground and vegetation surfaces (Kleffmann, et al., 2003; Vogel, et al., 2003; Zhou, et al., 2002a; Zhou, et al., 2003; Zhou, et al., 2002b). The source strength of this daytime source was estimated to be 200-1800 pptv/h (Ren, et al., 2003; Zhou, et al., 2003) or to be ~20 times faster than all night-time sources of HONO (Kleffmann, et al., 2003). The photolysis of nitrate and/or nitric acid on surfaces was postulated to explain these high daytime concentrations of HONO (Zhou, et al., 2002a; Zhou, et al., 2003). However, the exact mechanism of this photolytic HONO source still remains to be unanswered, e.g., the photolysis frequency of adsorbed HNO_3 was reported to be two orders of magnitude faster compared to the gas and the liquid phase, which is still unclear (Ramazan, et al., 2004; Zhou, et al., 2003). In addition, in a recent study in a large simulation chamber, the photolysis of HNO_3/nitrate was excluded to explain the observed photolytic HONO formation (Rohrer, et al., 2004).

Therefore, we investigated the effect of light (in the visible) on the uptake kinetics of NO_2 on various surfaces taken as proxies for dust particles. The selected approach was based on combining experimental determinations and 3D modelling.

2. Experimental

2.3. HORIZONTAL COATED WALL REACTOR WITH CHEMILUMINESCENCE DETECTION

The heterogeneous interactions of gaseous NO_2 were studied on bulk surfaces by exposing different concentrations of gaseous NO_2 mixtures to selected solid films. The experimental approach is based on measuring the reactant gas concentration i.e., NO_2 gas, at the exit of a cylindrical flow reactor as a function of the distance (which translates to time) that the NO_2 gas is in contact with the mineral surface.

The experiments were performed in a horizontal coated wall reactor (Figure 1). A detailed description of the experimental setup may be found in George et al., 2005. The horizontal flow tube approach for this study is similar to the one used in previous studies of heterogeneous reactions (Lovejoy et al., 1995) However, the horizontal reactor used in this work has been fitted with four halogen lamps (OSRAM Halostar starlite, 50 W) to study the effect of irradiation on the uptake of NO_2 gas on different minerals.

A Pyrex tube with an internal volume of approximately 17 cm^3 and an inner diameter of 0.525 cm was used in all experiments. The cell was maintained at a constant temperature using a Huber CC130 thermostatically controlled bath by circulating a methanol/water mixture through the outer jacket. All experiments were performed under atmospheric pressure and the temperature range was 278 to 308 K. The NO_2 reactant gas was introduced into the reactor via a movable Pyrex injector. It was monitored directly with a NOx chemiluminescence analyser (THERMO 42C). The uptake coefficients for NO_2 were determined by measuring the quantity of the NO_2 reactant gas absorbed by the dry solid film. The trace gas loss in the flow tube was measured as a function of the position (distance) of the movable injector, i.e., as a function of the gas/solid exposure time t. The maximum length l of the interaction zone (maximum length that the injector could be retracted) was about 20 cm. As shown in equation (I) below, the measured loss rate can be interpreted in terms of a first order process with respect to the gas phase concentration of the reactant.

$$\frac{\mathrm{n}-\Delta\mathrm{n}}{\mathrm{n}} = \exp(-k_w t) \tag{1}$$

In equation (1), t is the average carrier gas residence time and k_w is the first order rate coefficient for the reaction at the solid film surface. The first order rate coefficient k_w is:

$$K_w = \frac{\gamma_{geom}\langle c\rangle}{2r_{tube}} \tag{2}$$

In eqn. (2), r_{tube}, γ_{geom} and $\langle c\rangle$ are the flow tube radius, uptake coefficient and average molecular velocity, respectively.

An indirect detection of the produced HONO was made by means of a NO/NO_x-chemiluminescence detector (Thermo – 42C, coupled to a molybdenum converter reducing HONO and NO_2 to NO), in combination with a sodium carbonate denuder tube for removing HONO from the gas stream. This molybdenum converter/chemiluminescence detection system principally measures the NO_y-species NO, NO_2, and HONO with an equal analytical response. The sodium carbonate denuder tube may either be switched into the sampling line to measure the sum of the species NO and NO_2 or be

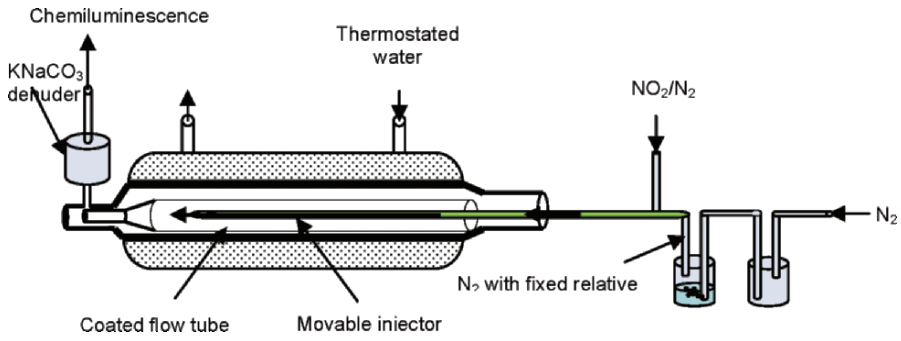

Figure 1. Schematic representation of the horizontal wall flow tube experimental approach used to measure the uptake of NO_2 on mineral dust

bypassed so that the CLD signal accounts for the sum of the species NO, NO_2 and HONO. The HONO concentration can therefore be expressed as the difference of the NO/NO_x-chemiluminescence detector signal without and with carbonate denuder in the sampling line. The NO concentration can be obtained from the detector signal, when the molybdenum converter is bypassed.

The various mineral oxide powders and dusts that were investigated, i.e., SiO_2 (DEGUSSA Aerosil 130) and TiO_2 (DEGUSSA, P25 80% anatase, 20% rutile; P25), were purchased from Degussa.

TiO_2 and SiO_2 (1.5 g) powder was dissolved in 20 ml of water and was dripped uniformly into the Pyrex flow tube and dried in an oven at 100°C overnight. The resulting film covered the entire inner area of the tube and, to the eye, was fairly uniform in thickness (Sullivan, et al., 2004).

2.2. DESCRIPTION OF THE MODEL TO TREAT INTERACTION BETWEEN AEROSOLS AND CHEMISTRY

INCA is a chemistry and aerosol model coupled to the Laboratoire de Météorologie Dynamique (LMD) General Circulation Model, LMDz. INCA is developed at the Laboratoire des Sciences du Cimat et de l' Environnement (LSCE) in collaboration with other laboratories.

LMDz-INCA accounts for emissions, transport (resolved and sub-grid scale), photochemical transformations, and scavenging (dry deposition and washout) of chemical species and aerosols interactively in the GCM. Several versions of the INCA model are currently used depending on the envisaged applications with the chemistry-climate model. The standard model resolution is 96 × 72 (3.75 × 2.5 degrees in respectively longitude and latitude) with 19 sigma-p hybrid vertical levels. The GCM also offers the possibility to zoom over specific regions, reaching horizontal resolutions

of 50×50 km^2. The model can be run in a nudged mode, relaxing to ECMWF winds and temperature. An off-line version of the GCM has also been developed in order to minimize the required computing time for transport simulations. This model is still under development and constitutes the atmospheric component of the IPSL coupled atmosphere-ocean-biosphere model.

The model has been used for the transport of inert tracers by Hourdin and Issartel (2000) with winds and temperature relaxed towards ECMWF reanalysis (nudging), and by Boucher et al. (2002) and Boucher and Pham (2002) for the simulation of the sulphur cycle. The relaxation of the GCM winds towards ECMWF meteorology is performed by applying a correction term to the GCM winds corresponding to a relaxation time of 2.5 for both u and v and over the whole model domain. The ECMWF fields are provided every 6 hours and interpolated onto the LMDz grid. In this study, we present the results obtained with the climatological version of LMDz. However, we are currently conducting simulations with the nudged version in order to follow the evolution of the main gases and aerosol species of interest during field campaigns that have taken place in Europe.

The LMDz version used here has a horizontal resolution of 3.8 degrees in longitude and 2.5 degrees in latitude (96×72). On the vertical, the model uses σ-p coordinates with 19 levels extending from the surface up to about 3 hPa. This corresponds to a vertical resolution of about 300-500 m in the planetary boundary layer (first level at 70 m height) and to a resolution of about 2 km at the tropopause (with 7-9 levels located in the stratosphere). Other versions of the model with higher horizontal (160×98 or 2.25° in longitude and 1.8° in latitude) and vertical (50 hybrid levels up to 0.07 hPa) resolutions are currently used. The primitive equations in the GCM are solved with a 3 min time step, large-scale transport of species is performed every15 min, and physical processes (including unresolved sub grid scale mixing) are calculated with a time step of 30 min. The transport and distribution of inert tracers (CO_2, SF_6, Kr85, CCl_3F and Rn222) has been compared with measurements and other model simulations to show that the model reproduced reasonable inter and intra-hemispheric transport times (Hauglustaine et al., 2003).

The aim for using such model is to be able to simulate interactively with the General Circulation Model the ozone chemistry both tropospheric and stratospheric, the different aerosol types (sulphate, carbonaceous, mineral and seasalts) together with the long-lived greenhouse gases (CO_2, CH_4, N_2O, (H)CFC). We have developed a chemistry/aerosol and emission model INCA (INTeractions of Chemistry with Aerosols) that allows to follow changes in atmospheric chemical composition due to human activities and their impact on climate. The model has built-in features that allow to follow back-trajectories, to do inverse modelling and assimilate chemical and aerosol

species. In addition, a near real-time forecast mode is used (*http://www-lsceinca.cea.fr/welcome_real_time.html*).

Two different versions have been developed to treat tropospheric chemistry, one that keeps the number of species to a limited number 33 species and treats CH_4–NOx–CO–O_3 as a chemical scheme representative of the background chemistry while lumping together non-methane hydrocarbons. In this version, species with a very short photochemical lifetime are not subject to transport, and only one photochemical family is formed (Ox = O_3 + $O(^1D)$ + $O(^3P)$). The scheme includes 19 photolytic reactions, 62 gas phase reactions and 4 heterogeneous reactions. The reaction rates are specified according to DeMore et al. (1997) and subsequent updates (Sander et al., 2000; 2002). These reaction rates are updated at each model time step based on the temperature, pressure, and water vapour distributions provided by the GCM.

Dry deposition is treated using a resistance in series scheme for gases and constant dry deposition velocities that depend whether the surface is covered by land or oceans. The sedimentation of the aerosol is based upon settling velocities calculated using Stokes relationship, taking into account their dependency on the lower air viscosity at higher altitude (Seinfeld, 1986). The adaptation of this scheme to be used with the spectral scheme for aerosol size distribution is detailed in Schulz et al. (1998).

2.3. TREATMENT OF THE HETEROGENEOUS REACTION OF NO_2 ON DUST

The gas uptake to the surface of the aerosol is described by a first order rate reaction in the model. The coefficient k_j (s^{-1}) which indicates the rate at which the gaseous species j is uptaken at the aerosol surface is:

$$k_j = \int_{r1}^{r2} k_{d,j}(r) n(r) \mathrm{d}r \tag{3}$$

where n(r)d is the number density of particles which sizes are included in the interval limited by r and r + dr. Kd, j (m^3 s^{-1}) denotes the coefficient of mass transfer that demands on the aerosol size and is computed based upon the Fuchs et Sutugin equation:

$$k_{d,j} = \frac{4\pi D_j V}{1 + K_n(\lambda + 4\dfrac{1-\gamma_j}{3\gamma_j}} \tag{4}$$

where Dj(m^2 s^{-1}) is the molecular diffusion coefficient of the trace gas involved in the reaction. Following the laboratory results described here the coefficient γj were set respectively to 1.e-4, 1.e-5 and 1.e-6.

The LMDz-INCA model is run for 13 months and only the last 12 months are analysed the first month ensuring that the spinup is over.

A future step in this work will be to have a better description of non-methane hydrocarbons using a more refined chemical scheme where several hydrocarbons are explicitly treated. This will allow to make a better quantification of the effects of this reaction upon NOx, NOy and HOx radicals.

3. Results

The uptake of NO_2 on bare glass was beyond the sensitivity of our horizontal coated wall reactor, which means that the uptake coefficient was below the detection limit of a few times 10^{-7}. Only a physical adsorption was observed i.e., the surface exposed by the glass flow tube was rapidly covered and saturated by NO_2 molecules. At this stage, no more uptake occurred on this surface. In the dark and at low relative humidity i.e., rh below 1%), there was no reaction on the bare glass surface.

The uptake of NO_2 in the dark was also studied on various mineral dusts. As an example, Figure 2 shows the raw data during a NO_2 uptake experiment in the dark on a surface made of TiO_2/SiO_2 at 1 wt% of TiO_2. When the surface of mineral was exposed to gaseous NO_2, nothing important happens which means that under our experimental conditions we could not observe any uptake of NO_2 on these minerals (despite the important specific surface of our samples). In the dark, NO_2 will not react on mineral dust as previously demonstrated or at a very slow rate which is beyond the possibility of our current set-up.

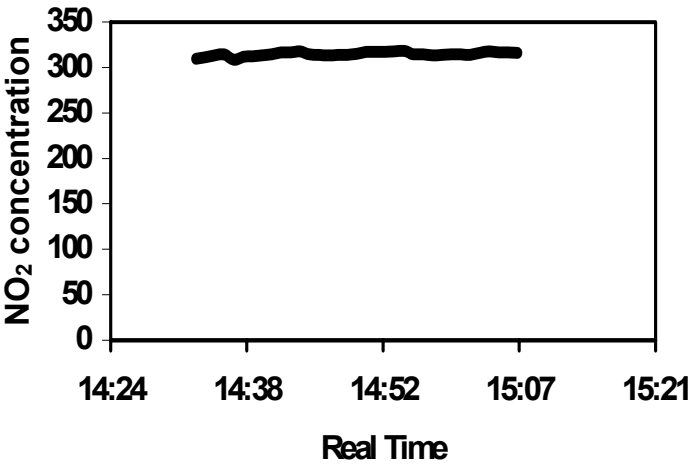

Figure 2. Raw data of the uptake of NO_2 over the surface of TiO_2 (1% wt)/SiO_2 surface in dark for different positions (30, 20, 10 cm) of the injector; 12.5% hr

Figure 3 shows the raw data for an uptake experiment on a on a surface made of TiO_2/SiO_2 at 1wt% of TiO_2 when the Pyrex flowtube was irradiated by the output of the halogen lamps. This has to be compared with data shown in Figure 2 (corresponding experiment but in the dark). It is obvious that in the dark only physical adsorption is occurring while under irradiation the uptake of NO_2 is driven by a chemical reaction on the solid film. Here the quantity of NO_2 that has reacted is depending "only" on the surface exposed to the gas phase. The uptake coefficient measured in this case is about 10^{-6} (or greater) i.e., at least an order of magnitude larger than without light.

The photocatalytic action of TiO_2 is initiated by the photo-production of an electron and a hole. The electron reduces the oxygen contained in the gas flow or the nitrogen dioxide while the hole oxidizes traces of water being also present in the gas flow.

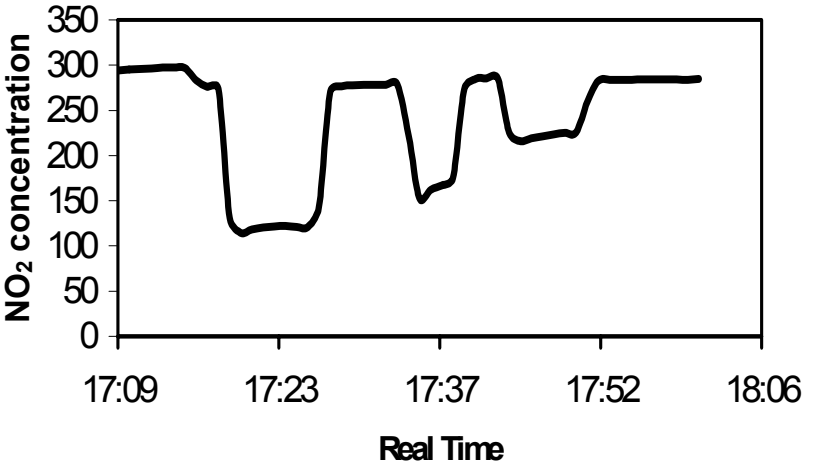

Figure 3. Raw data of the uptake of NO_2 over the surface of TiO_2 (1%wt)/SiO_2 with light for different positions (30, 20, 10 cm) of the injector at 297 K, 12.5 %hr

3.1. EFFECT OF TEMPERATURE, RELATIVE HUMIDITY, PERCENTAGE OF TIO_2 IN MIXTURE ON THE UPTAKE COEFFICIENT OF NO_2 ON TIO_2/SIO_2

The temperature dependence of the NO_2 uptake coefficient on the surface of TiO_2/SiO_2 was also studied between 288 and 298 K and the corresponding data are shown in Figure 4. One can note that the uptake coefficient is slightly dependent of the temperature as it increases as function of temperature (Figure 4).

On the other hand, the uptake coefficient appears to decrease with increasing relative humidity (Figure 5). While all experiments described above were performed under dry conditions (i.e., rh < 1%), we observed that adding

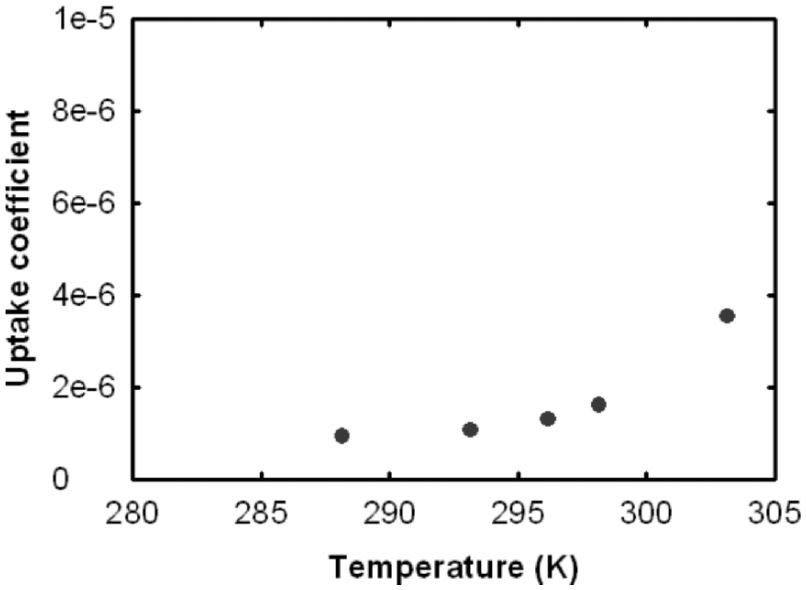

Figure 4. Uptake rate for NO_2 (197 ppb) on TiO_2 (5%wt)/SiO_2 as a function of temperature

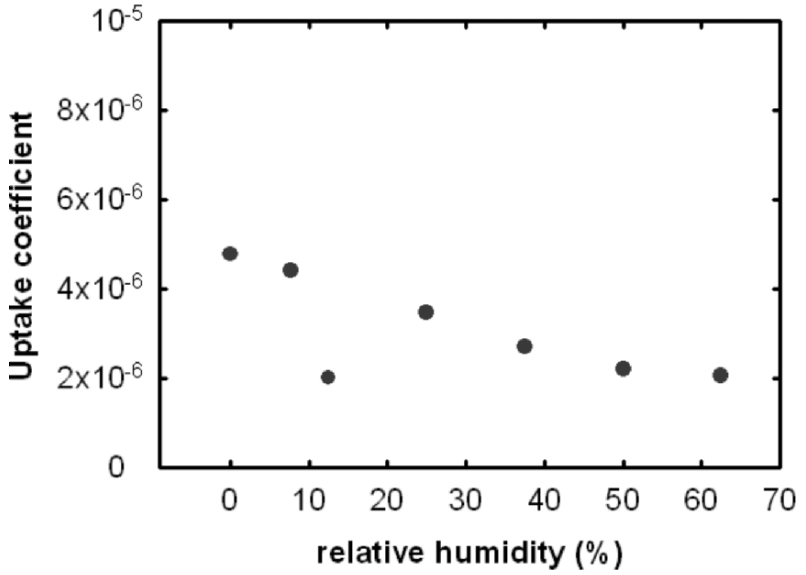

Figure 5. Uptake rate for NO_2 (197 ppb) on TiO_2(5%wt)/SiO_2 as a function of relative humidity

water vapour into the gas flow lead to a slight decrease of the uptake of NO_2. It appears certainly that water adsorbs more strongly on our films changing the properties of the surfaces and its ability to react with NO_2. Especially, the increasing amount of adsorbed water will lead to a stronger role in the associated chemical mechanism. Indeed, adsorbed water will be oxidised by TiO_2 and will produce OH radicals. This surface competition (in both adsorption and reactivity) may in turn affect the observed kinetics. This decrease can then be understood as the surface becoming less reactive toward NO_2, in connection to the fact that the molecules of waters, which are in the surface of the solid, prevent the reaction between NO_2 and TiO_2.

3.2. PHOTO-CONVERSION OF NO_2 to HONO

In our experimental approach, we used as mentioned a NO/NO_x-chemiluminescence detector. This molybdenum converter/chemiluminescence detection system principally measures the NO_y-species NO, NO_2, and HONO with an equal analytical response. This means that in any system where HONO can be potentially formed it will be detected as NOx. To prevent such interferences, a sodium carbonate denuder tube was inserted between the outlet

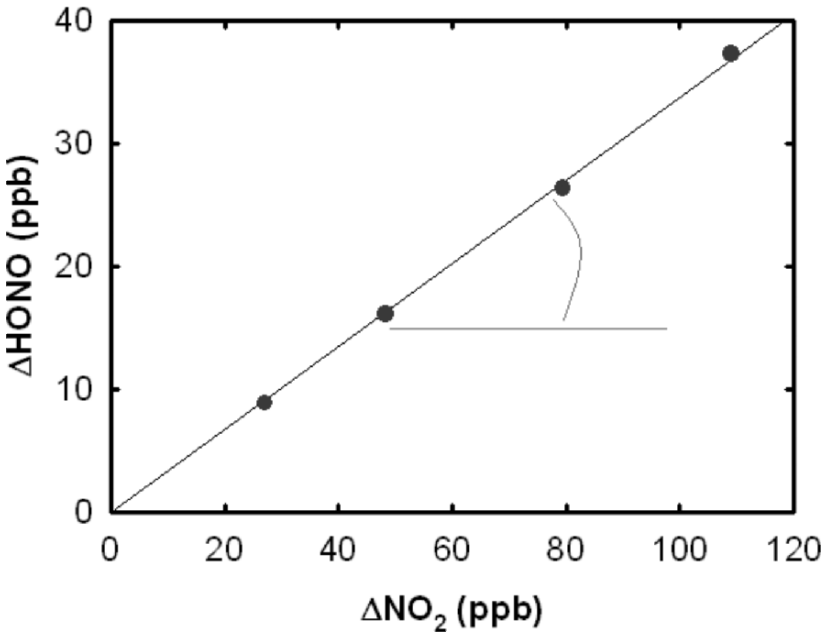

Figure 6. NO_2 (197 ppb) on TiO_2(5%wt)/SiO_2: dependence of the concentration of HONO produced on the concentration of NO_2 consumed observed at 298 K, and 50%hr

of the flowtube and the NOx analyser. This denuder removed from the gas flow any traces of nitrous acid and allowed a real detection of the NOx level along with the combination of the NOx + HONO level (by removing periodically the carbonate denuder). In other words, the sodium carbonate denuder tube was either be inserted into the sampling line allowing the determination of the sum of the species NO and NO_2 or may be bypassed that the sum of the species NO, NO_2 and HONO was measured. The HONO concentration can then be derived as the difference of the NOx-NOy level without and with carbonate denuder in the sampling line.

Using this procedure, HONO was detected as a product of NO_2 interaction with TiO_2/SiO_2. One can note that HONO production correlates with the kinetics of NO_2 consumption (Figure 6). The yield of HONO from the reaction of NO_2 with TiO_2 was determined as a ratio of the concentration of HONO formed and the concentration of NO_2 consumed. A few series of experiments were carried out where the HONO yield was determined under varied experimental conditions (temperature, relative humidity, and concentration of NO_2) and as a function of the TiO_2/SiO_2 masse deposit. All the experiments were conducted at room temperature (except the temperature dependence study) and 1 bar of pressure. The reduction of NO_2 to nitrous acid (HONO) on

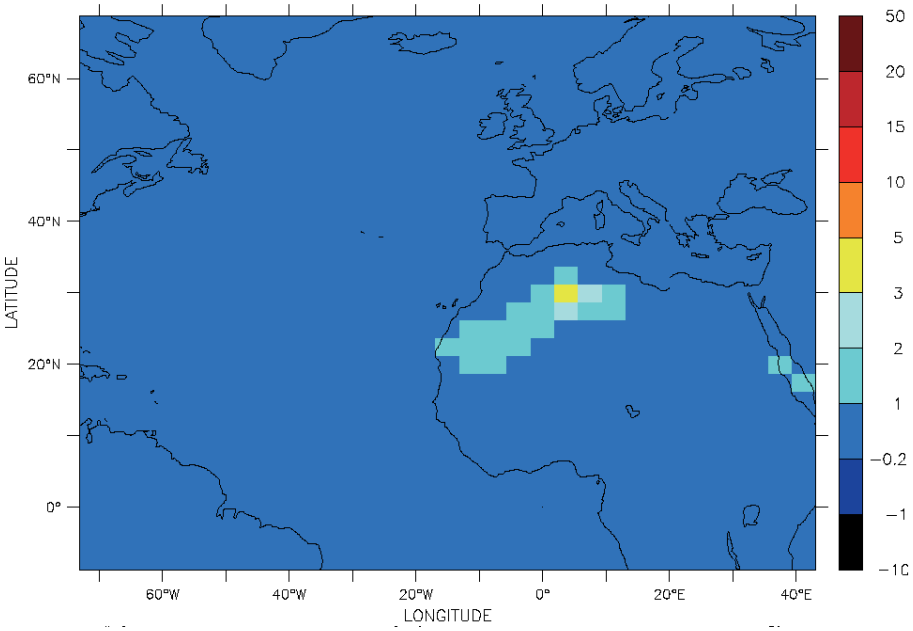

Figure 7. Percentage difference in NO_2 concentrations in the boundary layer (between 1005 and 714 mb) between a simulation with NO_2 uptake on mineral aerosol surfaces and the CONTROL RUN without the reaction, in this simulation the accommodation coefficient, γ was set to 10^{-5}

solid organic surfaces was observed in several laboratory studies (Arens et al., 2002; Leliére et al., 2004; George et al., 2005...). Figure 7 shows the dependence of HONO formed on the consumed concentration of NO_2; 33% yield of HONO was founding this present study.

From our findings, we can conclude that NO_2 is photochemically taken up by minerals containing traces of TiO_2 (in its anatase structure) and it forms nitrous acid as product but certainly particle bound nitrate (as the nitrous acid yield is not unity). The uptake coefficients reported in this preliminary study, have to be understood as lower limits as the irradiation used was mild i.e., below real solar irradiation. Accordingly, we do currently estimate the associated uptake coefficients as being in the range from 10^{-7} to 10^{-5}.

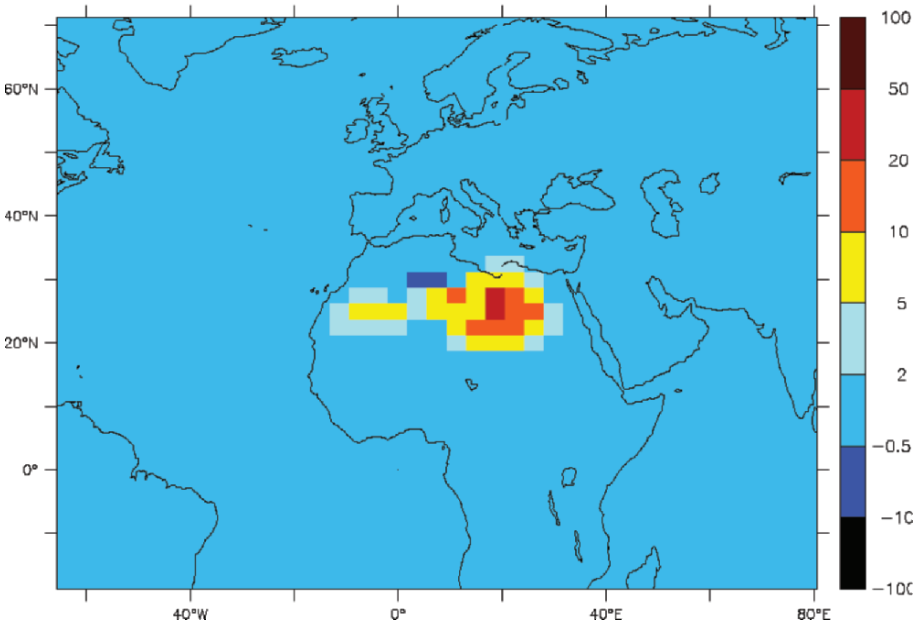

Figure 8. Percentage difference in NO2 concentrations in the closest layer to the surface (984 mb) between the simulation with the NO2 uptake on mineral aerosol surfaces and the CONTROL RUN without the reaction, in this simulation the accommodation coefficient, γ was set to 10^{-5}

3.3. 3-D MODELLING

An uptake coefficients of 10^{-5} which represents a lower limit given the results presented above was used in the model version with a chemical scheme representative of the background chemistry (CH_4–NOx–CO–O_3). The first results we obtained are shown in Figures 7 & 8. The July boundary layer concentrations of NO_2 are decreased by 1 to 5% even for a conservative value for the accommodation coefficient (Figure 7). The effect is particularly

pronounced in the vicinity of source regions (Sahara) and close to the surface where the aerosol surface available for the reaction is maximum. To illustrate the episodic nature of the uptake of NO_2, we show in Figure 8 that NO_2 concentrations during a dust outbreak that occurs on March 20th in the model can decrease by up to 30%. The main difference is that this NO_2 sink is photochemical (i.e., it will occur only during daytime) producing HONO that will in turn photodissociates producing OH and NO. Therefore the photocatalytic effect of dust particles (if existing in the environment) will affect the NO to NO_2 ratio drastically. We envisage quantifying this effect on the HOx radicals as well as onto NOx and NOy.

4. References

George, C., et al. (2005), Photoenhanced uptake of gaseous NO2 on solid organic compounds: A photochemical source of HONO?, *Faraday Discussions*, *130*, 195-210.

Kleffmann, J., et al. (2003), Measured and simulated vertical profiles of nitrous acid - Part I: Field measurements, *Atmos. Environ.*, *37*, 2949-2955.

Lovejoy, E. R., et al. (1995), Atmospheric fate of CF3OH. 2. Heterogeneous reaction, *Journal of Geophysical Research, [Atmospheres]*, *100*, 18,775-780.

Ramazan, K. A., et al. (2004), The photochemical production of HONO during the heterogeneous hydrolysis of NO2, *Phys. Chem. Chem. Phys.*, *6*, 3836-3843.

Ren, X., et al. (2003), OH and HO2 chemistry in the urban atmosphere of New York City, *Atmos. Environ.*, *37*, 3639-3651.

Rohrer, F., et al. (2004), Characterisation of the Photolytic HONO-Source in the Atmosphere Simulation Chamber SAPHIR, *Atmos. Chem. Phys. Discuss.*, *4*, 7881-7915.

Sullivan, R. C., et al. (2004), Ozone decomposition kinetics on alumina: Effects of ozone partial pressure, relative humidity and repeated oxidation cycles, *Atmospheric Chemistry and Physics*, *4*, 1301-1310.

Vogel, B., et al. (2003), Measured and simulated vertical profiles of nitrous acid - Part II. Model simulations and indications for a photolytic source, *Atmos. Environ.*, *37*, 2957-2966.

Zhou, X., et al. (2001), Snowpack photochemical production of HONO: A major source of OH in the Arctic boundary layer in springtime, *Geophys. Res. Lett.*, *28*, 4087-4090.

Zhou, X., et al. (2002a), Summertime nitrous acid chemistry in the atmospheric boundary layer at a rural site in New York State, *J. Geophys. Res.*, *107*, ACH13/11-ACH13/11.

Zhou, X., et al. (2003), Nitric acid photolysis on surfaces in low-NOx environments: significant atmospheric implications, *Geophys. Res. Lett.*, *30*, ASC 12/11-ASC 12/14.

Zhou, X., et al. (2002b), Photochemical production of nitrous acid on glass sample manifold surface, *Geophys. Res. Lett.*, *29*, 26/21-26/24.

GAS PHASE PROCESSES RELEVANT TO THE MEDITERRANEAN SOME NEW AND IMPORTANT TOPICS

IAN BARNES[1] AND IUSTINIAN BEJAN[1,2]
[1]*Bergische University Wuppertal, Fachbereich C – Physical Chemistry Department, Gauss Strasse 20, D-42119 Wuppertal, Germany*
[2]*Alexandru Ioan Cuza "University of Iasi, Faculty of Chemistry, Dept. of Analytical Chemistry, Carol I Boulevard 11, 700506 Iasi, Romania*

Key Words: Secondary organic aerosol; hydroxyl radicals; nitrate radicals.

Abstract This manuscript is a written version of the talk presented at the NATO ARW. The paper is not designed as a general overview of gas-phase processes, rather the intention has been to try and highlight work that has been going on gas-phase processes which have possible important conesquences for the complex chemistry occurring in the Mediterranean atmosphere. The manuscript is constrained to chemical processes involved in the gas-phase photooxidation of volatile organic compounds (VOCs).

1. Introduction

The Mediterranean region is rich in vegetation and the intense solar radiation and high temperatures result in high emissions of biogenic NMVOCs (non-methane volatile organic compounds) to the atmosphere. These biogenic emissions consist to a large extent of monoterpenes and isoprene. The biogenic VOC mix is often augmented by inflows of polluted air containing anthropogenic VOCs and nitrogen oxides (NO_x = NO + NO_2) emitted from industrial regions. The anthropogenic VOCs are often dominated by emissions from combustion sources, i.e., they contain substantial levels of aromatic compounds. There are indications that the summertime ozone (O_3) levels are considerably enhanced over the entire Mediterranean and that the aerosol radiative forcing is among the highest in the world (Lelieveld et al., 2002).

Both the biogenic and anthropogenic VOCs are subject to gas phase photooxidation, to a large extent by the hydroxyl radical (OH) during the daytime but for compounds containing unsaturated C=C bonds oxidation by ozone (O_3) can also be important. During the night reactions of VOCs with the nitrate radical (NO_3) dominate. These gas-phase oxidation processes lead to the formation of the high levels of ozone, other photooxidants and aerosol, which have been observed in the summertime Mediterranean

A. Mellouki and A.R. Ravishankara (eds.), Regional Climate Variability and its Impacts in the Mediterranean Area, 235–251.

(Lelieveld et al., 2002) and have serious detrimental consequences for human health and vegetation growth within the Mediterranean area. The average levels of summertime O_3 in the Mediterranean area can vary between 50 and 85 ppbv (Sanz and Millán, 1998; Kalabokas et al., 2007 and references therein).

Our understanding of the gas phase oxidation processes of VOCs has increased tremendously during the last two decades. The aim of the manuscript, as stated in the abstract, is not to give a general overview of gas-phase tropospheric processes but rather to show the typical VOC and oxidant levels prevailing in the Mediterranean area and highlight some of the main areas of uncertainty in our knowledge of the gas-phase processes, which often result in high levels of oxidant and aerosol formation in this region.

For anyone not familiar with the subject matter and who wishes a broad overview of the topic under discussion the following books and articles should be of assistance:

- general atmospheric chemistry (Finlayson-Pitts and Pitts, 2000)
- general chemistry of volatile organic compounds (VOCs) (Atkinson, 1989, 1990, 1994, 1998, 2000; Atkinson and Arey, 2003a)
- alkane chemistry (Atkinson, 1997)
- alkene chemistry (Atkinson, 1997; Calvert et al., 2000)
- aromatic hydrocarbon chemistry (Calvert et al., 2002)
- biogenic hydrocarbon chemistry (Atkinson and Arey, 2003b)
- oxygenated VOC chemistry (Mellouki et al., 2003)
- dimethyl sulphide chemistry (Barnes et al., 2006)

Good overviews of atmosphere aerosols can be found in Seinfeld and Pandis (1998) and Kanakidou et al. (2005). Actual kinetic data for the reactions of the atmospherically relevant reactive species OH and NO_3 radicals and O_3 with VOCs can be found in Atkinson et al. (2005).

2. VOC and Radical Levels in the Mediterranean

2.1. BIOGENIC AND ANTHROPOGENIC VOCS LEVELS

Biogenic volatile organic compounds such as isoprene (2-methyl-1,3-butadiene; $CH_2=C(CH_3)-CH=CH_2$) and monoterpenes are known to play key roles in the photooxidation chemistry of the Mediterranean (e.g., Fehsenfeld et al., 1992; Harrison et al., 2001; Cortinovis et al., 2005; Liakakou et al., 2007 and references therein). Although biogenic VOC emissions tend to dominate in the general Mediterranean area in some Mediterranean urban and industrial sites emissions of anthropogenic VOCs and NO_x are quite substantial. In addition, transport of polluted air from

other regions of Europe is also a source of anthropogenic VOCs, in particular, aromatic hydrocarbons (see for example: Cortinovis et al., 2005; Gros et al., 2003; Liakakou et al., 2007; Xu et al., 2003). The input of different levels of anthropogenic VOCs and NO_x leads to large variations in the VOC/NO_x ratio over the Mediterranean and thus the oxidising capacity of the affected area and the gas phase chemical processes, which occur within the area. Typical concentrations of aromatic hydrocarbons, which can be present in polluted air parcels in the Mediterranean, are shown in Table 1 (Xu et al., 2003).

TABLE 1. Anthropogenic aromatic hydrocarbon concentrations observed in polluted air masses in the Mediterranean, e.g., for Finokalia, Crete during the MINOS campaign, and mixing ratios in the Greater Athens Area (GAA) (Xu et al., 2003)

Compound	**mean+1σ (pptv)**	**Range (pptv)**	**GAA Mean (ppbv)**
toluene	11 ± 7	0.3 – 38	16
ethylbenzene	8 ± 6	0.2 – 21	20
p/m-xylene	11 ± 6	0.5 – 27	16
o-xylene	8 ± 5	0.3 – 18	11
propylbenzene	43 ± 36	6 – 250	48
1,2,3-trimethylbenzene	7 ± 4	0.2 – 22	43
1,35-trimethylbenzene	12 ± 7	1.7 – 33	–
benzacetaldehyde	25 ± 18	0.7 – 70	19

The levels of isoprene and monoterpenes emitted to the atmosphere can be highly variable (Guenther et al., 1992). In Finokalia/Crete, for example, the isoprene concentration has been observed to vary between 5-1200 pptv, the mean value in summertime is the area is around 100 pptv (Liakalou et al., 2007). The annual isoprene emissions in Greece alone from trees have been estimated to be (132 ± 29) kT yr^{-1} (Harrison et al., 2001). There are numerous papers reporting biogenic emissions from vegetation in the Mediterranean area, e.g., an overview of the emissions of the C5 and C10 hydrocarbons, isoprene and monoterpenes from different plant species in five different Mediterranean habitats can be found in Owen et al., (2001) and Parra et al., (2004) give estimates of the biogenic emissions of NMVOCs from vegetation in the North Western Mediterranean. Quantitative information on the emission rates of selected reactive gases from vegetation in the Mediterranean basin can also be found in reports from the European Community funded project BEMA (Biogenic emissions in the Mediterranean Area (Kesselmeier et al., 1996; *http://cordis.europa.eu/data/PROJ_ENV/ACTIONeqDndSESSIONeq12999200595ndDOCeq5ndTBLeqEN_PROJ.htm*).

2.2. RADICAL LEVELS

There have been virtually no direct measurements of the radical levels of OH and HO_2 in the Mediterranean area. Two campaigns in which OH was directly measured have shown high OH radical concentration maxima around midday during the summertime.

During the AEROBIC97 campaign OH and HO_2 radicals were measured over a forested region in north-western Greece during July and August 1997 (Carslaw et al., 2001). During the campaign mean averaged concentrations between 3.1-6.4 × 10^6 and 0.89-6.1 × 10^8 molecules cm^{-3} were measured for OH and HO_2 radicals, respectively. During the MINOS campaign, conducted at Finokalia on the north-eastern coast of Crete, OH radicals were measured between 28 July-18 August 2001 (Berresheim et al., 2003). The OH radical levels showed a strong diurnal variability with high maxima of ~2 × 10^7 molecules cm^{-3} occurring around13-14 h LT and nightime values below the detection limit of around 2.4 × 10^5 molecules cm^{-3}. The daily 24-hour average concentrations were found to vary between 3.6-6.7 × 10^6 molecules cm^{-3}.

A general overview of nitrate radicals in the troposphere can be found in Platt and Heintz (1994). However, as for OH and HO_2 radicals there have been very few measurements of NO_3 radicals in the Mediterranean area. During the above-mentioned MINOS campaign at Finokalia NO_3 radicals were measured simultaneously with OH. The NO_3 radical concentrations ranged from 3 × 10^7 to 9 × 10^8 radicals cm^{-3} with an average nighttime value of 1.1 × 10^8 radicals cm^{-3} (Vrekoussis et al., 2004). The measurements were continued for more than two years (June 2001 – September 2003) and showed that in the area the NO_3 radicals follow a distinct seasonal dependency with the highest seasonally average mixing ratios in summer, (5.5 ± 1.2) pptv, and the lowest in winter, (1.2 ± 1.2) pptv (Vrekoussis et al., 2007). The series has shown that the highest NO_3 mixing ratios are attained mainly in polluted air masses which originate from mainland Greece, Central and East Europe and Turkey. Measurements of O_3, NO_2 and meteorological parameters were also made during the two-year observation period and the NO_2 data set is currently the most comprehensive overview of NO_2 temporal variability for the area.

2.3. REACTIVITY OF VOCS TOWARDS OXIDIZING SPECIES IN THE ATMOSPHERE

As stated in the Introduction the most important oxidants in the atmosphere, which initiate the gas phase oxidation of VOCs are OH during daylight hours, the NO_3 radical during the hours of darkness, and O_3 continually. Different classes of VOC show different reactivity toward these oxidants.

TABLE 2. Typical rate coefficients for the reactions of different classes of VOC with the atmospherically important reactive species O_3, OH and NO_3

VOC Class	Ozone (O_3)	OH	NO_3	Most important removal process
Alkanes Cycloalkanes	$<10^{-23}$	$0.3^{-8} \times 10^{-11}$	$<10^{-17}$	***OH***
Oxygenated aliphatics	$<2.2 \times 10^{-21}$	$0.2^{-6} \times 10^{-11}$	$<1.4 \times 10^{-16}$	***OH***
Aromatics	$<6 \times 10^{-21}$	$0.1^{-6} \times 10^{-11}$	$<10^{-17}$	***OH***
Alkenes cycloalkenes	2×10^{-18} – 1.5×10^{-15}	$0.8^{-12} \times 10^{-11}$	6×10^{-17} – 3×10^{-11}	***(NO3) O3, OH, NO3***

The rate coefficients for the reactions of OH, NO_3 and O_3 with the various classes of VOC found in the Mediterranean are listed in Table 2.

The table also lists the oxidant, which is dominant in oxidising the class of VOC. In general biogenics VOCs (isoprene and monoterpenes) are very reactive compared to most anthropogenic VOCs and because of the presence a double bond in their molecular structure will be subject to oxidation by all three oxidants to differing degrees. The atmospheric lifetime of a VOC with respect to oxidation by OH, NO_3 or O_3 is given by:

$$\tau_{OH} = 1/(k_{OH}[OH]) \qquad \tau_{NO3} = 1/(k_{NO3}[NO_3]) \qquad \tau_{OH} = 1/(k_{O3}[O_3])$$

where k_{OH}, $k_{NO3,}$ and k_{O3} are the rate coefficient of the VOC with the reactive species and [OH], [NO_3], and [O_3] are the measured oxidant concentrations.

3. Current Issues in Gas Phase Chemistry Affecting the Mediterranean

3.1. ISOPRENE CHEMISTRY AND SECONDARY ORGANIC AEROSOL (SOA)

Isoprene is the second most abundant hydrocarbon emitted into the Earth's atmosphere. Up until a few years ago it considered that the gas phase chemistry with regard to its oxidation by OH radicals was well established the reaction leading to the formation of methacrolein, methyl vinyl ketone as major products and lower yields of hydroxynitrates, hydroxycarbonyls, 3-methylfuran and unsaturated-1,2-diols. It was assumed that all of these products remained in the gas phase and there was no indication from

laboratory studies for secondary aerosol formation. Extensive descriptions of the gas-phase chemistry of isoprene can be found in the Master Chemical Mechanism *http://www.chem.leeds.ac.uk/Atmospheric/MCM/mcmproj.html*) or Atkinson and Arey (2003a,b). A summary of heterogeneous and aqueous-phase transformations of isoprene can be found in Rudzinski (2006).

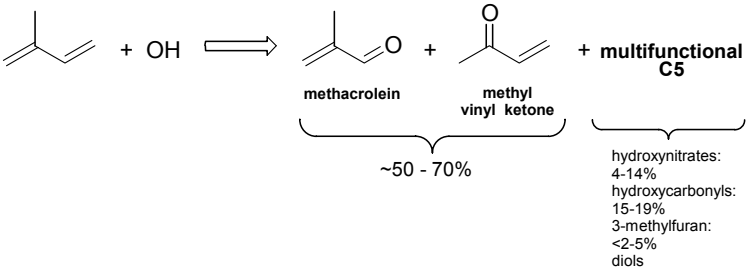

Figure 1. Products formed in the reaction of OH radicals with isoprene

In 2004 Claeys et al., (2004a, b) found two isomers of 2-methyl-butane-1,2,3,4-terols in aerosol samples collected over the Amazon rain forest and over the continental L-Pustzta forest in Hungary (Ion et al., 2005). Since then the tetrols have also found in aerosol samples in Melpitz, Germany (Böge et al., 2006), Hyytiälä, Finland (Kourtchev et al., 2005) and in the eastern United States (Edney et al., 2005; Xia and Hopke, 2006).

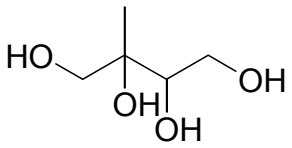

Figure 2. 2-methyltetrols: 2-methythreitol and 2-methylerythritol

Since the tetrols have the isoprene skeleton (see Figure 2), Claeys et al. (2004a) originally hypothesised that the tetrols were formed in the gas-phase oxidation of isoprene and condensed to aerosols. The proposed mechanism, however, required low NO_x conditions and since tetrols were also found under high NO_x conditions the gas-phase mechanism was later retracted (Claeys et al., 2004b) and acid-catalysed reaction of isoprene either heterogeneously or in the aqueous phase was proposed to explain the formation of the tetrols. Subsequent studies have also shown that isoprene may contribute to organic aerosol via heterogeneous or aqueous phase oxidation routes; these studies are summarised in Kroll et al. (2005) and Henze and Seinfeld (2006).

As isoprene is emitted in such large quantities to the atmosphere even a small SOA yield from it oxidation, as discussed by Henze and Seinfeld (2006), would have profound implications, not only for the sources of organic

aerosol in the Mediterranean area, but also globally. Since the publications of Claeys et al. (2004a, b) many studies have been made in many laboratories to try and establish whether the gas-phase oxidation of isoprene produces SOA. The results from these investigations have been mixed with some studies showing aerosol formation and others not. The extensive set of experiments are those from the Seinfeld group in the USA in which they have investigated the gas-phase oxidation of isoprene over a wide range of experimental conditions (Kroll et al., 2005; Kroll et al., 2006; Ng et al., 2006; Surratt et al., 2006). This set of comprehensive laboratory investigations supports that the OH radical initiated oxidation of isoprene forms SOA. SOA yields of 1-2% were found at high NO_x levels and around 3% at low NO_x levels (Kroll et al., 2005, 2006). The following bullet points list some of the important results, which emerged from the studies:

- at high NO_x yields were found to decrease substantially with increasing [NO_x] which is taken to indicate the importance of RO_2 chemistry (Kroll et al., 2006)
- time delay in SOA formation and continuous growth after complete consumption of isoprene suggests SOA is mainly coming from the further oxidation of first-generation products (Ng et al., 2006)
- a large fraction of SOA growth is likely related to the oxidation of methacrolein (Kroll et al., 2005; Ng et al., 2006; Surratt et al., 2006)

methacrolein: 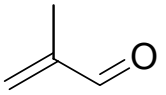

- oligomerization was observed to be an important SOA formation pathway under all conditions (Surratt et al., 2006)
- the nature of the oligomers depends strongly on the NO_x level (Surratt et al., 2006)
- acidic products formed only under high NO_x conditions (Surratt et al., 2006)
- further oxidation of the gas phase product methacrolein under high NO_x conditions produces polyesters involving 2-methylglyceric acid as a key monomeric unit (Surratt et al., 2006)
- these oligomers comprise ~22-34% of the high-NO_x SOA mass (Surratt et al., 2006)
- organic peroxides contribute significantly to the low-NO_x SOA mass (up to ~60%) (Surratt et al., 2006)

Because of the implications of the results from the Seinfeld group with respect to the yield of SOA from the oxidation of isoprene it is important that the results are validated in independent studies in other laboratories.

3.2. OZONOLYSIS OF ALKENES AND SOA

Klotz et al. (2004) have observed the formed of low yields of SOA in the ozonylsis of methyl vinyl ether. The results were reproducible and no formation of SOA was observed for the OH and NO_3 initiated oxidation of the ether.

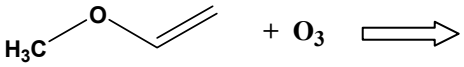

CH_3OCHO (formate) + HCHO + CH_2OO (*CI*) + CH_3OCHOO (*CI*) + SOA formation (< 1% yield)

At that time methyl vinyl ether (MVE) was the smallest reported molecule for which SOA formation had been observed. The mechanism leading to the SOA formation and the chemical composition of the SOA were not known. In subsequent studies on other small vinyl ethers, within the European Community project MOST, formation of SOA in 1-3% yields was also observed.

Sadezky et al. (2006) have also studied the ozonolysis of several alkyl vinyl ethers (EVE, PVE, n-BVE, t-BVE, EPE) and investigated the formation of SOA and also the chemical composition of the SOA using mass spectrometry. They measured SOA yields between 2 and 4% for the vinyl ethers. However, they found that the SOA was strongly reduced in the present of formic acid and water, both compounds, which efficiently scavenge the stabilised Criegee Intermediates (CI) formed in the ozonolyis. Chemical analysis of the SOA showed the formation of oligimeric compounds with repetitive chain units. These chain units had the mass as the major Criegee intermediates formed during the ozonolysis of the ethers:

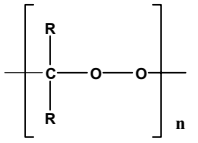

R = H,CH_3 etc.

The formation of oligomers in the ozonolysis of alkyl vinyl ethers observed by Sadezky et al. (2006), which contain the Criegee biradical structural entity, and the large decrease in the SOA yield on adding a CI scavenger to the reaction systems strongly support a major role of CI in the SOA formation observed in the "dry" ozonolysis of alkyl vinyl ethers, i.e. possible reaction of the CI with the double bond. If this is the case, addition of a CI scavenger, such as water or HCOOH, will very effectively transform the CI to highly volatile hydroperoxides thus hindering reaction of the CI with the alkyl vinyl ether double bond and reducing SOA formation.

If reaction of the Criegee biradical with the double bond in the ozonolysis of alkyl vinyl ethers is the major route to the SOA formation as the results

of Sadezky et al. (2006) appear to suggest then the SOA formation from the ozonolysis of alkyl vinyl ethers will be of negligible importance under atmospheric conditions due to scavenging of the Criegee biradicals by the high concentrations of water vapour constantly present in the atmosphere. However, if the SOA observed in the ozonolysis of alkyl vinyl ethers via reaction of the CI with the double bond is a general phenomenon for alkenes then it needs to be taken into account in all SOA studies on the ozonolysis of alkenes performed under dry conditions. This would also apply to the SOA formation studies for isoprene discussed in the section 3.1.

3.3. PHOTOOXIDATION OF BENZENE

The conventional wisdom for many years has been that the photooxidation of benzene, in contrast to the alkylbenzenes, does not form SOA. However, experiments performed in EUPHORE outdoor simulation chamber in Valencia, Spain have clearly demonstrated that this assumption is clearly in error (Martín-Reviejo and Wirtz, 2005). Experiments were performed for a variety of NO_x regimes and high aerosol yields have been obtained.

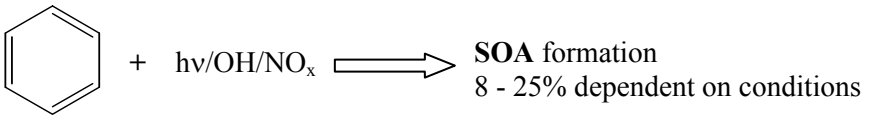

The SOA yields are comparable to those obtained during the photooxidation of other aromatic compounds under similar conditions. The work has clearly demonstrated the strong influence that the level of NO_x has on aromatic photooxidation systems and highlighted to need to perform SOA studies on the photooxidation of aromatic hydrocarbons at NO_x levels pertinent to the atmosphere.

3.4. NITOPHENOLS A NEW PHOTOLYIC SOURCE OF NITROUS ACID (HONO)

Among the different classes of anthropogenic VOCs emitted to the atmosphere aromatic hydrocarbons are of particular significance. They contribute appreciably to photooxidant and SOA formation and are associated with human health problems. Nitrophenols are a class of aromatic compound with carcinogenic and phytotoxic properties; it has been implied that they play a role forest decline.

Nitrophenols can be emitted directly into the atmosphere or they can be formed via the photooxidation of aromatic hydrocarbons (Harrison et al.,

2005). The reaction of all aromatic hydrocarbons with OH radicals in the presence of NO_x produce nitrophenols to differing degrees. The reaction of NO_3 radicals with hydroxylated aromatic compounds produces nitrophenols in high yields (Calvert et al., 2002).

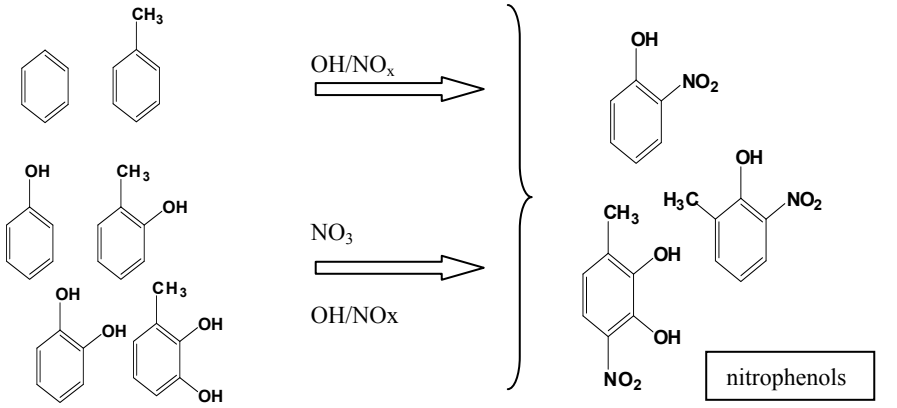

Until recently, very little was known about the atmospheric fate of nitrophenols. Rate coefficients have now been determined for the reaction of OH radicals with a number of nitrophenols (Bejan *et al*., 2006b, 2007)

TABLE 3. Rate coefficients for the reactions of OH radicals with nitrophenols at 298 K and atmospheric pressure (Bejan et al., 2006b, 2007)

Compound	$\mathbf{k_{OH}}$ **(cm^3 molecule^{-1} s^{-1})**
Nitrophenol (NP)	$\sim 1 \times 10^{-12}$
3-methyl-2-nitrophenol (3M2N)	$(3.69 \pm 0.70) \times 10^{-12}$
4-methyl-2-nitrophenol (4M2NP)	$(3.59 \pm 1.17) \times 10^{-12}$
5-methyl-2-nitrophenol (5M2NP)	$(6.72 \pm 2.14) \times 10^{-12}$
6-methyl-2-nitrophenol (6M2NP)	$(2.70 \pm 0.57) \times 10^{-12}$

Nitrophenols are only moderately reactive toward OH radicals; with the high OH radical levels prevailing in the Mediterranean during the summertime they will have atmospheric lifetimes ranging from 1-2 days up to ~5 h with respect to photooxidation by OH during this season. All nitrated aromatic hydrocarbons absorb in the atmospherically relevant actinic region 300-400 nm, an example is shown in Figure 3 for of the liquid phase absorption spectrum of 3-methyl-2-nitrocresol.

The gas-phase UV spectra of the nitrophenols are not expected to be very much different to those recorded in the liquid phase. Previously, photolysis of nitrophenols was thought to be fairly slow and the main photolysis pathway was thought to production of NO_2 and the corresponding hydroxylated

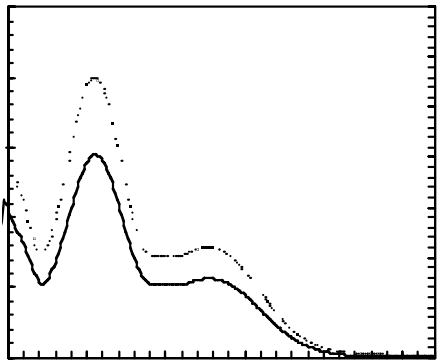

Figure 3. Liquid-phase absorption spectrum of 3-methyl-2-nitrocresol

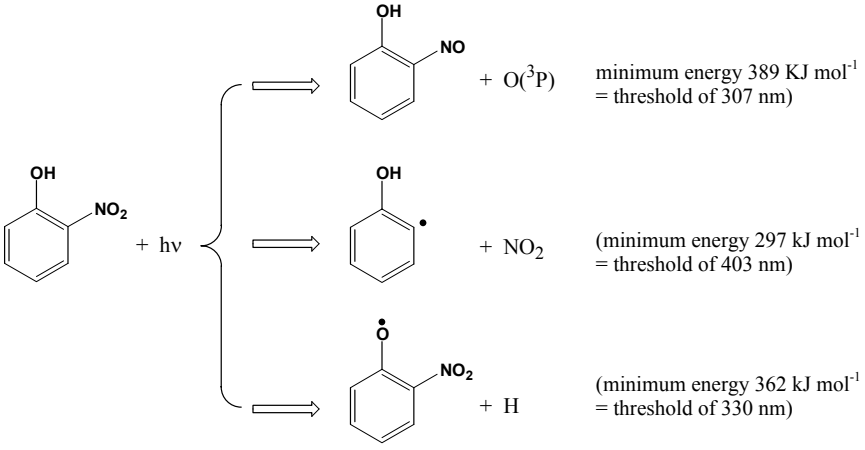

Figure 4. Pathways for the photolysis of 2-nitrophenol (Calvert et al., 2002)

phenyl radical (Calvert et al., 2002). Possible photolysis pathways for 2-nitrophenol are shown in Figure 4.

It has been shown recently that the photolysis of 2-nitrophenol and its methylated derivatives produce nitrous acid (HONO) (Bejan et al., 2006a). No evidence was found in these experiments for the production of NO_2. At present the photolysis mechanism is still speculative; it is though to involve an intramolecular H-atom transfer from the OH group to the NO_2 group substituent with subsequent cleavage of HONO and possibly formation of a biradical.

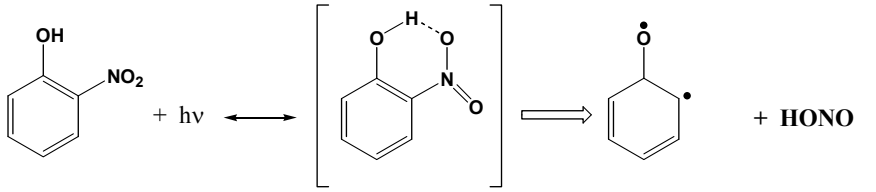

However, the measured HONO production rates and the measured nitrophenol photolysis frequencies suggest that a large fraction of the photolysis is producing products other that HONO, therefore, other pathways must also be occurring. The photolysis of the nitrophenols has been shown to be very effective in producing SOA, SOA formation is observed on conversion of very low concentrations of the compounds (Bejan, 2007). It is possible that their photolysis may play a key role in initiating the SOA formation observed in the photolysis of aromatic compounds. Atmospheric photolysis frequencies of between 40 min to 3 h have been estimated for the nitrophenols, which implies that photolysis will be the major gas-phase atmospheric loss process for the nitrophenols.

To our knowledge there have been no measurements of nitrophenols in the Mediterranean area, however, the large aromatic content of the polluted air masses which traverse the area (Gros et al., 2003; Liakakou et al., 2007; Xu et al., 2003) suggest that they should be present in appreciable quantities and active in the photochemistry of the area.

Nitrous acid is of considerable atmospheric interest since its photolysis leads to the formation of OH radicals, the key atmospheric oxidant in the degradation of most air pollutants and a crucial intermediate in the formation of photochemical smog in the troposphere. Recent field studies have demonstrated that the contribution of HONO to the oxidation capacity of the atmosphere has been greatly underestimated and demonstrated the existence of yet unknown daytime sources of HONO (Kleffmann et al., 2005; Kleffman, 2007). The photolysis of the nitrophenols to produce HONO as reported by Bejan et al. (2006a) can explain, at least partly, the large contribution of HONO to the oxidation capacity of the urban atmosphere recently established in field campaigns.

Although field measurements have highlighted the large contribution of HONO to the oxidising capacity of the atmosphere, HONO is a species, which is currently not represented in most atmospheric chemistry models. Because of the existence of diverse production pathways for HONO in the atmosphere, such as heterogeneous and gas phase photolytic pathways, the parameterisation of HONO in models will not be an easy task. It is an endeavour, which needs to be undertaken if the chemistry occurring in regions such as

the Mediterranean is to be correctly modelled and understood. Measurements of the atmospheric concentration levels and seasonal variability of HONO at different locations in the Mediterranean region should therefore be implemented.

3.5. NITRATE RADICAL CHEMISTRY

Nitrate radicals, NO_3, are formed in the atmosphere nearly exclusively through the reaction of NO_2 with O_3:

$$NO_2 + O_3 \rightarrow NO_3 + O_2$$

Equilibrium is quickly established between NO_3 und NO_2:

$$NO_3 + NO_2 + M \leftrightarrow N_2O_5 + M$$

Due to this equilibrium the behaviour of NO_3 und N_2O_5 in the atmosphere is strongly coupled. Nitrate radicals are rapidly destroyed during the day by photolysis and reaction with NO:

$$NO_3 + NO \rightarrow 2NO_2$$

$$NO_3 + h\nu\ (\lambda < 580\ nm) \rightarrow NO_2 + O$$

$$\rightarrow NO + O_2$$

The photolytic lifetime of the NO_3 radical during the day is globally on average ca. 5 s. Since the reaction of NO_3 with NO is very rapid (2.6×10^{-11} cm^3 $molecule^{-1}$ s^{-1} by 295 K) NO concentrations of ~0.4 ppbV are sufficient to limit the lifetime of NO_3 radicals in the troposphere also to 5 s. NO_3 radical concentrations are, therefore, very often less than 0.1 pptV during the day. In the night destruction of NO_3 via photolysis is not operative, and the NO concentrations are extremely low because of the reaction of NO with O_3; these circumstances allow measurable concentrations of NO_3 radicals to be formed. During the night the main sinks for NO_3 radicals are reactions with NMVOCs and heterogeneous reactions of NO_3 or N_2O_5 on surfaces.

Measurements performed at Finokalia, Crete have demonstrated quite vividly the important contribution of NO_3 radical chemistry to the nighttime chemistry of the Mediterranean area (Vrekoussis et al., 2004, 2006, 2007).

The Crete measurements constitute first time measurements on the seasonal variability of the NO_3 radical in the area. As stated in section 2.2, distinct seasonal pattern was observed for the NO_3 radical with the highest mixing ratios being observed in summer, (5.6 ± 1.2) pptv, and the lowest in winter, (1.2 ± 1.2) pptv. The highest NO_3 radical mixing ratios were detected in polluted air masses originating from other parts of Europe.

The work has demonstrated the important role of NO_3 in regulating the nighttime chemistry of dimethyl sulphide (CH_3SCH_3; DMS). The loss of

DMS during the night through reaction with NO_3 was estimated to be about 75% of that by the OH radical during the day. The initial pathway in the reaction of NO_3 with DMS is thought to result in the 100% conversion of NO_3 to nitric acid (Barnes et al., 2006).

$$CH_3SCH_3 + NO_3 \rightarrow CH_3SCH_2 + HNO_3$$

It was estimated that reactions of NO_3 and N_2O_5 account for about 21% of the total nitrate ($HNO_{3(g)} - NO_{3(g)}^-$) measured in the area. It has been estimated that nighttime NO_3 initiated VOC oxidation is also more important than that with OH radicals for the monoterepenes (Vrekoussis et al., 2007).

Hydroxylated aromatic compounds (phenols) are a class of VOC, which are very reactive toward NO_3 radicals (Calvert et al., 2002). As indicated in section 3.4 reaction of NO_3 with aromatic hydrocarbons, especially phenols, will lead to formation of nitrophenols, the photolysis of which will form HONO an important OH radical source. It would be interesting to make some field measurements of the levels of nitroaromatics in the region and estimate their contribution to HONO production and thus the oxidising capacity of the region.

4. Acknowledgments

Financial support for travel expenses by the European Community 6th Framework programme project EUROCHAMP is gratefully acknowledged.

5. References

Atkinson, R., 1989, Kinetics and mechanisms of the gas-phase reactions of the hydroxyl radical with organic compounds, *J. Phys. Chem. Ref. Data*, Monograph No. 1.

Atkinson, R., 1990, Gas-phase tropospheric chemistry of organic compounds: A review, *Atmos. Environ*. **24A**:1-41.

Atkinson, R., 1994, Gas-phase tropospheric chemistry of organic compounds, *J. Phys. Chem. Ref. Data*, Monograph No. **2**, 1-216.

Atkinson, R., 1997, Gas-phase tropospheric chemistry of volatile organic compounds: 1. Alkanes and alkenes, 1997, *J. Phys. Chem. Ref. Data* **26**(29):215-290.

Atkinson, R., 1998, Gas-phase degradation of organic compounds in the troposphere, *Pure & Appl. Chem.* **70**(7):1335-1343.

Atkinson, R., 2000, Atmospheric chemistry of VOCs and NO_x, *Atmos. Environ*. *34*:2063-2101.

Atkinson, R., Baulch, D.L., Cox, R.A., Crowley, J.N., Hampson, R.F., Jr., R.G. Hynes, R. G., Jenkin, M.E., Kerr, J.A., Rossi, M.J., Troe, J., 2005, *Summary of Evaluated Kinetic and Photochemical Data for Atmospheric Chemistry,* IUPAC Subcommittee on Gas Kinetics Data Evaluation for Atmospheric Chemistry, Web Version, www.iupac-kinetic.ch.cam.ac.uk, University of Cambridge, UK.

Atkinson, R., Arey, J., 2003a, Atmospheric degradation of volatile organic compounds, *Chem. Rev.*, **103**:4605-4638.

Atkinson, R., Arey, J., 2003b, Gas-phase tropospheric chemistry of biogenic volatile organic compounds: a review *Atmos. Environ*. **37**(2)*:*S197-S219.

Barnes, I., Hjorth, J., and Mihalopoulos, N., 2006, Dimethyl sulfide and dimethyl sulfoxide and their oxidation atmosphere, *Chem. Rev*. **106**:940-975.

Bejan, I., 2007, PhD thesis, Bergische University Wuppertal, Germany.

Bejan, I., Abd El Aal, Y., Barnes, I., Benter, Th., Bohn, B., Wiesen, P., and Kleffmann, J., 2006a, The photolysis of ortho-nitrophenols: a new gas phase source of HONO, Phys. Chem. Chem. Phys. **8**:2028-2035.

Bejan, I., Barnes, I., Olariu, R., and Zhou, S., 2007, Investigations on the gas-phase OH radical kinetics and photolysis of methylated *2*-nitrophenols, *Phys. Chem. Chem. Phys*., in press.

Bejan, I., Barnes, I., Olariu, R., Becker, K.H., and R. Mocanu, R., 2006b, FT-IR Study of the kinetic gas-phase reactions of the OH radical with a series of nitroaromatic compounds, in: *Environmental Simulation Chambers: Application to Atmospheric Chemical Processes,* I. Barnes and K.J. Rudzinski (eds), *NATO* Science Series, IV. Earth and Environmental Sciences, Vol. **62**, Springer, Amsterdam, pp. 155-162.

Berresheim, H., Plass-Dülmer, C., Elste, T., Mihalopoulos, N., Rohrer, F., 2003, OH in the coastal layer of Crete during MINOS: Measurements and relationship with ozone photolysis, *Atmos. Chem. Phys.* **3**:639-649.

Böge, O., Miao, Y., Plewka, A., and Herrmann, H., 2006, Formation of secondary organic particle phase compounds from isoprene gas-phase oxidation products: An aerosol chamber and field study, *Atmos. Environ*. **40**:2501-2509.

Calvert, J.G., Atkinson, R., Kerr, J.A., Madronich, S., Moortgat, G.K.; Wallington, T.J., Yarwood, G. *The Mechanisms of Atmospheric Oxidation of Alkenes*, **2000**, Oxford University Press, New York.

Calvert, J., Atkinson, R., Becker, K. H., Kamens, R., Seinfeld, J., Wallington, T., and Yarwood, G., 2002, *The Mechanisms of the Atmospheric Oxidation of Aromatic Hydrocarbons,* Oxford University Press.

Carslaw, N., Jacobs, P.J., Creasey, D.J., Harrison, D., Heard, D.E., Hunter, M.C., Lee, J.D., Lewis, A.C., Pilling, M.J., Saunders, S.M., Seakins, P.W., Jenkin, M.E., 2001. A Modelling study of OH and HO_2 Radical Chemistry in a Forested Region of North-Western Greece. *Atmos. Environ*. **35**:4725-4737.

Claeys M., Graham, B., Vas, G., Wang, W., Vermeylen, R., Pashynska, V., Cafmeyer, J., Guyon, P., Andreae, M.O., Artaxo, P., and W. Maenhaut, W., 2004a, Formation of secondary organic aerosols through photooxidation of isoprene, *Science* **303**:1173-1176.

Claeys M., Wang, W., Ion, A.C., Kourtchev, I., Gelencser, A., and Maenhaut, W., 2004b, Formation of secondary organic aerosols from isoprene and its gas-phase oxidation products through reaction with hydrogen peroxide, *Atmos. Environ.* **38**:4093-4098.

Cortinovis, J., Solmon, F., Serça, D., Sarrat, C., and Rosset, R., 2005, A simple modeling approach to study the regional impact of a Mediterranean forest isoprene emission on anthropogenic plumes, *Atmos. Environ*. **5**:1915-1929.

Edney, E.O., Kleindienst, T.E., Jaoui, M., Lewandowski, M., Offenberg, J.H., Wang, W., and Claeys, M., 2005, Formation of 2-methyl tetrols and 2-methylglyceric acid in secondary organic aerosol from laboratory irradiated isoprene/NO_x/SO_2/air mixtures and their detection in ambient $PM_{2.5}$ samples collected in the eastern United States, *Atmos. Environ*. **39**:5281-5289.

Fehsenfeld, F., Calvert, J., Goldan, P., Guenther, A.B., Hewitt, C.N., Lamb, B., Liu, S., Trainer, M., Westberg, H. and Zimmerman, P., 1992. Emissions of volatile organic compounds from vegetation and the implications for atmospheric chemistry. *Global Biogeochemical Cycles* 6 **4**, pp. 389-430.

Finlayson-Pitts, B.J., Pitts, J.N. Jr., 2000, *Chemistry of the Upper and Lower Atmosphere: Theory, Experiments and Applications,* Academic Press, San Diego, CA; London.

Gros, V., Williams, J., van Aardenne, J.A., Salisbury, Hofmann, G.R., Lawrence, M.G., von Kuhlmann, R., Lelieveld, J., Krol, M., Berresheim, H., Lobert, J.M., and Atlas, E., 2003, Origin of anthropogenic hydrocarbons and halocarbons measured in the summertime european outflow (on Crete in 2001), *Atmos. Chem. Phys*. **3**:1223-1235.

Guenther, A.B., Zimmerman, P.R., Harley, P.C., Monson, R.K. and Fall, R., 1993. Isoprene and monoterpene emission rate variability—model evaluations and sensitivity analyses. Journal of Geophysical Research **98** D7, pp. 12609-12617.

Harrison, D., Hunter, M.C., Lewis, A.C., Seakins, P.W., Nunes, T.V., and Pio, C.A., 2001, Isoprene and monoterpene emission from the coniferous species Abies Borisii-regis—implications for regional air chemistry in Greece, *Atmos. Environ*. **35**:4687-4698.

Harrison, M.A.J., Barra, S., Borghesi, D., Vione, D., Arsene, C., and Olariu, R.I., 2005, Nitrated phenols in the atmosphere: a review, *Atmos. Environ*. **39**:231-248.

Henze, D.K., and Seinfeld, J.H., 2006, Global secondary organic aerosol from isoprene oxidation, *Geophys. Phys. Res. Lett*. **33**:L09812, doi:10.1029/2006GL025976.

Ion, A. C., Vermeylen, R., Kourtchev, I., Cafmeyer, J., Chi, X., Gelencse´r, A., Maenhaut, W., Claeys, M., 2005, Polar organic compounds in rural PM2.5 aerosols from K-puszta, Hungary, during a 2003 summer field compaign: sources and diel variations, *Atmos. Chem. Phys.* **5**:1805-1814.

Kalabokas, P.D., Volz-Thomas, A., Brioude, J., Thouret, V., Cammas, J.-P., and Repapis, C.C., 2007, Vertical ozone measurements in the troposphere over the Eastern Mediterranean and comparison with Central Europe, *Atmos. Chem. Phys. Discuss*. **7**:2249-2274.

Kanakidou, M., Seinfeld, J.H., Pandis, S.N., Barnes, I., Dentener, F.J., Facchini, M.C., Van Dingenen, R., Ervens, B., Nenes, A., Nielsen, C.J., Swietlicki, E., Putaud, J.P., Balkanski, Y., Fuzzi, S., Horth, J., Moortgat, G.K., Winterhalter, R., Myhre, C.E.L., Tsigaridis, K., Vignati, E., Stephanou, E.G., and Wilson, J., 2005, Organic Aerosol and Global Climate Modelling: A Review, *Atmos. Chem. Phys*. **5**:1053-1123.

Kesselmeier, J., Schäfer, L., Ciccioli, P., Brancaleoni, E., Cecinato, A., Frattoni, M., Foster, P., Jacob, V., Denis, J., Fugit, J.L., Dutaur, L., Torres, L., 1996, Emission of monoterpenes and isoprene from a Mediterranean oak species Quercus ilex L. measured within the BEMA (Biogenic Emissions in the Mediterranean Area) project, *Atmos. Enviro*n. **30**(10-11):1841-1850.

Kleffman, J., 2007, Daytime sources of nitrous acid (HONO) in the atmospheric boundary layer, *Chem. Phys. Chem*., submitted.

Kleffmann, J., Gavriloaiei, T., Hofzumahaus, A., Holland, F., Koppmann, R., Rupp, L., Schlosser, E., Siese, M., and Wahner, A., 2005, Daytime formation of nitrous acid: A major source of OH radicals in a forest, *Geophys. Res. Lett*. **32**:Lo5818, doi: 10.1029/2005GL022524.

Klotz, B., Barnes, I., and Imamura,T., 2004, Product study of the gas-phase reacions of O_3, OH and NO_3 radicals with methyl vinyl ether, *Phys. Chem. Chem. Phys*. **6***:*1725-1734.

Kourtchev, I., Ruuskanen, T., Gelencse'r, A., Maenhaut, W., Claeys, M., 2005, Observation of 2-methyltetrols and related photooxidation products of isoprene in boreal forest aerosols from Hyytiälä, Finland. *Atmos. Chem. Phys.* **5**:2761-2770.

Kroll, J.H., Ng, N.L., Murphy, S.M., Flagan, R.C., and Seinfeld, J.H., 2005, Secondary organic aerosol formation from isoprene photooxidation under high-NOx conditions, *Geophys. Res. Letters*, **32**:L18808, doi:10.1029/2005GL023637.

Kroll, J.H., Ng, N.L., Murphy, S.M., Flagan, R.C., and Seinfeld, J.H., 2006, Secondary organic aerosol formation from isoprene photooxidation, *Environ. Sci Technol*, **40**:1869-1877.

Lelieveld, J., Berresheim, H., Borrmann, S., Crutzen, P.J., Dentener, F.J., Fischer, H., Feichter, J., Flatau, P. J., Heland, J., Holzinger, R. Korrmann, R., Lawrence, M.G., Levin, Z., Markowicz, K. M., Mihalopoulos, N., Minikin, A., Ramanathan, V., de Reus, M., Roelofs, G.J., Scheeren, H.A., Sciare, J., Schlager, H., Schultz, M., Siegmund, P., Steil, B., Stephanou, E.G., Stier, P., Traub, M., Warneke, C., Williams, J., and Ziereis, H., 2002, Global air pollution crossroads over the Mediterranean, *Science*, **298** (5594):794-799.

Liakakou, E., Vrekoussis, M., Bonsang, B., Donousis, Ch., Kanakidou, M., and Mihalopoulos, N., 2007, Atmos. Environ. **41**(5):1002-1012.

Martín-Reviejo, M. and Wirtz, K., 2005, Is benzene a precursor for secondary organic aerosol, *Environ. Sci Technol*, **39**:1045-1054.

Mellouki, A., Le Bras, G., and Sidebottom, H., 2003, Kinetics and mechanisms of the oxidation of oxygenated organic compounds in the gas phase, *Chem. Rev.* **103**:5077-5096.

Ng, N.L., Kroll, J.H., Keywood, M.D., Bahreini, R., Varutbangkul, V., Flagan, R.C., Seinfeld, J.H., Lee, A., and Goldstein, A.H., 2006, Contribution of first- versus second-generation products to secondary organic aerosols formed in the oxidation of of bigenic hydrocarbons, *Environ. Sci Technol*, **40**:2283-2297.

Owen, S.M., Boissard, C., and Hewitt, C.N., 2001, Volatile organic compounds (VOCs) emitted from 40 Mediterranean plant species: VOC speciation and extrapolation to habitat scale, *Atmos. Environ*. **35**(32):5393-5409.

Parra, R., Gassó, S. and Baldasano, J.M., 2004, Estimating the biogenic emissions of non-methane volatile organic compounds from the North Western Mediterranean vegetation of Catalonia, Spain, *Sci. Total Environ*. **329**(1-3):241-259.

Platt, U. and Heintz, F., 1994, Nitrate radicals in tropospheric chemistry, Israel J. Chem. **34**:289-300.

Rudzinski, K.J., 2006, Heterogeneous and aqueous-phase transformations of isoprene, in: *Environmental Simulation Chambers: Application to Atmospheric Chemical Processes,* I. Barnes and K.J. Rudzinski (eds), *NATO* Science Series, IV. Earth and Environmental Sciences, Vol. **62**, Springer, Amsterdam, pp. 261-277.

Sadezky, A., Chaimbault, P., Mellouki, A., Roempp, A., Winterhalter, R., Moortgat, G.K., Le Bras, G., 2006, Formation of secondary organic aerosol and oligmers from the ozonolysis of enol ethers, *Atmos. Chem. Phys*. **6**:5009-5024.

Sanz, M.J., and Millán, M.M., 1998, The dynamics of aged air masses and ozone in the Western Mediterranean: Relevance to forest ecosystems, *Chemosphere* **36**:1089-1094.

Seinfeld, J.H.; Pandis, S.N., 1998, Atmospheric Chemistry and Physics, J. Wiley, New York.

Surratt, J.D., Murphy, S.M., Kroll, J.H., Ng, N.L., Hildebrandt, L., Sorooshian, A., Szmigielski, R., Vermeylen, R., Maenhaut, W., Claeys, M., Flagan, R.C., and Seinfeld, J,H., 2006, Chemical composition of secondary organic aerosol formed from the photooxidation of isoprene, *J. Phys. Chem. A*, **110**:9665-9690.

Vrekoussis, M.; Kanakidou, M.; Mihalopoulos, M.; Crutzen, P. J.; Lelieveld, J.; Perner, D.; Berresheim, H.; Baboukas, E., 2004, Role of the NO_3 radical in the oxidation processes in the eastern Mediterranean troposphere during the MINOS campaign, *Atmos. Chem. Phys.* **4**:169-182.

Vrekoussis, M., Mihalopoulos, M., Gerasopoulos, E., Kanakidou, M., Crutzen, P., Lelieveld, J., 2007, Two-years of NO_3 radical observations in the boundary layer over the Eastern Mediterranean, *Atmos. Chem. Phys.* **7**:315-327.

Xia, X., and Hopke, 2006, Seasonal variation of 2-methyltetrols in ambient air samples, *Environ. Sci. Technol*. **40**(22):6934-6937.

Xu, X., Plass-Dülmer, W.C., Berresheim, H., Salisbury, G., Lange, L., and Lelieveld, J., 2003, GC×GC measurements of C_7-C_{11} aromatic and n-alkane hydrocarbons on Crete, in air from Eastern Europe during the MINOS campaign, *Atmos. Chem. Phys*. **3**:1461-1475.

OTHER PRESENTATIONS

CLIMATE CHANGE AND ITS IMPACTS IN MOROCCO

MOHAMMED-SAÏD KARROUK
University Hassan II, FLSH Ben M'Sick
Climatology Research Centre
BP 8220 Oasis, MA-20103 Casablanca - Morocco
CEREC@UnivH2M.Ac.Ma

Key Words: Climate change, Atmospheric circulation, Morocco, Mediterranean, Atlantic, Pacific, ENSO, NAO, Energy budget, Drought, Floods, Food security, Water resources, Agriculture.

Abstract Observed climatic changes at the planetary level, and these which are due to natural activities and especially human, are forced to upset the systems of global atmospheric circulation, and this is attributed to the change of the energy budget of the Earth and its Atmosphere.

The increase of the planetary temperature already observed (Figure 1), provoked by the accumulation of concentrations of gases of a high capacity of thermal energy absorption, such as the carbon dioxide (CO_2), methane (CH_4) and nitrous oxide (N_2O), is only one of the main results of the change at the level of the radiative contributions and losses of the planet Earth.

1. Energy Budget and Atmospheric Circulation

The radiative budget of Earth is made up of different games of the solar radiation, to a great extent visible part, penetrating to the summit of the atmosphere in the direction of Earth (radiative input), and the terrestrial radiation, mainly by infrared, exiting to space (radiative losses).

If the natural greenhouse effect stabilises, the average global temperature is around 15°C, and taking into account that radiative solar contributions are on the average stable, the increase observed of temperatures could only be conceived by a diminution of the radiative losses in the infrared domain; it is the human surplus to the effect of the greenhouse (Karrouk, M.S., 2002c).

Although the currently available means do not allow the distinction between what is natural to the human in this investigation on the increase of the greenhouse effect, the measures undertaken on the carottages have the demonstrated that the concentration of gases of the greenhouse effect has

A. Mellouki and A.R. Ravishankara (eds.), Regional Climate Variability and its Impacts in the Mediterranean Area, 253–267.

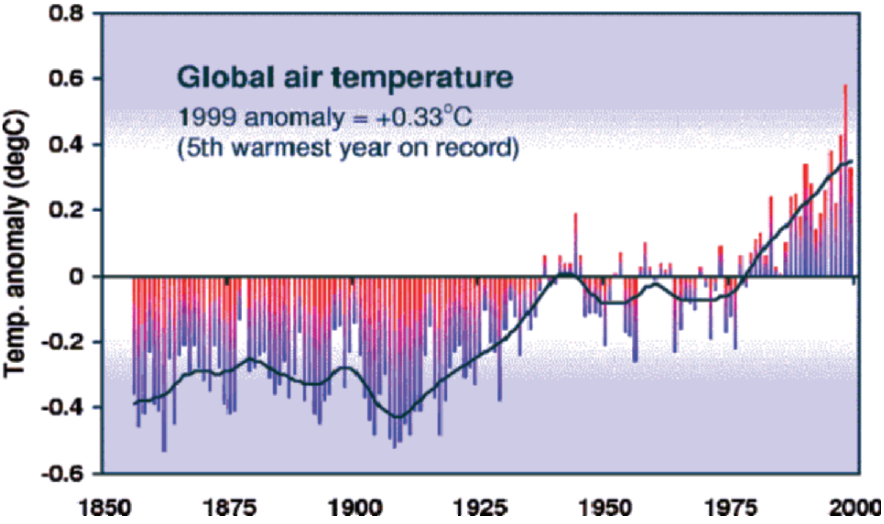

Figure 1. Evolution of Global Middle Temperatures 1861-2000 of the Earth as compared to the Average 1951-80 (CRU-UEA)

strongly increased since the preindustrial period (that is since 1750 approximately): the CO_2 has moved from 280 to near 360 ppbv[1], the CH_4 from 700 to 1720 ppbv and the N_2O from 275 to 310 ppbv approximately.

The latitudinal distribution of radiative inputs and losses on the hemispheric plan has led to a surplus of the energy in the intertropical zone, and to a deficiency in the extratropical latitudes, particularly in the winter season (Figure 2 ; Karrouk, M.S., 2003b).

In January (Figure 2A), 18th parallel North above Atlantic marks the reversal of the net radiation. The zone existing between this parallel and the north pole knows a negative budget, and that found in the south of this parallel down to the south pole know a positive[2] budget. Whereas in July (Figure 2C), it is the 10th parallel South that marks the energetic reversal on the planetary level all along the 20°W. This observation in the Atlantic is general on Earth. The energy budget follows a spatio-temporal zonal distribution. The geographical intervention of lands and oceans selectively modifies this distribution, especially to the west of the continents, but the zonality remains well-structured: an intertropical zone where the energy budget on the annual plan is permanently in excess in between 10°S and 18°N, and two other extratropical zones, one to the North of 40°N, and the other to the South of 37°S, where the energy budget is deficient on the annual average (Figure 2; Karrouk, M.S., 2003b).

[1] ppbv = parts by billion in volume. Quoted figures are valid for 1992.
[2] The zone of cover of ERBS is within the 68th parallel north and south.

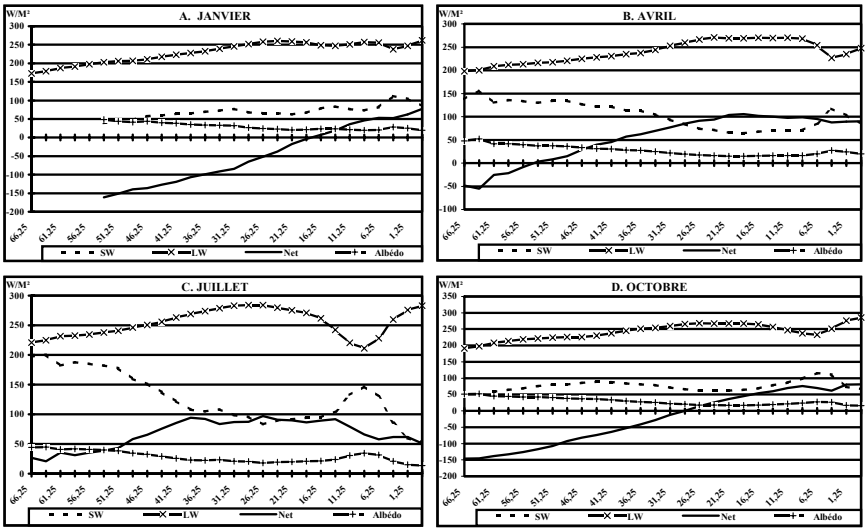

Figure 2. Middle Seasonal Energy Budget 1985-89 the long of 19°45' W (ERBS-NASA)

In intermediate seasons, the zone where the radiative budget is positive overlaps between 54°N and 26°S on the meridian 20°W in spring (Figure 2B), and 26°N and 49°S in autumn on the same meridian along the Atlantic (Figure 2D; Karrouk, M.S., 2004).

This situation creates a radiative gradient between the excess zone and the deficient zone on the hemispheric plan. A radiative exchange between the two zones becomes necessary (Karrouk, M.S., 1999). This causes the intertropical energetic surplus to be transferred to the deficient zone and vice-versa. The latitudinale circulation is thus established (Karrouk, M.S., 2002a). Its intensity varies between a winter maximum where the energetic gradient is important, and a summer minimum where this gradient is weak (Karrouk, M.S., 2004).

This atmospheric circulation is the result of two main factors: the solar radiation, and the spherical form of the earth in rotational movement on itself. This west-to-east terrestrial movement causes the superficial radio-thermal energy, which is sensitive and latent, in the subtropical zone to be accumulated in the equator due to the increase in the centrifugal force (Karrouk, M.S., 1999 & 2001a). The flows of the surface (called Trade winds), converge to the intertropical zone and thermo-mechanic ascendance becomes necessary, creating the equatorial low region pressure (whose center is the meteorological equator). Once in high troposphere, the temperature declines

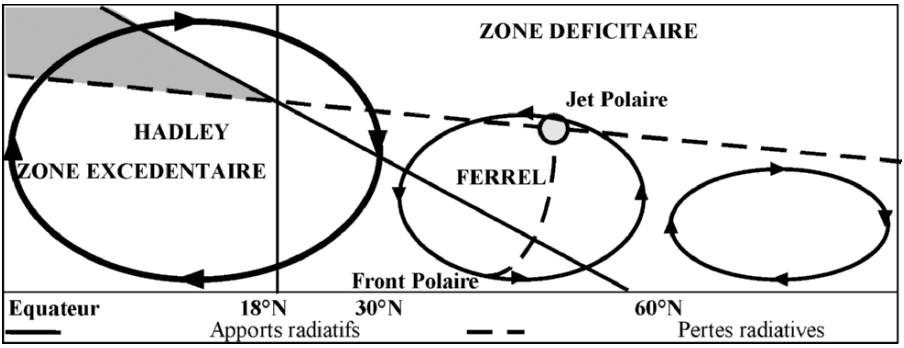

Figure 3. Schematic Representation of the Meridian Winter Circulation

and flows diverge to the north and to the south in the form of géopotential energy causing thus the intertropical radiative surplus to be transferred to deficient extratropical latitudes (Karrouk, M.S., 2001d & 2002a). Reaching the level of the reversal of the hemispheric energy budget, these meridian flows undergo a down action to the ground creating the anticyclonic subtropical centure. The subtropical circulation is thus established in the form of a large meridian cell of a horizontal axis called the circulation of Hadley (Figure 3; Karrouk, M.S., 1999, 2001a, b, d, 2002a, c & 2006; Wang, C., 2002).

Through the circulation of Hadley, subtropical anticyclones are fed in permanence by the transfer of the intertropical energy accumulation (Figure 4; Karrouk, M.S., 1999, 2001c, 2002a & 2004). Their divergent dynamics implies a superficial distribution to the North by means of Westerlies that constitute the superficial branch of the intermediate cell of Ferrel, and to the South by means of the Trade winds that constitute the superficial branch of the cell of Hadley. Depending on the intensity of the down branch of this cell of Hadley, one of the superficial flows overcomes the other (Figure 5; Karrouk, M.S., 2003a).

When the intertropical ascendance is more important than the normal (in phasis «El Niño» for the Atlantic, for example, Figure 6), the subtropical anticyclones are found strengthened as compared to their normal state (the Azores in the Atlantic and Hawaii in the Pacific, Figure 4), and occupy a more northern position (Karrouk, M.S., 2001b, 2002b & 2005). The zonal circulation of average latitudes is carried out rapidly in these energy conditions due to the energy gradient which is important between the subtropical zone and the moderate zone, and the West polar throw is therefore tense (Karrouk, M.S., 2006). The meridian exchange with average latitudes is minimal due to blockage imposed by the rapid West circulation, and the flow of the Trade winds overcomes the Westerlies winds.

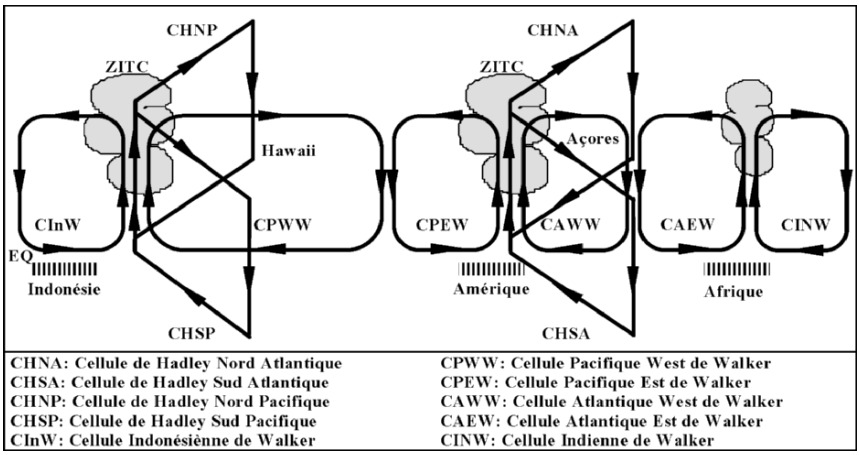

Figure 4. The Connections of Circulation of Hadley and Walker

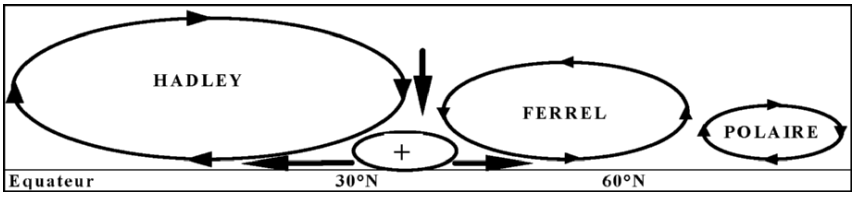

Figure 5. Schematic Representation of the Intensity of divergent Subtropical flows of surface

This situation emerges in the form of an increasing atmospheric stability of average latitudes that are invaded by the anticyclonic field. Winter «Droughts» appear in North Africa and in South-West Europe (Karrouk, M.S., 2001), and ordinary perturbations remain confined to the North of the polar front. The Trade winds become strengthened by the superficial energy surplus, and blow strongly on the equator; hot surface waters of the Pacific «SST»[3] migrate to the West and the normal situation returns.

In contrast, when the energy transfer through the superior branch of Hadley is less important than the normal (phase «La Niña» for the Atlantic, Figure 7), the subtropical anticyclones become less powerful and occupy southern latitudes (Figure 4). The meridian energetic gradient is weak and the West current throw is less tense. Planetary undulations are set up between the subpolar and subtropical air masses, the meridian exchanges are in full action throughout the valleys and the planetary crests, and the Westerlies become powerful.

[3] SST: Sea Surface Temperature.

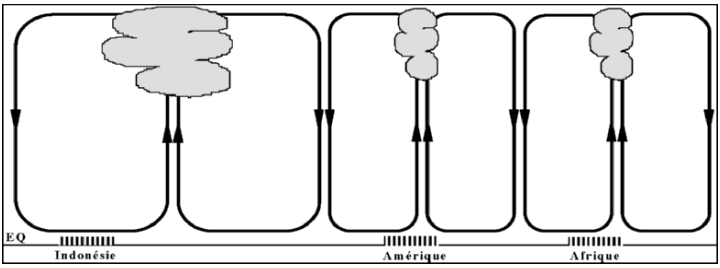

Figure 6. Diagram of the Circulation of Walker in Boreal Winter in phase El Niño

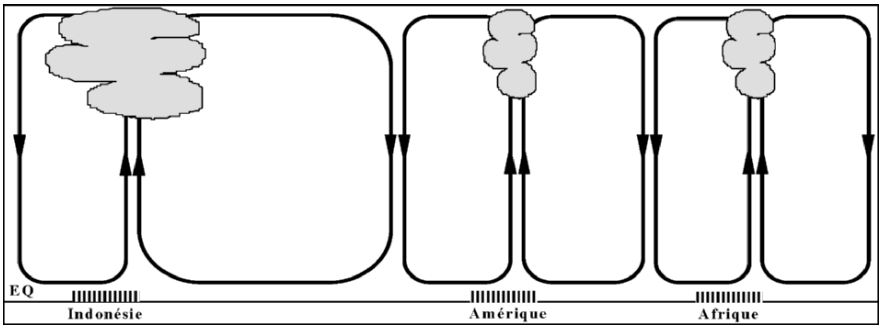

Figure 7. Diagram of the Circulation of Walker in Boreal Winter in phase La Niña

This energy situation is characterized by violent perturbations of average latitudes (Western Europe), and precipitations of transit latitudes (Europe of the Southwest and North Africa). The Trade winds weaken by reason of the important share of superficial energy displaced to the North by West flows. The superficial branch of Hadley is less powerful, hot waters of the Pacific «SST» are loosened to the East of the basin, and «El Niño» could re-establish again.

2. Climate Change and Atmospheric Circulation

Currently, this circulation is found shaken by the energy imbalance due to the surplus of greenhouse effect, which disturbs the usual spacial distribution of superficial temperatures, as well as the atmospheric flows, winds, temperatures, precipitations, humidity of soils and the other climatical variables, perhaps even the speed of the rotation of the earth that could be accelerated or slowed by extreme events such as «El Niño».

The atmospheric circulation at the hemispheric level as it has been presented above, is characterized by energy exchanges undertaken between the

low latitudes where the energy budget is in excess, and the high latitudes where this budget is deficient. It is indeed at the level of the reversal of these energy budgets that the atmospheric circulation should witness the large changes of mechanisms that manage it and should have the most important impacts on the natural ecosystems and the sociosystems.

The decrease of energy loss provoked by the increase of the greenhouse effect, should increase the energy surplus in the intertropical zone and to displace the zone of the reversal of global energy budgets of the Earth to the poles (Figure 8; Karrouk, M.S., 2002a), and thereby, the cell of Hadley of the meridian vertical circulation will be found strengthened and widened in latitude. The polar cell should keep its weak situation vis-à-vis the cell of Hadley, and the thermal gradient will have a tendency to weaken in temperate latitudes, but should probably keep the same gap between the high and the low latitudes. The current West throw would be forced to move to higher latitudes, as well as the polar front and its perturbations, due to the expansion of the zone which is occupied by subtropical anticyclones (Figure 9; Karrouk, M.S., 2002c & 2004). Whole climatic zones would therefore be displaced towards the poles.

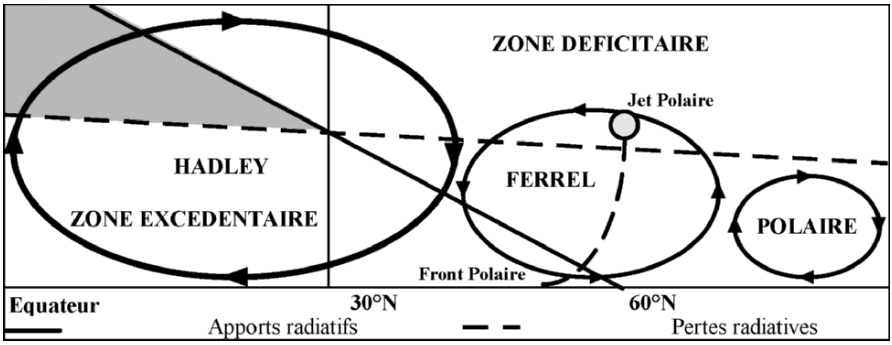

Figure 8. Schematic Representation of the Meridian Winter Circulation Expected

It is in the winter period and at average latitudes that the effects of the climatic change will be the most sensitive. The upheaval of the spacial distribution of energy budgets will give to atmospheric flows a new spacial distribution. The divergence center of subtropical anticyclones, situated at higher latitudes as compared to their usual space, will put whole regions situated to the West of continents, at the limit of the current influence of circumpolar circulation and Westerlies, under the dominance of the subtropical circulation and the Trade winds (Iberian peninsula and North Africa concerning the

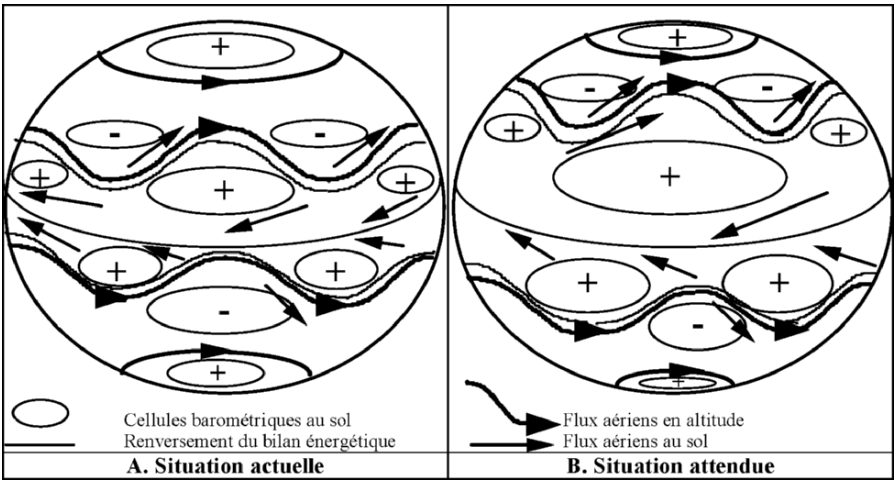

Figure 9. Schematic Representation of the Boreal Atmospheric Winter Circulation

Azores anticyclone). Thus one should expect an expansion of the zone of subtropical «Drought» in the direction of the poles vis-à-vis their current area, as well as the zone of influence of Westerlies, which should shrink at the subtropical side.

From this expected energy budget, a new spatial of the thermal and hydrologic budget should emerge. The energy stored in the low troposphere, especially in the oceans, will increase the energy surplus in the «ITCZ» [4] due to the superficial accumulation undertaken by flows of the Trade winds, and intertropical ascendance be strengthened. The circulation of Walker, under the influence of a superficial forcing should influence the system of intertropical precipitations by increasing the precipitable volume of water in this zone (Monsoons), as well as the frequency and the amplitude of the upwellings to the East of equatorial oceans which should intensify (events «El Niño» and «La Niña»); the consequences at the planetary level do not need to be demonstrated.

In the average latitudes, the temperatures should increase in the new areas invaded by subtropical anticyclones. The same thing affects the rates of evapotranspiration. The budget hydrologic should increase its deficit in these zones of transition. While in temperate regions, the increase of temperatures, especially in winter, and the progress of the Westerlies in latitudes should decrease snow, and increase winter precipitations and change the regime of flow; hence, the risk of repetitive storms and flooding above these latitudes at this period of the year.

[4] ITCZ: InterTropicale Convergence Zone.

3. Characteristics of the Current Atmospheric Circulation in Morocco

Information and observations concerning precipitations in Morocco during the past century, show us clearly that in more than 50% of cases, precipitations have been inferior to the normal in the major part of the national territory: 46.4% in Marrakech between 1900 and 1996, varying between a surplus of 291 mm in 1912, and a deficit of 162 mm in 1981, that is, 67% negative difference to the normal. In Casablanca, the deficient year frequency is 57.8% of cases between 1907 and 1996, varying between a surplus of 569 mm in 1996 and a deficit of 271 mm in 1981, that is, 64.1% negative difference to the normal. Therefore, this natural situation is structural and has well to be taken in consideration in all plans and projects of development (Figure 10; Karrouk, M.S., 2001, 2002b, 2003a & 2005).

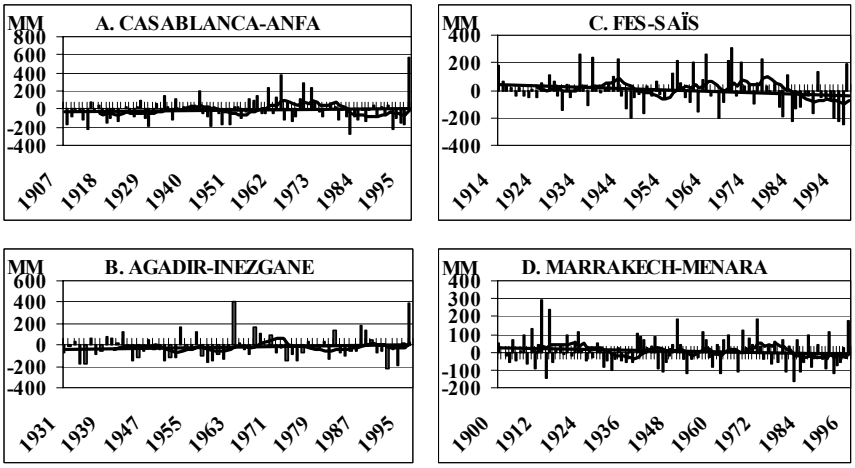

Figure 10. Interannual Variability of Gaps of Precipitations to 1961-90 in Morocco

This hygrometric situation of air in Morocco is linked to a macro-regional atmospheric circulation that makes this region sometimes submitted, to the subtropical climatic atmospheric predominance inhibiting precipitations, sometimes, to the influence of subpolar atmospheres which carry the humidity.

It is the anticyclone Azores in these Moroccan latitudes, along with the mobile low pressure and especially the Icelandic permanent center that controls the atmospheric situations carrying or not rains to Morocco. When the energetic and barometrical gradient between the center of Azores and that of the Iceland is important, the atmospheric circulation is rapid, tense and

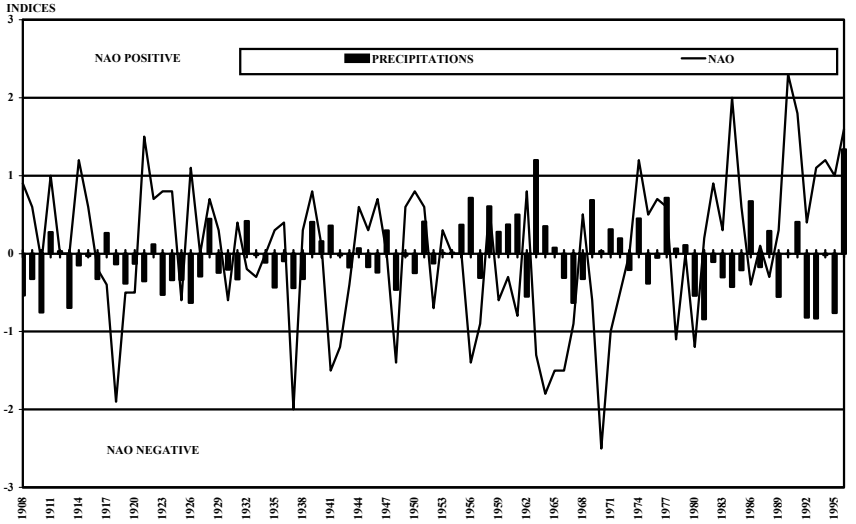

Figure 11. Interannual Variability of the NAO and Winter Precipitations in Casablanca

zonal. This situation does not allow meridian exchanges and Morocco is under the dominance of the regime of subtropical circulation. On the other hand, if these gradients are weak, the regional circulation is slow and undulant, North-South exchange are established and perturbations of the polar front reach Moroccan latitudes.

This situation of the alternation between regimes of subtropical and subpolar circulation finds its explanation in the variation of atmospheric event in North Atlantic named «North Atlantic Oscillation-NAO». This connection is determined especially by the index that measures the normalized pressure difference between the Azores and Iceland. A strong value of this indication corresponds to a zonal circulation west fort, whereas a weak corresponds to a situation of higher evoked freezing and to a slowing of the West circulation. A strong value «Positive NAO» of this indication is accompanied by «Drought» in Morocco, whereas a weak value of this indication «Negative NAO» is characterized by the return of precipitations (Figure 11).

It has been noticed, according to observations provided by satellites and meteorological observations, that «Droughts» in Morocco coincided with «El Niño» situations (1993, 1995). This power finds its origins in the «ITCZ» which is both due to oceanic superficial temperatures «SST», Atlantic and Pacific in this period «ENSO» (Figure 12).

In «El Niño» situation, the «CPEW»[5] in the eastern part of the Pacific feeds in excess the ascending branch of connecting it the cell of Hadley by reason of the increase of the superficial temperature of the sea «SST» (Figure

[5] CPEW: Pacific East Cell of de circulation of Walker.

4), and gives a remarkable power to the meridian circulation. This anomaly is manifested at the level of the cell of Hadley as a whole; hence, the emergence on the ground at the level of the descending branch (Azores) of an adiabatic compression abnormally high which constitutes thus a sensitive heat excess. Minimal temperatures decline in Morocco, and the positive index of the «NAO» is established; it is the establishment of the tropical regime and the «Drought» (examples of 1983, 1993, 1995 and 1998). This is characterized in Morocco, by a dry atmosphere and a perfect atmospheric stability in periods normally considered humid. On the other hand, during «La Niña», cold waters of the Pacific decrease the feeding of the cell of Hadley, and thereby, the anticyclone of Azores is found in a weak situation, the negative extreme of the index «NAO» is established, which allows perturbations of the polar front to reach northern Africa; it is the polar regime and the return of precipitations to Morocco that could be abundant (examples 1996 and 1997), perhaps even exceptional in several regions of the country (Figure 12).

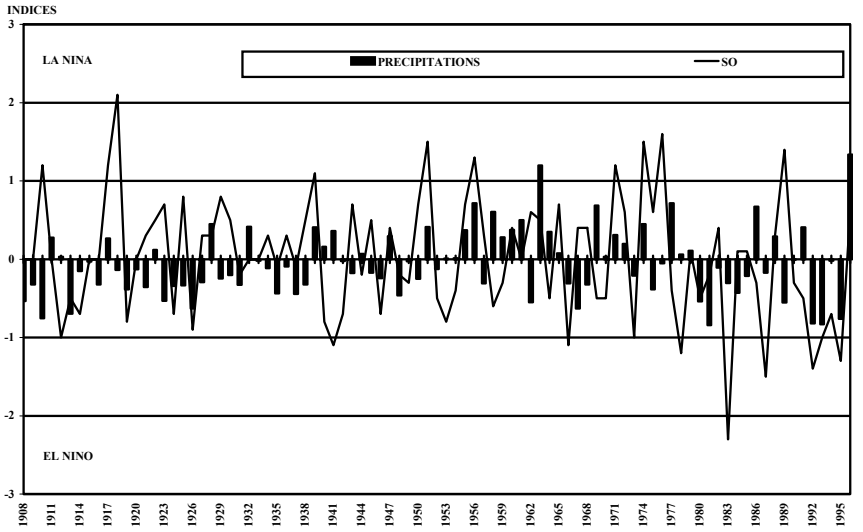

Figure 12. Interannual Variability of the SO and Winter Precipitations in Casablanca

4. Climate Change and Atmospheric Circulation in Morocco

Morocco, a country with a transition climate from the extreme Southwest of the Western Mediterranean, frequently knows disagreeable repercussions due to perturbations of the global climatical system, characterized by

«Droughts», sometimes severe, or even floods. The most recent «Drought», that has lasted more fifteen years according to regions, was interrupted in 1996 and started again in 1998, and that has been marked by two large episodes of global «Drought» in 1980-85 and 1991-95. Given the latitudinal position of the country (21-36°N) in relation to the usual vicissitudes of the reversal of the hemispheric energy budget, the region is confronted with the negative effects of the change of the atmospheric circulation that would place Morocco under the dominance of subtropical climate. This situation would make northern Africa submitted to «Drought» far more frequent and probably more long by reason of the strengthening of the anticyclonic system of the Azores and its widening in latitudes and longitudes, as well as to a rare return but certainly abundant of precipitations in humid period inducing floods by reason of increase of the pluvial capacity of the atmosphere.

This predictable atmospheric situation, based on physics and geographical logic of the tendency of the current evolution of the climatic change, will put in peril several socio-economic sectors in Morocco, the most important and the most vulnerable of which are water resources, humidity of the ground, agriculture, fishery and food security.

The frequencies studies of the evolutionary trends of the «NAO» in the Atlantic, and «ENSO» in the Pacific, to which are connected the precipitations in Morocco (Figure 13), allows us to distinguish three distinct periods:

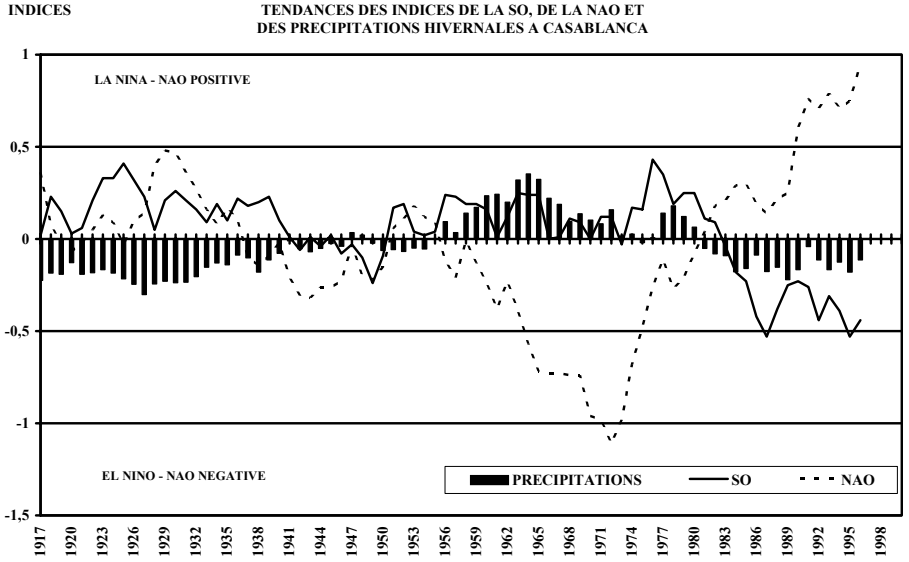

Figure 13. Interannual Variability of the Evolution of Trends of Index of the SO, the NAO and Winter Precipitations in Casablanca

The first dry, and begins from the beginning of the century[6] until the 1950s (from 1907 to 1954). The second humid, and extend from the 1950s to the end of the 1970s (from 1956 to 1980). And finally a third dry period that started at the beginning of 1980s and continues to our days.

The first period has been marked by a synchronic evolution of «La Niña», the «Positive NAO», and «Droughts» in Morocco; the second by the presence of «La Niña», the «Negative NAO» and precipitations; while the third was marked by the predominance of «El Niño», the «Positive NAO» and the «Drought» in Morocco.

If the second and current periods have appeared in conformity according to the theory of energy transfer presented higher, the first dry period (1907-1954) raises questions vis-à-vis events in the Pacific. Are we dealing with the change of the mechanisms of the global atmospheric circulation since this period?

The information provided by the dendrochronology[7] (Figure 14) on the duration of «Droughts» in Morocco since the year 1000 shows us that for the first time these durations have reached 8 years in the last two decades (Figure 10).

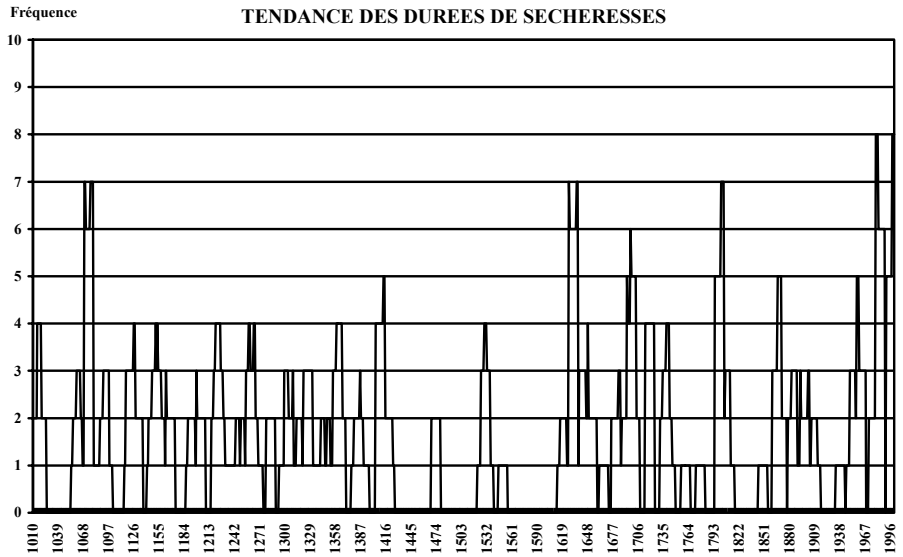

Figure 14. Dicennal Trend of Droughts Duration in Morocco

[6] According to available meteorological data. observations of the station of Cap Spartel to Tangier undertaken between 1894 and 1920 indicate us a globally humid tendency in this station.

[7] *Cedrus Atlanticus* 1000-1989, completed by current information of 1990-2000.

On the basis of these available data (Figure 10, 13 and 14), one clearly notices that the effects of global change are manifested in Morocco by an acuity of «Droughts» according to the analyses presented above.

5. Conclusion

The terrestrial climates affected by climate change are under the constraint to be upset by the new mechanisms that manage the global atmospheric circulation.

Hot average latitudes to which Morocco belongs represent the most vulnerable places to negative effects of this climatical upheaval given their position of transition between the climatical subpolar and subtropical zones. The sector that is most affected by this situation is *WATER* due to the prolonged «Droughts» already observed at the end of this century. And this is by reason of the new geographical distribution of the cycle of water that is established at our latitudes, and the enlargement of the area of subtropical evapotranspiration that has a tendency to emphasize hydric budgets which are deficient in Morocco.

6. References

Karrouk, M.S., 1999, TOPEX/POSEIDON, Monitoring and Predicting Precipitations in Morocco, *Conférence Internationale sur l'Observation de l'Océan pour le Climat, Centre National d'Etudes Spatiales*, Saint-Raphaël.

Karrouk, M.S., 2001a, Climate Change, Predicting Precipitations and Food Security in Morocco, *International Conference on*: *Understanding the Earth System, Compartment, Processes and Interactions, German National Committee on Global Change Research,* Springer-Verlag Berlin Heidelberg New York.

Karrouk, M.S., 2001b, Changement Climatique et Sécheresses au Maroc, *Séminaire AMAECO sur Les Aléas Climatiques et Politiques Agricoles*, Rabat.

Karrouk, M.S., 2001c, Climate Change, Water Resources and Food Security in Morocco, *Global Change Open Science Conference*, *Challenges of a Changing Earth, International Geosphere-Biosphere Programme (IGBP),* Amsterdam.

Karrouk, M.S., 2001d, Changement Climatique et Ressources en Eau au Maroc, MOSELLA, Tome XXV, N°3-4, Metz.

Karrouk, M.S., 2002a, Seasonal Climatic Forecast in Morocco : The Contribution of the Observations of Topex/Poseidon and the Energetic Method, *International Symposium "En route to GODAE", Centre National d'Etudes Spatiales,* Biarritz.

Karrouk, M.S., 2002b, Changement Climatique et Ressources en Eau au Maroc, *International WONUC Conference "Nuclear desalination, Chalenges and Options"* Marrakech.

Karrouk, M.S., 2002c, Changement Climatique, Circulation Atmosphérique et Climat du Maroc, *Premier Congrès de Géographie du Maroc: RGM 20*, Rabat.

Karrouk, M.S., 2003a, Climate change and its consequences in Morocco, *3rd IGBP Congress*, Banff.

Karrouk, M.S., 2003b, Climate Change and Moroccan Climate: The Contribution of the Energetic Method, *International Conference on Earth System Modelling*, Hamburg.

Karrouk, M.S., 2004, Climate Change and Recent Atmospheric Circulation in Morocco, *1st International CLIVAR Science Conference, Understanding and Predicting Our Climate System*. Baltimore, Maryland.

Karrouk, M.S., 2005, Climate Change, Water Resource and Food Security in Morocco, *International Conference on: Integrated Assessment of Water Resources and Global Change: A North-South Analysis*, Bonn.

Karrouk, M.S., 2006, Climate Change and Atmospheric Circulation in Morocco: The Contribution of the Energetic Method, *An Earth System Science Partnership, Global Environmental Change, Open Science Conference*, Beijing.

Wang, C., 2002a, Atmospheric circulation cells associated with the El Niño-Southern Oscillation, *J. Climate*, **15**, 399-419.

Wang, C., 2002b, Atlantic climate variability and its associated atmospheric circulation cells, *J. Climate*, **15**, 1516-1536.

THE EFFECT OF CLIMATE CHANGES ON THE DISPOSAL FACILITY OF NATURAL OCCURRING RADIOACTIVE MATERIALS IN EGYPT

MOHAMED ABDEL GELEEL MOHAMED
3 Ahmed el Zomor st., National center for Nuclear Safety and Radiation Control, Atomic Energy Authority, Cairo, Egypt

Key Words: Climate Change; NORM Wastes; Petroleum Industry; Disposal facility.

Abstract Oil and gas extraction and processing operations sometimes accumulate naturally occurring radioactive materials (NORM) at concentrations above normal in by-product waste streams. There are number of industries generates NORM contaminated waste in Egypt. Trench was used as a disposal facility for NORM contaminated waste at one site of the petroleum industry in Egypt.

The aim of this work is to calculate the risk and dose assessment received from trench disposal facility and salt caverns due to the climate changes after direct closure and after post closure (1000 year). RESRAD computer code with two different scenarios was used for this purpose. Results of this assessment can be helped to examine policy issues concerning different options and regulation of NORM contaminated wastes generated by petroleum industry in Egypt.

1. Introduction

Naturally Occurring Radioactive Material (NORM) is found in air and in soil. Oil and gas production and processing operations sometimes accumulate NORM at elevated concentrations in the by-product waste streams. The sources of most of the radioactivity are the isotopes of uranium-238 and thorium-232, which are naturally present in subsurface formations in which oil and gas are produced. The primary radionuclides of concern in NORM wastes are radium-226 of the U-238 decay series and radium-228 of the Th-232 decay series. Other radionuclides of concern include radionuclides that form due to decay of Ra-226 and Ra-228, such as radon-222 (Rn-222). The production waste streams which include produced water, scale, and sludge (Smith et al., 1997) are most likely contaminated by elevated radium concentrations. Radium, which is slightly soluble, can be mobilized in the liquid phase of a formation and transported to the surface in the produced water

A. Mellouki and A.R. Ravishankara (eds.), Regional Climate Variability and its Impacts in the Mediterranean Area, 269–277.

stream. Dissolved radium either remains in solution in the produced water or precipitates out in scales or sludge. Conditions that appear to affect the radium solubility or precipitation include water salinity, temperature, and pressure. Contamination of scale and sludge with NORM can occur when dissolved radium co-precipitates with other alkaline earth elements such as barium, strontium, or calcium (EPA, 1993; Tomasko, 1997; John et al., 1998).

The safe handling of these NORM in Egypt implies identification of the responsibilities of both the producers of the NORM and the Central Radioactive Management Authority. In Egypt, CRMA has a Hot Laboratory and Waste Management Centre (HLWMC) (El-Adham, 2000). Dealing with these wastes requires developing both the required technologies and the relevant regulations to determine the responsibilities and identify the safety requirements for the handling of such wastes. The responsibilities of the producer include waste collection, packaging of category 1 and interim storage of category 2. The responsibilities of the HLWMC include transporttation and long term storage of category 1.

The aim of this study, is to calculate the risk and dose assessment received from trench disposal facility after direct closure and after post closure (1000 year) was calculated. RESRAD computer code with two different scenarios was used for this purpose**.**

2. Experimental Procedure

2.1. COLLECTION OF MATERIALS AND METHODS

Five samples weighing about 1 kg each were collected from the NORM that will be disposed of into the trench or salt cavern. The waste samples contain the sludge and the scale formed in the production equipment, during oil and gas extraction, and those removed during the periodical maintenance. The samples pulverized to fine powder (200 mesh) and then dried over night at 110°C. Known amount of the samples (50 gm) were packed in a special counting container and carefully sealed for 8 weeks to reach secular equilibrium between ^{232}Th and ^{238}U progeny. The activity of ^{214}Bi, ^{214}Pb, and other progenies of ^{226}Ra in equilibrium with their parents were assumed to represent the ^{238}U activity. The activity of ^{228}Ac and other progenies of ^{232}Th were assumed to represent ^{232}Th activity. Sludge samples were stirred manually by a glass rod and filled in a plastic container for counting.

Radiometric analyses of different samples were carried out using a high resolution gamma ray spectrometric system. The system was comprised of high purity germanium detector (HPGe) with 81cm^3 sensitive volume. The detector has an energy resolution of 2.2 keV FWHM for the 1,332.5 keV of

gamma energy of ^{60}Co. To reduce environmental gamma background radiation, the detector was shielded with lead bricks of thickness 5-10 cms. A lining of 2 mm thick copper followed by 2 mm-thick aluminum was made to absorb the x-rays from lead and copper.

2.2. REGULATIONS CONCERNING NORM

TABLE 1. Recommended Dose Limits (Regulatory rule No: Pet-1, 1999)

	Occupational	**Public**
Effective Dose	20 mSv per year, averaged over defined periods of 5 years	1 mSv in a year

3. Result and Discussions

3.1. ACTIVITY LEVEL IN SCALE NORM WASTE

From above experiment the following radionuclides from the ^{238}U series having half-lives exceeding one day were identified: ^{234}Th, ^{234}U, ^{230}Th, ^{226}Ra, ^{222}Rn, ^{210}Pb, ^{210}Bi, ^{210}Po. From the ^{232}Th series we have: ^{228}Ra, ^{228}Th, ^{224}Ra. Highest level of radium isotopes (^{226}Ra, ^{228}Ra, ^{224}Ra) was observed from hard scale samples. The analysis result of radium activity - between 34 and 153 Bq/g are shown in Table 2.

TABLE 2. NORM concentration in different samples of hard scale

Sample no.	**NORM Concentration (Bq/g)**			
	^{226}Ra	**^{228}Ra**	**^{224}Ra**	**^{40}K**
1	71 ± 3	52 ± 4	34 ± 3	7 ± 1
2	82 ± 4	63 ± 3	49 ± 1	8.2 ± 1
3	153 ± 4	119 ± 1	72 ± 3	13 ± 1
4	138 ± 3	98 ± 5	64 ± 1	6.2 ± 1
5	106 ± 3	83 ± 3	55 ± 2	6.7 ± 1

3.2. ACTIVITY LEVEL IN SLUDGE NORM WASTE

Sludge containing NORM is produced from the cleaning of oil separator, storage tanks and other surface equipments. This waste contains less activity than the hard scale and that is shown in Table 3.

TABLE 3. NORM concentration in different samples of sludge

Sludge Sample no.	NORM Concentration (Bq/g)			
	^{226}Ra	^{228}Ra	^{224}Ra	^{40}K
1	35 ± 1	30 ± 1	23 ± 2	6.1 ± 0.9
2	72 ± 2	50 ± 2	39 ± 1	6.9 ± 1
3	121 ± 3	91 ± 1	52 ± 3	10.1 ± 1
4	113 ± 3	98 ± 5	64 ± 1	5.2 ± 1.1
5	86 ± 3	69 ± 1	38 ± 3	5 ± 1.1

Based on the obtained results, it is clear that, the activity in both hard scale and sludge are higher than the exempt activity levels for the Natural Occurring Radioactive Materials as recommended in the basic safety standards given by the IAEA. This means that, these wastes release natural radiation hazardous to environment in oil and gas production, which may causes health risk to the workers in this field through inhalation of radon gas from ^{226}Ra, ingestion and/or in touch of the contaminated production equipment therefore, dealing with these materials must be approached under controlled conditions. Also, ^{226}Ra is the main constituent in the NORM waste and represent 135, 121 Bq/g for both hard scale and sludge.

3.3. RESRAD COMPUTER CODE

The RESRAD code focuses on radioactive contaminants in soil and their transport in air, water, and biological media to a single receptor. The radiation dose calculated by the codes from the resulting exposure is defined as the effective dose equivalent (EDE) from external radiation plus the committed effective dose equivalent (CEDE) from internal radiation. The total dose is the sum of the external radiation EDE and the internal radiation CEDE and is referred as the TEDE.

1.1.1. Assuming

A 70 Kg weight man drinks 2 liters of ground water from a well-located 5000 m distance away from the disposal site.

The assumptions and the parameters used in this analysis depend on:

1- disposal site characterization (trench and salt caverns)
2- types of NORM arising
3- design of the disposal trench and salt caverns
4- the hydrology and geohydrology of the site
5- the worst case; there is no unsaturated zone
6- the cover and barrier is completely failed (no barrier exist)

The input data and the assumptions for trench disposal facility are:

Porosity	: 0.4
Precipitation	: 1m/y
Irrigation	: 0.2 m/y
Density	: 1.5 g/cm^3
Hydraulic conductivity	: 100 m/y
Hydraulic gradient	: 0.02

Figure 1 shows a relation between the total effective doses (mSv) with time (in years) that was received as a result of direct exposure. The maximum doses received from direct external exposure to all radionuclides are 8E-04 this may be due to the presence of ^{226}Ra. The excess cancer risks for all radionuclides and all pathways reached to 1.25E-07 and this is shown in Figure 2.

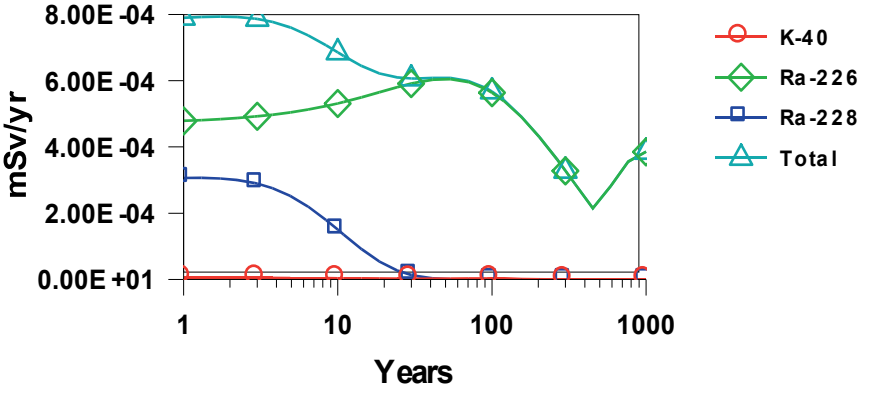

Figure 1. Total effective dose received from external exposure to all radionuclides and all pathways

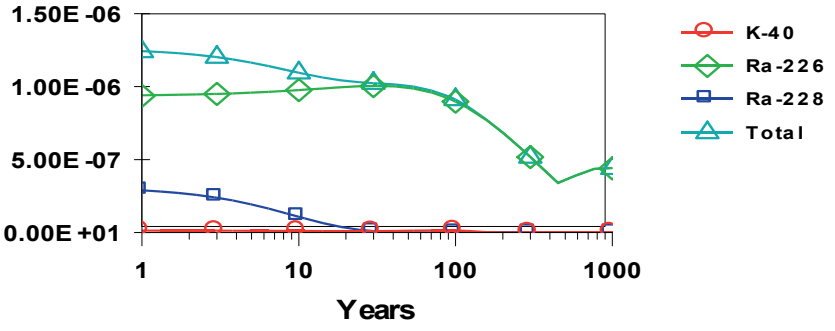

Figure 2. Excess cancer risk from external exposure to all nuclides and all pathways

Figure 3 shows a relation between a human risk against time and indicated that trench disposal of NORM waste poses a very low human health risk. It is clear from the radioactive dose assessment results that the total annual exposure dose to the whole body is less than the limit; 0.25 mSv (10 CFR 61). This means that trench disposal is safe to dispose of the NORM.

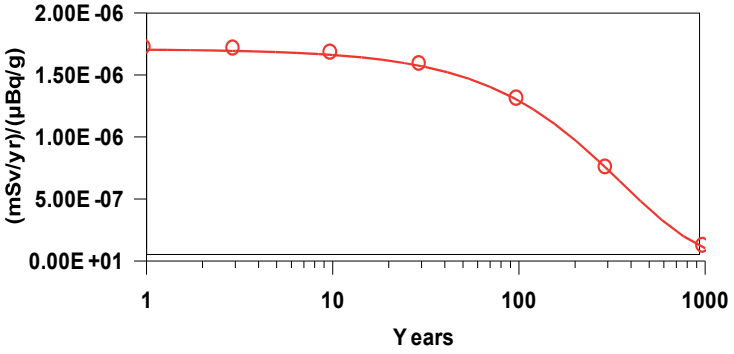

Figure 3. Dose/Source ratio for R a-226 (External and all pathways)

Figures 4, 5 show the relation between the effective dose per source ratio (mSv/yr)/ (µBq/g) against time (year). From these figures it's clear that the external exposure dose from all pathways decreases with increasing time. For Ra-228 and K-40 the doses per source reached to about zero after nearly 50 and 250 years respectively. The maximum value will be1.5E-06 (mSv/yr)/ (µBq/g) after 20 years for Ra-228 and will be 1.55E-07 (mSv/yr)/(µBq/g) After one year for K-40. The dose per source ratio for Ra-228 is greater than K-40. These values are acceptable according to the Egyptian regulations for NORM wastes (Regulatory rule No: Pet-1, 1999).

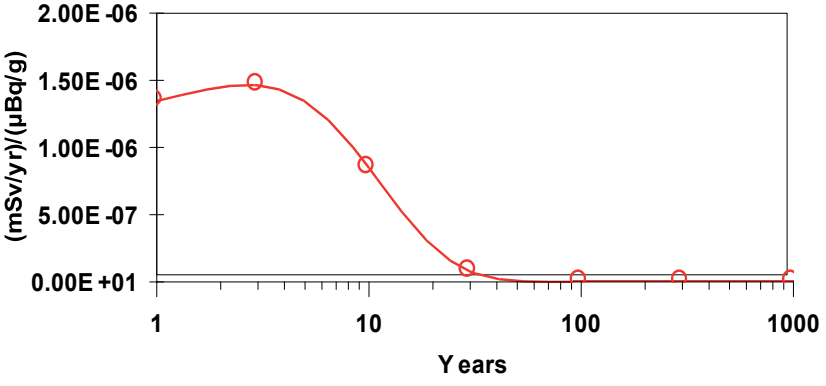

Figure 4. Dose/Source ratio for R a-228 (External and all pathways)

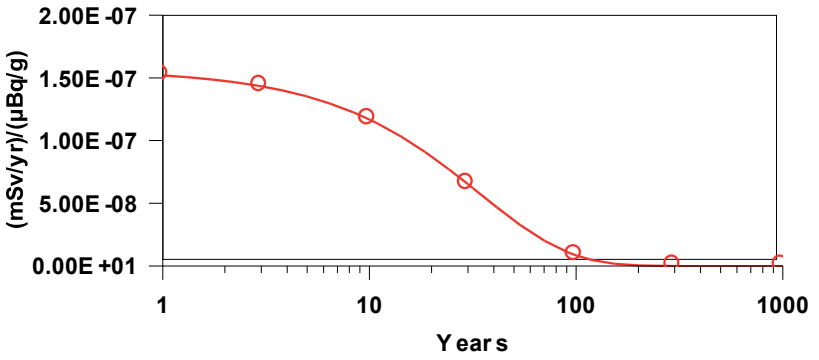

Figure 5. Dose/Source ratio for K-40 (External and all pathways)

Figures 6, 7 show the relations between the concentration of radium (µBq/g) in the contaminated zone soil with time (year). From these figures its clear that the concentration of radium decreases with time and it reach to about zero after 30 years for ^{228}Ra, while for ^{226}Ra the concentration reach to about zero after 1000 years this may be due to the long half life of ^{226}Ra (1599 y) compared to ^{228}Ra.

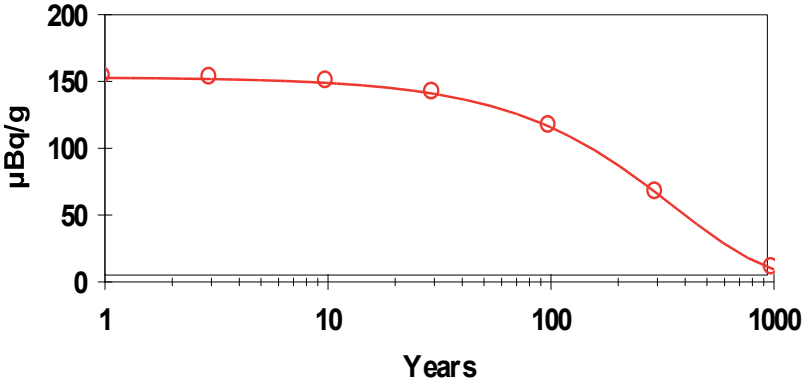

Figure 6. Concentration of Ra-226 in contaminated zone soil

The probability to cancer risk from drinking water increasing with the time increases and levels off at about 650 years as shown in Figure 8. From this figure its clear that ^{226}Ra is the main constituent to cancer while there is no effect from ^{228}Ra. This may be due to the high concentration of ^{226}Ra (135 Bq/g) rather than other radionuclides.

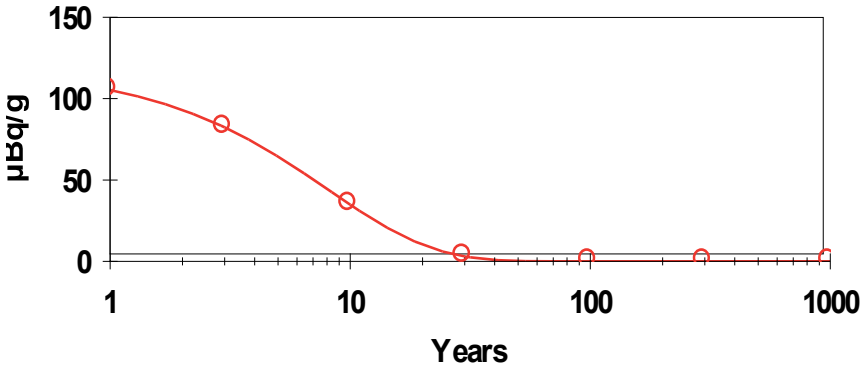

Figure 7. Concentration of Ra-228 in contaminated zone soil

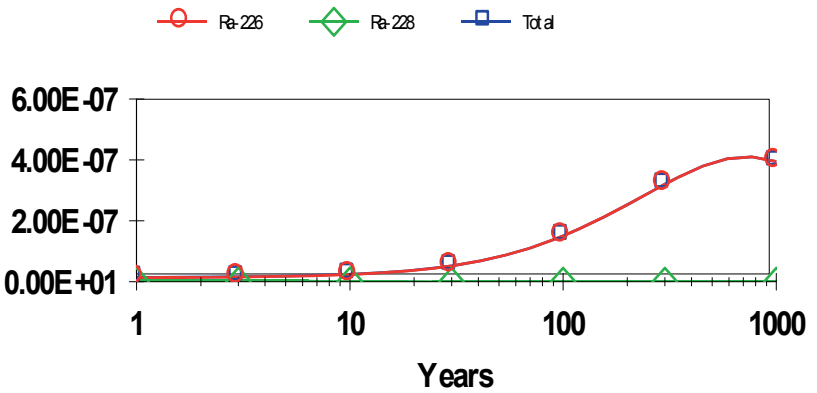

Figure 8. Excess cancer risk from drinking water to all nuclides

4. Conclusion

This study using the RESRAD computer code provides evidence that caverns disposal of NORM contaminated waste produced from oil and gas production poses a very low human health risk and is most likely technically feasible as compared with trench disposal facilities.

5. Acknowledgments

I would like to express my deepest gratitude and sincere thanks to the NATO program for security through science and to Dr. Wahid Mellouki for his kind cooperation and faithful help and for payment the travel and living expensive during the period of the workshop.

6. References

Berest, P., and B. Brouard, "Behavior of Sealed Solution-Mined Caverns," presented at the Spring Meeting of the Solution Mining Research Institute, New Orleans, LA, 1995.

EPA,"Draft Diffuse NORM-Waste Characterization and Preliminary Risk Assessment," U.S. Environmental Protection Agency, Office of Radiation and Indoor Air, Washington, DC. Pergamon Press, Oxford, United Kingdom,1993.

John A. Veil., Karen P. Smith, D. Tomasko, D. Elcock, D. Blunt, and G.P. William, "Disposal of NORM waste in salt caverns" Society for petroleum engineers international conference on health, safety and environment in oil and gas exploration and production, Caracas, Venezuela, 1998.

K. El-ADHAM, International conference on the safety of radioactive waste management, IAEA-CN-78/49 , 2000.

Langer, M., M. Wallner, and H. Wassman, "Gebirgsmechanische Bearbeitung von Stabilatsfragen bei Deponiekaverenen im Salzgebirge" (Geoengineering with Respect to Stability of Cavities Used for Disposal Purposes, in German), *Kali und Steinsalz*, 2, pp. 66-76, 1984.

McArthur A., M. Major, and D.J. Lowe "NORM disposal in class II wells" SEP paper 29713, presented at petroleum engineers/environmental protection agency exploration & production environmental conference, Houston, TX, 1995.

Scaife, W.W., S.G. Mueller, and D.R. Young, "Downhole Disposal of NORM Wastes in An Offshore Setting: Lessons Learned," in Proceedings of the International Petroleum Environmental Conference, Houston, TX, 1994.

Sipple-Srinivasan, M., M.S. Bruno, R.A. Bilak, and P.G. Danyluk "Field Experiences with oilfield waste disposal through fracture injection" SEP paper 38254, presented at 67th Annual Western Regional Meeting of the society of Petroleum engineers, Long Beach, CA, 1997.

Smith, K.P., D.L. Blunt, G.P. Williams, and C.L. Tebes, 1996, "Radiological Dose Assessment Related to Management of Naturally Occurring Radioactive Materials Generated by the Petroleum Industry," ANL/EAD-2, Argonne National Laboratory, Argonne, IL, 1996.

Tomasko, D., D. Elcock, J. Veil, and D. Caudle, "Risk Analyses for Disposing Nonhazardous Oil Field Wastes in Salt Caverns," prepared for U.S. Department of Energy, Office of Fossil Energy, Argonne National Laboratory, Argonne, IL, 1997.

Veil, J., D. Elcock, M. Raivel, D. Caudle, R.C. Ayers, Jr., and B. Grunewald, "Preliminary Technical and Legal Evaluation of Disposing of Nonhazardous Oil Field Waste into Salt Caverns," prepared for the U.S. Department of Energy, Office of Fossil Energy, by Argonne National Laboratory, Washington, DC, June1996 Washington, DC, June1996.

Wallner, M., "Frac-Pressure Risk in Rock Salt," presented at the Fall Meeting of the Solution Mining Research Institute, Amsterdam, 1986.

ANALYSIS OF DOWN LOOKING GPS OCCULTATION SIMULATED DATA USING LEAST SQUARES AND ABEL INVERSIONS

ASHRAF EL-KUTB MOUSA
National Research Institute of Astronomy and Geophysics, Helwan, Cairo, Egypt

TOSHITAKA TSUDA
Research Institute for sustainable humanosphere, Kyoto University, Kyoto, Japan

Key Words: GPS; Occultation; Down Looking; Abel; Least squares; simulation; Inversion; refractivity; water vapor.

Abstract Atmospheric refractivity profile can be retrieved from Down Looking (DL) GPS radio occultation data. The main observations are the bending angle of the ray as a function of the impact parameter. Abel inversion and least squares are the possible ways to invert the profile of bending angle to the vertical profile of refractivity.

The current paper uses simulated GPS data to compare the merits and limitations of the least squares and Abel techniques. The simulation uses model refractivity from MSIS dry Model, wet model and radiosonde data. The result shows that it is possible to produce accurate vertical refractivity profile using either least squares or Abel inversion. Abel inversion is slightly more accurate than least squares. The percentage of the relative error of the two methods is in the range of 0.2-0.25. Least squares technique is more sensitive to biases than Abel inversion. Abel inversion solution requires much less computation time compared to least squares one.

1. Introduction

When electromagnetic signal passes through the atmosphere it is refracted. The magnitude of the refraction depends on the gradient of refractivity normal to the path, which depends on the gradients of density and water vapor. Thus measurements of refraction will contain information on the density (and hence temperature) and the water vapor along the path. The effect is more pronounced when the signal traverses a long atmospheric limb path. A series of such a path at different tangent heights yields measurements

A. Mellouki and A.R. Ravishankara (eds.), Regional Climate Variability and its Impacts in the Mediterranean Area, 279–289.

containing information on the vertical profile of refractivity (Figrue 1). Refractivity can be converted to a profile of temperature and/or water vapor. At radio frequencies, it is not possible to make direct and accurate measurements of the refracted angle. However, if the transmitter and receiver are in relative motion, the refraction introduces a change in the Doppler shift of the received signal, and this can be related to the refracted angle (Eyre, 1994).

Space-based radio occultation (RO) measurements using GPS receivers on low Earth orbiting (LEO) satellites provide accurate atmospheric refractivity profiles (Kursinski et al., 1997; Rocken et al., 1997; Wickert et al., 2001). The RO technique has been widely used in the study of planetary atmospheres (e.g., Fjeldbo et al., 1971). The basic idea behind the radio occultation is to measure how radio waves are bent by the refractive index gradients in an atmosphere. Assuming spherical symmetry of the atmosphere, this bending information can be inverted with an Abel inversion to produce a vertical profile of refractive index.

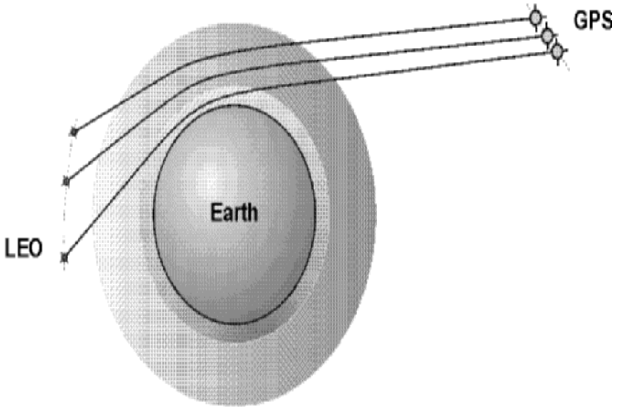

Figure 1. Concept of refractivity profiling using GPS radio occultation

RO measurements with a receiver inside the atmosphere, placed either on an airplane or a mountain top, for example, has been proposed by Zuffada et al. (1999). While GPS-LEO occultation data have the advantage of being global (one receiver in LEO can provide about 500 globally distributed occultation events per day), the sampling in any region is relatively sparse without a large number of orbiting receivers (e.g. Kursiniski et al., 1997). In contrast, a receiver located inside Earth's atmosphere can be used to provide data over specific areas of interest for the purpose of regional weather and climate studies.

A mountain-based or airborne receiver can track any GPS satellite as it sets or rise behind earth's limb. Therefore, data can be collected at both negative and positive elevation angles relative to the receiver local tangent (local horizon). Every occultation will produce a profile of refractivity below

the height of the receiver, with a diffraction-limited vertical resolution of 150-250m. An occultation with the receiver inside the atmosphere is known as a downward looking (DL) occultation.

Although fundamentally DL measurements are similar to the LEO measurements, it was originally thought that the limits of integration used in the Abel transform prevented its implementation when the receiver is inside the atmosphere (Zuffada et al., 1999). In fact, it is possible to use an Abel inversion for the DL case. The measurement geometry is similar to the one considered by Bruton and Kattawar (1997) when inverting solar occultation data.

This paper compares a least squares ray-tracing technique and the Abel inversion method for DL retrievals. Section two introduces the GPS occultation theoretical considerations and highlights the basics of the inversion techniques. Section three describes the results of the inversions using simulated data. Basic conclusions and discussion are given in Section four.

2. Theory of GPS Down Looking Occultation

For each GPS occultation event, the data analysis chain from the measured phase delay to the derivation of the refractivity can be divided into two main steps:

- Calculation of the atmospheric bending angle profile from the observed L1/L2 excess phase path time series (L1 and L2 are the phases of the two GPS carrier frequencies).
- Retrieval of the refractivity profile from the atmospheric bending angles.

2.1. CALCULATION OF BENDING ANGLE

In the geometric optics approximation, a ray passing through the atmosphere behaves according to Fermat's principle of least time. The ray travels along a curve defined by;

$$nr \sin(\varphi) = \text{constant} \equiv a \tag{1}$$

where r is the distance from the origin of symmetry to a point on the ray path, φ is the angle between the direction of r and the tangent to the ray path, and n is the refractive index at r (Figure 2).

Equation (1) corresponds to Snell's law in polar coordinates for a spherecally symmetric medium, and is known as Bouguer's formula. On this basis, a signal traveling in a spherically symmetric medium will bend by an angle α (Born and Wolf, 1980):

$$\alpha = -2a\int_{a}^{\infty} \frac{1}{n\sqrt{(n^2r^2 - a^2)}} \frac{dn}{dr} dr \tag{2}$$

where a is the impact parameter of the ray.

The basic GPS data from which the bending angles α are derived are the L1 and L2 phase delays. From knowledge of the position of the transmitter (r_t) and the receiver (r_r) and their clocks (Figure 2), the excess Doppler shift due to the atmosphere (compared to the Doppler shift in a vacuum) can be calculated. Then the bending angle is derived as a function of the impact parameter (a) from the Doppler shift (for more details see, e.g., Hajj et al., 1996). For this step, the geometry of Figure 2 is very important.

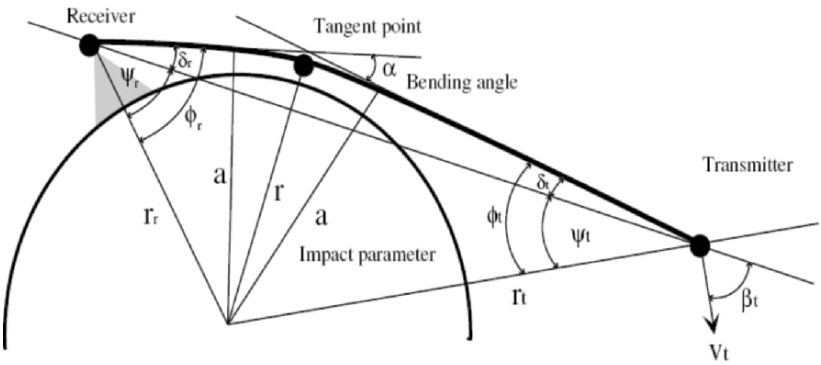

Figure 2. A schematic diagram defining the geometrical variables for a GPS transmitter/receiver link

2.2. INVERSION METHODS

The profile of bending angles as a function of impact parameter is the input data for the inversion. The Abel inversion for DL uses the difference between the bending angle observed at negative and positive elevation angles, while the least squares method uses the observed bending angle directly. However, least squares method requires an a priori model above the receiver to constrain the solution. Here, the basics of both the least squares and the Abel inversion methods are described.

2.2.1. Abel Inversion

The Abel inversion has been used extensively in seismic and astronomical inversions, as well as planetary and Earth occultation data (e.g., Fjeldbo et al., 1971; Kursiniski et al., 1997). Starting with the bending angle

determined from the GPS Doppler shift, Eq. (2) is inverted with Abel inversion to give the refractive index as (e.g., Tricomi, 1977):

$$n(x) = \exp\left(\frac{1}{\pi}\int_{a}^{\infty}\frac{\alpha(a)}{\sqrt{(a^2 - x^2)}}da\right) \tag{3}$$

where x = nr is the refractional radius.

Unlike the LEO case, in DL occultations there may be significant ray bending along sections of the path above the receiver position, so the bending will not be equal on both sides of the tangent point. However, Bruton and Kattawar (1997) noted that when the receiver is within the atmosphere, it is possible to observe rays at both positive and negative elevations. These refer to rays that intersect the receiver from above and below the local tangent. They also pointed out that, assuming spherical symmetry, for every negative elevation ray with bending angle $\alpha_{neg.}$ there is a corresponding positive elevation value α_P with the same impact parameter value. Subtracting α_P from $\alpha_{neg,}$ gives the partial bending angle α' (a) as;

$$\alpha'(a) = \alpha_{neg}(a) - \alpha_P(a) \tag{4}$$

where α' (a) is the bending that occurs along the section of path below the receiver. By definition, as the tangent point approaches the receiver distance r_r, the partial bending approaches zero.

The partial bending angle α' (a) can be written as:

$$\alpha'(a) = -2a\int_{a}^{n(r_r)*r_r}\frac{d\ln(n)/dx}{\sqrt{(x^2 - a^2)}}dx \tag{5}$$

where x = nr, n (r_r) is the refractive index at the receiver position and r_r is the receiver position. Equation (5) can be inverted with,

$$n(x) = n(r_r)\exp\left(\frac{1}{\pi}\int_{x}^{x(r_r)}\frac{\alpha'(a)}{\sqrt{(a^2 - x^2)}}da\right) \tag{6}$$

where x (r_r) is the refractional radius at the receiver position.

2.2.2. Least squares inversion

The observation vector is composed of a set of m_p positive and m_n negative elevation bending angle data. Since each bending measurement at negative

elevation is heavily weighted by the atmospheric structure at the layer where the tangent point resides, the atmospheric structure below the height of the receiver is expected to be strongly constrained by the bending measurements (Mousa and Tsuda, 2001). However, as the elevation angle increases, the data become strongly correlated, and we must rely on other a priori information to obtain a unique solution for the atmosphere at high altitudes. For this a priori information we introduce m_c refractivities taken from a climatological model above the receiver. These independent data are added as constraints and the problem becomes a constrained least squares calculation.

The atmosphere is thus modeled as a set of concentric layers of specified thickness, with refractivity varying exponentially as a function of radius with a fixed scale height for each layer. This exponential model consists of m layers, with $m = m_p + m_n + m_c$. The model is constrained such that the refractivity (but not its derivative) is continuous across the boundaries of different layers. Thus, refractivity can be formulated as a function of the radius r as:

$$N(r) = N_{norm} \exp\left(-\frac{r - R_j}{H_j}\right) \prod_{i=j}^{J_{norm}-1} \exp\left(+\frac{\Delta_i}{H_i}\right) \qquad j < j_{norm}$$

$$N(r) = N_{norm} \exp\left(-\frac{r - R_j}{H_j}\right) \prod_{i=j_{norm}}^{J-1} \exp\left(-\frac{\Delta_i}{H_i}\right) \qquad j > j_{norm} \qquad (7)$$

$$N(r) = N_{norm} \exp\left(-\frac{r - R_j}{H_j}\right) \qquad J = j_{norm}$$

where R_j is the lower boundary of the j^{th} layer, Δ and H_i are the i^{th} layer thickness and scale height, respectively. N_{norm} is a normalized refractivity, taken as the refractivity value at the lower boundary of an arbitrary layer referred to as the normalized layer. Initial values of the H_i are obtained from the a priori model. Note that the domain of the radius r given for each part of Eq. (7), is given by:

$$R_j \le r \le R_{J+1} \qquad (8)$$

The inversion consists of finding the optimal set of scale heights and an overall N_{norm} that best fits the measured bending angles. For the simulations, the bending angle is calculated using numerical integration of Eq. (2)

(Zuffada et al., 1999) and the a priori constraints, weighted by their respective measurement uncertainty. The error in the refractivity, used as constraints above the receiver position, is assumed to have a Gaussian distribution with standard deviation equals 0.05 N. The errors in bending angles are also assumed to be random with a standard deviation given by $0.01\alpha + 10^{-5}$ radians. Because the problem is highly nonlinear, a few iterations are required before a solution is obtained.

3. Results and Discussion

In order to compare the capability of the two algorithms to retrieve the refractivity when a receiver is inside the atmosphere, we constructed three sets of simulated measurements; a dry and a wet case from the MSIS-90 model atmosphere (Mass-Spectrometer-Incoherent-Scatter model, which describes the temperature and densities in Earth's neutral atmosphere from ground to thermospheric heights (Hedin, 1991)) and a wet case with some vertical variability given by a radiosonde profile. The receiver is assumed to be stationary at 3.8 km altitude and tracking GPS satellite signals at both positive and negative elevations.

In all cases, starting with a model refractivity to be the truth, a set of rays linking the transmitter to the receiver were constructed with specified tangent heights, ranging from the Earth's surface to the receiver's height. In a similar fashion, a set of rays linking the GPS satellite to the receiver was constructed to represent positive elevation angles above the receiver horizon. Like the negative measurements, the positive measurements have impact parameter given by Eq. (1), where r is the radius of the receiver but φ is between 90° (0° elevation) and 180° (zenith).

We start the simulation by calculating the bending angle as a function of impact parameter using the refractivity profile. Then white noises (random errors of zero mean) are added to the calculated bending angles (standard deviation, SD = $0.01\alpha + 10^{-5}$ radians). This random error is intended to include the error due to the spherical symmetry approximation and to receiver thermal noise. Next we used this profile of bending angle as input to the two inversion methods. The errors of the inversion, height range of the results as well as the computer CPU time are considered in the comparison. Results are summarized in Figure 3 through 6 in terms of the inversion errors for both cases.

The results show that the accuracies of both inversion methods are similar. The relative errors are always better than 0.2% (as is clear from Figure 3 through 5). The least squares method requires much more CPU time than the Abel inversion (the ratio is about 60 to one on a P4 PC running Windows XP). In addition, the least squares inversion requires an a priori model of refractivity, which is not required by the Abel inversion.

However, the least squares method can estimate the refractivity to about 2 km above the receiver positions in addition to elevations below the receiver, while the Abel method can only estimate the refractivity below the receiver.

We also compared the effect of biases in the bending angles on the two methods. A constant bias makes no difference at all for the Abel inversion. However, a constant bias greater than $1.454 * 10^{-4}$ radian (30 sec) in the

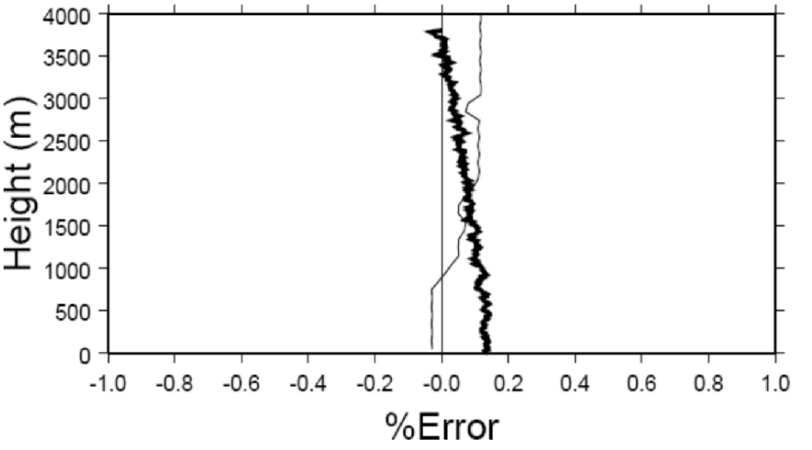

Figure 3. Refractivity retrieval error (%) for the dry model case. The receiver is at 3.8 km height. The thick line shows the results for abel while the thin line is used for least squars results

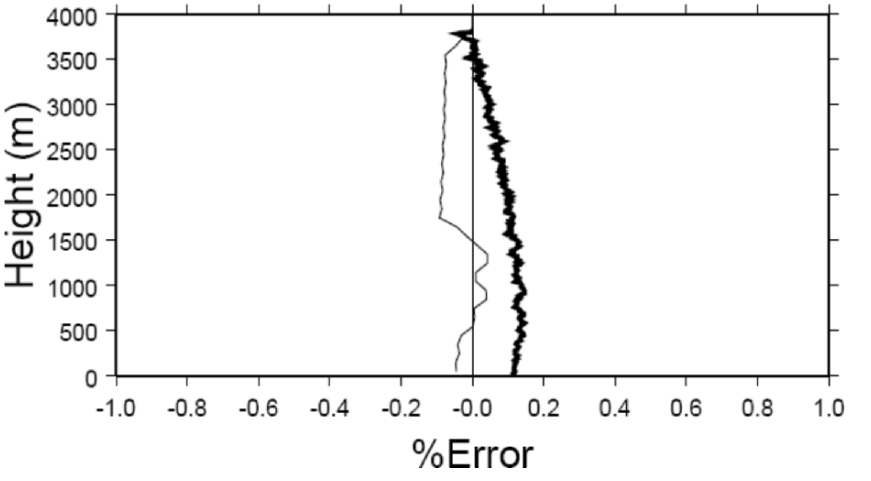

Figure 4. Refractivity retrieval error (%) for the wet model case. The thick line shows the results for abel while the thin line is used for least squars results

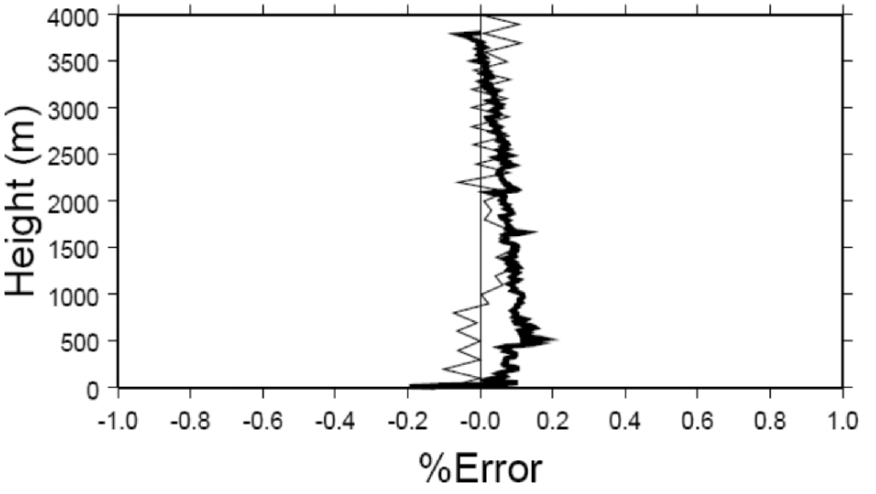

Figure 5. Refractivity retrieval error (%) for the radiosonde case. The thick line shows the results for abel while the thin line is used for least squares results

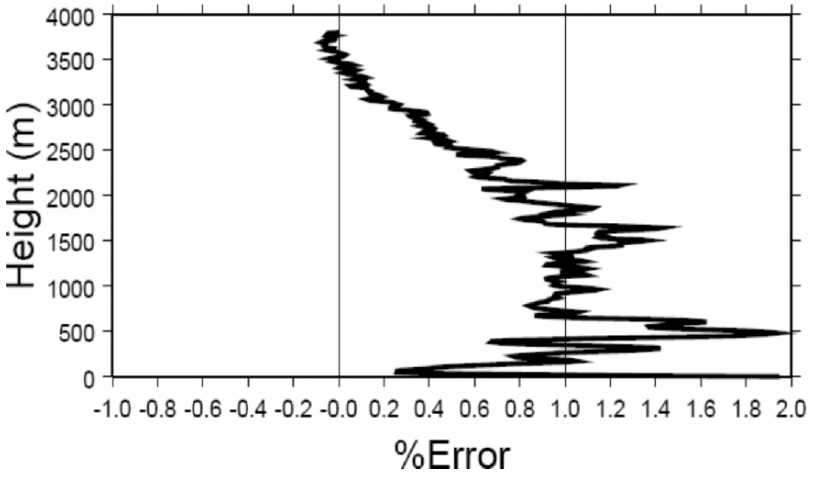

Figure 6. Refractivity retrieval error (%) for the radiosonde case for the Abel inversion. Elevation-dependant bias errors are added to the bending angles (about 10%)

bending angle prevents the convergence in the least squares method. An elevation-dependent bias (the value of the bias is taken as zero at the zero degree elevation angle and increases as a linear function of the elevation angle until it reaches 10% of the bending angle at the lowest elevation angle) prevents convergence for the least squares method. Table 1 summarizes the limitations and promises of the two methods.

TABLE 1. Overall comparison of both Least squares and Abel inversions

Items	Least Squares	Abel
Refractivity Model	Needed	Not needed
Accuracy	Better than 0.25%	Better than 0.2%
Constant bias	No convergence if >30 arc second ($1.454 * 10^{-4}$ radians)	No problem at all
Elev. Depen. bias	No convergence	Few errors
CPU time	> 5 sec.	< 0.08 sec.
Height range	~2km above receiver	Below receiver

4. Conclusions

Least squares and Abel inversion techniques are compared for retrieving DL GPS occultation data. Occultation data are simulated using profiles from a climatological model (MSIS-90) and radiosondes.

Both the least squares and Abel inversions can retrieve the refractivity with a very good accuracy. The relative errors are better than 0.2% for the observational error model used in this study. The least squares method can extend the height range to a few kilometers above the receiver but it requires an a priori refractivity model. However, the Abel inversion does not require an a priori model. The Abel inversion is also less sensitive to biases in the data. Abel inversion solution is much faster than least squares one.

5. References

Born, M., and E. Wolf: 1980. Principles of Optic*s*. 6th ed., Pergamon, New York, 952 pp.

Bruton, W. D., and G. W. Kattawar: 1997. Unique temperature profiles for the atmosphere below an observer from sunset images. Appl. Opt., vol. **36**, 27, 6957-6961.

Eyre, J. R.: 1994. Assimilation of radio occultation measurements into a numerical weather prediction system, Tech. Memo 199, Eur. Cent. for Medium-Range Weather Forecasts, Reading, England.

Fjeldbo, G., A. J. Kliore, and V. Eshleman: 1971. The neutral atmosphere of venus studied with the mariner V radio occultation experiments. *Astron. J*., vol. **76**, 2, 123-140.

Hajj, G. A., E. R. Kursiniski, W. I. Bertiger, S. S. Leroy, T. Meehan, L. J. Romans, and J. T. Schofield: 1996. Initial results of GPS-LEO occultation measurements of Earth's atmosphere obtained with GPS/MET experiment. *Proc. Symp. on GPS Trends in Precise Terrestrial, Airborne, and Spaceborne Applications*, Springer-verlag, New York, 144-153.

Hedin, A. E.: 1991. Extension of the MSIS Thermospheric Model into the Middle and Lower Atmosphere, *J. Geophys. Res*. vol. **96**, 1159-1991.

Kursinski, E. R., G. A. Hajj, K. R. Hardy, J. T. Schofield, and R. Linfield: 1997. Observing Earth's atmosphere with radio occultation measurement using the Global Positioning System. *J. Geophys. Res*., vol. **102**, 23429-23465.

Mousa, A. K., and T. Tsuda: 2001 Retrieval of key climate variables using occultation geometry of a mountain top GPS receiver. *ION GPS 2001 proceedings*, 1117-1126.

Rocken, C., R. Anthes, M. Exner, D. Hunt, S. Sokolovskiy, R. Ware, M. Gorbunov, W. Schreiner, D. Feng, B. Herman, Y.-H. Kuo, and X. Zou: 1997. Analysis and validation of GPS/MET data in the neutral atmosphere. *J. Geophys. Res*, vol. **102**, D25, 29849-29866.

Tricomi, F. G.: 1977. *Integral Equations*. Dover, Mineola, New York, 238 pp.

Wickert, J., C. Reigber, G. Beyerle, R. Konig, C. Marquardt, T. Schmidt, L. Grunwaldt, R. Galas, T. K. Meehan, W. G. Melbourne, and K. Hocke: 2001. Atmospheric sounding by GPS radio occultations: first results from CHAMP. *Geophys. Res. L*, vol. **28**, 17, 3263-3266.

Zuffada, C., G. A. Hajj, and E. R. Kursiniski: 1999 and A Novel approach to atmospheric profiling with a mountain-based or airborne GPS receiver, *J. Geophys. Res.*, vol. **104**, D20, 24435-24447.

PRESENTATION OF MADEPODIM PROJECT

ABBÈS AZZI
Laboratoire de Mécanique Appliquée
Faculté de Génie Mécanique
Université des Sciences et de la Technologie d'Oran
BP 1505 El-Mnaouar, 31000, Oran, Algérie
Abbes.Azzi@gmail.com ou abbesazzi@yahoo.fr
url : www.madepodim.org

Abstract In this contribution we intend to present a summary of a joint European project in frame of MEDA-TEMPUS program. The main aim of this project is to set up in Algeria (USTO University) a Master Degree that will focus on Air Pollutant Dispersion Modelling. To the best knowledge of the author, this is the first time that this level of diploma in this specialized field is setup in Algeria. The first promotion will be composed by ten Master and then will be conducted successively. In parallel, the future Master candidate will be involved in PhD thesis and post doctoral research. Another great advantage of that project is the creation of a very high quality computing center (80 Xeon node, 160 Go of Ram memory and 4 To of storage capacity). This will be also the first and more powered computing center in Algeria and will be used mainly to run atmospheric models as the eta/skiron, CAMx codes. Among other partners the project is supported by the highly skilled *Atmospheric Modelling & Weather Forecasting Group* from Athens. The ten students involving in the first promotion will beneficiate from six month training in France and Greece and will be involved in different research areas such as:

- Study of the cyclogenesis in the Mediterranean Region.
- Investigation of the dust budget in the Mediterranean Region.
- Evaluation of the operational photochemical model CAMx.

1. Specific Objectives of the TEMPUS JEP MADEPODIM project

The main aim of this TEMPUS project is to create a high level curriculum and a Master degree diploma at the USTO University that focus on Air Pollutant Dispersion Modelling.

A. Mellouki and A.R. Ravishankara (eds.), Regional Climate Variability and its Impacts in the Mediterranean Area, 291–294.

This large training project also lies in:

1. Improving teaching abilities of the staff members,
2. Creating a computing centre,
3. Setting up all teaching equipments,
4. Training Master Degree researchers.

It is expected that, at the end of the MADEPODIM project, a centre of excellence for Environmental sustainability training and research centre will be established and will provide consulting and services to industry and regulatory bodies. The Algerian academic staff trained and the international co-operation network that will be created during the project will be the background to setup a specialized and very high level teaching team in the Faculty of Mechanical Engineering, USTO and ENSET. Technical and human infrastructure set up by the present JEP will be used to open successive Master degrees after the end of the project.

2. The Project Actions

The first JEP year (2004-2005) has been devoted to enhance the skills of teaching staff and to prepare the necessary conditions to start the master degree courses:

- Kick-off meeting,
- Special courses and training for Algerian teachers in Greece, France and Algeria,
- Creation of a specialised library (software, books and academic journals) on air pollution modelling,
- Preparing and purchasing all necessary teaching equipments and updating the existing material (computers, video-projector…etc),
- Organising a national competitive exam in order to select the future Master students (ten students),
- Development of specific curricula and courses at international standards,
- First year meeting: project monitoring, progress report and financial report.

During **the second year (2005-2006)**, the following activities are currently running:

- Theoretical lectures at USTO led by Algerian teachers,
- Intensives courses (blocked weeks at USTO) given by French and Greek specialists,
- Dissemination seminars for non consortium people,
- Submission of Master projects which will be supervised conjointly by Algerian and European teachers,
- Second year meeting: course and lecture evaluations, progress report and financial report.

The third year (2006-2007) will be spent by the students to prepare their Master Thesis.

- Mobility of students and teachers will be planned in both directions,
- Accomplishment and presentation of the Master research projects,
- Dissemination seminars for non consortium people,
- Publication of the JEP results on the web,
- Final meeting: Overall evaluation of the JEP, perspectives on further developments and co-operative programs, final report.

3. Summary of lectures

General lectures: (Semester I)

- Numerical methods.
- Experimental methods & statistics.
- Heat & mass Transfer.
- Turbulence modelling.
- Technical English.

Specific lectures: (Semestre II)

- General meteorology and moist atmospheric processes.
- Regional meteorology.
- Regional water modelling.
- Turbulence in the lower atmosphere.
- Transport and dispersion of pollutants in urban areas.
- Introduction to atmospheric particle pollution.
- Introduction to Computational Fluid Dynamic (projects for environmental flows).
- Photochemistry of the atmosphere.
- Photochemistry modelling.

4. Final year projects

Cooperation with *Atmospheric Modelling & Weather Forecasting Group, Athens University*

- Study of the cyclogenesis in the Mediterranean Region.
- Investigation of the dust budget in the Mediterranean Region.
- Evaluation of the operational photochemical model CAMx.

Cooperation with AIAS Ltd, Thessaloniki, Greece

- Assessing the influence of small scale phenomena to local/meso-scale simulation results by two-way model coupling. Part I: Fast chemistry module implementation & vertical fluxes calculation.
- Assessing the influence of small scale phenomena to local/meso-scale simulation results by two-way model coupling. Part II: Mesoscale simulations.

Cooperation with École Centrale de Nantes (France)

- Transferts thermiques entre batiment et atmosphere, etude d'une relation entre flux de chaleur convectif et ecoulement de proche paroi.
- Dépôt des particules atmosphériques sur les facades des batiments.
- Modélisation de la turbulence produite par le trafic automobile urbain.
- Simulation numérique du bilan d'énergie de la canopée urbaine en site hétérogène : application aux données, de la campagne CLU-ESCOMPTE (Marseille, 2001).
- Etude numérique du comportement d'un traceur passif dans l'atmosphère urbaine de Marseille pendant, la campagne CLU-ESCOMPTE (Marseille, 2001).

LIST OF PARTICIPANTS

Arsene Cecilia
Environmental Chemical Processes Laboratory
Department of Chemistry, University of Crete
P.O.Box 2208, Voutes, GR-71003 Heraklion, Greece
carsene@chemistry.uoc.gr

Azzi Abbès
Département de Génie-Maritime, Faculté de Génie-Mécanique
Université des Sciences et de la Technologie d'Oran (USTO)
BP. 1505 El-Mnaouar, 31000, Oran, Algeria
abbes.azzi@gmail.com

Balafrej Taha
Ministère de l'Aménagement du Territoire, de l'Eau et de l'Environnement
Point Focal de la CCNUCC
Agdal Rabat, Morocco
balafrej@minenv.gov.ma

Bani-Aameur Fouzia
Laboratoire de Recherche sur la Variabilité Génétique
Université Ibn Zohr, Faculté des sciences, Département de Biologie
BP 28/S, 80 000 Agadir, Morocco
baniaameur@hotmail.com

Barnes Ian
Physikalische Chemie / Fachbereich C
Bergische Universitaet Wuppertal
Gauss Strasse 20, D-42097 Wuppertal, Germany
barnes@uni-wuppertal.de

Becker Karl H.
Institute of Physical Chemistry
Department of Chemistry, University Wuppertal
Gauss-Str. 20, D-42097 Wuppertal, Germany
khbecker@uni-wuppertal.de

Bennani Abdelfdil
Université Ibn Zohr
B.P. 32/S, 80 000 Agadir, Morocco
bennani@esta.ac.ma

Bergametti Gilles
Laboratoire Inter-Universitaire des Systèmes Atmosphériques (LISA)
Faculté des Sciences et Technologie
61 avenue du Général de Gaulle, F-94010 Créteil Cedex, France
bergametti@lisa,univ-paris12.fr

Born Kai
Universitaet zu Koeln
Institut fuer Geophysik und Meteorologie
Kerpener Str. 13, D-50937 Cologne, Germany
kai.born@uni-koeln.de

Bounoua Lahouari
Biospheric Sciences Branch, Code 614.4
NASA - Goddard Space Flight Center
Greenbelt MD 20771, USA
bounoua@ltpmail.gsfc.nasa.gov

Chahed Rafik
Institut National de La Météorologie
BP 156-2035, Tunis, Tunisia
chahed@meteo.tn

Chehbouni Ahmed
Université Cadi Ayyad, Faculté des Sciences Semlalia
BP 2390, Marrakech, Morocco
chehbouni@ucam.ac.ma

Daële Véronique
CNRS, Laboratoire de Combustion et Systèmes Réactifs (LCSR)
1C, Avenue de la recherche scientifique
F-45071 Orléans cedex 02, France
daele@cnrs-orleans.fr

Dakkina Abdelali
Centre d'Information sur l'Energie Durable et l'Environnement (CIEDE)
Ministry of Environment
Rabat, Morocco
dakina2002@yahoo.fr

Dhaou Hanen
Laboratoire d'erémologie et lutte contre la désertification
Institut des Régions Arides Médenine
Route du djorf km 22.4119 Médenine, Tunisia
hanen_dhaou@yahoo.fr

Doussin Jean-François
Laboratoire Inter-Universitaire des Systèmes Atmosphériques (LISA)
Faculté des Sciences et Technologie
61 avenue du Général de Gaulle, F-94010 Créteil Cedex, France
doussin@lisa.univ-paris12.fr

El-Araby Tarek
Cairo University Center for Environmental Hazard Mitigation P. O
Box: 453 Al Orman, Giza, 12612, Egypt
tmelaraby@hotmail.com

Elmaimouni Lahcen
Laboratoire de Chimie Physique, département de Chimie
FSA, Agadir, Morocco
lelmaimouni@yahoo.fr

George Christian
Laboratoire d'Application de la Chimie à l'Environnement (LACE)
Domaine Scientifique de la Doua, Batiment J. Raulin
43 Bd du 11 Novembre 1918, F-69622 Villeurbanne Cedex, France
Christian.George@univ-lyon1.fr

Habib Khaled
Environmental Sciences Department
KISR, P.O.Box 24885 SAFAT 13109, Kuwait
khaledhabib@usa.net

Haddouche Amal
Centre de Développement des Energies Renouvelables (CDER)
El Machaar El Haram, BP 509, Issil-Marrakech, Morocco
a.haddouche@cder.org.ma

Hjorth Jens
Institute for Environment and Sustainability (IES)
The European Commission Joint Research Centre
TP 290, 21020 ISPRA (VA), Italy
jens.hjorth@jrc.it

Kanakidou Maria
Environmental Chemical Processes Laboratory
Department of Chemistry, University of Crete
P.O.Box 2208, Voutes, GR-71003 Heraklion, Greece
mariak@chemistry.uoc.gr

Karrouk Mohamed-Saïd
Université Hassan II Centre de Recherche de Climatologie (CEREC)
Laboratoire de Climatologie et de Télédétection (CLIMTEL)
BP 8220 Oasis, MA-20103 Casablanca, Morocco
Karrouk.MS@UnivH2M.Ac.Ma
KarroukSaid@Yahoo.Com

Knidiri Mohamed
Association Grand Atlas
149, Avenue Mohamed El Bakali N° 2
B.P. 682, Gueliz -Marrakech, Morocco
fnapmarrakech@yahoo.fr

Kubilay Nilgün
Institute of Marine Sciences
Middle East Technical University
PO Box 28, Erdemli-Mersin, Turkey
kubilay@ims.metu.edu.t

Laknifli Abdellatif
Département de Chimie
Faculté des Sciences d'Agadir
BP 8106, cité Dakhla, 80000 Agadir, Morocco
abdelaknifli@yahoo.fr

Le Bras Georges
CNRS, Laboratoire de Combustion et Systèmes Réactifs (LCSR)
1C, Avenue de la recherche scientifique
F-45071 Orléans cedex 02, France
lebras@cnrs-orleans.fr

Mahmoud Narmine S.
Atomic Energy Authority
National Centre for Nuclear Safety and Radiation Control (NCNSRC)
Material and Nuclear Fuel Cycle Dept.
3 Ahmed El-Zomer St. Nasr City, 11762, Cairo, Egypt, P.O.Box 7552
natonarmine@yahoo,com

Maione Michela
Universita' di Urbino Istituto di Scienze Chimiche
6, Piazza Rinascimento, 61029 Urbino, Italy
michela@uniurb.it
project.office@accent-network.org

Mallet Marc
Laboratoire d'Aérologie (LA), Observatoire Midi-Pyrenees
14 av Edouard Belin, F-31400 Toulouse, France
malm@aero.obs-mip.fr

Mellouki Wahid
CNRS, Laboratoire de Combustion et Systèmes Réactifs (LCSR)
1C, Avenue de la recherche scientifique
F-45071 Orléans cedex 02, France
mellouki@cnrs-orleans.fr
wmellouki@laposte.net

Melouki Ali
Ministère de l'énergie et des mines
Marrakech, Morocco
alimelouki@yahoo.fr

Mihalopoulos Nikos
Environmental Chemical Processes Laboratory
Department of Chemistry, University of Crete
P.O.Box 1470, Voutes, GR-71409 Heraklion, Greece
Mihalo@chemistry.uoc.gr

Millán Millán
Fundacion CEAM
Parque tecnologico c/4, Sector Oeste, Paterna
46980 Valencia, Spain
pilarz@ceam.es

Mohamed Mohamed A.
Atomic Energy Authority
National Centre for Nuclear Safety and Radiation Control (NCNSRC)
Material and Nuclear Fuel Cycle Dept.
3 Ahmed El-Zomer St. Nasr City, 11762, Cairo, Egypt, P.O.Box 7551
mageleel2000@yahoo.com

Moukrim Abdelatif
Université Ibn Zohr
B.P. 32/S, 80 000 Agadir, Morocco
moukrim@esta.ac.ma

Mousa Ashraf
Crustal Movements Laboratory
National Research Institute of Astronomy and Geophysics
Elmarsad St., Helwan, Cairo, 11421, Egypt
ashrafkm@yahoo.com

Niedojadlo Anita
AGH University of Science and Technology
Faculty of Mining Surveying and Environmental Engineering
Department of Management and Protection of Environment
Al. Mickiewicza 30, C4, 30-059 Cracow, Poland
niedan@poczta.fm

Pilling Mike
School of Chemistry
University of Leeds
Leeds LS2 9JT, United Kingdom
M.J.Pilling@leeds.ac.uk

Prospero Joseph M.
RSMAS/MAC, University of Miami
4600 Rickenbacker Causeway
Miami, FL 33149, USA
jprospero@rsmas.miami.edu

Ravishankara A.R. (Ravi)
Chemical Sciences Division, Earth System Research Laboratory
NOAA, R/CSD 2
325 Broadway, Boulder CO 80305, USA
A.R.Ravishankara@noaa.gov

Rubio Jose L.
Centro de Investigaciones sobre Desertificacion-CIDE
(CSIC, Universitat de Valencia, Generalitat Valenciana)
Cami de la Marjal, s/n, Apartado Oficial, 46470 Albal, Valencia, Spain
jose.l.rubio@uv.es

Sahabi Salah
Groupe Etudes & Recherche Climat Applications au Développement
GERCAD - ARCE, BP 4250 (Ibn Rochd) 31037 Oran, Algeria
salah_sahabi@yahoo.com

Sahi Zahra
Inspection Régionale de l'Aménagement du Territoire, de l'Eau et
de l'Environnement
Marrakech, Morocco
zahirasahi@hotmail.com

Saliba Najat A.
IBSAR - American University of Beirut
American University of Beirut
P.O.Box 11-0236 Riad El-Solh, Beirut 1107 2020, Lebanon
ns30@aub.edu.lb

Sinan Fouad
Département de Chimie
Faculté des Sciences d'Agadir
BP 8106, cité Dakhla, 80000 Agadir, Morocco
fouadsinan @yahoo.fr

Tanimoto Hiroshi
National Institute for Environmental Studies
Asian Environment Research Group Regional Atmospheric Modeling
Section & Center for Global Environment Research
16-2 Onogawa, Tsukuba, Ibaraki 305-8506, Japan
tanimoto@nies.go.jp

Touzani Abderrahmane
Ecole Mohammadia d'Ingénieurs
Avenue Ibnsina B.P. 765 Agdal
Rabat, Morocco
touzani@emi.ac.ma
craste@emi.ac.ma

Wahid Nadya
Laboratoire d'Analyse et de Valorisation des Ressources
Environnementales, Département de Biologie,
Université Cadi Ayyad, Faculté des Sciences et Technique de Béni-Mellal
BP 523, Béni-Mellal, Morocco

Wiesen Peter
Physikalische Chemie / Fachbereich C
Bergische Universitaet Wuppertal
Gauss Strasse 20, D-42097 Wuppertal, Germany
wiesen@uni-wuppertal.de

Yahyaoui Abdelaziz
FLSH Marrakech
Département de Géographie
BP 2410 Quartier Amerchich, Marrakech, Morocco
ayahyaoui2006@yahoo.fr

Zaghlol Gihan Mounier
Helwan University
Ain Helwan, Cairo, 11795 Egypt

AUTHOR INDEX

SUBJECT INDEX